Molecular characterisation of NAADP-gated two-pore channels

Robert Hooper

A thesis submitted for the degree of Doctor of Philosophy

The Department of Cell & Developmental Biology
University College London

September 2011

Declaration

I, Robert Hooper, hereby confirm that the work presented in this thesis is my own. Where information has been derived from other sources, I confirm that it has been duly acknowledged. This work has not been submitted in any previous application for a higher degree.

The data presented in this thesis was collected from September 2008 to September 2011.

Signature of the candidate: Date:

Acknowledgements

I'd first like to acknowledge those who gave me the opportunity to come to UCL and study for my PhD, including John Carroll, then head of the (former) Physiology Department. I'd also like to thank Shamshad Cockcroft, with whom I spent my initial placement. Shamshad started me off on the process of completing my PhD, for which I'm eternally grateful, and she remains a good source of advice. Nico Carvou, Michelle Li and Roman Holic in Shamshad's lab were all accommodating the early days. I'd also like to acknowledge Jonathan Gale, with whom I spent my third rotation placement. Jonathan honed my micro-dissection skills and first taught me calcium imaging, both have proved invaluable skills.

Choosing which of my rotation projects to extend in to a full three year PhD was always going to be a hard choice, but Sandip Patel, being a young PI, working at the bench, full of enthusiasm, drive and optimism swung it. How times have changed! A few grey hairs have crept in and he's increasingly desk bound writing grants and papers. They clearly had to make him a Professor sooner or later and he richly deserves it. Sandip still remains enthusiastic in directing the lab and a superb supervisor. He's ridiculously knowledgeable about anything even remotely related to calcium signalling. Sadly he also beats us regularly when playing pool in the pub.

I probably owe Dev Churamani a few drinks for his saint-like patience, always taking the time to help and teaching me most of the techniques I use in the lab (even if he then forgets them and I have to teach them back to him). He's also a great friend and has made the whole PhD process more enjoyable than it probably should be. I'd like to thank former lab members George Dickinson and Latha Ramakrishnan for all their help. I'll leave the lab with happy memories and a good scar to talk about, the result of attempting to give George a piggy-back down Piccadilly after the now infamous Christmas party of 2008. Les Dale has also been a good friend and a regular source of conversation about science and just about anything else over a coffee.

I'd like to thank Michael Duchen, as graduate tutor and Bogue Fellowship Committee chair, for giving me the opportunity to travel to the US and learn from Eugen Brailoiu (Temple) and Jonathan Marchant (Minnesota), both of whom I'm also grateful to for their time and help. I'd also like to acknowledge Colin Taylor (Cambridge) for the generous use of his lab equipment and Dave Prole for help with the FRET analysis. I've enjoyed my PhD immensely and that is a reflection of the people I've worked with, as much as the exciting and stimulating science.

Finally I'd like to thank my partner Katie, for always being a source of support and keeping me on the straight and narrow (despite Dev's efforts). Her hard work during her PhD, which has been far more stressful and arduous than mine, is an inspiration and I'm glad she's also made it to the end. Her sage advice of "don't get too drunk and don't end up in A & E" is usually, but not always, heeded.

Abstract

Nicotinic acid adenine dinucleotide phosphate (NAADP) is a potent intracellular calcium (Ca^{2+})-mobilising second messenger implicated in a variety of physiological processes. Unusually, NAADP mediates Ca^{2+} release from acidic organelles, such as the lysosome, and not the endoplasmic reticulum. Recently, members of the voltage-gated ion channel super-family, the two-pore channels (TPCs), have been identified as molecular targets of NAADP. The aim of this thesis is to investigate the molecular properties of these poorly characterised ion channels. In this study, I present the cloning of a novel TPC isoform from the sea urchin, an extensively used model organism for NAADP signalling, and the subsequent characterisation of the complete ancestral sea urchin TPC family. Sea urchin TPCs appeared to be N-glycosylated in an isoform-specific manner, displayed anomalous migration upon fractionation, similar to endogenous NAADP-binding proteins, and localised to the endo-lysosomal system. To characterise the properties of human TPCs, antibodies suitable for Western blot and immunocytochemistry analyses were identified. The topology of human TPCs was examined using *in silico* prediction methods, combined with fluorescence protease protection assays and the mapping of TPC antibody epitopes and N-glycosylation sites. Human TPCs conformed to a twelve transmembrane region model with cytosolic termini. The quaternary structure of TPCs was investigated using FRET analysis, sucrose density gradients, gel filtration, co-immunoprecipitation, and chemical cross-linking of both full-length TPCs and individual hydrophobic domains. TPCs likely assemble as dimers possibly within a high molecular weight protein complex. Finally, I show that the N-terminus of TPC1 regulates NAADP-mediated Ca^{2+} release and identify a potential physiological role for TPC2 in pigmentation.

Table of contents

List of figures

Chapter 1 – Introduction

1.1. Ca^{2+} signalling overview

Calcium (Ca^{2+}) is the most abundant and ubiquitous cation in the body, enabling it to act as widespread means of signalling and mediate a vast array of physiological processes from fertilisation to apoptosis (Berridge *et al.*, 2000). This one ion can elicit such a range of specific effects due to the highly defined amplitude, frequency, duration and location of its release into the cytoplasm, the so-called Ca^{2+} "signature". The resting cytosolic free Ca^{2+} concentration is low at ~ 100 nM, therefore a Ca^{2+} signal can be generated with a relatively small increase in cytosolic Ca^{2+}. Cytosolic Ca^{2+} can increase by influx from the extracellular space or release from internal Ca^{2+} storing organelles. The cytosolic Ca^{2+} concentration is tightly defined by a range of buffering, extrusion and reuptake mechanisms. The cell can then "encode" external stimuli by the production of intracellular second messengers and the generation of a subsequent Ca^{2+} signature. This signature is then "decoded" by Ca^{2+} sensitive processes to modulate downstream physiological events.

1.2. Ca^{2+}-release mechanisms

The majority of intracellular Ca^{2+} is stored in the endoplasmic reticulum (ER), a network of membrane bound cisternae emanating from the perinuclear region of the cell. The ER has a luminal Ca^{2+} concentration of ~ 100 μM. Two well characterised ligand-gated Ca^{2+} release channels are located on the ER, the inositol trisphosphate (IP_3) receptor and the ryanodine receptor.

1.2.1. IP_3 receptors

The release of cytosolic Ca^{2+} by the IP_3 receptor is one of the most extensively characterised signalling pathways. After stimulation by the agonist 5-HT, levels of IP_3 were shown to be elevated preceding intracellular Ca^{2+} release (Berridge, 1983) leading to speculation that IP_3 may be acting as a diffusible intracellular second messenger. IP_3 was subsequently shown to mobilise Ca^{2+} from the endoplasmic reticulum of permeabilised pancreatic acinar cells (Streb *et al.*, 1983) confirming second messenger activity. The production of IP_3 is mediated by activation of the enzyme phospholipase C (PLC) which hydrolyses phosphatidylinositol 4,5-bisphosphate (PIP_2) to form diacylglycerol (DAG) and IP_3 (Huang, 1989). IP_3 induces Ca^{2+} release from the ER by interaction with the eponymously named IP_3 receptor (IP_3R). IP_3R1 was first cloned from cerebellar Purkinje neurons (Furuichi *et al.*, 1989) and two further isoforms were subsequently identified (Yamamoto-Hino *et al.*, 1994), each differing in their affinity for IP_3 (Newton *et al.*, 1994). The IP_3 receptor protein has a predicted molecular weight of ~ 300 kDa and comprises of six transmembrane regions and an extended cytosolic N-terminus (Patel *et al.*, 1999). IP_3 receptors are divalent-selective cation channels, IP_3R1 having a Ca^{2+} conductance of ~ 50 pS (Foskett *et al.*, 2007). The binding of IP_3 to an N-terminal domain elicits a conformational change in the receptor coupled to activation (Mignery & Sudhof, 1990). Cytosolic Ca^{2+} had also been shown to regulate IP_3 receptors in a biphasic manner (Bezprozvanny *et al.*, 1991) when low concentrations acted as a co-agonist of activation whereas high Ca^{2+} concentrations were inhibitory. The functional IP_3 channel is formed by homo or hetero-tetramers of receptor isoforms. These tetramers can then associate to form clusters in response to IP_3, which is turn modulates the individual channels sensitivity to IP_3 and Ca^{2+} (Taufiq *et al.*, 2009;Rahman & Taylor, 2009). Furthermore IP_3 receptors are increasingly implicated in signalling microdomains, whereby disparate Ca^{2+} channels come into proximity or interact to regulate one another. IP_3 receptors have been shown to interact with TRPP2 to potentiate Ca^{2+} release (Sammels *et al.*, 2010) with similar observations for interactions with TRPC3 (Adebiyi *et al.*, 2011) and Orai1 (Lur *et*

al., 2011). Clustering and microdomain formation represents a higher order of dynamic IP_3 receptor regulation.

1.2.2. Ryanodine Receptors

The second family of ER-localised Ca^{2+} release channels is composed of the three ryanodine receptor isoforms (RyR1-3) which share ~ 70% sequence homology (Fill & Copello, 2002). RyR1 is the most abundant isoform in skeletal muscle (Takeshima *et al.*, 1989), RyR2 predominates in cardiac tissue (Nakai *et al.*, 1990;Otsu *et al.*, 1990) whereas RyR3 has a widespread tissue distribution (Fill & Copello, 2002). The receptors were named after the plant alkaloid ryanodine, high concentrations (> 100 μM) of which irreversibly inhibit channel opening. Ryanodine receptors (RyRs) have a predicted molecular mass of ~ 550 kDa (Lai *et al.*, 1988) and comprise either five (Ludtke *et al.*, 2005) or possibly six (Samso *et al.*, 2005) transmembrane spanning regions (which is yet to be conclusively proven) clustered towards the C-terminus of the protein, leaving an extensive N-terminal region, much like the IP_3 receptor. Functional ryanodine receptors exist as a homotetrameric complex of > 2 mDa (Lai *et al.*, 1989) forming a pore ~ 3 Å wide (Tinker & Williams, 1993) and ~ 10.4 Å in length (Tinker & Williams, 1995). Ryanodine receptors are poorly selective for Ca^{2+}, however they have a high conductance of ~ 100 pS (Tinker & Williams, 1992). The receptors are best characterised in their role mediating excitation-contraction coupling of striated muscle, where they interact with T-tubule L-type voltage-gated Ca^{2+} channels, the dihydropyridine receptors (DHPRs) (Fill & Copello, 2002). Depolarisation of the T-tubule induces a conformational change in the DHPR leading to RyR activation, intracellular Ca^{2+} release and subsequent muscle contraction. In cardiac excitation-contraction coupling the activation of RyR2 also requires the influx of Ca^{2+} through the DHPR to activate RyR2 and initiate Ca^{2+}-induced Ca^{2+} release (CICR). Low cytosolic Ca^{2+} concentrations (1-10 μM) have been shown to activate the channel while high concentrations (1-10 mM) inhibit channel function (Fill & Copello, 2002). Luminal Ca^{2+} may also modulate RyR function, with increased sensitivity to cytosolic stimuli

at high luminal ER Ca^{2+} levels (Gyorke & Gyorke, 1998). As well as Ca^{2+}, RyRs are believed to be activated by the intracellular second messenger cyclic ADP-ribose (cADPR) (Lee, 1997). cADPR was shown to release Ca^{2+} from sea urchin egg homogenate that had been desensitised to IP_3 (Clapper *et al.*, 1987;Lee *et al.*, 1989). cADPR is formed by the cyclisation of NAD by a family of ADP-riboysl cyclases (ARCs) (Lee & Aarhus, 1991). It has been proposed that cADPR may not bind ryanodine receptors directly but instead modulate the activity of ryanodine receptors via an accessory protein. This was based on the observation of photo-affinity labelling studies which suggested cADPR binds protein targets of 100 and 140 kDa (Walseth *et al.*, 1993), much smaller than ryanodine receptors. Ryanodine receptors may also be regulated by interactions with other Ca^{2+} conducting channels. Signalling by RyR2 in the heart is sensitive to expression of TRPP2, which interacts via its N-terminus with RyR2 (Anyatonwu *et al.*, 2007). Like IP_3 receptors, receptor interactions may therefore add another layer of RyR2 regulation, modulating Ca^{2+} signalling in the heart.

1.3. Ca^{2+} Influx

1.3.1. Voltage-gated Ca^{2+} channels

In addition to intracellular Ca^{2+} release by ligand-gated ion channels, cytosolic Ca^{2+} signals may also be generated by Ca^{2+} influx across the plasma membrane. The voltage-gated ion channel superfamily consists of ~ 140 channels that conduct Ca^{2+} (Ca_v), K^+ (K_v) or Na^+ (Na_v) ions (Yu *et al.*, 2005). Each member of the family is a variant upon a structurally homologous domain consisting of six transmembrane spanning α–helix regions (S1-S6) with a re-entrant pore-forming loop between the S5 and S6 helices (Minor, Jr. & Findeisen, 2010). The pore region of the voltage-gated channel primarily determines the ion selectivity and conductance properties of the channel (Heinemann *et al.*, 1992). Functional voltage-gated Ca^{2+} (and Na^+) channels expresses four pore domains as a single protein, in contrast voltage-gated

K^+ channels (K_vs) have a single pore domain in each in protein, and are tetrameric. This pore-forming protein is termed the α1 subunit and comprises the core of the channel. The S4 region in each domain serves as the primary voltage-sensor in voltage-gated channels, containing highly conserved, positively charged amino-acids (Liman *et al.*, 1991). Upon depolarisation of the membrane, this S4 region undergoes a structural change in conformation whereby the α–helix of S4 moves towards the extracellular face of the protein, allowing channel gating by functional coupling to the pore through the S4-S5 linker (Catterall, 2011). By this mechanism the channel is voltage-gated.

There are ten distinct α1 subunits of voltage-gated Ca^{2+} channels, divided into three groups based on sequence homology (Catterall, 2011). The Ca_v1 α1 subunits share ~ 75% amino acid identity and mediate high-voltage activated (HVA) L-type Ca^{2+} currents. Ca_v1 α1 subunits have a range of functions including excitation-contraction coupling in skeletal muscle, as mentioned previously, endocrine secretion and regulation of gene expression. Ca_v2 α1 subunits have < 40 % homology with the Ca_v1 subunits and also mediate HVA currents (N, P, Q and R) to initiate fast synaptic transmission. The Ca_v3 α1 subfamily has little homology (< 25 %) to other α1 channels. This family are low-voltage activated (LVA) and conduct T-type currents, responsible for repetitive action potentials and pacemaker activity in rapidly firing cells such as cardiac myocytes.

The α1 subunit of HVA channels do not exist in isolation however, multiple accessory subunits are associated with the pore-forming protein to create a channel complex. While the α1 subunit determines the main biophysical properties of the channel the accessory subunits can modulate channel function. Cytoplasmic β-subunits bind to the "α-interaction domain" (AID) in the S1-S2 linker of α1 subunits (Richards *et al.*, 2004) and modulate the kinetics and amplitude of Ca^{2+} influx as well as contributing to membrane targeting of the channel (Dolphin, 2009). Membrane-anchored $\alpha_2\delta$ subunits may interact with the extracellular face of the α1 subunit to promote trafficking of the channel (Davies *et al.*, 2007). Finally a

membrane-spanning γ-subunit is also proposed to modulate Ca^{2+} currents and inactivation properties of skeletal muscle L-type channels (Freise *et al.*, 2000), although the exact function of this subunit has not been conclusively demonstrated.

1.3.2. TRP channels

The transient receptor potential (TRP) channels are a diverse group of cation channels which also belong to the voltage-gated ion channel superfamily (Yu *et al.*, 2005). Like voltage-gated K^+ channels, the basic structure of a TRP channel consists of six transmembrane spanning regions with a pore-loop between the fifth and sixth membrane spans. TRP channels are therefore believed to form tetramers to preserve the four pore arrangement of a functional voltage-gated ion channel. TRP channels are key modulators of sensory physiology, allowing the cell to react to changes in the environment such as temperature or pressure (Venkatachalam & Montell, 2007). The diversity of the TRP family arises from their polymodal activation. Not only is the TRP channel family activated by a range of stimuli but a single TRP channel isoform may have more than one mode of activation. TRP channels are primarily, but not exclusively, localised to the plasma membrane and are cation selective with many conducting Ca^{2+}. The TRP channel family is divided into six subfamilies in mammals TRPC, TRPV, TRPM, TRPA (classed as group 1 channels), TRPP and TRPML (group 2).

Mammalian TRP canonical family members (TRPC1-7) localise to the plasma membrane with a broad tissue expression profile. All TRPC isoforms are activated by phospholipase C (PLC) stimulation, with some isoforms also activated specifically by diacylglycerol (DAG) (Montell, 2005). TRPC channels had been implicated in store-operated Ca^{2+} entry (SOCE) although more viable candidates for this process have emerged (discussed below). TRP vanilloid (TRPV1-6) channels were so named when TRPV1 was shown to be activated by the inflammatory vanilloid compound capsaicin, the molecule that gives chilli peppers their apparent heat (Venkatachalam & Montell, 2007). The TRPV channels are calcium permeable

and activated by a range of noxious compounds (such as piperine and allicin), acidic pH and temperature. The TRPV isoforms act as thermosensors with a range of temperature activation thresholds from around 27 ºC (TRPV4) to greater than 52 ºC (TRPV2). TRP melastatin channels (TRPM1-8) have a range of activation mechanisms and permeability to cations. Ca^{2+}-permeable TRPM2 is activated by ADP-ribose and Ca^{2+} (Toth & Csanady, 2010). TRPM4 and M5 are activated by Ca^{2+} yet impermeable to this ion, with TRPM5 implicated in taste cell sensory transduction. TRPM8 does conduct Ca^{2+} and is activated by low temperatures and compounds which give the apparent sensation of cold (menthol, icilin). The single TRPA (ankyrin) isoform may also be activated by cold temperatures as well as acting as a nociceptor for pungent compounds such as isothiocyanates (found in wasabi, horseradish and mustard) and acrolein (a component of tear gas). Ca^{2+} influx through TRPA1 can be both potentiated (Zurborg *et al.*, 2007) and inhibited by extracellular Ca^{2+} (Wang *et al.*, 2008).

Group 2 TRP channels are evolutionary distinct from group 1 channels. They are distinguished by a long linker region between the first and second transmembrane regions. TRP polycystic (TRPP2, 3, 5) channels were characterised in the context of TRPP2 mutations causing polycystic kidney disease (PKD). PKD is a common inherited disorder and the greatest single cause of kidney failure (Gabow *et al.*, 1997). Mutations in either PKD1 or PKD2 (TRPP2) (Mochizuki *et al.*, 1996) can give rise to the disease, although the exact mechanism of TRPP2 mediated Ca^{2+} signalling is not known. Finally TRP mucolipin (TRPML1-3) proteins are localised to intracellular membranes of the endo-lysosomal system. TRPML1 may regulate lysosomal pH and mutations in TRPML1 are responsible for the lysosomal storage disorder mucolipidosis IV (MLIV), characterised by severe neurodegeneration. The exact role of TRPML1 in the progression of this disease is not known, however it is speculated that TRPML1 may regulate late-endosome/lysosome fission, perturbation of which leads to an accumulation of macromolecules in the lysosome, a characteristic of the disease (Lloyd-Evans *et al.*, 2010).

1.3.3. Store-operated Ca^{2+} entry

Store-operated Ca^{2+} entry (SOCE) refers to the specific coupling of ER Ca^{2+} store depletion with Ca^{2+} influx across the plasma membrane, as a mechanism for "re-filling" ER Ca^{2+} stores (Varnai *et al.*, 2009;Smyth *et al.*, 2010). It was noted that depletion of ER Ca^{2+} stores elicited a specific Ca^{2+} current across the plasma membrane, initially termed the I_{CRAC} current (Hoth & Penner, 1992). Subsequently it was demonstrated that depletion of ER Ca^{2+} leads to decreased binding of Ca^{2+} to the luminal EF hand of stromal interaction molecule 1 (STIM1) protein which acts as a Ca^{2+} sensor in the ER (Liou *et al.*, 2005;Roos *et al.*, 2005). STIM1 then relocates and clusters at ER/ plasma membrane junctions (Wu *et al.*, 2006) where it is believed the cytoplasmic domain of the protein can directly interact with the channel mediating I_{CRAC} Ca^{2+} influx across the plasma membrane (Varnai *et al.*, 2009). This CRAC current was later shown to be conducted by Orai1, based on knockdown and mutagenesis studies (Yeromin *et al.*, 2006;Prakriya *et al.*, 2006). The Orai1 channel protein consists of four putative transmembrane spanning regions with cytoplasmic N and C termini, the C-terminus being crucial for activation by STIM1 (Li *et al.*, 2007;Muik *et al.*, 2008). Upon interaction with STIM1, Orai1 dimers associate to form a tetrameric functional channel to mediate Ca^{2+} entry (Penna *et al.*, 2008).

1.4. Regulation of cytosolic Ca^{2+}

As I have discussed, the cytosolic Ca^{2+} signature is generated either by release of Ca^{2+} from intracellular stores or Ca^{2+} influx from outside the cell. To control the location, amplitude and duration of Ca^{2+} release events and therefore to generate specific Ca^{2+} signals (such as transient, sustained or oscillatory signals) Ca^{2+} must be either buffered or removed from the cytosol.

1.4.1. Ca^{2+} buffers and Ca^{2+} binding proteins

Ca^{2+} binding proteins fall into two broad categories; those that buffer Ca^{2+} and those that sense Ca^{2+} and translate this into a signal. The resting intracellular Ca^{2+} concentration of the cytosol is ~ 100 nM therefore to achieve tight spatial regulation of Ca^{2+} signals within a cell, Ca^{2+} is heavily buffered. Ca^{2+} is known to regulate synaptic transmission, and Ca^{2+} influx into the pre-synapse is heavily buffered to prevent uncontrolled neurotransmitter release across the synapse and subsequent nerve firing. As Ca^{2+} enters the pre-synapse, the area in which it exceeds 1 μM is restricted to > 250 nm of each point of entry (Roberts, 1993), consistent with effective buffering. Three of the principle diffusible, cytosolic Ca^{2+} buffering proteins are calretinin (Rogers, 1987), calbindin-D28k (Wasserman & Taylor, 1966) and parvalbumin (Arif, 2009). These proteins contain multiple Ca^{2+} binding EF hands (Kawasaki *et al.*, 1998) with affinity for Ca^{2+} in the micromolar to nanomolar range. Differences in the binding and dissociation kinetics of these proteins determine their physiological role as fast or slow onset buffers (Schwaller *et al.*, 2002). To effectively buffer Ca^{2+}, these proteins are found in micromolar concentrations within the cytosol (Hackney *et al.*, 2005). Ca^{2+} binding proteins not only act as buffers but also sensors to translate Ca^{2+} signals into a physiological response. The most studied intracellular Ca^{2+} sensor implicated in signal transduction is calmodulin. Calmodulin binds Ca^{2+} via four EF hand motifs and undergoes a subsequent change in conformation or localisation to interact with a broad range of target proteins to transduce signals (Chin & Means, 2000).

1.4.2. Ca^{2+} removal – Ca^{2+} pumps, exchangers and mitochondria

Not only is free cytosolic Ca^{2+} buffered in the cell, but ultimately Ca^{2+} is either removed from the cell or recycled back into intracellular Ca^{2+} stores. Two well characterised mechanisms exist for Ca^{2+} extrusion across the plasma membrane of eukaryotic cells (Brini & Carafoli, 2011). The first is the plasma membrane Ca^{2+} ATPase (PMCA) (Schatzmann, 1966) and the second is by Na^{+}/Ca^{2+} exchange

(Reuter & Seitz, 1968;Baker & Blaustein, 1968). The PMCA can be activated by direct binding of calmodulin (Larsen & Vincenzi, 1979), facilitating binding to the PMCA and activation of the pump. The PMCA removes Ca^{2+} with a stoichiometry of one Ca^{2+} ion for one molecule of ATP hydrolysed and a counter-flux of H^{+} ions. Although the PMCA has a high affinity for Ca^{2+}, it operates with slow kinetics (Brini & Carafoli, 2011). This in contrast to the Na^{+}/Ca^{2+} exchanger which has a low affinity yet high capacity for Ca^{2+} exchange. The Na^{+}/Ca^{2+} exchanger transports three Na^{+} ions for a single Ca^{2+} ion, either into or out of the cell, depending on the net electrochemical gradient acting on the exchanger (Blaustein & Lederer, 1999).

Ca^{2+} is not only extruded from the cell, but also recycled back into intracellular stores to so that signals may be sustained. As previously discussed, the primary intracellular Ca^{2+} store is the endoplasmic reticulum (or the sarcoplasmic reticulum in smooth and striated muscle). Ca^{2+} is taken up into the ER (or SR) primarily by the sarco/endoplasmic reticulum Ca^{2+}-ATPase (SERCA) (Lytton & MacLennan, 1988;Gunteski-Hamblin *et al.*, 1988) The SERCA pump hydrolyses one molecule of ATP for two molecules of Ca^{2+} transported with a counter-flux of H^{+} ions leaving the ER, similar to the PMCA. The SERCA pump can be inhibited by thapsigargin (Thastrup *et al.*, 1990), which binds irreversibly to lock the pump in an inactive conformation and prevent ion transport (Sagara *et al.*, 1992).

Mitochondria also act as a sink for cytosolic Ca^{2+}, sequestering Ca^{2+} upon release from intracellular channels then slowly releasing it back for reuptake. Like Ca^{2+} buffering proteins, mitochondria can therefore act to define the Ca^{2+} signature (Boitier *et al.*, 1999). The mechanism of uptake is believed to be through the mitochondrial calcium uniporter (mCU), whereby Ca^{2+} is drawn across by the negative mitochondrial potential (Santo-Domingo & Demaurex, 2010). Mitochondria have been shown to be in close juxtaposition to ER Ca^{2+} release channels to modify Ca^{2+}-induced Ca^{2+} release feedback mechanisms on these channels (Rizzuto *et al.*, 1993).

Cytosolic Ca^{2+} levels are buffered by mitochondria and cytosolic proteins, extrusion from the cell and reuptake into intracellular stores. Cytosolic Ca^{2+} signals are therefore generated by influx and release from intracellular stores and subsequent control and termination of these signals. The intracellular Ca^{2+}-mobilising second messenger NAADP, represented a completely novel signalling pathway, targeting a hitherto uncharacterised receptor located on a novel Ca^{2+} store.

1.5. NAADP-mediated Ca^{2+} signalling in the sea urchin egg: The early days

The sea urchin had long been a model organism for developmental biologists when it emerged as a prominent tool for the investigation of intracellular Ca^{2+} signalling. Upon fertilisation, the sea urchin egg undergoes a rapid increase in intracellular Ca^{2+} from the point of sperm entry, which propagates as a wave across the cell (Swann & Whitaker, 1986) representing a crucial step for the initiation of egg development. This wave was shown to be generated by the release of Ca^{2+} from intracellular stores (Jaffe, 1983). Hong Cheung Lee demonstrated IP_3 could mobilise Ca^{2+} from non-mitochondrial stores in broken cell preparations of the sea urchin egg (Clapper & Lee, 1985) providing the basis for much subsequent work in this organism. Lee followed this by showing the pyridine nucleotide metabolites NAD and NADP could also stimulate Ca^{2+} release from egg preparations that had previously been desensitised to IP_3 (Clapper *et al.*, 1987). Release of intracellular Ca^{2+} by NAD was later found to be due to the conversion of NAD to cADPR (Lee *et al.*, 1989) now known to be produced via a cyclisation reaction mediated by ADP-ribosyl cyclases (Lee & Aarhus, 1991;Churamani *et al.*, 2007;Davis *et al.*, 2008;Ramakrishnan *et al.*, 2010). The rapid Ca^{2+} mobilisation elicited by NADP was shown to be evoked by a contaminant of commercial NADP, identified by high resolution mass spectroscopy as NAADP (Lee & Aarhus, 1995). Intracellular Ca^{2+} release displayed a lack of heterologous desensitisation between IP_3, cADPR and NAADP stimulation (Clapper *et al.*, 1987;Lee & Aarhus, 1995) while IP_3 and cADPR antagonists proved unable to

inhibit NAADP responses in egg homogenates (Lee & Aarhus, 1995). NAADP-mediated Ca^{2+} release was independent of cytosolic Ca^{2+} concentration (Chini & Dousa, 1996) in contrast to the Ca^{2+}-induced Ca^{2+} release, a marked property of IP_3 and cADPR signalling. Furthermore it was shown that sub-threshold concentrations of NAADP could desensitise subsequent stimulation with maximal concentrations of NAADP (Aarhus *et al.*, 1996;Genazzani *et al.*, 1996) another facet of NAADP-mediated Ca^{2+} release that is unique from the properties of IP_3 and cADPR. This evidence suggested that NAADP was mobilising Ca^{2+} through a novel receptor.

Both IP_3 and cADPR had been shown to elicit Ca^{2+} release from the ER, however NAADP appeared to be acting upon a novel intracellular Ca^{2+} store. Fractionation of sea urchin egg homogenates by Percoll density centrifugation revealed Ca^{2+} release from a wide range of vesicles in response to NAADP, whereas only a limited subset, enriched in ER markers, were sensitive to IP_3 and cADPR (Lee & Aarhus, 1995). Stratification of intact sea urchin eggs resulted in cADPR and IP_3 mobilising Ca^{2+} from the nuclear pole, whereas NAADP could only trigger release from the distal pole, indicative of NAADP acting upon a non-ER Ca^{2+} store (Lee & Aarhus, 2000). As well as physical separation, discrimination of second messenger sensitive Ca^{2+} stores was demonstrated pharmacologically. Unlike cADPR and IP_3, NAADP signalling in broken cell preparations was insensitive to the SERCA pump inhibitor thapsigargin (Genazzani & Galione, 1996), which depletes the ER of Ca^{2+} (Thastrup *et al.*, 1990). The NAADP-sensitive Ca^{2+} store was subsequently identified as the reserve granule in the sea urchin egg when it was shown that pre-treatment with the lysomotropic agent Glycyl-L-phenylalanine (GPN) could ablate responses to NAADP (Churchill *et al.*, 2002). GPN is a peptide substrate of cathepsin C and causes osmotic lysis of lysosomes and related organelles when hydrolysed (Jadot *et al.*, 1984). Furthermore subcellular fractionation of sea urchin egg homogenates revealed NAADP-sensitive stores coincided with lysosomal markers such as β-galactosidase (Churchill *et al.*, 2002), likely corresponding to the reserve granule, an organelle analogous to the lysosome in sea urchin eggs. Uptake into the NAADP-sensitive store was prevented by the V-H^+-ATPase pump inhibitor bafilomycin A1

(Bowman *et al.*, 1988), consistent with the notion that Ca^{2+} uptake into lysosomes is dependent on a proton gradient, likely through a Ca^{2+}/H^{+} exchanger. It therefore appeared that NAADP-mobilised Ca^{2+} from novel acidic Ca^{2+} stores and not the ER, in stark contrast to IP_3 and cADPR.

It soon became apparent that despite NAADP targeting a novel receptor on a novel Ca^{2+} store, a high degree of cross-talk existed between signalling pathways in the intact sea urchin egg. When both IP_3 and ryanodine receptors are blocked or ER Ca^{2+} depleted with thapsigargin, NAADP-evoked Ca^{2+} signals were diminished in the intact egg (Churchill & Galione, 2000). Moreover, NAADP could also trigger long-lasting Ca^{2+} oscillations in the intact sea urchin eggs (Churchill & Galione, 2001). This was despite potent homologous desensitisation and the lack of cytosolic Ca^{2+} regulation of NAADP signalling in broken cell preparations. These findings were rationalised in the context of a "two-pool" mechanism of action, whereby NAADP primes subsequent ER Ca^{2+}-induced Ca^{2+} release by IP_3 and cADPR to produce Ca^{2+} oscillations through cycles of ER Ca^{2+} release and uptake. The clear pharmacological distinction between NAADP and IP_3 or cADPR-mediated Ca^{2+} release in egg homogenates most likely reflected the loss of functional coupling between stores by homogenisation.

1.6. Sea urchin NAADP receptors

NAADP was shown to act on a novel receptor located on a novel Ca^{2+} store, however the receptor was poorly characterised and its identity unknown. The use of radiolabelled [^{32}P]NAADP provided a key tool in the subsequent characterisation of the target protein. NAADP appeared to bind with high affinity to a single class of sites in sea urchin egg homogenates (Aarhus *et al.*, 1996;Patel *et al.*, 2000;Billington & Genazzani, 2000). Kinetic analysis revealed NAADP did not substantially dissociate from the receptor binding site under physiological conditions making binding to all intents irreversible (Aarhus *et al.*, 1996;Patel *et al.*, 2000;Billington & Genazzani, 2000). The binding site was closely related to the Ca^{2+} release properties

of the receptor, as the potency of NAADP analogues to compete with the binding of [^{32}P]NAADP (Patel *et al.*, 2000b), matched their ability to release Ca^{2+} (Lee & Aarhus, 1997). Binding of NAADP was shown to be insensitive to Ca^{2+} and pH changes (Patel *et al.*, 2000a) however a requirement for phospholipids was demonstrated in the association between NAADP and its target receptor (Churamani *et al.*, 2005). The receptor also appeared to be regulated by K^+ ions as ligand binding in buffer lacking K^+ was largely reversible, indicative of multiple receptor conformations (Dickinson & Patel, 2003). An important tool in the characterisation of NAADP-sensitive Ca^{2+} signalling came with the identification of an NAADP antagonist, Ned-19 by virtual screening (Naylor *et al.*, 2009). Analogues of Ned-19 have provided evidence for multiple binding sites on the NAADP target protein. Ned-20 inhibited NAADP binding and desensitisation by sub-threshold concentrations of NAADP without effect on Ca^{2+} release by activating concentrations (Rosen *et al.*, 2009). In contrast Ned-19.4 prevented Ca^{2+} release without altering NAADP binding. These data support the hypothesis of a high affinity (inactivating) and a low-affinity (activating) site on the putative NAADP-receptor.

The biochemical properties of the endogenous receptor were further investigated by utilising the irreversible nature of NAADP binding to sea urchin egg homogenates. This enabled effective solubilisation and tracking of the target protein during fractionation without dissociation of radiolabelled NAADP. Thus the apparent molecular mass of the target protein when analysed by gel filtration column was found to be 400-470 kDa (Berridge *et al.*, 2002). However when analysed by sucrose density centrifugation, the protein was considerably smaller at 120-150 kDa. The reason for this anomalous migration may be due to the dissociation of oligomers by high-speed centrifugation. Alternatively the association of the receptor with lipids (Churamani *et al.*, 2005) may reduce its buoyant mass and therefore underestimate the weight of the protein on sucrose gradients. The ligand-protein complex also exhibited a "molecular memory" whereby the stability of the complex was dependent on the length of exposure to NAADP (Churamani *et al.*, 2006;Genazzani

et al., 1996). Thus short exposure to NAADP resulted in more rapid dissociation of the ligand from the receptor. This was reported to be due to stabilisation of the receptor upon ligand binding, perhaps by a low-affinity, irreversible binding site (Churamani *et al.*, 2006).

1.7. NAADP as a wide-spread signalling molecule

The Ca^{2+}-mobilising properties of NAADP are not restricted to the sea urchin. NAADP-induced Ca^{2+} release been demonstrated in echinoderms (starfish) (Santella *et al.*, 2000), ascidians (Albrieux *et al.*, 1998), gastropods (aplysia) (Chameau *et al.*, 2001), amphibians (frogs) (Brailoiu *et al.*, 2001) and mammals (Cancela *et al.*, 1999) including humans (Berg *et al.*, 2000) making NAADP a wide-spread signalling molecule. NAADP-mediated Ca^{2+} signalling in the sea urchin had been localised to the reserve granule, an acidic organelle analogous to the mammalian endo-lysosomal system. Accordingly, there is much evidence that NAADP mobilises Ca^{2+} from the lysosomes, endosomes, and other related acidic organelles in mammalian cells (Galione, 2006;Mandi & Bak, 2008).

Lysosomes are membrane-bound organelles (0.1-1 μm diameter) that form the terminal degradative compartment of the endocytic pathway (Luzio *et al.*, 2007). Lysosomes have a luminal Ca^{2+} concentration of ~ 400-600 μM and an acidic pH of 4.6-5 maintained by an H^+-ATPase proton pump (Christensen *et al.*, 2002). Inhibition of this pump by bafilomycin A1 has been shown to decrease luminal Ca^{2+} concentration in the lysosome while subsequent acidification enabled rapid recovery of Ca^{2+} content (Christensen *et al.*, 2002). This indicated that lysosomal Ca^{2+} concentration is maintained by the proton gradient therefore loading of Ca^{2+} may occur via a H^+/ Ca^{2+} exchanger.

The initial characterisation of NAADP in a mammalian cell type utilised the pancreatic acinar cell in the context of cholecystokinin (CCK) signalling (Cancela *et al.*, 1999). CCK is a peptide hormone that acts on pancreatic acinar cells to stimulate

the release of pancreatic digestive enzymes in a Ca^{2+}-dependent manner. While CCK signalling is sensitive to IP_3 and cADPR blockade, it was also found that CCK signalling is abolished with desensitising NAADP concentrations (Cancela *et al.*, 1999). CCK signalling likely involves an NAADP-mediated Ca^{2+}-release which is subsequently amplified by ryanodine receptors and IP_3 receptors. Indeed NAADP levels were shown to increase 6-fold within 10 seconds of stimulation by a physiological concentration of CCK and precede cADPR production (Yamasaki *et al.*, 2005). CCK induced Ca^{2+} oscillations in pancreatic acinar cells are affected by thapsigargin targeting the ER Ca^{2+} uptake or GPN targeting lysosomes, suggesting a role for both in CCK signalling (Yamasaki *et al.*, 2004). Studies in pancreatic acinar cells have revealed that, similar to the sea urchin, NAADP targets acidic Ca^{2+} stores of the endo-lysosomal system and release of Ca^{2+} from these stores is amplified by the ER through Ca^{2+}-induced Ca^{2+} release. This has been dubbed the "Trigger hypothesis" (Patel *et al.*, 2001;Yamasaki *et al.*, 2005a;Cancela *et al.*, 1999).

One hallmark of signalling observed in mammalian cells but not in the sea urchin are the unique inactivation properties of NAADP. High (micromolar) concentrations of NAADP resulted in decreased Ca^{2+} release relative to lower (nanomolar) concentrations giving rise to a "bell-shaped" concentration-effect relationship in mammalian cells (Berg *et al.*, 2000). Consistent with its role as an intracellular second messenger, direct measurements of cellular NAADP using a radioreceptor assay (Churamani *et al.*, 2004;Lewis *et al.*, 2007) have identified many Ca^{2+} mobilising agonists that are coupled to production of NAADP (Galione *et al.*, 2010). Similarly, downstream of messenger production, a diverse range of physiological processes have also been linked to NAADP, three of which are discussed below.

A role for NAADP in smooth muscle signalling was first established by Yusufi et al when NAADP-mediated Ca^{2+} release and NAADP synthesis were demonstrated in rat vascular smooth muscle cells (Yusufi *et al.*, 2001). Furthermore, NAADP was capable of eliciting Ca^{2+} release from smooth muscle cell microsome preparations in a dose-dependent manner, independently of ryanodine and IP_3 receptors (Yusufi *et*

al., 2002). NAADP triggered restricted "bursts" of Ca^{2+} release that were propagated into a global Ca^{2+} wave and smooth muscle cell contraction, the latter being prevented by thapsigargin depletion of sarcoplasmic reticulum (SR) stores or RyR blockade (Boittin *et al.*, 2002). These findings supported a two-pool model whereby the initial, restricted, NAADP-mediated Ca^{2+} release is amplified into a global event via recruitment of ryanodine receptors on the sarcoplasmic reticulum. Local NAADP-mediated Ca^{2+} release events were subsequently shown to originate from lysosomes and then propagate by via lysosome/SR junctions forming a trigger zone for Ca^{2+} release (Kinnear *et al.*, 2004) which specifically included the RyR3 isoform (Kinnear *et al.*, 2008). This was demonstrated for NAADP-dependent Ca^{2+} signalling by the vasoconstrictor hormone, endothelin-1 (Kinnear *et al.*, 2004). NAADP was directly linked to smooth muscle contraction when it was implicated as a key second messenger in oxytocin-mediated contraction of uterine muscle. Muscle contraction was impaired both by the NAADP-receptor antagonist Ned-19 and disruption of acidic Ca^{2+} stores by bafilomycin A1 while conversely contraction could be stimulated by the addition of cell-permeant NAADP-AM (Aley *et al.*, 2010b). Furthermore, oxytocin was demonstrated to stimulate an increase in NAADP levels within uterine smooth muscle tissue.

NAADP has also been implicated in the modulation of neuronal differentiation. Several transcription factors such as NF-AT are Ca^{2+} sensitive (Shaywitz & Greenberg, 1999) and Ca^{2+} chelators prevent differentiation in neurons (Gu & Spitzer, 1995). Liposome delivery of NAADP was utilised in PC12 cells to evoke a sustained increase in cytosolic Ca^{2+} concentration that was GPN and bafilomycin A1 sensitive, consistent with lysosomes acting as NAADP-sensitive Ca^{2+} stores (Brailoiu *et al.*, 2006). NAADP also altered cell morphology by recruiting ER stores to form prolonged Ca^{2+} signals, a cue for differentiation in PC12 cells. Once neurons are formed, NAADP has been demonstrated to potentiate neurite outgrowth by stimulating Ca^{2+} release from bafilomycin A1 sensitive stores and subsequent amplification of this signal by CICR from the ER (Brailoiu *et al.*, 2005).

Finally, NAADP is also active in the modulation of endothelial cell signalling. In aortic endothelial cells, acetylcholine stimulation coupled to NAADP signalling, increased cytosolic Ca^{2+} by the mobilisation of acidic Ca^{2+} stores (Brailoiu *et al.*, 2010c). This was distinct from stimulation by thrombin and ATP which were not solely dependent on acidic Ca^{2+} stores. The action of NAADP was attributed directly to endothelial cells where nitric oxide production was stimulated and cells were hyperpolarised leading to dilation of aortic ring preparations. This physiology was expanded into a whole animal when intravenous administration of NAADP-AM lead to a fall in mean arterial pressure in anesthetised rats, providing a direct role for NAADP in regulating blood pressure.

A more comprehensive summary of physiological roles for NAADP is found in Table 1.1.

Organ	Tissue/Cell	Physiological Process	Reference
Reproductive System	Eggs (starfish)	Fertilisation potential	(Moccia *et al.*, 2004)
	Eggs (sea urchin)	Cortical flash	(Churchill *et al.*, 2003)
	Eggs (sea urchin)	Luminal pH regulation	(Morgan & Galione, 2007)
	Oocytes (ascidian)	Ca^{2+} current inhibition	(Albrieux *et al.*, 1998)
	Leydig cells	Testosterone secretion	(Hwang *et al.*, 2009)
	Uterine smooth muscle	Contraction	(Aley *et al.*, 2010b)
Nervous System	Neuromuscular junction (frog)	Neurotransmitter release	(Brailoiu *et al.*, 2003)
	Cortical neurons	Neurite extension	(Brailoiu *et al.*, 2005)
	PC12 cells	Differentiation	(Brailoiu *et al.*, 2006)
	Astrocytes	Autophagy	(Pereira *et al.*, 2011)
	Medulla neurons	Depolarisation	(Brailoiu *et al.*, 2009b)
	Buccal ganglion (aplysia)	Neurotransmitter release	(Chameau *et al.*, 2001)
Cardiovascular System	Platelets	Cell surface phosphatidyl-serine exposure	(Mushtaq *et al.*, 2011)
	Cardiac myocytes	Contraction	(Macgregor *et al.*, 2007)
	Coronary artery smooth muscle	Contraction	(Zhang *et al.*, 2006)
	Pulmonary artery smooth muscle	Contraction	(Boittin *et al.*, 2002)
	Endothelial cells	NO production	(Brailoiu *et al.*, 2010c)
		Hyperpolarisation	(Brailoiu *et al.*, 2010c)
		vWF secretion	(Esposito *et al.*, 2011)
	Aorta	Relaxation	(Brailoiu *et al.*, 2010c)

Organ	Tissue/Cell	Physiological Process	Reference
Immune System	T cells	Proliferation	(Dammermann *et al.*, 2009)
		NFAT translocation	(Dammermann *et al.*, 2009)
			(Dammermann *et al.*, 2009)
		Cytokine production	(Cordiglieri *et al.*, 2010)
		Stable arrests	(Cordiglieri *et al.*, 2010)
		Invasive capacity	(Cordiglieri *et al.*, 2010)
	Lymphokine-activated killer cells	Migration	(Rah *et al.*, 2010)
Pancreas	Beta cells	Insulin secretion	(Kim *et al.*, 2008)
		Insulin-stimulated ERK phosphorylation	(Alejandro *et al.*, 2010)
Other			
Gut	Taenia caecum smooth muscle	Contraction	(Tugba Durlu-Kandilci *et al.*, 2010)
Bladder	Detrusor smooth muscle	Contraction	(Tugba Durlu-Kandilci *et al.*, 2010)
Skeletal Muscle	C2C12 cells	Differentiation	(Aley *et al.*, 2010a)
Connective Tissue	Fibroblasts	Endo-lysosomal lipid transfer	(Zhang *et al.*, 2011)

Table 1.1 Physiological processes regulated by NAADP. Examples of cellular processes, shown to be regulated by NAADP, are grouped by organ system.

1.8. Candidate NAADP-sensitive Ca^{2+} channels

Despite extensive characterisation of NAADP-mediated Ca^{2+} signalling and the identification of a host of physiological processes assigned to this messenger, the molecular identity of the NAADP-sensitive Ca^{2+} release channel remained elusive. A number of candidate channels were proposed.

1.8.1. Ryanodine receptors

The initial characterisation of NAADP-mediated Ca^{2+} signalling suggested a novel receptor acting on acidic organelles, representing a then novel Ca^{2+} store. However the first candidate to emerge as a possible NAADP-sensitive channel was the ryanodine receptor, previously shown to be located on the ER and sensitive to cADPR.

The ability of NAADP to directly activate ryanodine receptors was first demonstrated in preparations of RyR2 from the heart, incorporated into lipid bilayers. It was found that NAADP increased the open-probability of single channels in a concentration-dependent manner (Mojzisova *et al.*, 2001). These findings were subsequently extended to purified RyR1 (Hohenegger *et al.*, 2002). Furthermore it was demonstrated that NAADP triggered a rapid Ca^{2+} release from heavy sarcoplasmic reticulum (HSR) stores in skeletal muscle which could be antagonised with the ryanodine receptor blockers ruthenium red and ryanodine. The Ca^{2+} release properties of NAADP, in combination with known ryanodine receptor agonists, were shown to be non-additive, suggesting NAADP was working directly through the ryanodine receptor. The use of the ryanodine receptor antagonist dantrolene implicated RyRI in NAADP-mediated insulin release in pancreatic β-cells (Mitchell *et al.*, 2003) while in pancreatic acinar cells, NAADP was shown to mobilise Ca^{2+} from a thapsigargin-sensitive store in the nuclear envelope (Gerasimenko *et al.*, 2003). This Ca^{2+} release could again be blocked by ryanodine and ruthenium red.

The apparent ability of NAADP to mediate Ca^{2+} release through ryanodine receptors was also observed in T-lymphocytes. Ca^{2+} release upon microinjection of NAADP could be abolished by co-injection of ryanodine or ruthenium red (Dammermann & Guse, 2005;Langhorst *et al.*, 2004). Release was also insensitive to bafilomycin A1 however thapsigargin could ablate responses (Steen *et al.*, 2007). These data suggested neither a novel receptor nor novel store were responsible for NAADP-mediated Ca^{2+} release in T lymphocytes. The use of BZ194, a nicotinic acid derivative was a potent antagonist of proliferation when co-injected with NAADP into mature T-cells (Dammermann *et al.*, 2009). Using purified RyR1 and high-affinity [^{3}H]ryanodine binding, which is proportional to channel opening, revealed NAADP increased association of ryanodine binding to its receptor, consistent with it activating the receptor. The observed increase in NAADP-mediated channel openings was antagonised by BZ194.

Despite the evidence for a direct effect of NAADP on ryanodine receptors, contradictory data suggests NAADP is acting on a distinct receptor and that perhaps disentanglement of the two signalling pathways may be hard to achieve. Application of cADPR in the presence of high, desensitising concentrations of NAADP could still elicit normal Ca^{2+} release from the nuclear envelope of pancreatic acinar cells (Gerasimenko *et al.*, 2003). This suggests that each messenger is acting upon a separate receptor. It may be that there is a close, perhaps even physical, association between ryanodine receptors and NAADP-sensitive channels that make disentanglement of the two difficult (Patel *et al.*, 2010). In arterial myocytes, for example, RyR3 forms dense perinuclear clusters that colocalise with lysosomal markers, suggesting the formation of a trigger zone for NAADP-mediated signalling (Kinnear *et al.*, 2008). Preincubation of the cells with dantrolene abolishes global Ca^{2+} waves but not the spatially restricted Ca^{2+} bursts evoked by NAADP dialysis, suggesting ryanodine receptors are responsible for Ca^{2+} signal propagation but not the initial release. The endo-lysosomal system is highly dynamic and if NAADP is

acting as the trigger for downstream ER mediated Ca^{2+} release, it seems likely that signalling microdomains between the two organelles exist.

1.8.2. TRPML1

The lysosomal Ca^{2+}-release channel TRPML1 has also been suggested to be NAADP-sensitive. Electrophysiological recordings made from planar lipid bilayers into which lysosomal Ca^{2+} release channels were reconstituted, displayed NAADP sensitivity which was dose-dependently attenuated by a TRPML1 polyclonal antibody (Zhang & Li, 2007;Zhang *et al.*, 2009). Human fibroblast TRPML1 knock out cells did not respond to NAADP but responses could be rescued by subsequent introduction of a TRPML1 transgene into the cells (Zhang *et al.*, 2011). These findings lack independent verification and a recent study by a different group observed NAADP-evoked Ca^{2+} signals were identical in wild-type and TRPML1 knock out mouse pancreatic acinar cells (Yamaguchi *et al.*, 2011).

1.8.3. TRPM2

A third candidate to be proposed as an NAADP-sensitive channel was another member of the TRP channel superfamily, TRPM2. Both NAADP and cADPR had been shown to potentiate TRPM2 activity in synergy with ADPR albeit at levels far greater than NAADP-mediated Ca^{2+} release which had previously been recorded (Lange *et al.*, 2008). TRPM2 was also reported to be functioning as a Ca^{2+} release channel located in lysosomal compartments (Lange *et al.*, 2009). However a subsequent study could find no enhanced activation of TRPM2 by ADPR in the presence of NAADP and Ca^{2+} release by NAADP could only be achieved at concentrations higher than physiologically relevant (Toth & Csanady, 2010). Additionally, NAAD was also shown to be a direct activator of TRPM2, suggesting the reported effects of NAADP were not specific.

1.9. Plant TPCs show the way

More recently, the mammalian two-pore channels (TPCs) have also been proposed as NAADP-sensitive Ca^{2+} release channels. At present, these channels, which I characterise in this thesis, are the strongest candidates for the long-sought target of NAADP (Galione, 2011;Patel *et al.*, 2011).

The two-pore channel (now referred to as TPC1) was first cloned from rat kidney by Ishibashi et al. in 2000 (Ishibashi *et al.*, 2000). The channel had an estimated molecular weight of 94 kDa and comprised two homologous domains each consisting of six predicted trans-membrane regions with a putative pore between the 5^{th} and 6^{th} membrane spanning regions. The structure was thus similar to voltage-gated Ca^{2+} and Na^{+} channels except that TPC1 contained two, as opposed to four, repeated domains leading to speculation that the two-pore channels may form dimers. However, no currents were recorded upon heterologous expression of rat TPCs in *Xenopus* oocytes and it was proposed that TPC1 may localise to intracellular membranes (Ishibashi *et al.*, 2000). The function of the animal TPCs was therefore unknown.

A year after the publication describing the cloning of a rat TPC, a TPC was cloned from the plant *Arabidopsis,* encoding an 84.9 kDa protein (Furuichi *et al.*, 2001). The protein appeared to be structurally homologous to the mammalian TPC, with the exception that the plant protein possessed two putative Ca^{2+}-binding EF hands (Hashimoto *et al.*, 2004). Initially AtTPC1 was shown to be a ubiquitously expressed and seemingly localised to the plasma membrane (Furuichi *et al.*, 2001). However upon re-examination, AtTPC1 was demonstrated to localise to the vacuole where it was shown to be the channel responsible for the intracellular slow vacuolar (SV) Ca^{2+} current (Peiter *et al.*, 2005). Electrophysiological recordings revealed SV Ca^{2+} currents were abolished in TPC1 knockout mutants and potentiated in TPC1 over-expressing lines.

Despite the link between AtTPC1 and the SV current, some early evidence suggested that AtTPC1may not actually be physiologically functional *in vivo*. When TPC1 knock-out, over-expressing and wild type cells were compared they revealed no role for the channel in mediating germination, guard cell Ca^{2+} signalling, abiotic or bacterial stress responses (Ranf *et al.*, 2008). Isalm et al also discounted a direct role for AtTPC1 mediated-CICR in abscisic acid and jasmonate-mediated stomatal closure by guard cells however it was conceded that TPC1 could be involved in priming S-type anion channels, which require elevated cytosolic Ca^{2+} (Islam *et al.*, 2010).

A functional role for AtTPC1 was demonstrated in leaf wound response by a gain-of function mutation of TPC1. Wounding of a plant leads to production of jasmonates by lipoxygenases, with an associated transient rise in cytosolic Ca^{2+} levels in the vicinity of the wound (Glauser *et al.*, 2008). A genomic screen linked the fatty acid oxygenation up-regulated 2 (fou2) mutation of TPC1 to increased jasmonate biosynthesis in response to wounding (Bonaventure *et al.*, 2007). This mutation manifested as lower activation potentials and faster conductivity of the TPC1 channel, highlighting a positive feedback mechanism for Ca^{2+} flux on JA synthesis. The mutation occurs in the putative voltage-sensing region of TPC1 (D454N) and was subsequently implicated in luminal Ca^{2+} sensing (Beyhl *et al.*, 2009), conferring increased tolerance to raised luminal Ca^{2+} on the channel and leading to sustained channel activation.

Plant TPC1 is a Ca^{2+} release channel located on the vacuolar membrane. The vacuole is the largest Ca^{2+} store in plants, with a typical Ca^{2+} concentration of 1.5-2.3mM, approximately 1000-fold higher than the surrounding cytosol (Peiter, 2011). The plant vacuole is analogous to the lysosome in mammalian cells. The vacuole, like the lysosome therefore, represents an acidic Ca^{2+} store (Patel & Docampo, 2010;Patel & Muallem, 2011). This raised the possibility that TPCs may localise to the lysosome in mammalian cells and could be the long sought-after NAADP-mediated Ca^{2+} release channel.

1.10. The TPC family in animals

Plants possess one (or perhaps two very closely related) TPC isoform. However in the animal kingdom the TPC family has undergone both gene loss and multiplication (Patel *et al.*, 2010). Animals are primarily classified into one of the two major phyla, protostomes or deuterostomes, dependent on whether the blastopore forms the mouth or the anus (respectively) during embryonic development. TPC genes are not present in protostomes such as flies (*Drosophila*) or worms (*C.elegans*) (Patel *et al.*, 2010). Humans are classed in the deuterostome phyla along with the model organism of NAADP signalling, the sea urchin, which represents a basal deuterostome. The majority of deuterostomia, including sea urchins, frogs and most mammals have three TPC isoforms although sequence similarity is remarkably low (< 40%) (Brailoiu *et al.*, 2009a) compared to other intracellular Ca^{2+} channels, such as IP_3 (Patel *et al.*, 1999) and ryanodine receptors (Fill & Copello, 2002) (~ 70%). Humans and rodents however, possess only two TPC genes encoding proteins with predicted molecular masses of ~94 kDa (TPC1) and ~85 kDa (TPC2). In primates, the gene encoding the third TPC isoform has degenerated into a pseudogene, in what is a relatively rare and recent event. Syntenic analysis of comparable chromosome regions between humans and other mammals revealed a partial TPC3 sequence corresponding to an N-terminal region of TPC3 (Brailoiu *et al.*, 2010a).

The degeneration of TPC3 from primates occurred ~25-40 million years ago in a common ancestor of Apes and Old World monkeys (Cai & Patel, 2010). TPC3 is likely to be intact in New World Monkeys and Prosimians however, suggesting selective constraints on the channel are still present in these groups.

The function of the TPCs in animals was unknown, therefore TPC isoforms were characterised in the context of being possible NAADP-sensitive Ca^{2+} release channels.

1.11. 2009: Animal TPCs as NAADP targets - initial characterisation

Within a short period in 2009, three independent publications emerged demonstrating that animal TPCs were NAADP-sensitive Ca^{2+} release channels. Brailoiu et al focussed on TPC1 (Brailoiu *et al.*, 2009a) whereas publications by Calcraft et al. (Calcraft *et al.*, 2009) and Zong et al. (Zong *et al.*, 2009) primarily investigated TPC2.

As discussed, NAADP-mediated Ca^{2+} release had been demonstrated in a wide variety of cell types and implicated in a range of physiological processes. Northern blot analysis published by Ishibashi et al in the original report of rat TPC1 cloning, had showed that TPC1 transcripts were detectable in numerous tissues (Ishibashi *et al.*, 2000). Brailoiu et al confirmed TPC expression in sea urchin, rat and human cell lines and furthermore quantitative analysis revealed that TPC1 was the most abundantly expressed isoform (Brailoiu *et al.*, 2009a). When the TPCs were overexpressed in SKBR3 cells they appeared to colocalise with markers of the endo-lysosomal system, consistent with the localisation of plant TPC1 to the analogous vacuolar compartment. While TPC2 was almost exclusively localised to the lysosome, TPC1 had a more heterogeneous distribution, showing part colocalisation with endosomal and lysosomal markers. In SKBR3 cells loaded with fura-2 to measure cytosolic Ca^{2+} levels, over-expression of TPC1 mediated a robust response to microinjection of NAADP, at a concentration that was sub-threshold in wild type cells. This response could be abolished by pre-treatment with bafilomycin A1, providing evidence that Ca^{2+} was mobilised from acidic stores upon microinjection of NAADP. Furthermore responses were diminished (but not ablated) in the presence of ryanodine, suggesting ryanodine receptors may contribute to the amplification of NAADP-mediated Ca^{2+} signals. RNA interference of TPC1 in wild type cells diminished typical responses to high concentrations of NAADP, demonstrating the contribution of endogenous TPCs to NAADP-mediated signalling.

An amino acid sequence alignment of the putative pore regions of TPCs revealed conserved leucine residues in each pore. Mutation of leucine 273 in pore I, to a helix-breaking proline eliminated the potentiating effect of TPC1 overexpression on NAADP responses. This suggests the pore-mutant may be acting in a dominant-negative manner on the endogenous receptor, indicative of oligomer formation. These data provide direct evidence that TPC1 is an NAADP-sensitive Ca^{2+} release channel.

The publications of Calcraft et al (Calcraft *et al.*, 2009) and Zong et al (Zong *et al.*, 2009) focussed on TPC2 as a possible NAADP-sensitive Ca^{2+} release channel. As with rat TPC1 (Ishibashi *et al.*, 2000), Calcraft et al reported a widespread tissue expression of human TPC2 transcripts by Northern blot (Calcraft *et al.*, 2009). Both endogenous and overexpressed TPC2 in HEK cells colocalised with lysosomal markers and this localisation was confirmed by sub-cellular fractionation. The distribution of TPC2 was in contrast to TPC1 and (chicken) TPC3 which appeared to localise in endosomes and other unidentified organelles. Flash photolysis of caged NAADP and dialysis of NAADP by patch pipette both revealed a biphasic release of Ca^{2+} in cells over-expressing TPC2. Initial low amplitude, slow release of Ca^{2+} was followed by a large, rapid Ca^{2+} transient. Both phases of NAADP-mediated Ca^{2+} release were abolished by pre-treatment with bafilomycin A1 while the IP_3 receptor antagonist heparin only abolished the second phase. This suggests the first phase may represent NAADP-mediated Ca^{2+} release from acidic stores which is subsequently amplified by IP_3 mediated Ca^{2+} release from the ER. Dialysis of NAADP into cells over-expressing TPC2 also revealed the characteristic "bell-shaped" dose-response relationship of NAADP. Electrical responses in isolated pancreatic β-cells from wild-type and TPC2 knock-out mice upon intracellular dialysis of NAADP were compared. In wild-type cells, NAADP elicited oscillatory currents which were absent in TPC2 knock-out cells, consistent with a role for TPC2 in mediating NAADP-evoked Ca^{2+} release. Radiolabelled [^{32}P]NAADP revealed enhanced binding of NAADP to membranes over-expressing TPC2 although this

was modest and no comparison was made of binding in wild-type and TPC2 knock-out mouse tissue.

Completing the triumvirate of publications, Zong et al characterised mouse TPCs as NAADP-sensitive channels (Zong *et al.*, 2009). Mouse TPCs, like their human orthologues, were shown to have a wide tissue distribution with TPC1 transcripts the most abundant. Heterologous expression of mouse TPC2 in HEK cells also showed a lysosomal location, although partial localisation with an ER marker was also apparent. Whole cell dialysis of NAADP into HEK cells loaded with fura-2 revealed potentiated Ca^{2+} transients upon over-expression of TPC2 compared to wild-type cells whereas over-expression of TPC1 was without effect. This response to NAADP in TPC2 expressing cells again exhibited a "bell-shaped" dose-response relationship and could be diminished by bafilomycin A1 although not, intriguingly, thapsigargin. This suggested that the NAADP mediated response in TPC2 expressing cells is not reliant on ER Ca^{2+} stores, an observation the authors were unable to explain.

The three publications had therefore reached a consensus on the TPCs as NAADP-mediated Ca^{2+} release channels, localised to the endo-lysosomal system. Equally though, the publications did raise points for discussion, most notably the role of TPC1. While Brailoiu et al reported a rapid, global Ca^{2+} signal in response to NAADP (Brailoiu *et al.*, 2009a), Calcraft et al. reported only localised transients (Calcraft *et al.*, 2009) while Zong et al failed to record any responses and concluded TPC1 was inactive (Zong *et al.*, 2009). The kinetics of the TPC2-mediated Ca^{2+} response also varied between groups. As with TPC1, Brailoiu et al witnessed a rapid Ca^{2+} transient in TPC2 expressing cells evoked by NAADP that peaked in seconds and was comparable to endogenous responses that had previously been characterised (Brailoiu *et al.*, 2009a). In contrast Calcraft et al and Zong et al recorded transients that peaked minutes after NAADP application (Calcraft *et al.*, 2009;Zong *et al.*, 2009). A recent study by Ogunbayo et al examined NAADP-evoked responses in HEK293 cells (as utilised by Calcraft et al) expressing TPC1 and observed global

Ca^{2+} transients (Ogunbayo *et al.*, 2011) comparable to those recorded by Brailoiu et al (Brailoiu *et al.*, 2009a). The reason for discrepant data between publications remains unresolved however.

1.12. Electrophysiology: the gold standard of ion channel status

The three research groups that had initially identified the TPCs as NAADP-sensitive Ca^{2+}-release channels published again in rapid succession to define the electrophysiological properties of TPCs. The intracellular localisation of TPCs presented a technical challenge to obtain electrophysiological recordings and interestingly the three groups employed different methodologies, each with its own advantages and disadvantages to circumvent this difficulty.

Brailoiu et al redirected TPC2 to the plasma membrane, rendering the channel accessible to patch-clamp recording (Brailoiu *et al.*, 2010b). This was achieved by mutation of a dileucine motif ($TPC2^{L11/12A}$) in the N-terminal region of TPC2, which forms a consensus sequence for lysosomal targeting of membrane proteins. TPC1 also contains such motifs in both the N- and C-termini, however mutation of these failed to redirect the protein to the plasma membrane. Coupling of wild-type TPC2 to ryanodine receptors on the ER was demonstrated by inhibition of peak Ca^{2+} signals after microinjection of NAADP into cells overexpressing TPC2 in the presence of ryanodine. Bafilomycin A1 further abolished all NAADP-mediated Ca^{2+} release confirming TPC2 is located on acidic organelles. When cells expressed TPC2 with a mutation in the dileucine targeting motif, ryanodine had no effect on Ca^{2+} signal amplitude. Bafilomycin A1 moderately enhanced Ca^{2+} release, most likely due to lack of sequestration of cytosolic Ca^{2+} by the acidic stores. Removal of extracellular Ca^{2+} from these cells abolished NAADP evoked signals, providing evidence that TPC2 targeted to the plasma membrane was uncoupled from ryanodine receptor activation and instead mediated Ca^{2+} influx. Inhibitory effects of

ryanodine on NAADP responses observed previously (Churchill & Galione, 2000) are thus likely due to disruption of amplification.

With TPC2 expressed at the plasma membrane and uncoupled from ryanodine receptors, the single-channel properties of TPC2 could be assessed by the patch-clamp technique, first by whole-cell recordings. NAADP was demonstrated to evoke slightly inwardly-rectifying currents with Cs^+ as the charge carrier. Recordings from inside-out patches of the cell plasma membrane expressing TPC2 revealed NAADP rapidly and reversibly elicited a unitary Cs^+ conductance of ~ 130 pS which could be blocked by the addition of *trans*-Ned19. Interestingly, TPC2 appeared to be largely voltage insensitive, despite the presence of basic residues in the fourth transmembrane spanning region of each domain, which confer voltage sensitivity on other ion channels (Liman *et al.*, 1991). The conductance of the channel could also be reduced to ~ 10 pS by the mutation of a conserved leucine residue in the putative pore region to a helix-breaking proline, indicating TPC2 is the pore-forming subunit of the NAADP-activated cation channel. The Ca^{2+} permeability of TPC2 was demonstrated when Ca^{2+} was used as the charge carrier and a unitary conductance of ~ 40 pS was recorded in presence of 500 nM NAADP.

Schieder et al used a novel method to record NAADP-mediated currents through mouse TPC2 on intact lysosomes (Schieder *et al.*, 2010a). HEK293 cells over-expressing TPC2 were treated with vacuolin to enlarge the lysosomes before these were isolated by centrifugation (Schieder *et al.*, 2010b). The enlarged lysosome was then attached to a < 1μm hole in a planar glass chip to enable "whole lysosome" recordings by planar patch clamp. NAADP-dependent current (which they termed I_{NAADP}) could be activated at low (60 nM) but not at high (5 μM) concentrations of NAADP (Schieder *et al.*, 2010b) consistent with previous findings showing self-inactivation (Berg *et al.*, 2000;Cancela *et al.*, 1999). The current was found to be non-rectifying with a reversal potential of ~ 45 mV that matches the theoretical reversal potential for Ca^{2+} (42.5mV) (Schieder *et al.*, 2010b). TPC2 was also shown to have a >1000 permeability ratio for Ca^{2+} over K^+. In accordance with the

localisation of TPC2 on acidic lysosomes, they found that increasing luminal pH to 7.2 abolished TPC2 currents. The group also mapped an acidic residue previously shown to modulate cation selectivity in TRPV channels to domains I and II of TPC2. Mutation of this residue in domain II of TPC2 manifested as a decrease in the selectivity ratio of Ca^{2+} over K^+ from >1000 to 8, suggesting this residue is key for the high level of selectivity for Ca^{2+} observed with TPC2.

Pitt et al reconstituted immunopurified TPC2 into artificial membrane bilayers for electrophysiological analysis (Pitt *et al.*, 2010). NAADP activated TPCs upon addition to the *cis* but not the *trans* chamber, which equates to NAADP binding the cytosolic face of the protein. The channel was shown to have a reversal potential of -21 mV indicative of cation selectivity and a Ca^{2+} conductance of 15 ± 1.5 pS, much smaller than IP_3 and ryanodine receptors. Using equimolar ratios of K^+ and Ca^{2+}, a permeability ratio of 2.6 for Ca^{2+} over K^+ was determined, suggesting the channel does not heavily discriminate for divalent over monovalent cations. This contrast with the findings of Schieder et al (Schieder *et al.*, 2010b). It was speculated that due to the overall small unitary conductance of TPC2, Ca^{2+} signalling could only be propagated by close proximity to ER/SR stores or if TPC2 channels were closely clustered and gating was coordinated. The group observed synchronised episodic gating of multiple channels which supports the latter hypothesis (Pitt *et al.*, 2010).

TPC2 channel activation reached a plateau at 1 μM NAADP when the NAADP concentration was increased cumulatively. However if 1 mM NAADP was applied without prior activation, the channel inactivated, suggesting a high affinity activation site and a low affinity inactivation site. The EC_{50} for TPC2 activation was 500 nM NAADP, higher than the Kd of NAADP binding to isolated membranes from cells over-expressing TPC2 (Calcraft *et al.*, 2009). The modulation of the TPC2 by regulatory factors was therefore investigated. When the luminal (*cis*) Ca^{2+} concentration was increased, the NAADP concentration-effect curve shifted to the left with a reduction in the EC_{50} to 5 nM. It therefore appears that luminal calcium regulates opening of TPC2 with low NAADP concentrations able to trigger channel

opening when lysosomal Ca^{2+} is high then as lysosomal Ca^{2+} stores are depleted, release is attenuated to enable refilling of stores.

The effect of pH on modulating TPC2 was also explored. When the pH was decreased from 7.2 to 4.8, TPC2 was still activated by low (nM) concentrations of NAADP however the channel inactivates at high NAADP concentrations. It was therefore concluded that changes in pH may alter the conformation of an NAADP binding site so that NAADP can dissociate from TPC2. This "bell-shaped" concentration-effect relationship at acidic pH is in accordance with the findings of Schieder et al (Schieder *et al.*, 2010b). However, Pitt et al were able to record currents at neutral pH (Pitt *et al.*, 2010), in contrast to Schieder et al. who concluded TPC2 was inactive when pH increased (Schieder *et al.*, 2010b). Pitt et al also demonstrated that 1 μM Ned-19 inhibited channel activity but surprisingly increased the open-probability at low, nanomolar, levels (Pitt *et al.*, 2010). This could indicate that Ned-19 is acting as a high affinity activator of the channel but at high concentrations becomes a non-competitive inhibitor.

The three studies reach a consensus that TPC2 is an NAADP-gated ion channel but again controversies arose between data sets. While Schieder et al demonstrated a thousand-fold selectivity for Ca^{2+} over K^{+}, Pitt et al found little discrimination in the cation permeability of the channel. As TPC2 is expressed on an acidic Ca^{2+} store, a role for pH regulation may be expected. Schieder et al observed that low luminal pH (comparable to within a lysosome) was a prerequisite for channel function (Schieder *et al.*, 2010b) whereas both Pitt et al and Brailoiu et al were able to record channel activity at neutral pH (Pitt *et al.*, 2010;Brailoiu *et al.*, 2010b). Furthermore Pitt et al found TPC2 self-inactivates with increasing NAADP at low pH (Pitt *et al.*, 2010). Finally, whereas Brailoiu et al reported a rapid reversal of channel activity upon washout of NAADP (Brailoiu *et al.*, 2010b), Pitt et al found TPC2 activation to be irreversible (Pitt *et al.*, 2010). It is possible that these discrepancies arise from the varied methodologies employed however it is important that consensus is reached regarding fundamental properties of the channel.

1.13. Coming full circle: Physiological roles for TPCs

In light of the identification of the TPCs as a molecular target of NAADP, recent studies have examined the role of TPCs in physiological effects in which NAADP had been previously implicated.

As discussed above (section 1.7), a role for NAADP in mediating contraction of smooth muscle had been reported in several preparations (Yusufi *et al.*, 2001;Yusufi *et al.*, 2002;Boittin *et al.*, 2002;Kinnear *et al.*, 2004). Tugba Durlu-Kandilci et al. examined the role of TPC2 in smooth muscle contraction. NAADP evoked contraction of smooth muscle with a characteristic "bell-shaped" dose-response relationship (Tugba Durlu-Kandilci *et al.*, 2010). Contraction mediated by NAADP was insensitive to ryanodine and thapsigargin treatment, but could be abolished by bafilomycin A1 and high, inactivating, concentrations of NAADP. NAADP failed to produce contraction in TPC2 knock-out mouse detrusor smooth muscle. Comparison of wild-type and knock-out mice responses to carbachol revealed that around 20% of the contractile response was dependent on functional TPC2. This was independent of ER Ca^{2+} stores, although it is possible that compensation in the transgenic animals had occurred to maintain contractions mediated by agonists.

Aley et al. examined the role of TPC1 and TPC2 in differentiation of skeletal muscle (Aley *et al.*, 2010a). Previous studies had demonstrated a messenger-specific role for NAADP in differentiation of PC12 cells (Brailoiu *et al.*, 2006). Cell permeable NAADP-AM was shown to stimulate early- and late-stage differentiation events which could be blocked by Ned-19 (Aley *et al.*, 2010a). During differentiation and skeletal muscle development TPC2 was down-regulated suggesting a role in early differentiation events while siRNA knock-down of both TPC1 and TPC2 manifested as a decreased differentiation index score in skeletal muscle, suggesting a role for both TPC isoforms in this process.

NAADP was demonstrated to mediate histamine-induced Ca^{2+}-release via H1 receptors on endothelial cells (Esposito *et al.*, 2011). Activation of H1R leads to increased intracellular NAADP and signalling through H1R evokes Ca^{2+} release from the ER and acidic organelles. This could be inhibited by the NAADP-mediated signalling antagonist, Ned-19 and inactivating concentrations of NAADP. Furthermore knock-down of both TPC isoforms abolished histamine-mediated release of von Willebrand factor from endothelial cells, a key component of the blood coagulation process.

1.14. Aims

Cytosolic Ca^{2+} is a ubiquitous means of signalling, mediating a vast array of cellular processes. This diversity is encoded by a tightly regulated Ca^{2+} "signature". Release of Ca^{2+} from intracellular stores can be mediated by the production of second messengers including IP_3, cADPR and NAADP. NAADP was first described as a calcium-mobilising molecule in 1995 (Lee & Aarhus, 1995), the cloning of the first mammalian TPC followed five years later (Ishibashi *et al.*, 2000) but it was nearly a decade before the two were linked (Brailoiu *et al.*, 2009a;Calcraft *et al.*, 2009;Zong *et al.*, 2009). The pace of progress in this field since 2009 has been impressive and the data presented in this thesis has hopefully contributed to that progress. The primary focus of my PhD was to investigate the molecular properties of the TPCs that contribute to their role as NAADP-mediated Ca^{2+} release channels. To achieve this I therefore aimed to:

1) Characterise TPCs in the model organism of NAADP signalling, the sea urchin
2) Identify suitable TPC antibodies to examine the molecular properties of TPCs
3) Define the topology of TPCs
4) Investigate the assembly of TPCs
5) Probe the regulation and physiology of TPC isoforms

Chapter 2 - Molecular cloning and characterisation of sea urchin TPC isoforms

2.1 Introduction

Following the identification of mammalian TPCs as likely NAADP targets, attention turned to the sea urchin, in which NAADP-mediated Ca^{2+} release had been extensively characterised. Would the observed properties of endogenous NAADP-sensitive Ca^{2+} release in sea urchin egg preparations be recapitulated with the cloning and characterisation of the sea urchin (Sp)TPCs?

The biochemical properties of the endogenous NAADP receptor in the sea urchin egg had previously been probed by exploiting the irreversible nature of NAADP ligand binding. Thus, egg homogenate preparations labelled with [^{32}P]NAADP could be effectively solubilised with mild detergents, without appreciable ligand dissociation. This allowed the target protein to be tracked during various fractionation procedures (Berridge *et al.*, 2002). Results from electrophoresis on native and pH gradient gels indicated that NAADP bound to a protein with an isolelectric point of ~ 6 (Berridge *et al.*, 2002). The apparent molecular weight of the labelled protein when analysed by gel filtration was 400-470 kDa. However, the protein appeared much smaller (~150 kDa) on sucrose density gradients. The reasons for this anomalous migration were unclear but it was initially proposed that sucrose density gradient centrifugation dissociates oligomeric TPC complexes (Berridge *et al.*, 2002). Subsequently the association of the endogenous receptor with lipids was established (Churamani *et al.*, 2005). This may reduce the buoyant molar mass of TPCs, thereby underestimating the protein weight on sucrose gradients.

It was also demonstrated that NAADP mobilised Ca^{2+} not from the ER but from a novel Ca^{2+} store, likely acidic organelles of the reserve granule. This was shown by

fractionation of sea urchin egg homogenates (Lee & Aarhus, 1995), stratification of intact eggs (Lee & Aarhus, 2000) and pharamacological discrimination between Ca^{2+} stores (Genazzani & Galione, 1996). The human TPCs were subsequently localised to the endo-lysosomal system (Calcraft *et al.*, 2009;Brailoiu *et al.*, 2009a). Additionally, potentiation of NAADP-mediated Ca^{2+} release by TPC overexpression could be abolished by bafilomycin A1, an inhibitor of acidic store Ca^{2+} uptake (Calcraft *et al.*, 2009;Brailoiu *et al.*, 2009a).

The size of the endogenous sea urchin protein responsible for NAADP-mediated Ca^{2+} release was therefore ambiguous, however the source of intracellular Ca^{2+} release was clearly localised to the endo-lysosomal system and not the ER. The aim of this chapter was to characterise the properties of sea urchin TPCs.

2.2 Materials and methods

Molecular cloning of SpTPC3

SpTPC3 was predicted by Gnomon, based on genomic contig SpuUn_WGA76937_2 (hmm 271542). Using gene-specific primers (5'-CAGGATCATATCCCATGCAG-3' (forward) and 5'-ATCACTGGATGAAACGCACA-3' (reverse)), a 2698 base pair (bp) clone was amplified from cDNA of *S.Purpuratus* embryos 54 hours post fertilisation (provided by Latha Ramakrishnan) by 35 cycles of PCR using Pfu Ultra II (Stratagene) with an annealing temperature of 55°C. 124 bp of 5' and 51 bp of 3' untranslated region (UTR) were included. This SpTPC3 product was sub-cloned into the pCR®-Blunt II-TOPO® cloning vector and sequenced in both directions. The sequence was deposited in EMBL (Accession # FN598568). The SpTPC3 coding sequence (2523 bp), lacking the stop codon, was then cloned into pCS2+GFP at the BamH1/XhoI restriction site using 5'-*CACC*GGATCCAAGATGGAGGGGCCAAAG-3' (forward) and 5'- AGGCTCGAGTGCTATGTTATCCACGGAAAGA-3' (reverse) primers to introduce a C-terminal GFP tag.

Plasmids

The SpTPCs were subsequently cloned into the pCS2+mRFP expression vector. All three isoforms were subject to restriction digest at their original ligation sites from pCS2+GFP vectors and ligated into pCS2+mRFP. SpTPC1 was digested at EcoRI/XhoI, SpTPC2 at ClaI/XhoI and SpTPC3 at BamHI/XhoI. SpTPC1 was also cloned into pCS2+ with five N-terminal *myc* tags at EcoRI/XhoI ligation sites from a sub-clone in pCR®II-TOPO®. Successful ligation was confirmed by sequencing across vector/insert junctions. The cloning of SpTPC1-GFP, SpTPC2-GFP and *myc*-SpTPC2 is detailed in Brailoiu et al 2010 (Brailoiu *et al.*, 2010a).

DNA products were resolved on a 1% w/v agarose gel for 30 min, 100 v alongside the 1 Kb plus DNA ladder (Invitrogen). Gel extraction was performed with the QIAquick gel extraction kit (QIAgen). DNA was transformed into One Shot® TOP10 Chemically Competent *E.coli* (Invitrogen) and purified with QIAprep Spin Miniprep Kit (QIAgen). Sequencing was performed with BigDye® Terminator v1.1 Cycle Sequencing Kit (Applied Biosystems).

The TPC constructs utilised in this chapter are summarised in Figure 2.1.

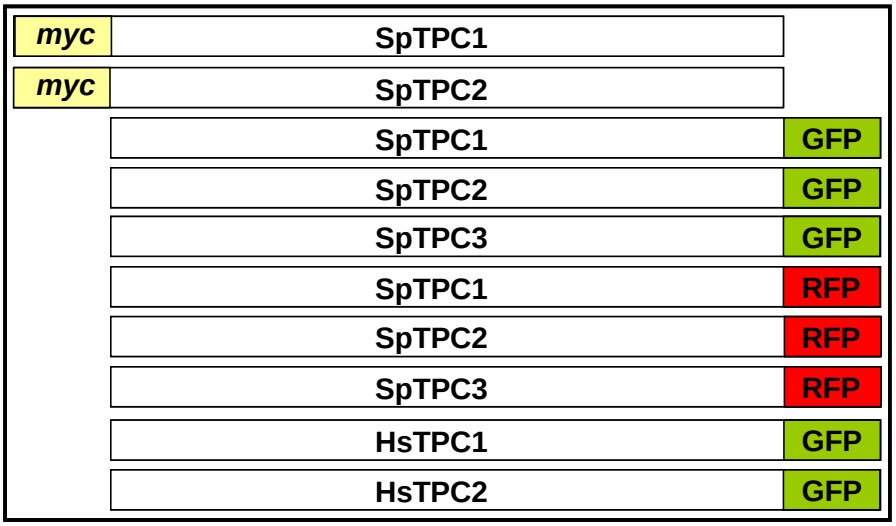

Figure 2.1. TPC clones utilised in the characterisation of SpTPCs. TPCs were tagged at either the N-terminus with five *myc* tags or at the C-terminus with GFP or mRFP.

Multiple sequence alignment and sequence homology analysis

TPC sequences were aligned using ClustalW2 (http://www.ebi.ac.uk/Tools/msa/clustalw2/) and the alignment (ALN) file generated then analysed by BoxShade 3.21 (http://www.ch.embnet.org/software/BOX_form.html). Amino acid identity and similarity between TPC isoforms and orthologues was calculated from pair-wise ClustalW2 alignments using the MacVector programme.

Cell culture

Human embryonic kidney (HEK 293) cells were maintained in DMEM supplemented with 10% (v/v) fetal bovine serum (FBS, Gibco Invitrogen). Cells were cultured in the presence of 100 U/ml penicillin and 100 μg/ml streptomycin at 37°C in a humidified atmosphere of 95% air and 5% CO_2.

Transfection

HEK cells (~80-90% confluent) were transfected using branched polyethylenimine (PEI, Sigma). A stock of 10 mM PEI in H_2O was prepared, neutralised with HCl (to pH 7) and diluted to a working concentration of 0.7 mM. A transfection mixture was prepared consisting of 1.3 μl of 0.7 mM PEI, 6.67 μl DNA (1 mg/ml) and 666 μl DMEM per 10 cm^2 of cells plated. This mixture was incubated at room temperature (RT) for 20 min before addition to cells in standard antibiotic and FBS-supplemented media. Five hours post addition of the transfection mixture, cells were washed with fresh media.

Preparation of solubilised protein

HEK cells expressing tagged SpTPCs were harvested 24 hours post transfection. Cells were scraped, washed by resuspension in phosphate-buffered saline (PBS) and centrifugation (500x*g*, 5 min) then resuspended in solubilisation medium (10 μl / cm^2 adherent cells) comprising 20 mM Tris (pH 7.2), 50 mM NaCl, 10 mM MgAcetate, 1% Triton X-100 (Pierce) and an EDTA-free protease inhibitor mixture (Roche). The suspension was rotated for 60 min at 4°C then centrifuged (90,000 x *g*, 60 min, 4°C). Supernatant containing solubilised protein was then reserved. The protein concentration of solubilised material was estimated by the bicinchoninic acid (BCA) assay (Smith *et al.*, 1985) against a standard dilution curve of known concentrations of bovine serum albumin (BSA, 0.03125 – 2 mg/ml) prepared in a

96-well plate. Absorbance was measured at 540 nm after 30 min incubation at 37 °C.

Sodium dodecyl sulfate polyacrylamide gel electrophoresis (SDS-PAGE) and Western blotting

Protein samples were prepared for SDS-PAGE analysis in NuPAGE LDS sample loading buffer (Invitrogen) supplemented with 100 mM DTT and incubated at 50°C for 60 min before loading. In initial experiments, Western blotting of SpTPCs following SDS-PAGE gave faint signals (Figure 2.2). Typical Western blot protocols entail denaturation of the protein at 95°C for five minutes in loading-buffer prior to SDS-PAGE. However heating at a lower temperature of 50°C for 60 minutes enabled a more robust visualisation of protein bands by Western blot. This heating step in sample preparation was subsequently refined to a 10 minute incubation of samples in loading-buffer at room temperature.

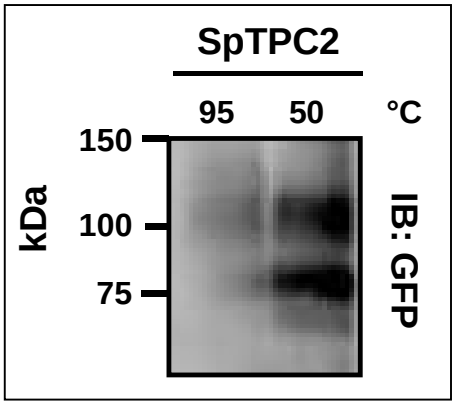

Figure 2.2. TPC protein is temperature sensitive. Western blot of SpTPC2-GFP solubilised from HEK cells. The homogenate was denatured in loading-buffer before resolution with SDS-PAGE either by heating at 95°C for 5 min or at 50°C for 60 min.

SDS-PAGE was performed using NuPAGE® Novex 4-12% Bis-Tris 1.5 mm, 10 well gels (Invitrogen) with Dual-Color Precision Plus protein standards (Bio-Rad).

The iBlot® Dry blotting system (Invitrogen) was utilised for protein transfer onto nitrocellulose membrane (iBlot® Transfer Stacks, Invitrogen). Membranes were blocked in a solution of 5% (w/v) powdered skimmed milk in PBS supplemented with 0.1% Tween-20 (Sigma) overnight at 4°C. Membranes were then probed by Western blotting with primary antibodies then secondary antibodies coupled to horse radish peroxidase (HRP), was typically at 1:2000 dilution in 2.5% milk blocking solution for 60 min at RT. Primary antibodies used were: polyclonal rabbit anti-GFP (Roche # ab290) and mouse anti-c-*myc* 9E10 (Insight Biotechnology Limited # sc-40, 200 µg/1.0 ml). Secondary antibodies used were goat anti-mouse IgG-HRP (# sc-2005) or goat anti-rabbit IgG – HRP (# sc-2004) both from Santa Cruz Biotechnology. Blots are developed with either Pierce ECL Western Blotting Substrate (Fisher Scientific) or ECL Advance Western Blotting Detection Kit (GE Healthcare).

PNGase F treatment

The protein concentration of solubilised HEK cell homogenates, transiently transfected with SpTPC protein, was estimated by BCA assay then 10 µg of protein was treated with PNGase F (NEB UK). Treatment was according to manufacturer's instructions, with the exception of the glycoprotein denaturing buffer step, which was omitted. Samples were incubated with PNGase F at 37 °C for 1 h before resolution by SDS-PAGE. In parallel, samples were mock treated with H_2O in place of PNGase F.

Sucrose density gradient centrifugation

HEK cells expressing GFP-tagged SpTPCs were harvested and solubilised as described above. Solubilised HEK homogenate (200 µl) was layered onto a 1.8 ml, 5-20% w/v sucrose density gradient (in 3% increments) prepared in solubilisation buffer. Samples were centrifuged in a swing-out rotor at 166,000 x *g* for 3.5 h at 4 °C. Fractions (195 µl) were collected from the top of the gradient and 20 µl

aliquots of each fraction were resolved by SDS-PAGE then probed by Western blot for GFP. The distribution of SpTPCs was compared to protein standards (2 mg/ml) run in parallel and detected by BCA protein assay. Standards utilised were cytochrome C (12 kDa), alcohol dehydrogenase (150 kDa), β-amylase (200 kDa) and apoferritin (443 kDa).

Gel filtration analysis

HEK cells transiently transfected with SpTPCs were harvested and solubilised as described above. Solubilised protein (200 µl) was injected onto a Superdex 200 HR 10/30 column linked to an AKTA FPLC system (Amersham Biosciences) equilibrated with solubilisation buffer. 1 ml fractions were collected at a flow rate of 0.5 ml/min and concentrated by Microcon YM-10 centrifugal filter devices (Millipore) to ~ 60 µl. The concentrated fraction (25 µl) was then resolved by SDS-PAGE and Western blot for GFP. The fraction profile of SpTPCs visualised by Western blot was compared to the UV absorbance profile of protein standards (10 mg/ml) in solubilisation buffer. Protein standards used were cytochrome C (12 kDa), alcohol dehydrogenase (150 kDa), apoferritin (443 kDa) and thyroglobulin (669 kDa).

Confocal microscopy

HEK cells (~ 70% confluent) were plated on poly-l-lysine (20 μg/ml) coated glass coverslips for transfection. Post transfection, cells were fixed in PBS containing 4% paraformaldehyde, for 10 min at RT then washed in PBS. Coverslips were mounted on glass slides with polyvinal mounting medium DABCO (Fluka) and sealed. Confocal images were captured using the LSM510 confocal scanner (Zeiss) attached to a Zeiss Axiovert 200M microscope through the Plan-Apochromat 63x/1.4 oil immersion objective. The excitation/emission wavelengths for GFP were 488 and 505-550 nm and mRFP 543 and 560-615 nm respectively. The image optical slice was 1 μm and the pinhole was 164 μm for the 488 nm channel and 216 μm for the 543 nm channel.

2.3 Results

2.3.1 Molecular cloning of SpTPC3

As discussed in Chapter 1, only a single TPC isoform exists in plants, while an expanded family of up to three isoforms are found in the animal kingdom (Brailoiu *et al.*, 2009a;Calcraft *et al.*, 2009), with evidence for both gene loss and multiplication (Cai & Patel, 2010). The two human TPC isoforms had been previously cloned and characterised as NAADP-mediated calcium-release channels (Brailoiu *et al.*, 2009a;Calcraft *et al.*, 2009). Sea urchins, the original model organism for NAADP-mediated signalling, have the full complement of three TPC isoforms present, including the TPC3 isoform, not functionally expressed in humans. Here I report the molecular cloning of SpTPC3.

The exact sequence of SpTPC3 was unknown, however the presence of the isoform was predicted by Gnomon based on genomic contig SpuUn_WGA76937_2. A product corresponding to the open reading frame (ORF) of the gene was amplified by polymerase chain reaction (PCR) from cDNA of *S.Purpuratus* embryos 54 hours post fertilisation as shown in Figure 2.3A. Amplification was from embryos 54 h post fertilisation due to the previously demonstrated developmental profile of SpTPC3, which had been shown not to be expressed in unfertilised sea urchin eggs. (Brailoiu *et al*., 2009a). The clone consisted of 2698 bp encompassing 124 bp of 5' and 51 bp of 3' untranslated region. (Figure 2.3B). The SpTPC3 ORF product was sub-cloned and sequenced to ascertain the coding sequence of the gene. The sequence was deposited in the EMBL nucleotide sequence database (Accession # FN598568). SpTPC3, along with SpTPC1 and SpTPC2, were ligated into expression vectors with either *myc*, GFP or mRFP tags, to enable the characterisation of these channels.

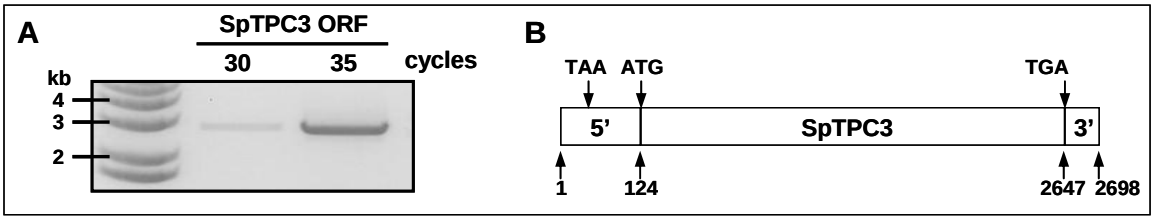

Figure 2.3. PCR amplification of an SpTPC3 ORF product yields a 2.7 kb product. (A) Agarose gel showing a 2698 bp clone of SpTPC3 was amplified from cDNA of *S.Purpuratus* embryos using gene specific primers. **(B)** Schematic of ORF SpTPC3 clone, encompassing 5' UTR containing a a possible stop codon (TAA) and putative start site (ATG). The position of the likely 3' stop codon (TGA) is also indicated. DNA base number of each site is indicated below the schematic.

2.3.2 Multiple sequence alignment of sea urchin and human TPC isoforms

With the cloning of SpTPC3, the full complement of sea urchin (Sp) and human (Hs) TPCs were available for characterisation. The predicted molecular weights (mW) of SpTPC1-3 are 101, 92 and 98 kDa, respectively. The five protein sequences were subject to a multiple sequence alignment and the identical and similar amino acids highlighted (Figure 2.4). Predicted pore regions are also marked. From the multiple sequence alignment, it is clear that there is little conservation across isoforms and species throughout the protein with particular divergence at the termini. A high degree of homology appears to exist in the predicted pore regions however (Figure 2.4).

Homology between TPC sequences was quantified from pair-wise alignments. Overall amino acid identity and similarity were calculated between orthologues and isoforms of human and sea urchin TPCs (Table 2.1). This revealed similarity between TPC isoforms to be between 33-37% within a species. Between orthologues HsTPC1 is 60% similar to SpTPC1 while HsTPC2 is 57% similar to SpTPC2. SpTPC3 has a higher similarity to SpTPC1 (37%) than SpTPC2 (35%). SpTPC3 is also more similar to SpTPC1 than SpTPC2 is to SpTPC1 (33%).

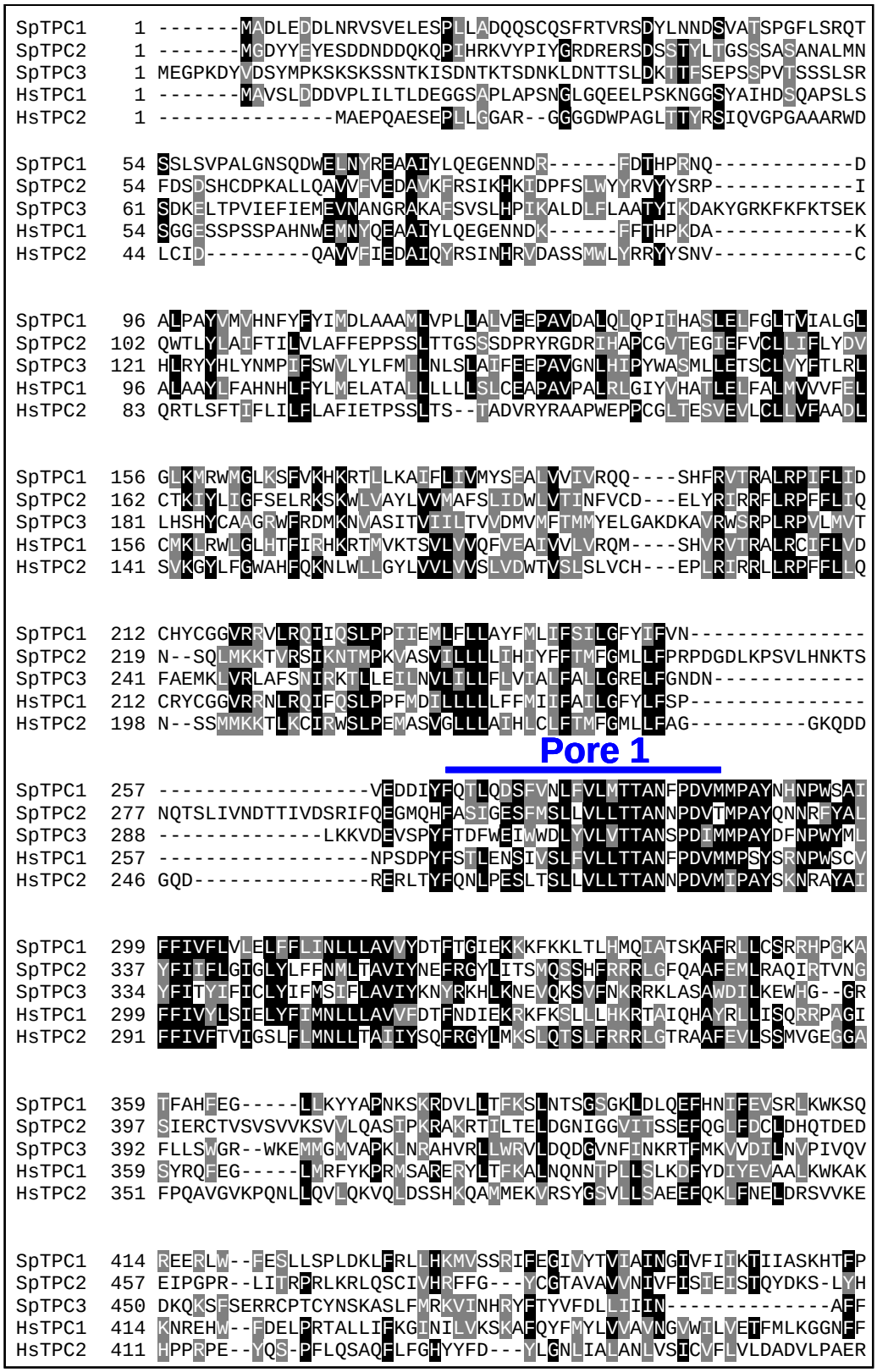
Pore 1

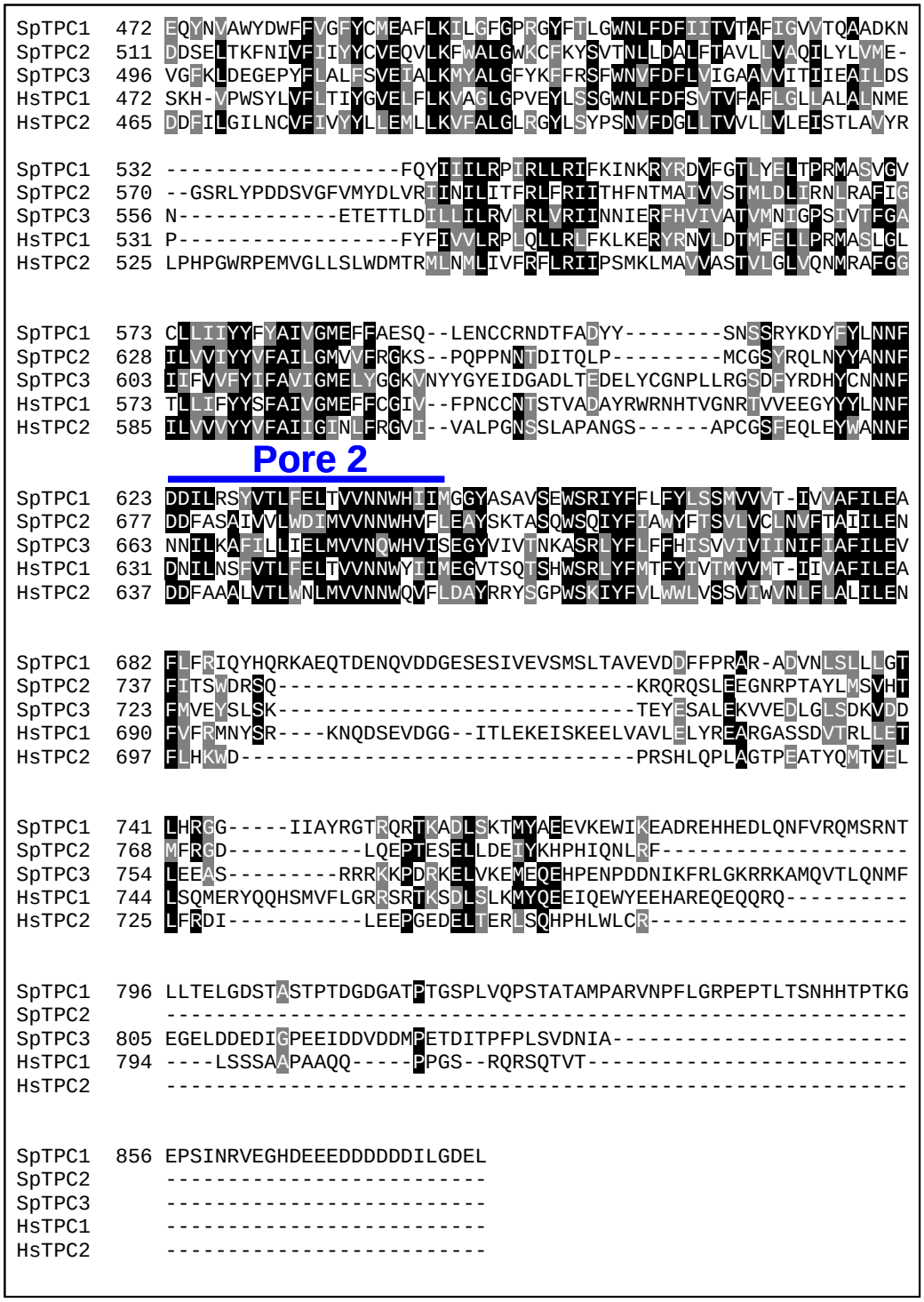

Figure 2.4. A multiple sequence alignment of sea urchin (Sp) and human (Hs) TPCs. Identical amino acids (black shading) and similar amino acids (grey shading) are highlighted. Pore regions predicted by homology to HsTPCs are also marked.

	HsTPC1	HsTPC2	SpTPC1	SpTPC2	SpTPC3
HsTPC1	**100**	**37**	**60**	**36**	**39**
HsTPC2	**21**	**100**	**33**	**57**	**34**
SpTPC1	**42**	**19**	**100**	**33**	**37**
SpTPC2	**20**	**40**	**18**	**100**	**35**
SpTPC3	**21**	**18**	**19**	**21**	**100**

Table 2.1. Overall amino acid percentage identity and similarity between isoforms and orthologues of the TPC family reveals a divergent family of proteins. Amino acid identity (below the grey diagonal) and similarity (above) % values were calculated from pairwise alignments between human (Hs) and sea urchin (Sp) TPCs.

Due to the overall low homology of TPCs and the apparent divergence seen in termini from the multiple sequence alignment, sequence analysis was extended to the examination individual domains of the protein. Figure 2.5 shows percentage similarity of human and sea urchin TPCs compared to the domains of an ancestral plant (*Arabidopsis thaliana*) TPC1. This confirms that conservation between TPCs is highest in the hydrophobic domain I and II regions (41 – 51%) while lowest in the termini, in particular the C-terminus (10 – 32%).

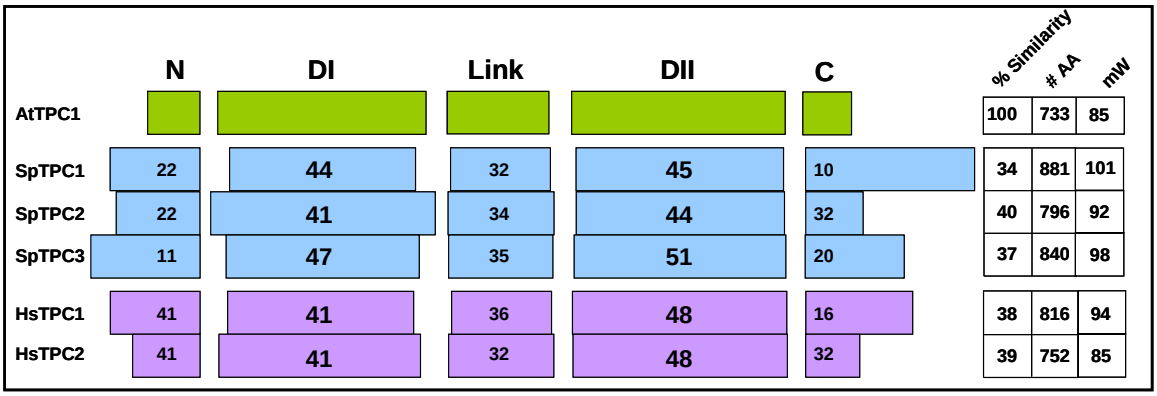

Figure 2.5. Analysis of TPC domains reveals sequence conservation is highest between hydrophobic domains. TPC domain sequence similarity was calculated from pair-wise alignment with domains of AtTPC1. The overall percentage similarity as well as the number of amino acids and predicted mW of the TPC proteins is displayed in the table on the right.

Sea urchin TPCs therefore share low sequence homology between isoforms, particularly outside of the hydrophobic domains. They are also clearly divergent from human TPC orthologues. Would the molecular properties of the SpTPCs be distinct from those defined thus far for the human TPCs? The molecular properties of the SpTPC isoforms were therefore explored.

2.3.3 SpTPCs are glycoproteins

In the initial characterisation of the TPCs, both human and mouse TPCs were shown to be N-glycosylated (Calcraft *et al.*, 2009;Zong *et al.*, 2009). N-glycosylation is a co-translational modification whereby oligosaccharide side-chains are added to luminal asparagine residues (Kukuruzinska & Lennon, 1998). It was therefore investigated whether SpTPCs are also glycosylated. N-glycosylation of proteins can be monitored by the addition of the N-glycosidase enzyme PNGase F to solubilised protein samples before resolution on SDS-PAGE. The enzyme cleaves oligosaccharide side chains from their associated asparagine residues between the innermost oligosaccharide monomer and the amino acid. This manifests as a decrease in size of the protein by SDS-PAGE.

As shown in Figure 2.6, both SpTPC1 and SpTPC2 are PNGase F sensitive, as witnessed by a decrease in the apparent size of the treated (+) protein. Untreated SpTPC1 (-) appears as a protein band of ~ 105 kDa which is reduced to ~ 95 kDa by PNGase F treatment. SpTPC2 appears to exist as two species, an upper protein band of ~ 88 kDa, likely corresponding to a fully glycosylated form (Figure 2.6. indicated by an arrow at F), and a lower band of ~ 70 kDa, likely representing a core glycosylated species (arrow at C). The two species are consolidated into a single deglycosylated form of ~ 65 kDa upon PNGase F addition (arrow at D). Western blotting SpTPC2 further reveals the presence of a dimer-sized band of ~160 kDa which is also PNGase F sensitive (arrow at 2). SpTPC3 however, appears to be insensitive to PNGase F treatment and is therefore not N-glycosylated. Of note is the apparent discrepancy between the predicted native molecular weights of *myc*-SpTPC2 (102 kDa) and SpTPC3-GFP (125 kDa) with those observed by Western Blot of the un-glycosylated proteins (65 kDa and 70 kDa, respectively).

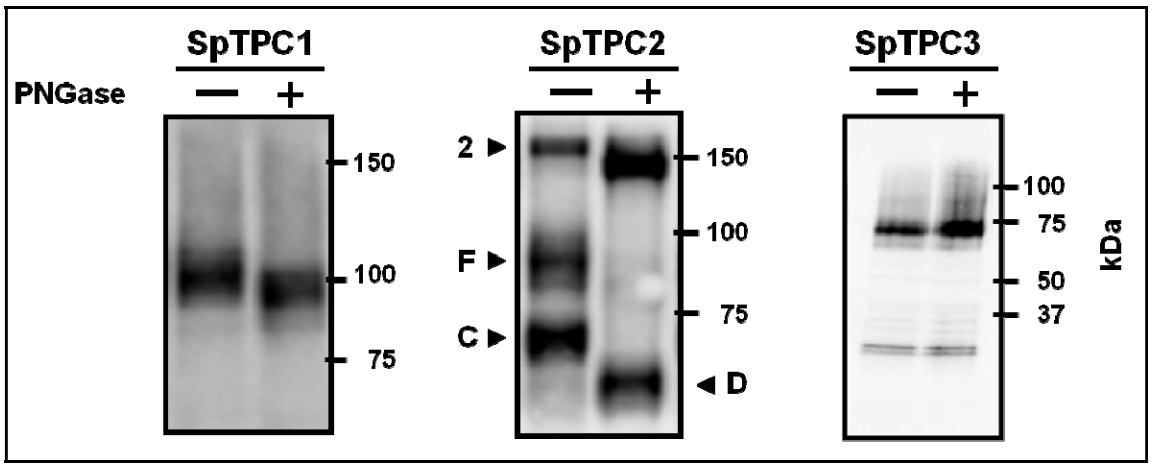

Figure 2.6. SpTPCs exhibit isoform selective N-glycosylation. Western blot of HEK cell homogenates expressing either *myc*-SpTPC1, *myc*-SpTPC2 or SpTPC3-GFP. Homogenates were either mock treated (-) or treated with PNGaseF (+) to remove oligosaccharide side-chains before resolution by SDS-PAGE. SpTPC2 is expressed as fully glycosylated (F) and core glycosylated (C) proteins which are consolidated into a single deglycosylated form upon PNGase F treatment. A protein band is also resolved which corresponds to a dimer of SpTPC2 (2).

2.3.4 Migration of SpTPCs on sucrose density gradients

As discussed in the introduction to this chapter (Section 2.1), [^{32}P]NAADP was shown to bind an endogenous protein ~200 kDa in size as assessed by sucrose density gradient centrifugation (Berridge *et al.*, 2002). The identity of this protein was unknown, but in light of TPCs being revealed as NAADP-sensitive calcium-release channels and speculative binding studies (Calcraft *et al.*, 2009), would migration of SpTPCs reflect that of the endogenous sea urchin NAADP-binding protein?

Protein centrifuged on a sucrose gradient reaches a point on the gradient, where due to the increasing density of sucrose, it can migrate no further. This is the buoyant mass of the protein and is proportional to its size. The determination of the molecular weight of the protein by sucrose density gradient could also reveal the native size of the TPC protein, for example do TPCs exist as a native oligomer?

Homogenates solubilised from HEK cells transiently transfected with SpTPCs were separated on a 5-20% w/v sucrose density gradient. Post centrifugation, the gradient was fractionated and TPC migration monitored by Western blot (Figure 2.7 A). This was compared to fractionation of protein standards of known molecular weights (Figure 2.7B). SpTPC1-GFP appeared in fractions corresponding to 150-200 kDa. The fraction profile of SpTPC2 was more restricted but also correlated to this size, as did SpTPC3. This molecular weight is approximately double the predicted monomeric size of a TPC and would therefore correspond to a protein dimer. In SpTPC2 expressing homogenates, protein bands corresponding to monomeric (Figure 2.7A, arrow at 1) and dimeric (arrow at 2) protein species were again visualised by Western blot, suggesting SpTPC2 may natively exist as a dimer and is somewhat resistant to deoligomerisation by SDS-PAGE resolution.

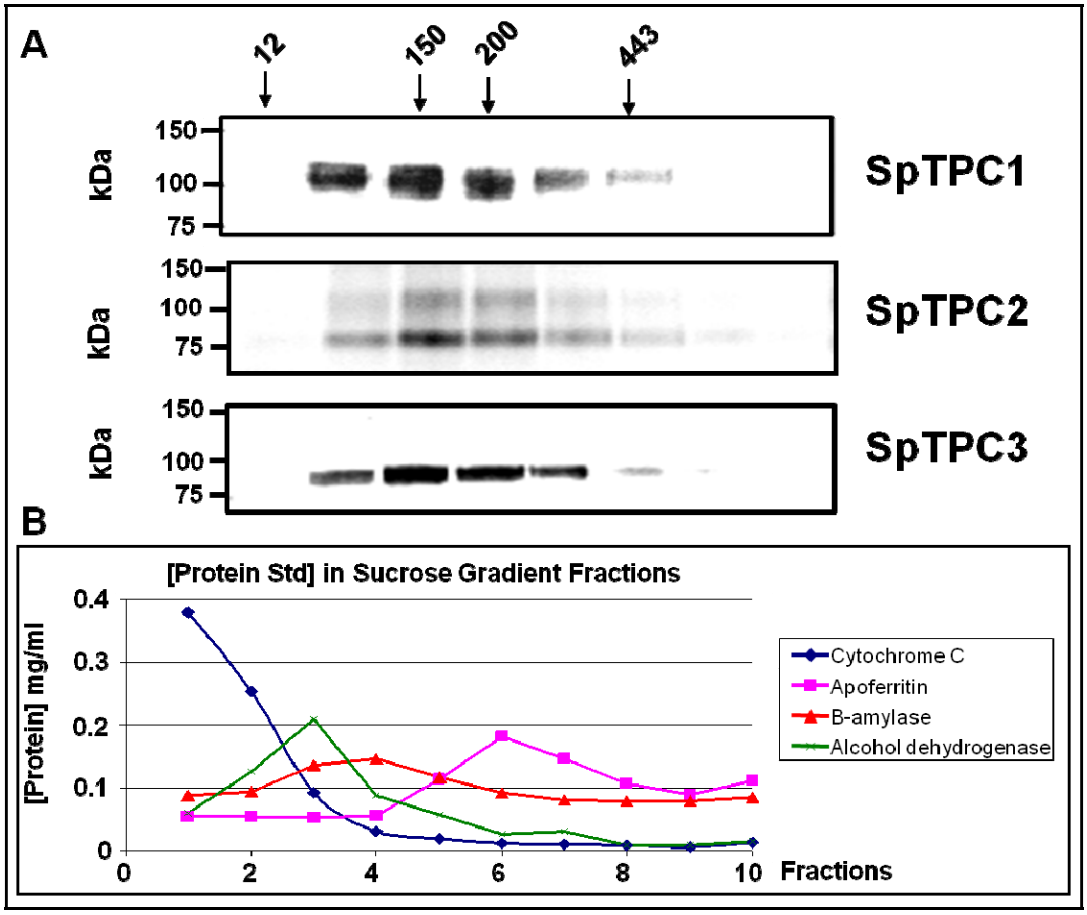

Figure 2.7. Fractionation of SpTPC homogenates following sucrose density gradient centrifugation reveals TPCs exist as dimer-sized (~ 200 kDa) complexes. Western blot of homogenates from HEK cells expressing SpTPCs separated on a 5-20% sucrose gradient. Post centrifugation the gradient was fractionated and fractions visualised for SpTPCs **(A)**. The fraction profile was compared to that of protein standards of a known mW (kDa) as monitored by BCA assay **(B)**. SpTPC1 and SpTPC3 are tagged at the C-terminus with GFP, SpTPC2 is tagged at the N-terminus with five *myc* tags and appears as both monomeric (1) and dimeric (2) species.

2.3.5 Migration of SpTPCs by gel filtration chromatography

The migration of native SpTPCs was also examined by gel filtration chromatography. Using this technique, solubilised protein material is loaded onto a gel filtration column where it is separated by the Stokes Radius of the protein. The column consists of a bed of porous beads whereby smaller proteins interact with the column bed more than larger proteins and therefore have a greater elution time. As

with the sucrose density gradient, the elution profile of the SpTPCs was analysed by Western blot of fractions collected from the column and compared to the elution profile of proteins of known sizes (Figure 2.8B).

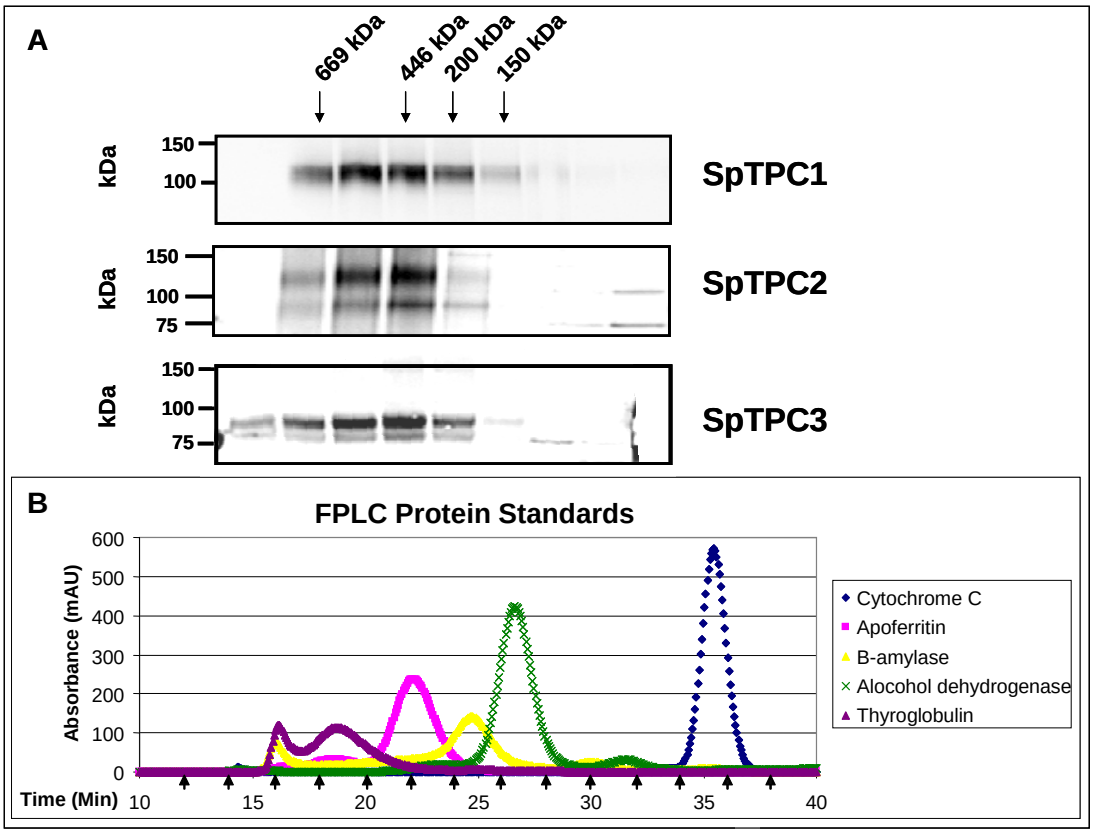

Figure 2.8. Fractionation of SpTPCs by gel filtration chromatography reveals TPCs exist as large (≥ 446 kDa) complexes. Western blot of homogenate fractions from HEK cells expressing GFP-tagged SpTPCs. Homogenates were injected onto a gel filtration column to separate protein according to native size then fractionated **(A)**. The elution profile was then compared to protein standards of known sizes as visualised by UV absorbance detection **(B)**. Homogenate fractions after gel filtration separation are donated by black arrows.

SpTPCs were found to elute from the column in fractions comparable to proteins 400-600 kDa in size, suggesting the complex they form is much larger than a dimer. This size is discrepant from that proposed by sucrose gradient centrifugation and therefore no consensus can be reached as to the size of the native channel complex using these two methods.

2.3.6 Localisation of SpTPCs

Studies of NAADP action in intact sea urchin eggs and mammalian cells had suggested that NAADP was acting upon a receptor located on a novel calcium store, distinct from the ER. It was shown that the source of calcium mobilised by NAADP was acidic organelles of the reserve granule in sea urchin eggs and the analogous endo-lysosomal system of mammalian cells. With the initial characterisation of the TPCs as NAADP-mediated calcium-release channels, three independent groups were in accordance that mammalian TPCs were indeed localised to the endo-lysosomal system. The localisation of heterologously expressed SpTPCs, tagged with either GFP or mRFP fluorophores, was therefore examined by confocal microscopy of HEK cells. The distribution of SpTPCs was compared to the expression of organelle markers for the lysosome (LAMP1-RFP) and the endosome (Endo-GFP, RhoB).

Expression of the three SpTPC isoforms appeared to be punctate and intracellular when imaged by confocal microscopy (Figure 2.9 A-C). SpTPC1 partially colocalised with the lysosomal marker LAMP1 but not with the endosomal marker (2.9A). SpTPC2 appeared to almost exclusively colocalise with LAMP1 (2.9B). SpTPC3 colocalised only with the endosomal marker Endo-GFP (2.9C), showing no colocalisation with the lysosomal marker, in contrast to the other two isoforms. The SpTPC isoforms were therefore localised to the endo-lysosomal with distinct distributions.

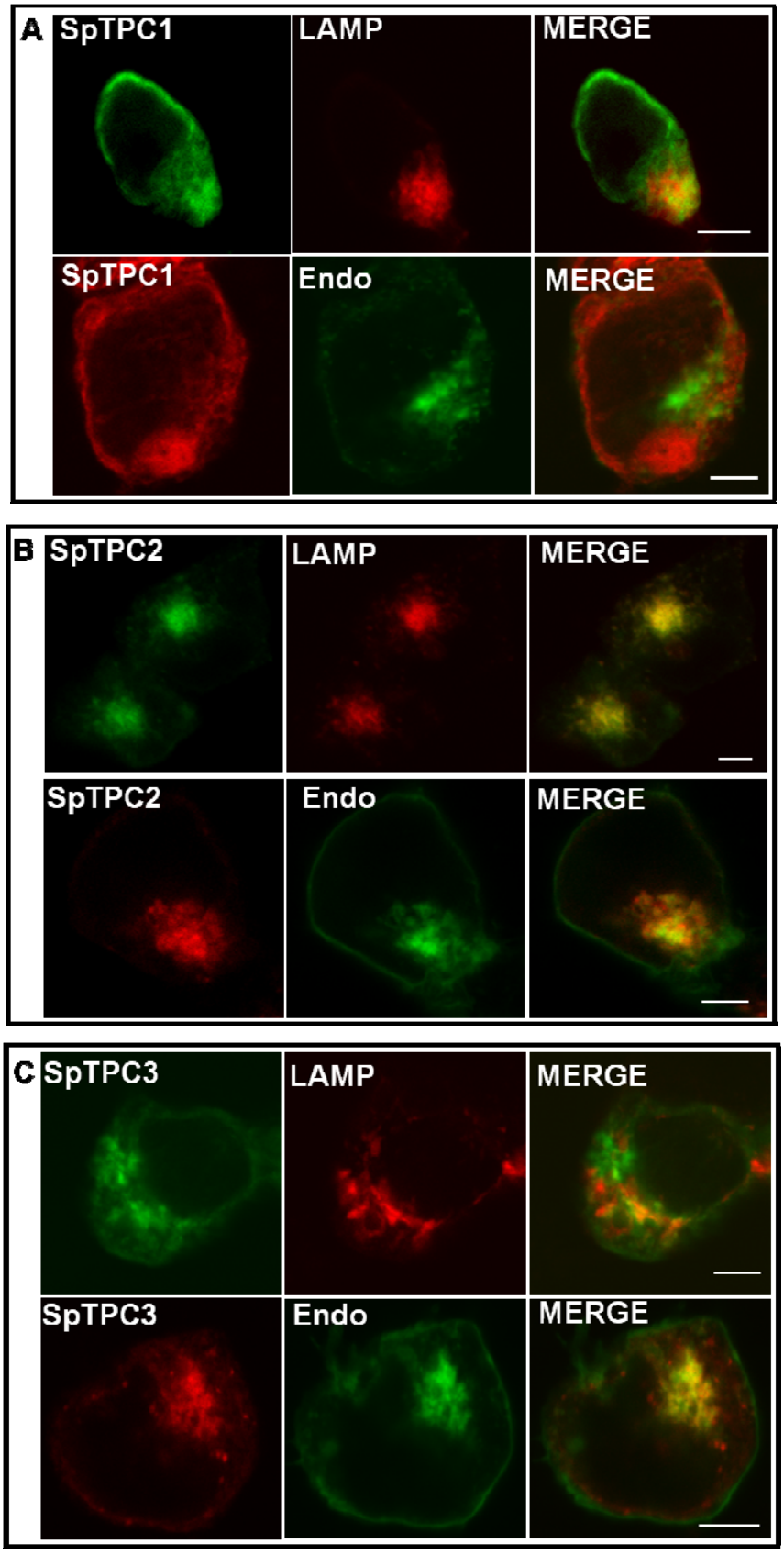
A
SpTPC1
LAMP
MERGE
SpTPC1
Endo
MERGE
B
SpTPC2
LAMP
MERGE
SpTPC2
Endo
MERGE
C
SpTPC3
LAMP
MERGE
SpTPC3
Endo
MERGE

Figure 2.9. SpTPCs localise to the endo-lysosomal system when heterologously expressed in HEK cells. SpTPC1 **(A)**, SpTPC2 **(B)** and SpTPC3 **(C)** tagged with either GFP (green) or mRFP (red) were expressed in HEK cells with organelle markers for lysosomes (LAMP1-RFP) or endosomes (Endo-GFP). Cells were fixed and imaged by confocal microscopy. Scale bar 5μm.

.

The distribution of SpTPC isoforms relative to their human orthologues was also compared. Both SpTPC1 (Figure 2.10A) and SpTPC2 (Figure 2.10B) colocalised with HsTPC1 and HsTPC2 respectively, suggesting sea urchin TPCs are trafficked to the same compartments even when heterologously expressed.

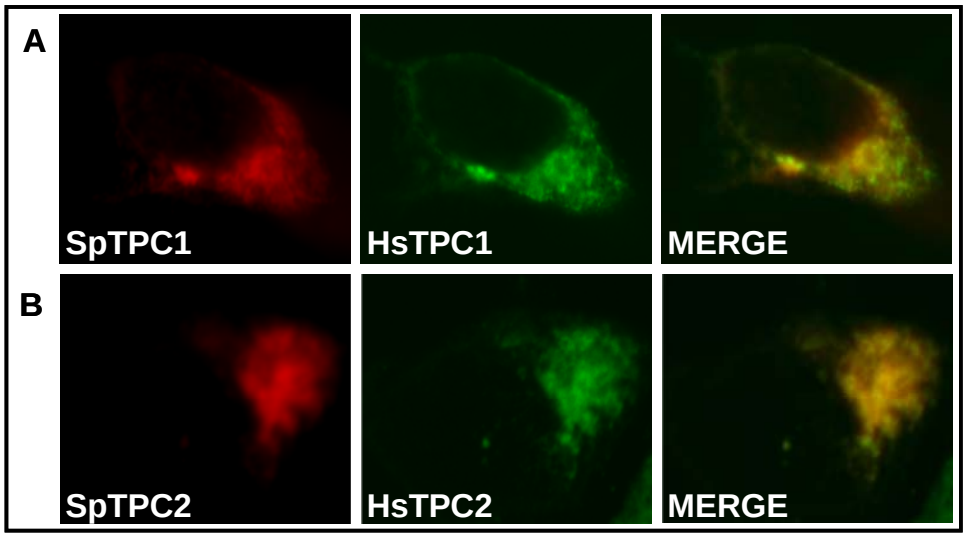

Figure 2.10. SpTPC isoforms colocalise with human TPC orthologues. HEK cells coexpressing mRFP-tagged SpTPCs and GFP-tagged HsTPCs were fixed and imaged by confocal microscopy.

2.4 Discussion

In this chapter, the cloning of a novel TPC isoform, SpTPC3, is reported and the molecular characteristics of the SpTPC family explored. Analysis of sea urchin and human TPC sequence revealed low overall homology between isoforms and orthologues, however TPC sequence displayed the greatest homology within hydrophobic domains. SpTPC1 and SpTPC2, but not SpTPC3 were shown to be glycoproteins. All three SpTPC isoforms migrate by SDS-PAGE smaller than their predicted size. Sucrose density centrifugation of SpTPCs gave an apparent native size of ~150-200 kDa, although gel filtration analysis suggested the native size to be >400 kDa. The native size of the channel complex was therefore not able to be determined. The SpTPCs were localised to the endo-lysosomal system when heterologously expressed and furthermore colocalised with their human orthologues.

Some problems were encountered with Western blotting the TPCs as the channels were intolerant to the high denaturing temperatures required by standard SDS-PAGE protocols. Heating the TPCs to 95°C before SDS-PAGE may have lead to aggregation resulting in incomplete entry into the gel, thereby limiting detection by Western blot. Interestingly SpTPCs were also smaller than their predicted molecular weight when visualised by SDS-PAGE and Western blot. Both of these may stem from the hydrophobic nature of the proteins. As TPCs are membrane-spanning channel proteins, large regions of the protein would be expected to be hydrophobic. Hydrophobic domains may not linearise fully during denaturation by SDS and so the full length of the protein may not be accessible to the anionic charge addition that SDS-PAGE migration relies upon. Size may therefore be underestimated by this technique.

TPCs have much lower sequence homology between isoforms (< 40%) than other intracellular calcium release channels such as ryanodine receptors (Fill & Copello, 2002) and IP_3 (Patel *et al.*, 1999) (~70%). This could be due to the differential expression of TPCs throughout the acidic organelles of the highly dynamic endo-

lysosomal system. TPCs may therefore be subject to a much wider range of selective pressures than if they were localised to a single organelle such as the ER. Interestingly SpTPC3 was consistently more similar to TPC1 isoforms than TPC2, perhaps suggesting it is more closely related to TPC1 evolutionarily. Examining the divergent regions of TPC isoforms and carrying out structure/ function analysis will no doubt reveal which amino acids are important for distinguishing the properties of different TPC isoforms.

As well as our publication on the cloning and characterisation of the SpTPCs (Brailoiu *et al.*, 2010a), TPCs from the sea urchin were also subsequently cloned by Ruas et al (Ruas *et al.*, 2010). Sequence similarity between the SpTPC clones of each group was ~97% with some degree of difference perhaps expected due to the high levels of polymorphic variation in sea urchins.

SpTPC1 and SpTPC2 are N-glycosylated while SpTPC3 is not. Many lysosomal proteins, including the often used lysosomal marker LAMP1, are glycosylated (Carlsson *et al.*, 1988). This is proposed to protect the luminal face of the protein from the harsh acidic environment of the lumen. However, glycosylation is also a method of protein regulation. Glycosylation has been shown to regulate protein expression, trafficking and function (Kukuruzinska & Lennon, 1998). The differences in the glycosylation state of SpTPCs could be due to SpTPC3 existing in the less acidic environment of the endosome (~ pH 6), opposed to ~ pH 4.8 in the lysosome (Luzio *et al.*, 2007) and therefore the addition of oligosaccharides to protect the luminal face of the channel is not required. Glycosylation of SpTPC1 and 2 but not SpTPC3 could also be a means of differential regulation of the isoforms. Perhaps SpTPC3 lost the need to be glycosylated during evolution? The reason for the lack of glycosylation of SpTPC3 is not known, but it may be informative to look at glycosylation of TPC3 isoforms in other species and examine if or how SpTPC3 glycosylation evolved. For example, are TPC3 isoforms in higher order mammals glycosylated, or if not, are more ancient TPC3 isoforms glycosylated? This would suggest either a loss or gain of glycosylation during evolution. In other species,

TPC1 and TPC2 may have evolved glycosylation as a means of regulation. Is glycosylation consistent throughout the TPC1 and TPC2 lineage? Ruas et al were in agreement with our data that SpTPC2 was glycosylated but SpTPC3 was not. However they were unable to demonstrate glycosylation for SpTPC1 in contrast to our findings. We found the change in mobility upon PNGase F treatment was much more subtle for SpTPC1 than SpTPC2. Perhaps this represented a failure to resolve a change in size by SDS-PAGE (Ruas *et al.*, 2010) or perhaps polymorphic variation again accounts for the differences seen.

The native channel size of SpTPCs was not adequately resolved by sucrose density gradients and gel filtration analysis as these two methods gave different apparent sizes. Sucrose density gradients revealed the SpTPCs to be ~200 kDa while by gel filtration TPCs eluted with the profile of a 400-600 kDa protein. This aberrant migration did however mirror that seen by Berridge et al. of the native sea urchin NAADP-binding protein (Berridge *et al.*, 2002). Berridge et al. speculated that high-speed centrifugation could dissociate oligomeric TPC complexes. Later however, the association of the endogenous receptor with lipids was demonstrated (Churamani *et al.*, 2005) and it was proposed that the buoyant molar mass of the NAADP-binding protein may be underestimated by this association. This lipid association may therefore be occurring with the SpTPCs. Overall the anomalous migration profile of the SpTPCs between these two methods is strikingly similar to that reported for the endogenous sea urchin NAADP-binding protein (or complex). Complementing the data presented in this chapter, Ruas et al also showed that NAADP bound to SpTPC1 and SpTPC3 with nanomolar affinity while dissociation of NAADP was sensitive to K^+ (Ruas *et al.*, 2010). These replicated findings previously observed with NAADP binding to endogenous protein in sea urchin egg homogenates (Dickinson & Patel, 2003) and would suggest that NAADP binds to SpTPCs either directly or with a tightly associated binding protein.

The SpTPC isoforms were found to localise to the endo-lysosomal system with a distinct but over-lapping profile within this system. SpTPC1 was partially lysosomal

but appears to have a broad distribution amongst acidic organelles (Calcraft *et al.*, 2009;Brailoiu *et al.*, 2009a). SpTPC2 was almost totally lysosomal, similar to HsTPC2 (Calcraft *et al.*, 2009;Brailoiu *et al.*, 2009a;Zong *et al.*, 2009) while in contrast SpTPC3 was exclusively endosomal. Overlap in localisation could point to a degree of functional redundancy between TPC isoforms but could also raise the possibility that if TPCs oligomerise, they could potentially form heteroligomers, introducing another layer of complexity into the regulation of a functional TPC channel. Ruas et al also localised SpTPCs to the endo-lysosomal system although specific localisation of the channels was ambiguous, they are generally in agreement with our assessment (Ruas *et al.*, 2010). Both labs were in agreement that SpTPC Ca^{2+} transients could be ablated by the addition of bafilomycin A1 while Ruas et al also used the IP_3 receptor antagonist heparin to dissect the TPC mediated Ca^{2+} "trigger" from amplification by CICR through ER IP_3 receptors.

We have shown that overexpression of SpTPC3 (along with SpTPC1 and SpTPC2) enhances intracellular calcium release upon microinjection of NAADP (Brailoiu *et al.*, 2010a). The effect was more modest in SpTPC3 than the other two isoforms but release was nevertheless potentiated. One significant difference from our publication with that of Ruas et al was their apparent lack of function recorded for SpTPC3 (Ruas *et al.*, 2010). They report that SpTPC3 did not mediate calcium release upon application NAADP-AM and furthermore inhibited endogenous responses in a dominant negative manner.

Any differences between the findings of the groups could be accounted for by the polymorphic variation between the two clones. It would seem unlikely that polymorphic variation could account for such a drastic change as complete lack of function, however it can not be discounted until demonstrated otherwise. An alignment of the two clones reveals some charged residues in our clone which are neutralised in the Ruas clone and these could fundamentally alter the stability of the channel or possible channel interactions (Figure 2.11).

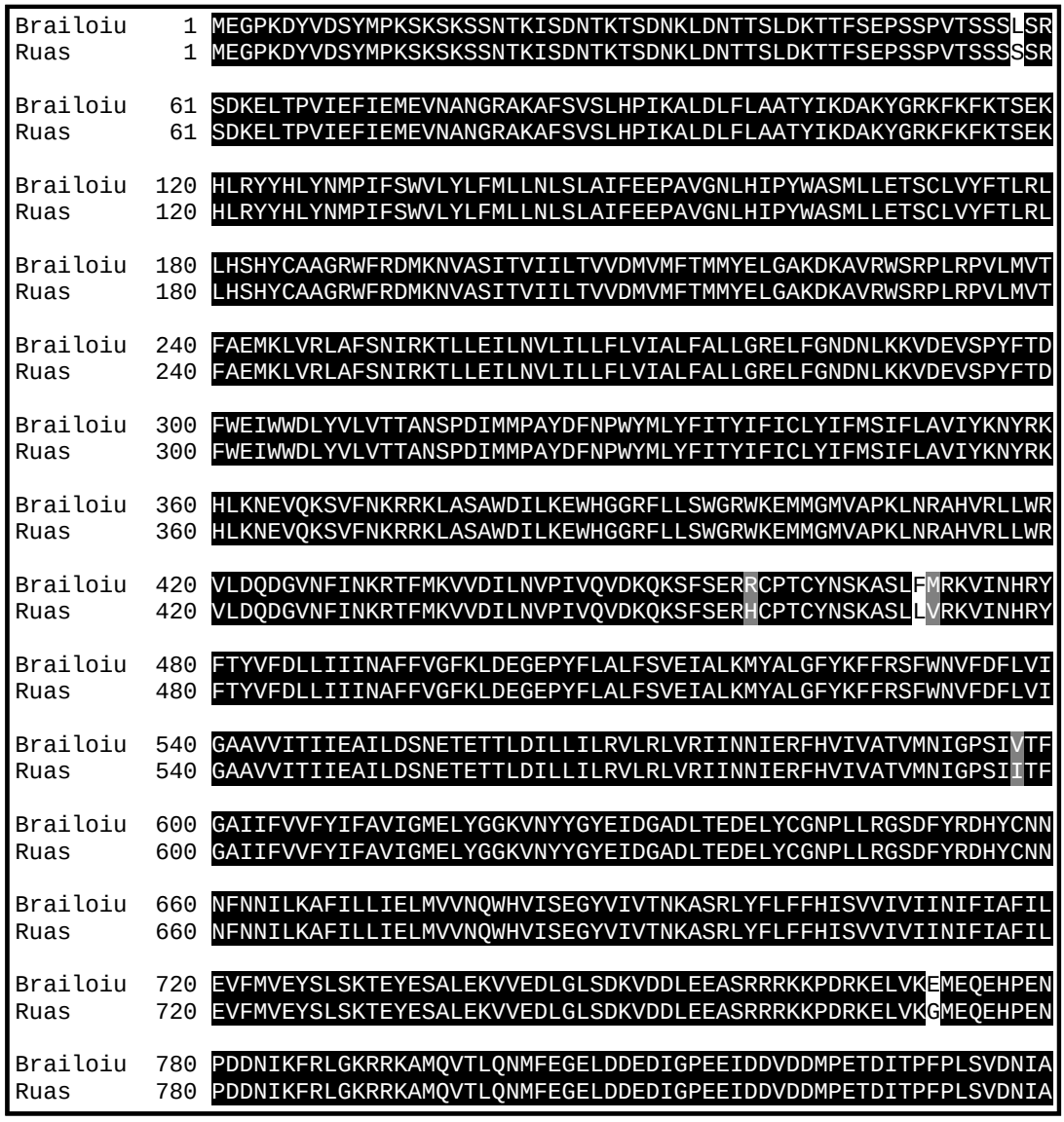

Figure 2.11. Sequence alignment between Ruas and Brailoiu SpTPC3 clones reveals polymorphic variation. Alignment of the protein sequence of the Ruas and Brailoiu SpTPC3 clones shaded to reveal identical (black), similar (grey) and mismatched (white) amino acids.

In summary, SpTPCs are a divergent family of channels with low sequence similarity, especially outside of the two hydrophobic domains. They are N-glycosylated and show anomalous migration on sucrose density gradients and gel filtration columns. SpTPCs also localised to the endo-lysosomal system where they have been demonstrated to be NAADP-sensitive Ca^{2+} release channels.

Chapter 3 - Characterisation of TPC antibodies

3.1 Introduction

To fully characterise the molecular properties of the TPCs, it is necessary to have the appropriate molecular tools. One of the most important tools for a molecular biologist is an antibody specific to the protein of interest. With the ever increasing interest in TPCs, life science companies are responding by producing an expanding repertoire of antibodies to these channels. In order to utilise these tools, it is first necessary to validate them and test qualities such as specificity and affinity for the target proteins.

The aim of this chapter is to therefore characterise a range of commercially available and custom-made anti-TPC antibodies which can then be utilised to explore the molecular properties of the TPCs further. To achieve this, the ability of the antibodies to detect TPCs by Western blot and immunocytochemistry will be examined for both overexpressed and endogenous protein.

3.2 Materials and methods

Plasmids

The HsTPC clones utilised in this chapter are schematically depicted in Figure 3.1. The molecular cloning of HsTPC1-GFP, mRFP-HsTPC1 and HsTPC2-GFP is described in Brailoiu et al. 2009 (Brailoiu *et al.*, 2009a). The cloning of C-terminal *myc*-tagged HsTPCs is described in Yamaguchi et al 2011 (Yamaguchi *et al.*, 2011).

The TPC constructs utilised in this chapter are summarised in Figure 3.1.

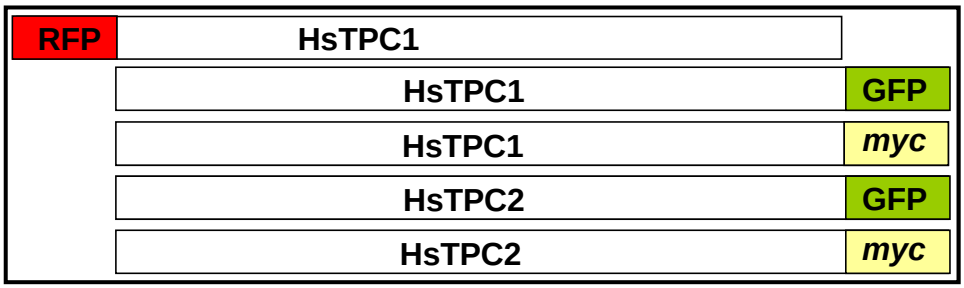

Figure 3.1. HsTPC clones utilised in the characterisation of TPC antibodies. HsTPC1 was tagged at the N-terminus with mRFP. HsTPC1 and HsTPC2 were tagged at the C-terminus with either GFP or *myc*.

Immunocytochemistry

HEK293 cells were plated on poly-l-lysine coated glass coverslips for transfection by PEI as stated in the methods of Chapter 2 or left untransfected as required. SKBR3 cells were also plated on poly-l-lysine coated coverslips; however Lipofectamine^{TM} 2000 transfection agent (Invitrogen) was used as per the manufacturers' instructions in place of PEI. With both methods, cells were washed into fresh antibiotic supplemented media five hours post transfection.

Following transfection, both SKBR3 and HEK cells were fixed in PBS with 4% PFA, for 10 min at room temperature (RT), then washed in PBS and permeabilised in PBS + 0.1% Triton X-100 for 10 min at RT with agitation. Cells were washed again before being incubated for 60 min at RT in blocking solution (5% FBS, 1% BSA in Ca^{2+}/Mg^{2+} free PBS) with agitation. Primary antibody was diluted in blocking solution and incubated with cells at 37°C for 60 min. Cells were washed three times in PBS 0.1% Tween® 20 (Sigma) before incubation in secondary antibody diluted in blocking solution. After the secondary antibody was washed, coverslips were mounted on slides with polyvinal mounting medium DABCO (Fluka) and sealed.

A range of commercially available anti-TPC antibodies were utilised. Anti-TPC1 antibodies were obtained from Abcam (ab80961) and from Santa Cruz Biotechnology (SC-67973). To test antibody specificity, a blocking peptide (SC-67973P) was also used in the presence of the Santa Cruz antibody, both at 4 μg/ ml. The antibody was incubated, with or without the blocking peptide for 30 min at RT with agitation in blocking solution. Images shown (+ / - blocking peptide) were taken at the same gain settings (639) in the green fluorescence channel A commercially available anti-TPC2 antibody was obtained from Sigma-Aldrich (HPA016561).

Affinity-purified rabbit polyclonal antibodies produced by Eurogentec were raised to peptide sequences corresponding to human TPCs. TPC1 antibodies # 76 and # 77 were raised to C-terminal epitopes as it is predicted the C-terminus is cytosolic and therefore readily accessible to detection of the native protein. The sites in the C-terminus were also chosen to have minimal mismatch between human, rat and mouse sequence so that antibodies could potentially be utilised against animal tissue. TPC2 antibody # 34 was raised to a luminal site between predicted TM region 1-2 of domain I and # 35 to the pore I region. It was envisaged that antibody # 35 may prevent ion conduction through the pore. With all antibodies, fixing, secondary

antibody incubation and mounting were as above. The concentration at which these antibodies were utilised is defined in Table 3.1.

For organelle markers, the mouse monoclonal anti-LAMP1 antibody H4A3, a lysosome marker, was obtained from The Developmental Studies Hybridoma Bank (University of Iowa). An anti-EEA1 antibody, a marker of early endosomes, was obtained from Abcam (#ab2900). Antibodies were used at a dilution of 1:100 for HEK and SKBR3 cells, with the exception of anti-LAMP1 in SKBR3s which was used at 1:200.

Secondary antibodies utilised were Invitrogen Alexa Fluor® 488 rabbit anti-goat IgG (H+L) 2 mg/ml (# A-11078), Invitrogen Alexa Fluor® 568 Donkey anti-rabbit (# A-10042), Alexa Fluor® 633 goat anti–mouse IgG antibody (#A21052). All secondary antibodies were diluted 1:100 for use.

Confocal settings were as described in Chapter 2.

A summary of TPC antibodies utilised, the sequence epitope they bind and dilutions used for Western blotting and immunocytochemistry are given in Table 3.1.

TPC Isoform	Company	Ab #	Epitope	Epitope Location	Host	WB Dilution	Immuno OE	Immuno Endog.
TPC1	Abcam	ab80961	Not Defined	C-terminus	Rabbit	1000	40	20
TPC1	Santa Cruz	sc67973	Not Defined	C-terminus	Goat	1000	100	50
TPC1	Custom	76	RMNYSRKNQDSEVDG	Proximal C-terminus	Rabbit	1000	20	20
TPC1	Custom	77	GRRSRTKSDLSLKMY	Distal C-terminus	Rabbit	1000	20	20
TPC2	Sigma	HPA016561	ENFLHKWDPRSHLQPLAGT PEATYQMTVELLFRDILEEPE EDELTERLSQHPHLWLCR	C-terminus	Rabbit	1000	40	40
TPC2	Custom	34	GGKQDDGQDRERLTY	DI S5-P1 linker	Rabbit	1000	20	20
TPC2	Custom	35	DVRYRAAPWEPPCGCL	DI SI-SII linker	Rabbit	1000	20	20

Table 3.1. Summary of TPC antibodies characterised in this chapter. The name and product number for each antibody is given as well its isoform selectivity, the epitope the antibody was raised to and the region on the TPC this epitope corresponds to. The working dilution for Western blot (WB) and immunocytochemistry (Immuno) to both overexpressed (OE) and endogenous (Endog.) are also given.

Mouse pancreas preparation

Pancreata from four month old wild-type, TPC1 heterozygous and TPC1 knock-out mice were kindly provided by Dr Sean Davidson (Hatter Institute, UCL). The tissue was homogenised by 3 x 5 sec sonication in SET buffer (0.25 M sucrose, 1mM EDTA, 10 mM Tris-HCl pH 7.4 with a protease inhibitor cocktail (Roche)) at 10 % w/v. The homogenate was centrifuged at 1000 x g for 10 min at 4 °C to pellet unbroken cells and the nuclear fraction. The supernatant was recovered and subject to a further 100,000 x g centrifugation for 1 h at 4 °C to pellet organelle membranes. The supernatant was discarded and the pellet was resuspended in SET buffer. The protein concentration was estimated by BCA assay as per Chapter Two. Protein preparation (40 μg) was resolved by SDS-PAGE then probed by Western blot with an anti-TPC1 antibody (Abcam) as detailed in Table 3.1.

Recurrent molecular biology methods

Cell culture, transfection, protein preparation, SDS-PAGE (typically 20μg of protein) and Western blotting were as described in Chapter 2.

3.3 Results

3.3.1 Mapping TPC antibody epitopes

An increasing number of anti-TPC antibodies are becoming commercially available as interest in the field grows. Here we examine some of the initial antibodies commercially produced, as well as antibodies custom-made to our specifications. Three commercially available antibodies and four custom-made antibodies are characterised in this chapter. The antibodies used are anti-HsTPC1 antibodies from Abcam and Santa Cruz, anti-HsTPC2 from Sigma and two custom-designed antibodies each for TPC1 (# 76 & # 77) and TPC2 (# 34 & # 35). The epitope sequences to which these antibodies are raised are highlighted in Figure 3.2.

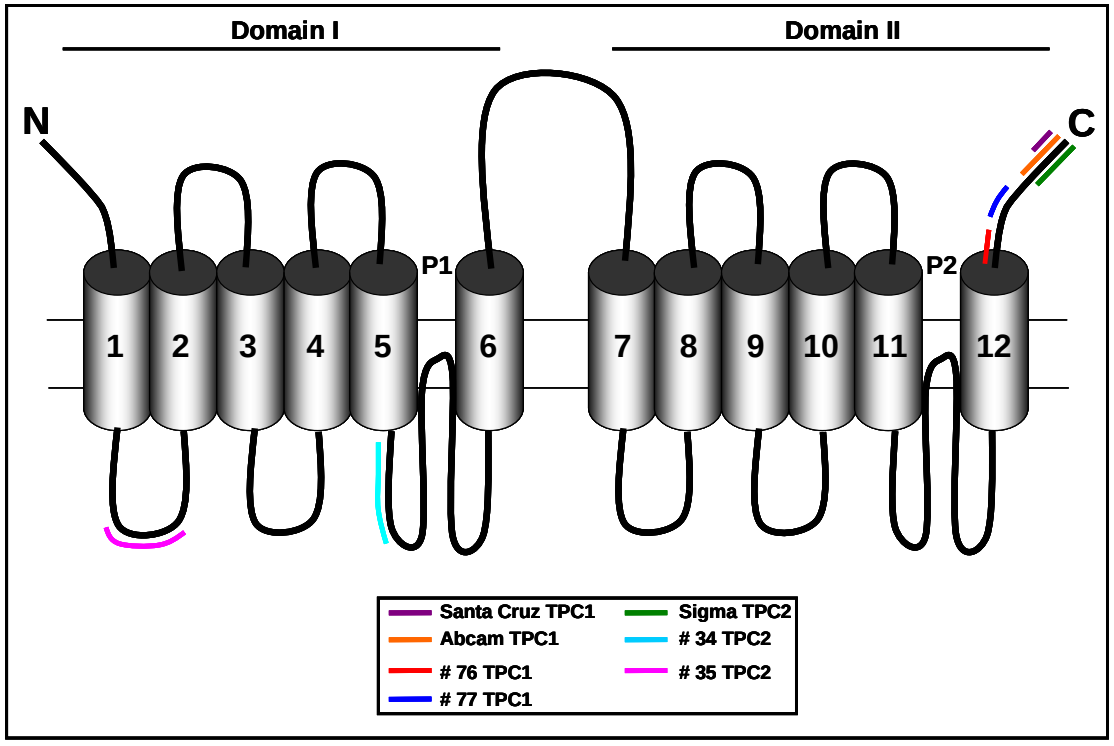

Figure 3.2 TPC antibody epitopes. Schematic of a TPC showing the predicted two domain repeats each with six membrane-spanning regions and a pore region (P1/P2) between the transmembrane region 5-6 of each domain. Epitopes of the TPC antibodies examined are marked.

The exact epitope varies between the antibodies (and is not always defined for commercial antibodies) however all TPC1 antibodies tested are raised against peptides corresponding to epitopes in the C-terminus. The Sigma TPC2 antibody was also raised to a C-terminal epitope, however the custom antibodies were raised to quite distinct regions. Antibody # 34 is raised to a peptide corresponding to the domain I pore region of TPC2 while # 35 was raised to the TM region 1-2 linker in domain I.

3.3.2 Western blotting of overexpressed TPCs

The affinity of these antibodies to TPCs was first examined by Western blot using homogenates of cells over-expressing TPC protein. The ability of the four TPC1 antibodies to detect TPC1-GFP or TPC1-*myc* was first explored (Figure 3.3). The predicted mW of GFP-tagged HsTPC1 construct is 122 kDa and for the *myc*-tagged construct is 104 kDa.

The Abcam TPC1 antibody detected prominent protein bands at ~130 and 100 kDa likely corresponding to overexpressed HsTPC1-GFP (Fig 3.3A). As we have seen with the SpTPCs, the doublet may represent the fully and partially N-glycosylated forms of the TPC. A smaller double band of ~120 and 90kDa was detected in the lane corresponding to HsTPC1-*myc*, indicative of the lower mW of the *myc* tag (15 kDa) compared to the GFP tag (27 kDa). No protein was detected in lanes corresponding to overexpressed TPC2, suggesting that the antibody is specific for TPC1.

The Santa Cruz TPC1 antibody detected protein at ~90 and 110 kDa in lanes corresponding to mock transfected cell homogenate and homogenate over-expressing mRFP-TPC1, tagged at the N-terminus, and TPC1-GFP, tagged at the C-terminus (Figure 3.3B). Proteins tagged at opposite termini were probed to control for the C-terminal tag interfering with the antibody binding to a C-terminal epitope. The protein bands were almost identical across all three homogenates in size and

intensity. This suggests that the antibody is not discriminating between tagged and endogenous protein.

Custom TPC1 antibody # 76 recognised a range of bands in homogenates expressing either TPC1 or TPC2 isoforms (Figure 3.3C). The antibody appears to detect five bands in mock transfected cell homogenate between ~ 100 and 40 kDa with combinations of these same five bands present in GFP and *myc* tagged protein, across both isoforms and with no apparent change in size or intensity. This suggests the antibody is highly non-specific.

Custom TPC1 antibody # 77 failed to visualise any prominent protein bands above background and those bands that were visible appeared across all isoforms and tags (Figure 3.3D).

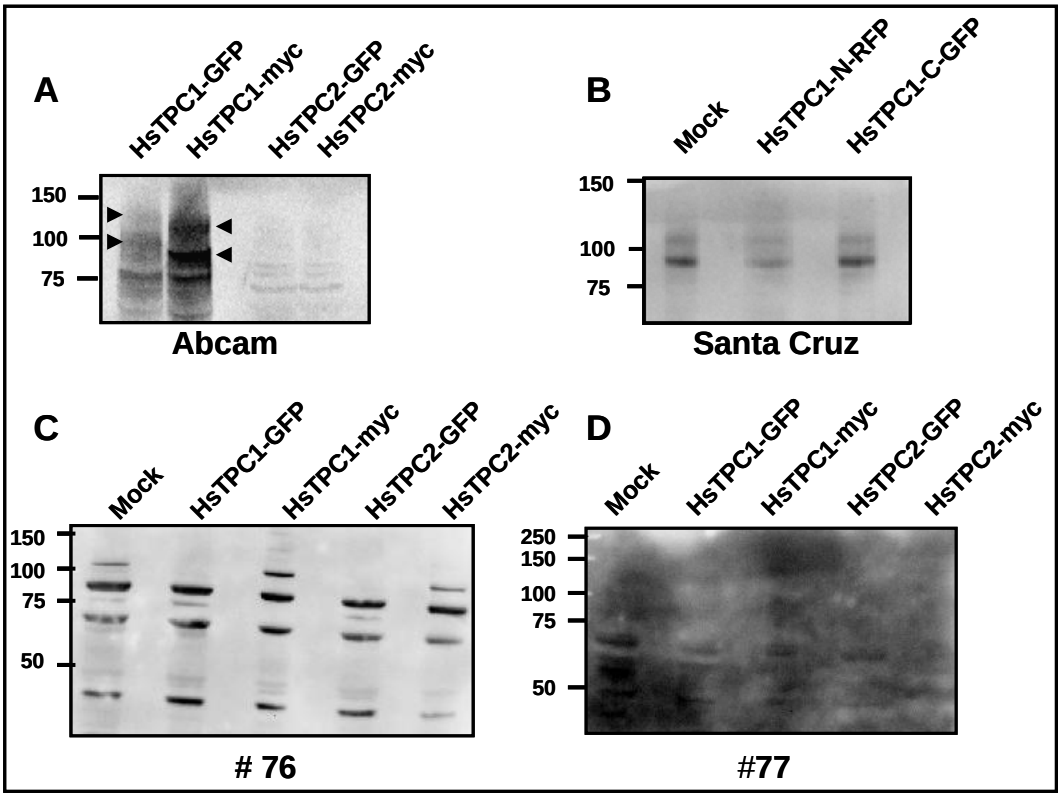

Figure 3.3. Western blotting of overexpressed TPCs with TPC1 antibodies identifies an antibody suitable for TPC1 detection. HEK cell homogenates expressing the indicated construct were probed with TPC1 antibodies. **(A)** Abcam (protein marked by arrows), **(B)** Santa Cruz **(C)** TPC1 antibody #76 and **(D)** TPC1 antibody # 77 were used.

The ability of TPC2 antibodies to specifically recognise TPC2 protein by Western blot was next explored using overexpressed TPC2-GFP and TPC2-*myc*. The predicted mW of TPC2-GFP is 113 kDa and TPC2-*myc* is 95 kDa. As shown in Figure 3.4A, Sigma TPC2 antibody specifically recognised protein corresponding to TPC2 and not TPC1. The antibody detected two protein bands at ~90 and 70 kDa corresponding to TPC2-GFP which were reduced in size to ~80 and 60 kDa when the channel is *myc*-tagged. This suggests the Sigma TPC2 antibody can discriminate between TPC isoforms and further resolve size differences between tags. The Sigma TPC2 antibody is therefore suitable for Western blot detection of overexpressed TPC2.

The custom TPC2 antibodies were probed together in a single Western blot (Fig. 3.4B). A protein band was detected at ~ 140kDa and this was present with both TPC1-*myc* and TPC2-*myc* protein homogenates. No protein was detected in TPC-GFP or mock transfected homogenates, suggesting the antibody may specific to the *myc* tagged vector and not to the TPC isoform. This renders these antibodies unsuitable for use in Western blot detection of TPC2.

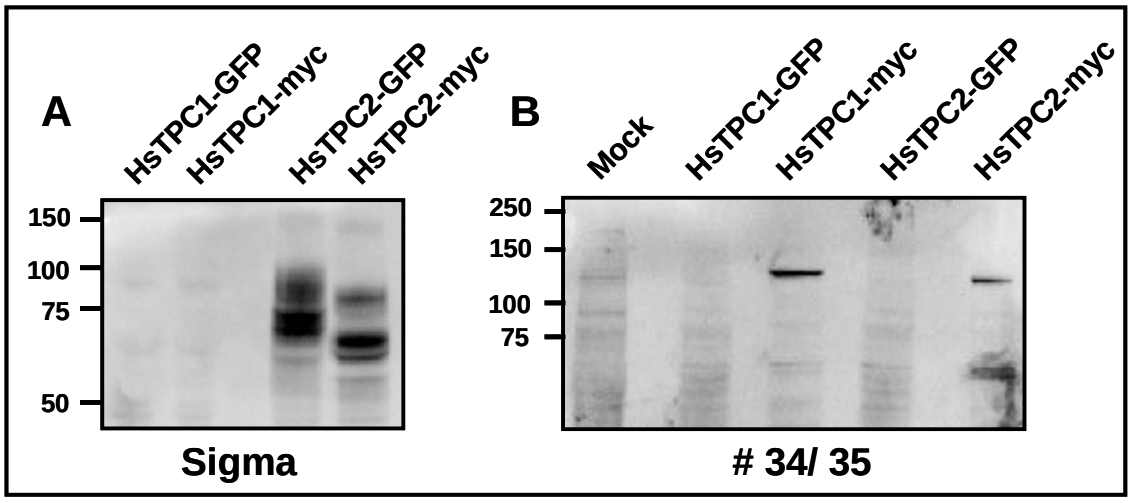

Figure 3.4. Western blotting of overexpressed TPCs, with TPC2 antibodies, identifies an antibody suitable for TPC2 detection. HEK cell homogenate was probed by Western blot with Sigma TPC2 **(A)** or custom antibodies **(B)** for affinity and specificity to TPC2.

3.3.3 Immunocytochemistry of overexpressed TPCs

The ability of the TPC antibodies to recognise overexpressed TPCs in their native, folded structure was probed by immunocytochemistry. HEK cells overexpressing fluorescently tagged TPCs were probed with TPC antibodies, to examine if expressed protein could be detected. Figure 3.5 demonstrates that the majority of anti-TPC antibodies were capable of recognising overexpressed TPC protein. At the gain settings used (variable for each antibody), staining was specific for over-expressed protein with no endogenous protein visible (as seen for TPC1 SC and TPC2 Sigma antibodies in Fig. 4.9)

In each case the detected protein was intracellular and punctate, to varying degrees. The majority of antibodies colocalised with overexpressed protein (Merge), with the exception of TPC1 Ab # 76 which showed no evidence of TPC1 recognition. These results indicate that all but one of the antibodies can be used for the recognition of overexpressed TPC1 protein.

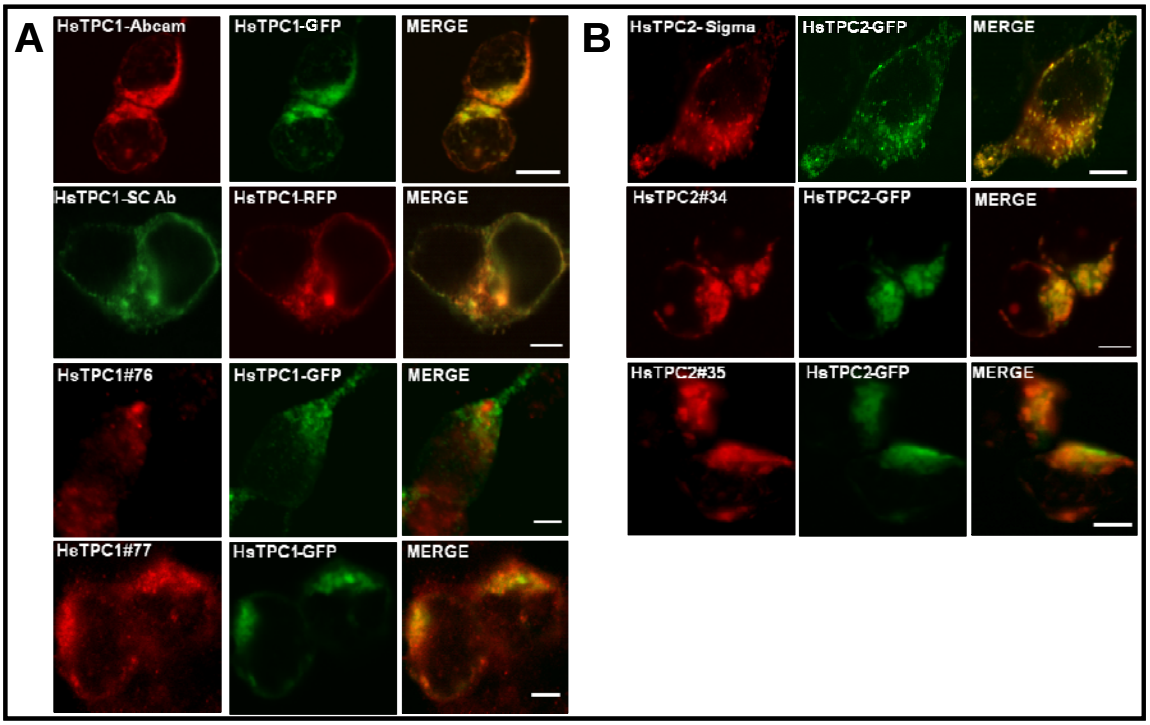

Figure 3.5. A range of TPC antibodies recognise overexpressed TPC protein by immunocytochemistry. Confocal images of HEK cells overexpressing fluorescently-tagged TPCs then probed with either **(A)** TPC1 or **(B)** TPC2 antibodies for recognition of the protein. Scale bar 5μm.

3.3.4 Western blotting of endogenous TPCs

Having established the capability of TPC antibodies to recognise overexpressed protein, their ability to recognise endogenous protein from untransfected cells was probed, first by Western blotting. The TPC1 antibody from Abcam and the TPC2 antibody from Sigma had been shown to successfully recognise overexpressed TPC protein by Western blot, therefore these antibodies were selected for analysis. The predicted mW of endogenous HsTPC1 protein is 94 kDa and TPC2 is 85 kDa.

The Abcam anti-TPC1 antibody detected a single protein band in HEK and SKBR3 homogenates at ~90 kDa (Figure 3.6A). When HEK homogenates were probed with the TPC2 antibody, a single band of ~115 kDa was visualised, and a faint band observed in SKBR3 homogenates (Figure 3.6B). The size of the protein bands visualised was different to those observed for over-expressed protein and did not appear as a doublet. To determine antibody specificity, a Western blot of pancreas homogenates from wild-type, TPC1 heterozygous and TPC1 knock-out mice was probed with the Abcam anti-TPC1 antibody (Figure 3.6C). A protein band of ~ 100 kDa apparent molecular weight was detected in the wild-type and heterozygous TPC1 mouse homogenates, that was not present in the knock-out mouse preparation. This suggests the Abcam TPC1 antibody is specifically recognising TPC1 protein, but does not explain the discrepant sizes between cell types.

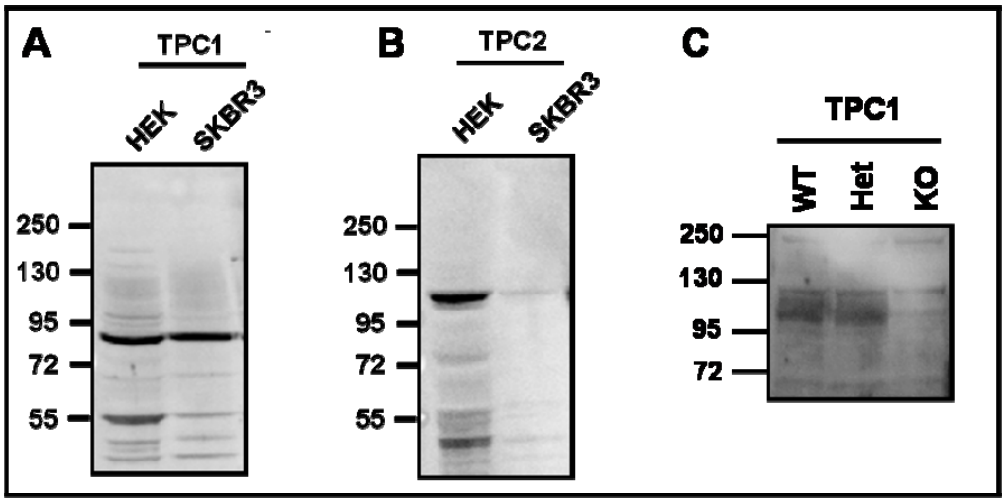

Figure 3.6. TPC antibodies detect endogenous protein from untransfected cell homogenates. Abcam TPC1 (**A**) and Sigma TPC2 (**B**) antibodies were used to probe untransfected cell homogenates by Western blot. (**C**) The anti-TPC1 antibody was shown to be specific for TPC1 by probing a Western blot of wild-type, heterozygous and knock-out TPC1 mouse pancreas homogenates.

3.3.5 Immunocytochemistry of endogenous TPCs

Untransfected SKBR3 cells were probed for endogenous TPC1 protein by immunocytochemistry using the Abcam TPC1 antibody. This antibody detected a protein with a widespread, punctate, intracellular localisation at levels above background (Figure 3.7). This protein did not however colocalise with endogenous lysosomal (LAMP1) or early-endosomal (EEA1) markers, at variance with the known distribution of recombinant HsTPC1 (Brailoiu *et al.*, 2009a;Calcraft *et al.*, 2009).

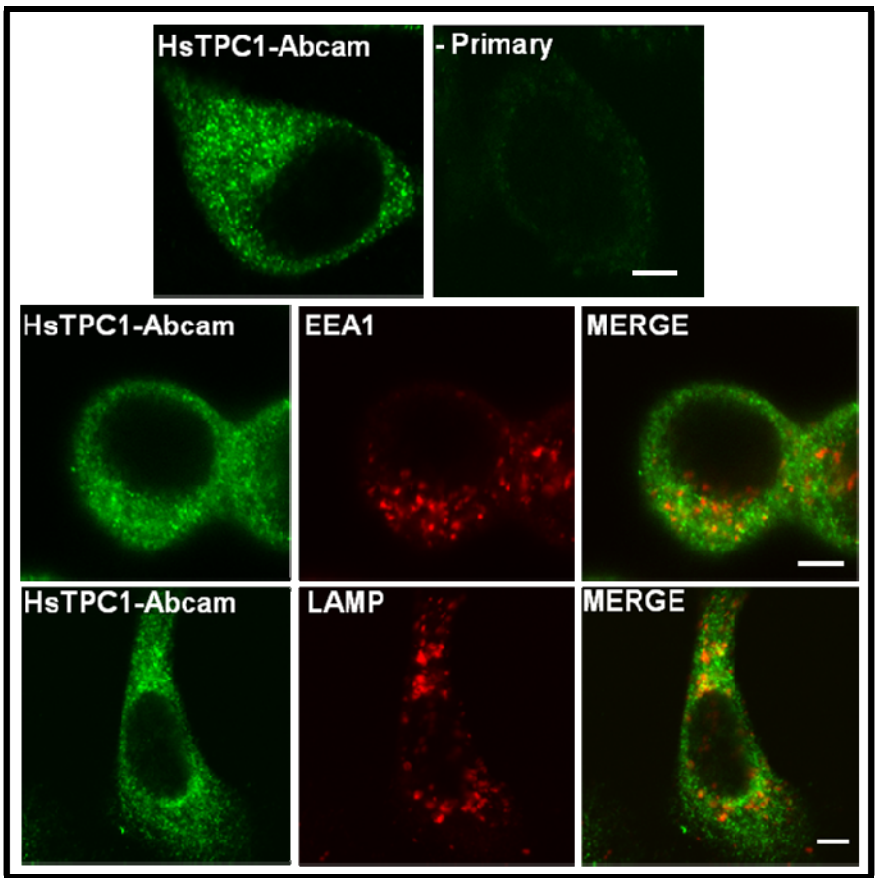

Figure 3.7. Abcam TPC1 antibody detects a protein with a punctate, intracellular distribution. Untransfected SKBR3 cells were probed with the Abcam TPC1 antibody and organelle markers for either early-endosomes (EEA1) or lysosomes (LAMP1), with no colocalisation observed between the two. Scale bar 5μm.

A similar pattern was visualised when the Santa Cruz TPC1 antibody was used in both HEK (Figure 3.8A) and SKBR3 (Figure 3.8B) cell lines, where antibody immunostaining failed to colocalise with endogenous organelle markers. This was also observed with the custom TPC1 antibodies # 76 and # 77 (Figure 3.9).

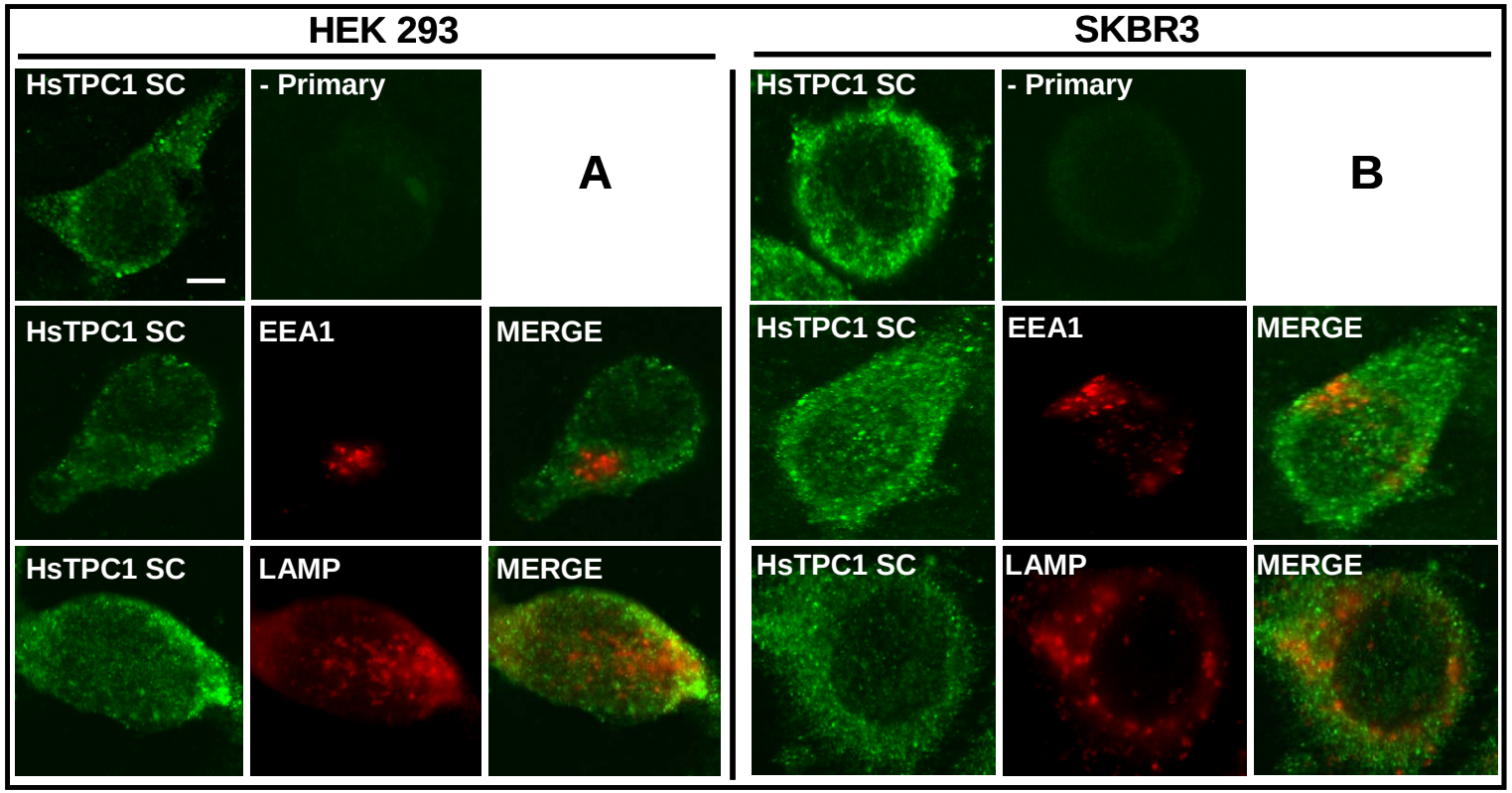

Figure 3.8. Santa Cruz TPC1 antibody detects a protein with a punctate, intracellular distribution. Confocal images of untransfected HEK **(A)** and SKBR3 cells **(B)** probed with the Santa Cruz TPC1 antibody and organelle markers for early-endosomes (EEA1) and lysosomes (LAMP1). Detected protein was above non-specific secondary antibody immunostaining (-Primary). Scale bar 5µm.

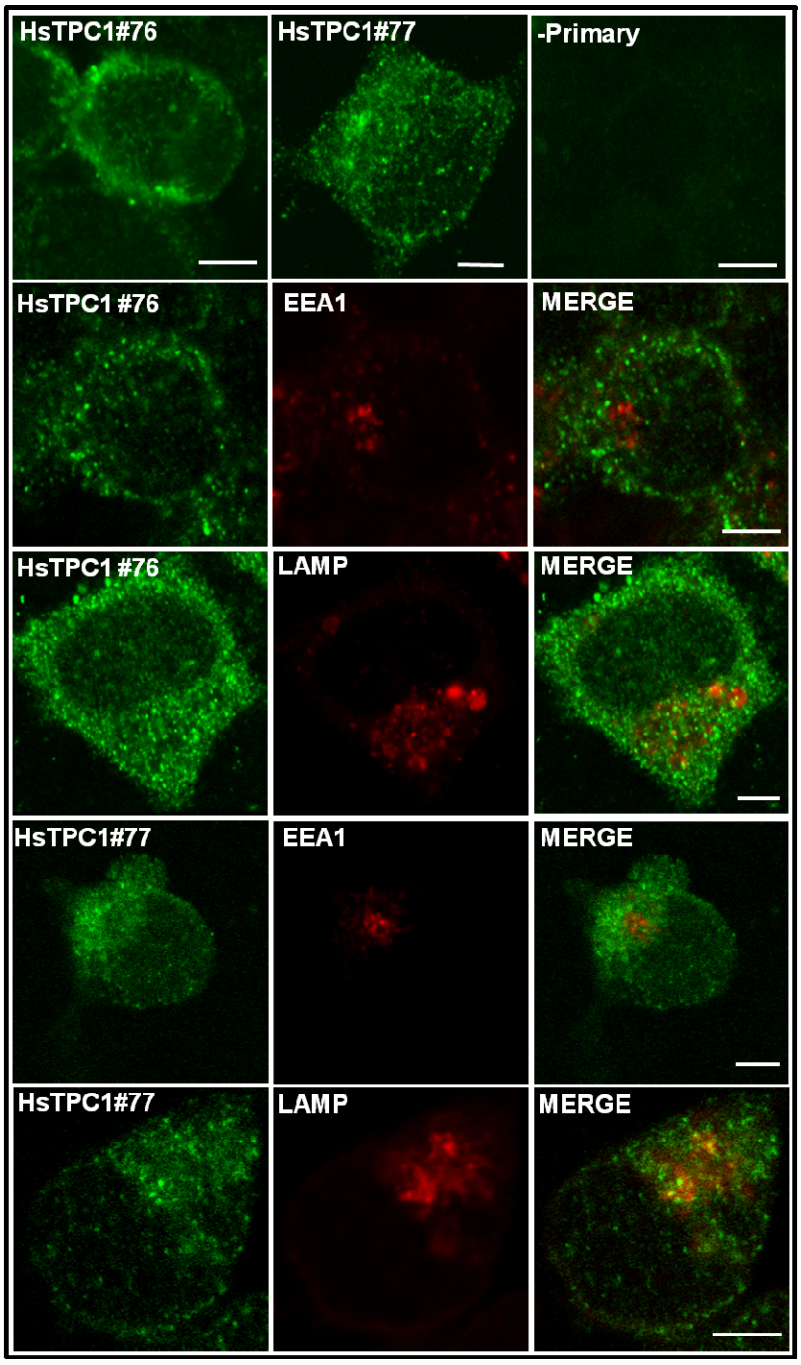

Figure 3.9. Custom TPC1 antibodies detect a protein with a punctate, intracellular distribution. Confocal images of SKBR3 cells probed with the custom TPC1 antibodies # 76 and # 77 and markers of the endo-lysosomal system (LAMP/ EEA1). Detection was above non-specific secondary antibody immunostaining (-Primary). Scale bar 5μm.

The specificity of the Santa Cruz TPC1 antibody was tested with the relevant blocking peptide. Both endogenous and overexpressed TPC1 protein were probed with the Santa Cruz antibody, incubated with (+) or without (-) the blocking peptide corresponding to the epitope sequence. As shown in Figure 3.10A, incubation with the TPC1 antibody visualised a protein with the typical widespread, intracellular puncta. In the presence of the blocking peptide, immunostaining was greatly reduced. In both cases the protein visualised was above non-specific secondary antibody staining (- primary).

When TPC1-mRFP was overexpressed (Figure 3.10B), antibody staining was saturating at comparable confocal settings used to image antibody binding to endogenous protein. In the presence of blocking peptide, this staining was still present but much reduced to non-saturating levels. This suggests that while some staining remains in the presence of the blocking peptide, a large proportion of protein visualised is specific to the target epitope of TPC1.

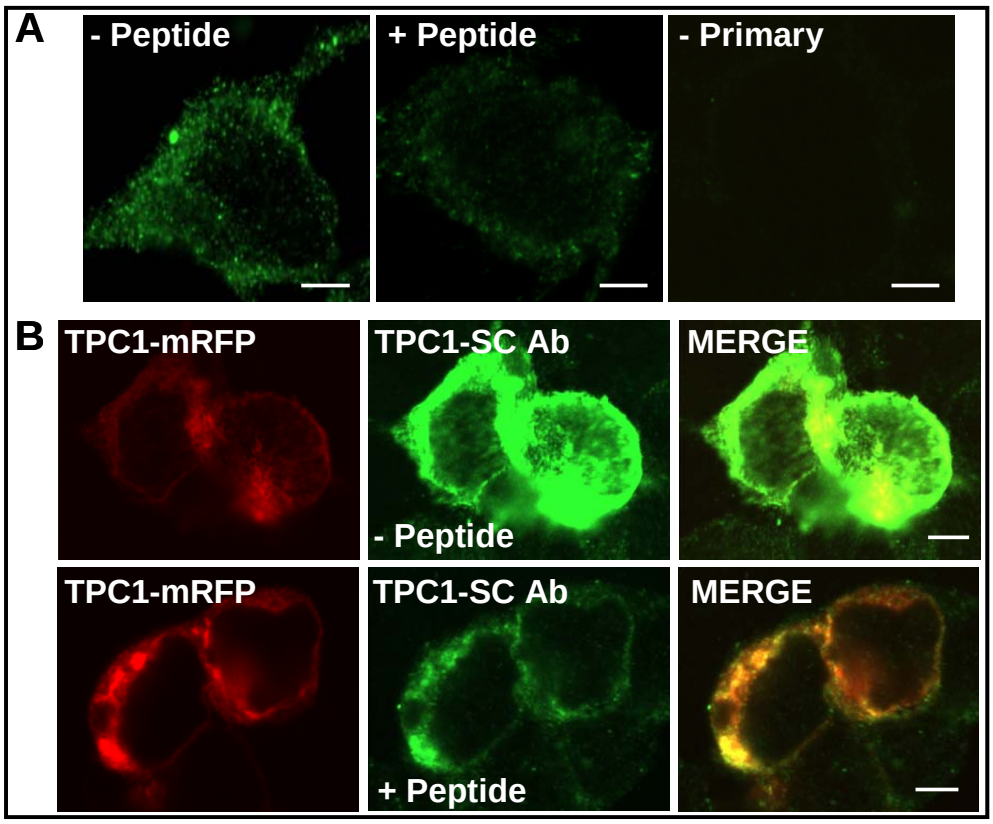

Figure 3.10. Immunostaining by the TPC1 Santa Cruz antibody is reduced in the presence of a blocking peptide. The Santa Cruz TPC1 antibody binds a protein with a widespread, punctate intracellular distribution which is above background immunostaining (-primary) **(A)**. This is reduced in the presence of blocking peptide (+ peptide) **(A)**. The antibody is able to recognise overexpressed mRFP-tagged TPC1 **(B)**. Binding to the overexpressed protein is also reduced in the presence of blocking peptide **(B)**. Scale bar 5µm.

In summary, the Abcam, Santa Cruz and custom TPC1 antibodies all recognise an endogenous protein with a similar punctate, intracellular distribution. Immunostaining of the endogenous protein and overexpressed TPC1-mRFP is reduced in the presence of the blocking peptide, suggesting the antibody is binding specifically to the epitope peptide sequence.

Following from the examination of the TPC1 antibodies to probe for endogenous TPC1 localisation, the same rationale was applied to the TPC2 antibodies, with much the same results. The Sigma TPC2 antibody detected a protein in SKBR3 cells, above background staining, which appeared to have an intracellular, punctate

distribution. This protein failed to colocalise with endogenous organelle markers to endosomes (EEA1) and lysosomes (LAMP) (Figure 3.11). Interestingly an intense region of protein is also detected in an area that appears to be nuclear (white arrow).

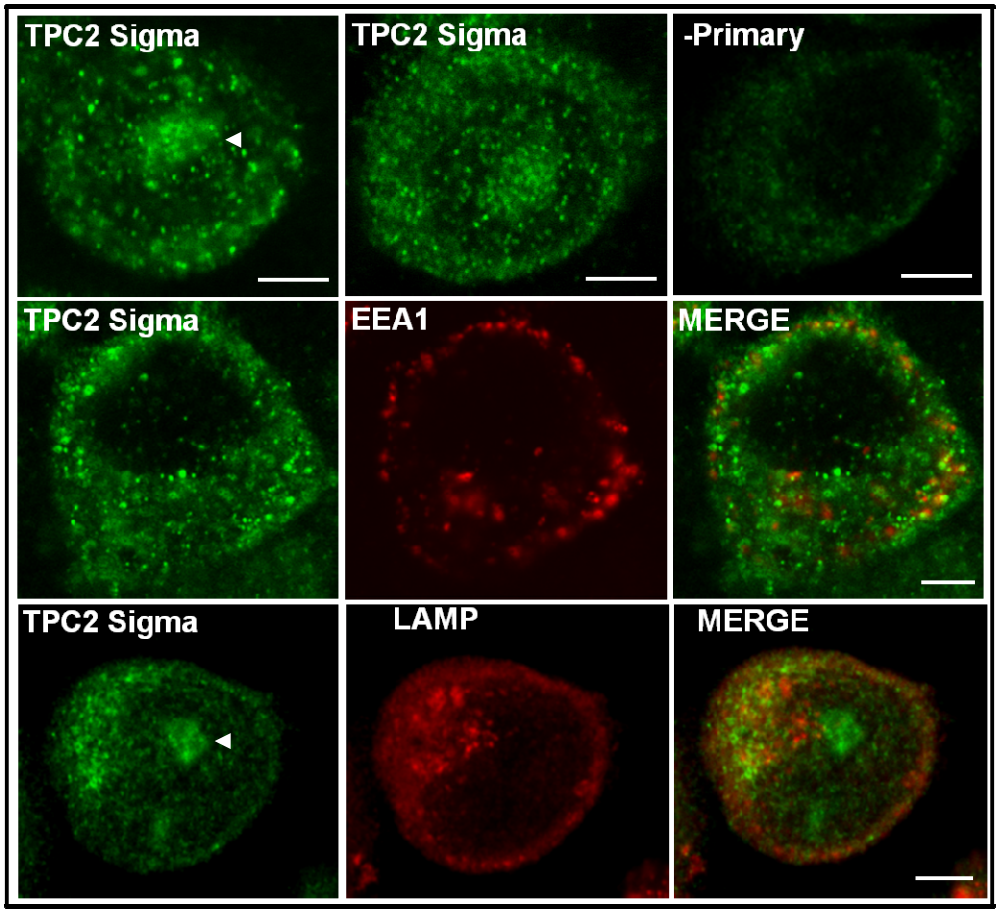

Figure 3.11. A Sigma TPC2 antibody detects a protein with a punctate, intracellular distribution. Confocal images of SKBR3 cells probed with the Sigma TPC2 antibody and markers of the endo-lysosomal system (LAMP/ EEA1). Detection was above non-specific secondary antibody immunostaining (-Primary). Scale bar 5µm.

A punctate intracellular distribution was also apparent for custom TPC2 antibody # 34 immunostaining, which failed to colocalise with organelle markers (Figure 3.12). Nuclear staining was also observed, most starkly with the TPC2 antibody # 34 where a small number of large, dense puncta were visible in what appears to be the nucleus (white arrow, Figure 3.12). Staining of protein with TPC2 antibody # 35 was poor and of low intensity.

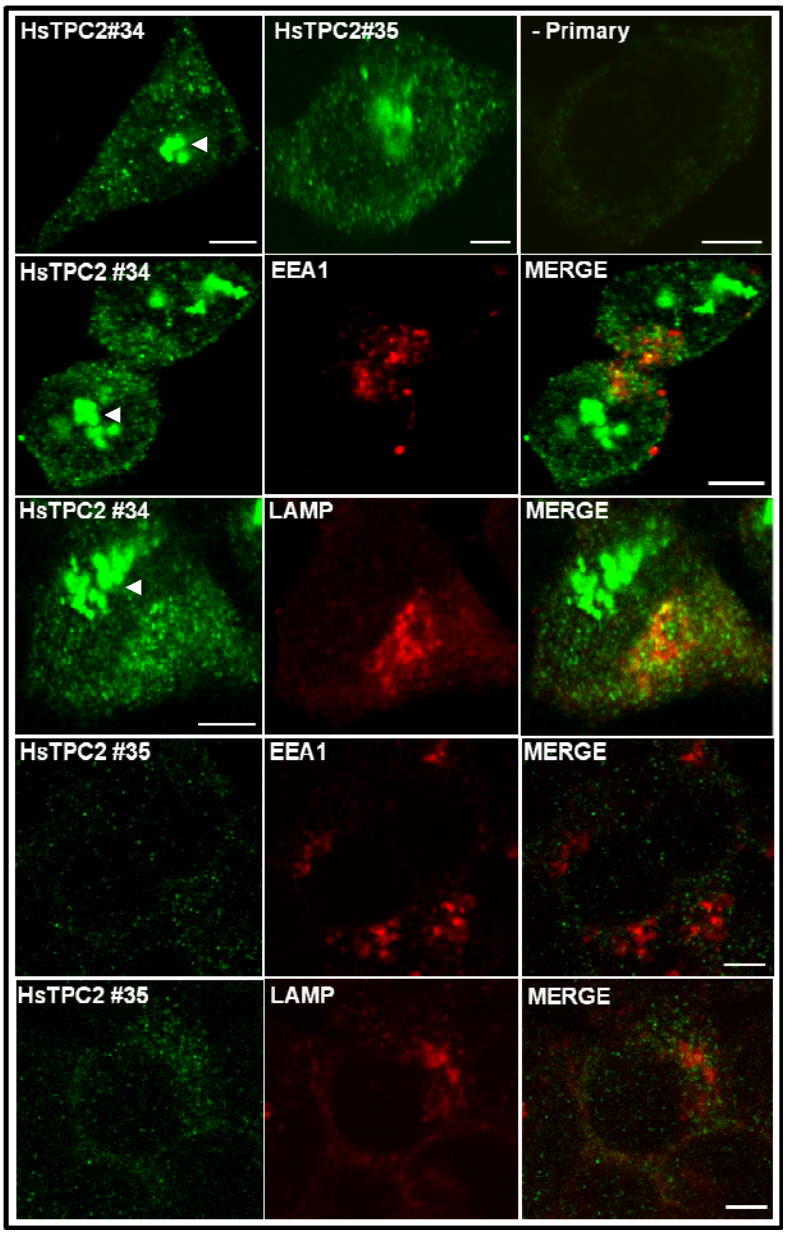

Figure 3.12 Custom TPC2 antibodies detect a protein with a punctate, intracellular distribution. SKBR3 cells were probed with the custom TPC2 antibodies # 34 and # 35 and organelle markers for endosomes (EEA1) and lysosomes (LAMP). Detection was above non-specific secondary antibody immunostaining (-Primary). Scale bar 5µm.

As with TPC1, TPC2 antibodies immunostain an endogenous protein, with a punctate, intracellular distribution. This staining fails to coincide with that of endogenous protein organelle markers, suggesting the protein is not localised to the endo-lysosomal system.

3.4 Discussion

A range of seven antibodies to human TPCs were tested for their ability to recognise both overexpressed and endogenous TPC proteins by Western blotting and immunocytochemistry. The Abcam TPC1 and Sigma TPC2 antibodies were found to be capable of detecting overexpressed TPC protein by Western blot. These two antibodies also recognise an endogenous protein by Western blot. All but one of the antibodies, TPC1 # 76, were able to detect overexpressed TPCs expressed in HEK cells by immunocytochemistry. Finally the majority of antibodies tested, with the exception of TPC2 # 35, bound an endogenous protein that had a widespread, punctate intracellular distribution. These detected proteins failed to colocalise with markers for the early endosome or the lysosome. The ability of antibodies to detect protein by Western blot and immunocytochemistry is summarised in Table 3.2.

TPC Isoform	Company	Ab #	WB OE	WB Endog.	Immuno. OE	Immuno. Endog.
TPC1	Abcam	ab80961	++	++	+	++
TPC1	Santa Cruz	sc67973	X	X	++	++
TPC1	Custom	76	X	X	X	++
TPC1	Custom	77	X	X	+	++
TPC2	Sigma	HPA016561	++	+	++	++
TPC2	Custom	34	X	X	+	++
TPC2	Custom	35	X	X	+	+

Table 3.2 Summary of the TPC antibody set and their applications. A range of TPC1 and TPC2 antibodies to varying epitopes were tested for their ability to recognise overexpressed and endogenous protein by Western blot and immunocytochemistry. Antibodies were not suitable for certain applications (X) or had varying affinity (+/++). Western blot (WB), overexpressed (OE), immunocytochemistry (Immuno).

The Abcam TPC1 antibody specifically detected overexpressed TPC1 protein as evidenced by visualisation of TPC1-GFP and TPC1-*myc* at their predicted sizes. The Santa Cruz antibody detected a doublet at ~ 110 and 90 kDa, however this was

present at the same intensity and size between mock and overexpressed protein homogenates. A decrease in size for untagged protein and a decrease in intensity of signal between overexpressed and endogenous protein would have been expected. It is therefore highly improbable that the protein bands detected truly correlate to TPC1. With the custom-designed TPC1 antibody # 76; several protein bands were visualised with no apparent logical pattern. There was no size shift between tags, no isoform specificity and no change in intensity between overexpressed and untransfected homogenates. Using antibody # 77, no prominent protein bands were visualised above background. Using both antibodies it is unlikely any of these bands correspond to TPC1. Turning to TPC2, the antibody commercially available from Sigma was capable of specifically recognising HsTPC2 by Western blot and could visualise the size shift between GFP- and *myc*-tagged proteins. The custom antibodies were again incapable of specifically recognising TPC2 protein.

The majority of antibodies tested, with the exception of TPC1 # 76, were capable of detecting overexpressed TPC protein in HEK293 cells by immunocytochemistry. This suggests that when the protein is in abundance and folded with its native tertiary structure the antibodies are able to recognise and bind their epitope sequences. During SDS-PAGE, the epitope, to which the antibody is raised, may be linearised by the reducing conditions of the process and therefore lose any natural tertiary structure. The antibody may rely on the tertiary structure of the epitope to bind the target protein and this may explain why antibodies incapable of binding TPC protein during Western blotting can bind protein by immunocytochemistry.

The Abcam TPC1 and Sigma TPC2 antibody can therefore be used to detect overexpressed TPCs by Western blot and six antibodies are able to recognise overexpressed protein by immunocytochemistry. These will be used in Chapters 4-6 to characterise the TPCs.

The ability of this repertoire of antibodies to recognise endogenous TPC protein was far from clear. By Western blot, the Abcam TPC1 antibody detected a single major

band at ~ 90 kDa while the Sigma TPC2 antibody visualised a single band at ~ 110 kDa. The predicted size of native TPC1 is 94 kDa, comparable with the band visualised, however TPC2 is predicted to be 85 kDa, significantly smaller than the observed size. Furthermore with the overexpressed protein, TPC2 is consistently smaller than TPC1, raising doubts about the specificity of the apparent endogenous protein band. This could perhaps be explained if TPC2 bound with an accessory protein that was not dissociated during the reducing conditions of SDS-PAGE. To assess the specificity of the protein band visualised by the Abcam TPC1 antibody, pancreas homogenates from wild-type, TPC1 heterozygous and TPC1 knock-out mice were probed. A protein band of ~ 100 kDa was detected with the Abcam TPC1 antibody in wild-type and heterozygous mouse homogenates that was not present in knock-out mouse homogenates. This suggests the protein detected is TPC1. The apparent size of the protein was greater than that observed by the TPC1 antibody in HEK homogenates. This could be indicative of different splice variants of TPC1 existing in different cell-types.

There is also some doubt as to the identity of the protein labelled by TPC antibodies during immunocytochemistry. The specificity of Santa Cruz TPC1 antibody to its epitope sequence was tested using the corresponding blocking peptide. This peptide corresponds to the sequence epitope to which the antibody was raised to. Using the blocking peptide greatly reduced the antibody signal, although some residual staining remained. This may be true non-specific immunostaining or could be due to incomplete block by the peptide. However, the greatly reduced signal does suggest that the antibody is predominately binding its target peptide sequence. The exact TPC1 C-terminal epitope the antibody was raised to is not specifically defined by Santa Cruz.

Furthermore, all evidence, both molecular and functional, has thus far pointed to TPC2 having a highly defined lysosomal localisation. From endogenous staining of lysosomes in SKBR3 and HEK293 cells a restricted, punctate, perinuclear distribution of lysosomes is visualised by the antibody to the lysosomal marker

protein LAMP1. The TPC antibodies consistently show a punctate, intracellular but broadly distributed protein localisation which fails to colocalise with either of the endo-lysosomal system markers. This staining is not an artefact of non-specific secondary antibody, as when the primary antibody is omitted, no immunostaining is seen with secondary alone. It therefore seems unlikely that the antibodies are recognising TPC protein, however this distribution is consistent across a range of epitopes. Furthermore, TPC2 antibodies to three different epitopes all intriguingly visualise a protein that has a high level of very punctate, nuclear staining. If this was an artefact of non-specific recognition of another protein, it seems unusual that three different epitopes would correlate to one protein with such a uniquely striking appearance. The identity of this possible nuclear organelle immunostained by the TPC2 antibodies was not determined.

There appears to be much doubt as to the ability of these TPC antibodies to recognise endogenous TPC protein, therefore one should be wary in using them to characterise the endogenous properties of TPCs.

Other groups have utilised TPC antibodies in to characterise the TPCs. Calcraft et al showed that endogenous TPC2 in HEK293 cells colocalised with the LAMP2 lysosomal marker, comparable to overexpressed tagged TPC2 (Calcraft *et al.*, 2009). The custom-made TPC2 polyclonal antibody was raised to epitopes in the pore I region and domain I-II linker. This antibody was also shown to apparently immunoprecipitate tagged overexpressed (~80 kDa) and endogenous (~ 70kDa) TPC2. Overexpressed protein bands were however, not prominent. Moreover, tagged TPC2 appeared as a doublet despite PNGase F treatment. As we have seen in this chapter, some caution should be observed when considering protein bands by Western blot as specific.

Zong et al utilised a TPC2 antibody raised to a C-terminal epitope to show that overexpressed (untagged) mouse TPC2 is N-glycosylated, appearing as a fully and partially glycosylated doublet (~80kDa) that is reduced to a single deglycosylated

form upon PNGase F treatment (~70 kDa). This is consistent with our ability to detect overexpressed TPC2 protein using an antibody to a predicted cytosolic C-terminal epitope.

New antibodies continue to become available and these may show better specificity and affinity than the initial cohort of TPC antibodies. Sigma has released a TPC2 antibody to the predicted cytosolic domain I-II linker region, an epitope not previously tested (HPA027080). Similarly Abcam now produce a TPC1 antibody to epitopes in the N-terminus (ab94731). It would be interesting to test if these second generation antibodies prove more capable of detecting endogenous TPC protein than those characterised here.

The ultimate test of specificity of these antibodies however, would be to examine protein recognition in TPC knock-out mouse models. If the protein bands visualised by Western blot or the widespread punctate staining seen by immunocytochemistry is abolished then it seems safe to conclude the antibodies are recognising TPC protein. Selectivity was demonstrated for the Abcam anti-TPC1 antibody during Western blotting. Further work is required to test the specificity of the TPC2 antibody.

In summary, antibodies capable of detecting TPC protein by both Western blot and immunocytochemistry have been established. These tools can now be used in the molecular characterisation of TPCs.

Chapter 4 - Defining TPC topology

4. 1 Introduction

To fully understand the function and regulation of a channel protein it is necessary to elucidate its basic architecture. TPCs are members of the voltage-gated ion channel superfamily (Yu *et al.*, 2005). This family encompasses, well-characterised voltage-gated Ca^{2+} (Ca_Vs) , Na^+ (Na_vs) and K^+ (K_vs) channels, as well as the TRP channel family, calcium-activated potassium channels (K_{Ca}), inwardly-rectifying potassium channels (K_{ir}) and the TPCs. The minimum requirement for a channel pore is two transmembrane (TM) regions flanking a pore loop, such as represented by the K_{ir} channels (Hibino *et al.*, 2010). Voltage-gated K^+ channels such as K_v1-9 consist of 6 TM regions with a pore loop between TM5 and TM6 (Grottesi *et al.*, 2005). During evolution, a 2 TM pore-forming protein was thought to have fused with a 4 TM region protein, which conferred voltage sensitivity on the pore (Liman *et al.*, 1991). Like K^+ channels, TRP channels such as TRPML1 also have 6 TM regions and a single pore region in each protein (Clapham *et al.*, 2001). In contrast, voltage-gated Ca^{2+} and Na^+ channels have four domain repeats, each comprised of 6 TM regions and a pore (Catterall, 2011). Phylogenetic analysis reveals that TPCs are most closely related to TRPML and TRPP channels (Yu *et al.*, 2005) and may represent evolutionary intermediates between TRP channels and voltage-gated Ca^{2+} and Na^+ channels. In this context, the initial report of rat TPC1 cloning by Ishibashi et al (Ishibashi *et al.*, 2000) proposed the protein had two homologous domains, each containing six TM regions and a putative pore loop between TM 5 and 6 of each domain. A schematic of this arrangement is shown in Figure 3.2 (Chapter 3).

The prediction by Ishibashi et al was based on consensus alignments with domains III and IV of voltage-gated Ca^{2+} and Na^+ channels as well as hydropathy plots (Ishibashi *et al.*, 2000). The two-repeat domains of 6 TM regions make the TPCs structurally homologous to half a voltage-gated Ca^{2+}or Na^+ channel (Yu *et al.*, 2005). Ishibashi et al therefore recognised that TPC1 may form a dimer to preserve the

four-pore arrangement that comprises a functional Ca_V/Na_V channel (Ishibashi *et al.*, 2000). A Kyte-Doolittle hydropathy plot also indicated that both termini and the domain linker are hydrophilic and therefore possibly located in the cytoplasm. The plot was ambiguous however in defining TM regions, clearly predicting 15 regions with positive hydropathy ratings. It was also noted that the similarity of TPC regions with Ca^{2+} and Na^{+} channels was lower than the similarity between these four-repeat channels. This suggests that alignments should not be relied on to form conclusions as to the topology of the channel. However the architecture of TPCs has become dogma based on predictions by Ishibashi et al (Ishibashi *et al.*, 2000). The basic topology of the TPCs was not experimentally addressed in the initial characterisation of the channels, although schematics of TPC topology were shown in these publications (Calcraft *et al.*, 2009;Zong *et al.*, 2009). Indeed a hydropathy plot by Calcraft et al displays at least 14 clear peaks with a positive hydropathy index (Calcraft *et al.*, 2009) at variance with the proposed 12 TM region model. Therefore the aim of this chapter is to investigate domain architecture of TPCs and experimentally determine the topology of the TPCs.

4.2 Materials and methods

In silico prediction of TPC transmembrane domains and N-glycosylation sites

The transmembrane prediction algorithms listed in Table 4.1 were used to predict TPC domain structure.

Program	Web Address	Reference
Das	http://www.sbc.su.se/~miklos/DAS/	[1]
SOSUI	http://bp.nuap.nagoyau.ac.jp/sosui/sosui_submit.html	[2]
TMHMM	http://www.cbs.dtu.dk/services/TMHMM/	[3]
HMMTOP	http://www.enzim.hu/hmmtop/	[4]
TMpred	http://www.ch.embnet.org/software/TMPRED_form.html	[5]
SPLIT	http://split.pmfst.hr/split/4/	[6]
TMMOD	http://liao.cis.udel.edu/website/servers/TMMOD/scripts/frame.php?p=submit	[7]
Phobius	http://phobius.sbc.su.se/	[8]

Table 4.1. Transmembrane domain prediction algorithms. The name and program web address are listed along with a primary reference relating to that algorithm. 1. (Cserzo *et al.*, 1997), 2. (Hirokawa *et al.*, 1998), 3. (Juretic *et al.*, 2002), 4. (Kahsay *et al.*, 2005), 5. (Hofmann & Stoffel, 1993), 6. (Kall *et al.*, 2004), 7. (Krogh *et al.*, 2001), 8. (Tusnady & Simon, 1998)

N-glycosylation sites were predicted by ScanProsite:

(http://prosite.expasy.org/scanprosite/)

Plasmids

The molecular cloning of HsTPC1-GFP, HsTPC1-mRFP, HsTPC2-GFP and HsTPC2-mRFP is described in Brailoiu et al. 2009 (Brailoiu *et al.*, 2009a). The cloning of mRFP-HsTPC1, mRFP-HsTPC2, HsTPC1$^{1-628}$ GFP and HsTPC2$^{1-339}$ GFP is described in Hooper et al 2011 (Hooper *et al.*, 2011).

Using HsTPC1-GFP as a template, three putative N-glycosylated residues; Asn-599, Asn-611 or Asn-616 were mutated to Gln using the Stratagene QuikChange® Site-

directed mutagenesis kit and mutagenic primers listed in Table 4.2. The TPC1^{N3Q}-GFP triple mutant was created by first generating the N616Q mutation using primer pair 3F and 3R and the N599Q mutant as the template. To the N599/616Q double mutant the N611Q mutation was introduced using primer pair 4Fand 4R.

Mutant	Primer	Sequence
N599Q	1F	CCCCAACTGCTGCCAAACGAGTACAGTGG
	1R	CCACTGTACTCGTTTGGCAGCAGTTGGGG
N611Q	2F	GCCTACCGCTGGCGCCAACACACCGTGGGCAACAGG
	2R	CCTGTTGCCCACGGTGTGTTGGCGCCAGCGGTAGGC
N616Q	3F	CCACACCGTGGGCCAAAGGACCGTGGTGG
	3R	CCACCACGGTCCTTTGGCCCACGGTGTGG
N3Q	4F	GCCTACCGCTGGCGCCAACACACCGTGGGCCAAAGG
	4R	CCTTTGGCCCACGGTGTGTTGGCGCCAGCGGTAGGC

Table 4.2 Primers for the creation of N-glycosylation defective HsTPC1 mutants. The primer pair for the creation of each mutant is listed with sequences for the forward (F) and reverse (R) primer (5' to 3' direction).

The TPC constructs utilised in this chapter are summarised in Figure 4.1.

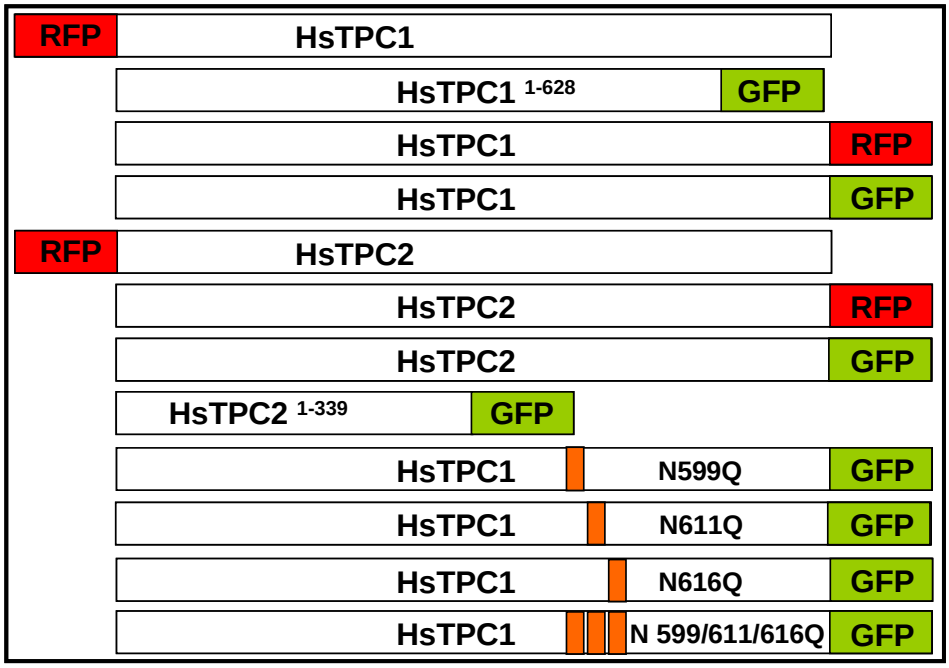

Figure 4.1. HsTPC clones utilised in the characterisation of channel topology. Tagged full-length, truncated and mutated TPC proteins were used to assess topology.

Cell culture and transfection

HEK293 and SKBR3 cells were cultured and transfected as per the methods in Chapter 2.

Fluorescence Protease Protection (FPP) assay

The Fluorescence Protease Protection (FPP) assay is based on methods originally outlined by Lorenz et al. (Lorenz *et al.*, 2006). HEK cells were transfected with the indicated fluorescently tagged construct. Cells were washed in HEPES-buffered saline followed by selective permeabilisation of the plasma membrane by 50 μM digitonin for 7 min at 20ºC. Digitonin was prepared in intracellular-like buffer consisting of 110 mM K^+acetate, 2 mM $MgCl_2$ and 20 mM NaHEPES (pH 7.2). Cells were washed twice in intracellular-like media before imaging. Cells were then imaged by a CCD camera using an inverted epifluorescence microscope (Olympus IX71) with a 20x objective and a monochromator light source (T.I.L.L photonics). At 3 second intervals, emission of GFP fluorescence (> 500 nm) or mRFP fluorescence (> 570 nm) was captured after excitation at 488 nm and 543 nm, respectively. After 60 s, 4 μM trypsin was added to the coverslip. Signals in individual cells were corrected for background and normalised to baseline before addition of trypsin.

Immunocytochemistry and confocal microscopy

The use of indicated antibodies and the protocol for immunocytochemistry is as described in Chapter 3. For epitope mapping experiments, cells were either permeabilised with Triton X-100 as previously described or the plasma membrane was selectively permeabilised by the addition of 50μM digitonin in intracellular-like buffer for 6 min at RT. TPC topology was mapped using a Santa Cruz TPC1 antibody (sc67973), a Sigma TPC2 antibody (HPA016561) or custom TPC2

antibody # 34. Details of antibody epitope sequences and conditions of use are outlined in Chapter 3, Table 3.1.

Recurrent molecular biology methods

PNGase F treatment, SDS-PAGE and Western blots were performed as described in Chapter 2.

4.3 Results

4.3.1 *In silico* prediction of TPC transmembrane regions

To objectively assess the domain architecture of TPCs, an unbiased *in silico* prediction approach was applied. This utilised eight web-based transmembrane (TM) prediction algorithms (detailed in table 4.1). The output of each algorithm was compared to a transmembrane region model, based on consensus with sequence alignments to voltage-gated Ca^{2+} and Na^{+} channels (Ishibashi *et al.*, 2000). As shown in Figure 4.2, there is no clear consensus on the number and position of TM regions for HsTPC1 (Figure 4.2 A) or SpTPC1 (Figure 4.2 B). Algorithms predicted between 9 and 13 TM regions for HsTPC1 and SpTPC1. While there was clear convergence on TM regions 1, 2, 3, 5 and 6 of domain I in both cases, and corresponding TM regions in domain II, TM regions 4 and 10 were poorly predicted, especially in SpTPC1. Many algorithms also predicted the putative pore loop as a TM region. The topology of the whole channel therefore remains unclear with no consensus on the overall channel architecture.

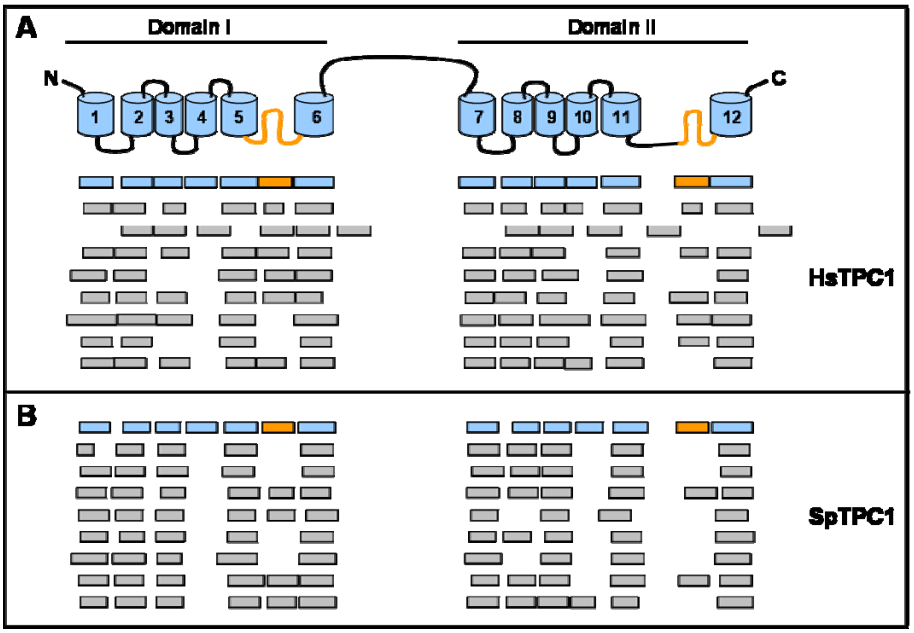

Figure 4.2. Transmembrane prediction algorithms do not reach a clear topology consensus for TPC1 isoforms. (A) Model of a TPC (top) with putative TM regions (blue) and pore loop (orange) corresponding to a HsTPC1 consensus (blue and orange bars) based on alignment with Ca_V and Na_V. Each row of grey bars represents the output of one prediction algorithm in the order given in Table 4.1. **(B)** Similar analysis for SpTPC1.

A lack of consensus between prediction algorithms was also apparent when this analysis was extended to TPC2 and TPC3 isoforms (Figure 4.3). The majority of programs predict an odd number of TM regions for these isoforms, which would place termini on opposite sides of the intracellular organelle membrane. Remarkably putative TM region 4 was not predicted by any algorithms in SpTPC2.

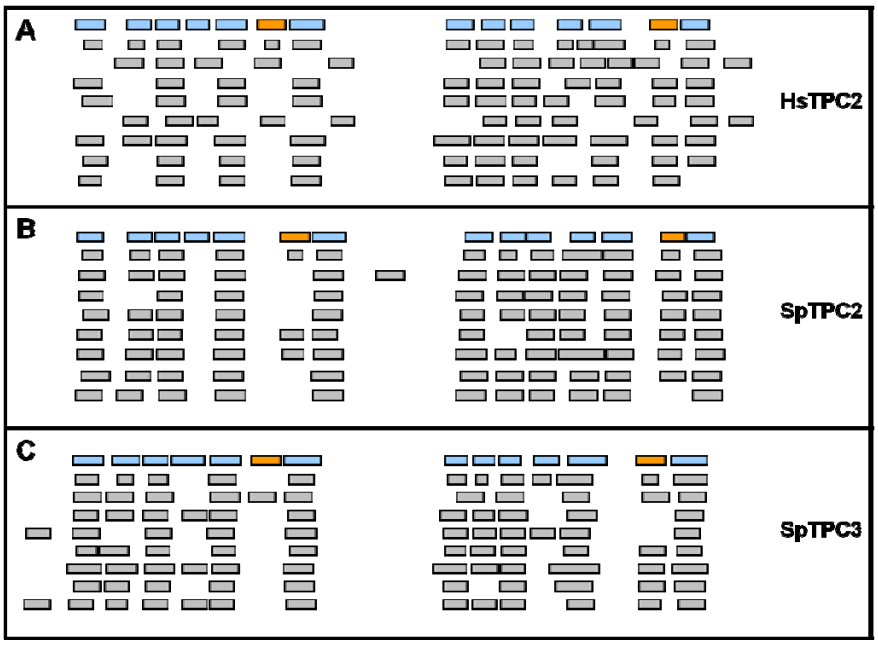

Figure 4.3. Transmembrane prediction algorithms do not reach a clear topology consensus for TPC2 or TPC3 isoforms. (A) Consensus transmembrane (TM) regions (blue bars) and pore loop (orange bars) based on alignment with Ca_V and Na_V. Each row of grey bars represents the output of one prediction algorithm in the order given in Table 4.1. **(B)** Similar analysis for SpTPC2 and **(C)** SpTPC3.

The total number of TM regions predicted for HsTPC1-2 and SpTPC1-3 isoforms by each of the eight algorithms is given in Table 4.3.

Program	Predicted Number of TM				
	HsTPC1	SpTPC1	HsTPC2	SpTPC2	SpTPC3
DAS *	13	10	14	13	12
SOSUI	11	10	13	13	10
TMHMM	12	12	11	11	11
HMMTOP	10	10	11	12	11
Tmpred #	12	10	11	12	11
SPLIT	11	9	12	13	12
TMMOD	10	12	10	12	10
Phobius	12	12	11	11	13

Table 4.3. The total number of TPC TM regions predicted by each algorithm varies considerably. A range of online prediction algorithms were used to predict TM regions based on TPC amino acid sequence. *Loose cut-off used. # Strongly preferred model used.

In summary prediction algorithms failed to produce a clear consensus as to the domain architecture of the TPCs with anywhere between 9 and 14 TM regions predicted.

4.3.2 Fluorescence protease protection assays

A non-biased assessment of TPC domain architecture highlighted ambiguities between various prediction algorithms. It was therefore deemed necessary to experimentally investigate the topology of the TPCs. The first method employed was a fluorescence protease protection (FPP) assay based on methods described by Lorenz *et al* (Lorenz *et al.*, 2006). The principle of this technique is demonstrated in Figure 4.4. As shown previously, over-expressed TPC protein has an intracellular localisation on organelle membranes of the endo-lysosomal system. After selective permeabilisation of the plasma membrane by digitonin, the addition of trypsin leads to degradation of fluorophores that are cytosolic (Figure 4.4A). However if a fluorophore is tagged onto the channel at a luminal location, it is inaccessible to trypsin addition and protected from degradation (Figure 4.4B). By monitoring the

fluorescence of TPCs differentially tagged at either predicted cytosolic or luminal positions, the location of the tag can be assessed and topology inferred.

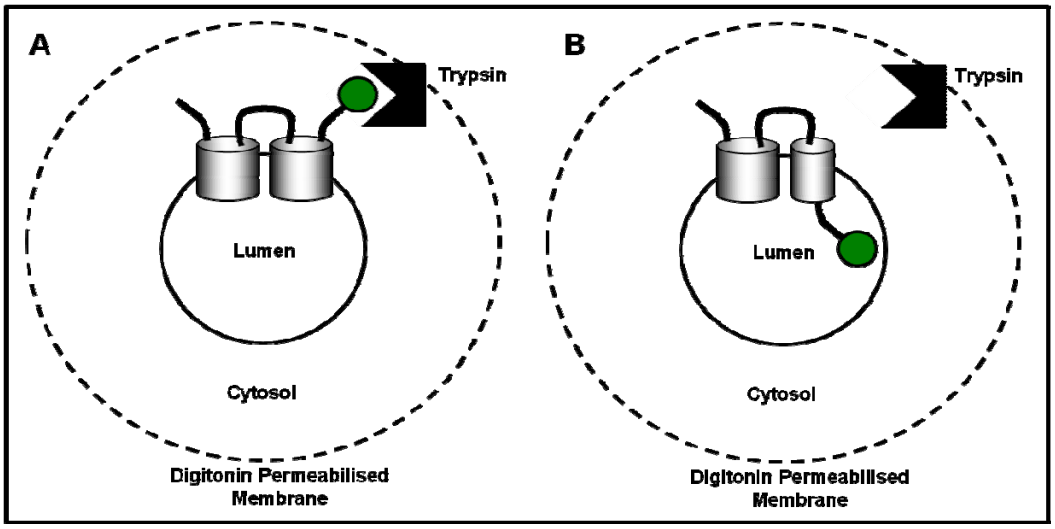

Figure 4.4. FPP assays discriminate between fluorophores tagged at cytosolic and luminal locations. Upon trypsin addition to a digitonin permeabilised cell, a cytosolic fluorophore will be degraded (**A**) while a luminal fluorophore is protected (**B**).

The topology of HsTPC1 was first investigated by expression of protein tagged at either the N or C termini. Upon addition of trypsin to cells expressing mRFP-TPC1, there is a marked decrease in fluorescence by ~50%. This would indicate that the N-terminus of TPC1 is cytosolic (Figure 4.5A). Addition of trypsin to C-terminally tagged TPC1 likewise causes a decrease in fluorescence, which, however, is much more rapid and complete (~ 95%). This is similar whether a GFP or mRFP tag is employed, suggesting that the use of tag itself does not greatly determine the rate or extent of fluorescence decrease (Figure 4.5B). These results indicate that TPC1 has cytosolic N- and C-termini and therefore an even number of TM regions.

A TPC1 construct truncated at amino acid 628 was also investigated. A fluorophore at this position is either luminal in a twelve-TM region model or cytosolic, if the poorly predicted TM region 10 is absent, as suggested by *in silico* prediction (Figure 4.2). Addition of trypsin does lead to a slight decrease in fluorescence, however the extent is less than for any other construct at ~ 33% (Figure 4.5C). This lead to the

conclusion that the fluorophore tag is in a luminal location and serves to confirm the specificity of degradation upon trypsin addition.

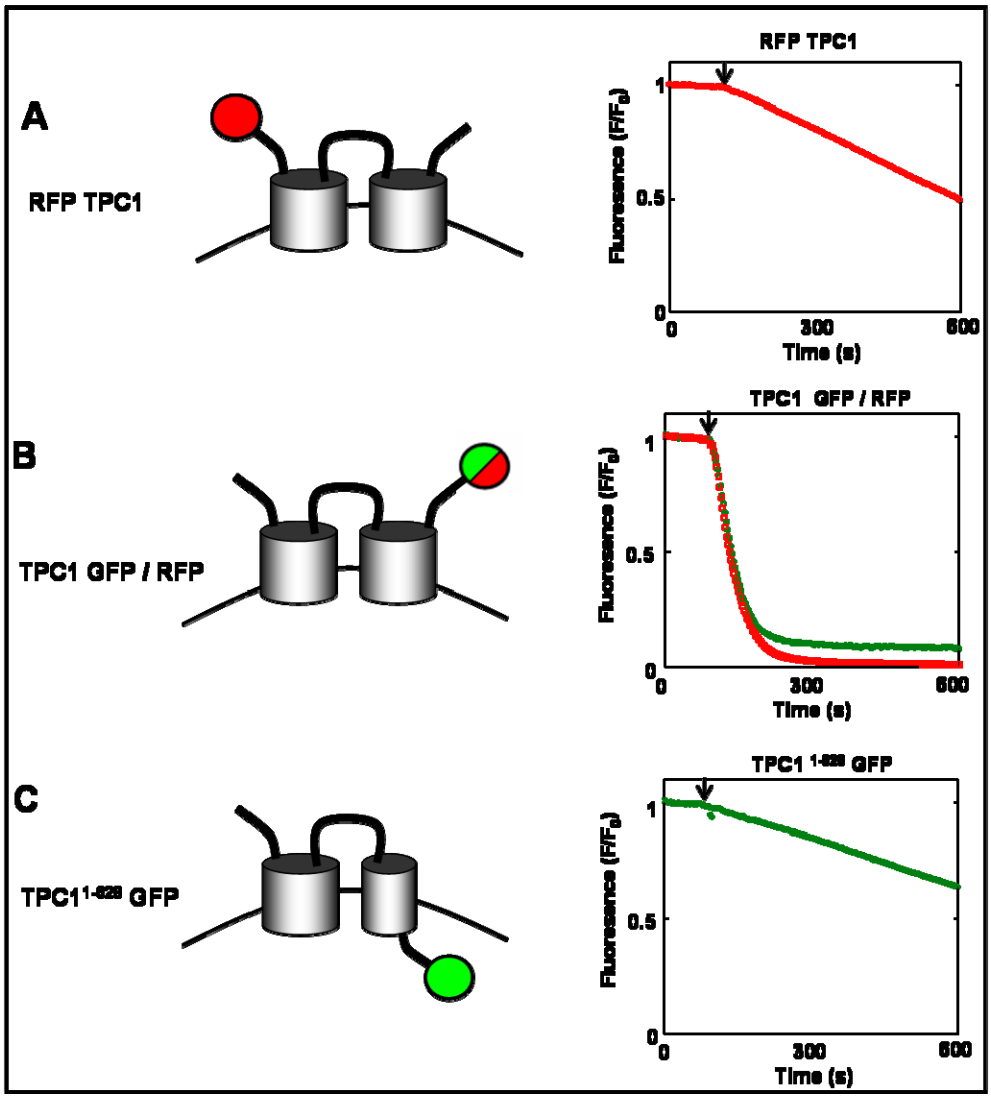

Figure 4.5. FPP analysis of differentially-tagged HsTPC1 indicates an even number of TM regions. HEK cells were transiently transfected with the indicated fluorescently-tagged TPC construct. After selective permeabilisation with digitonin, addition of trypsin (arrow) lead to a decrease in fluorescence intensity over time, which was less marked with TPC1$^{1-628}$ GFP.

The investigation of TPC domain architecture was extended to TPC2. The addition of trypsin caused a marked decrease in fluorescence intensity by ~ 88% from baseline in cells expressing mRFP-TPC2 (Figure 4.6A). The decrease in

fluorescence was less pronounced when TPC2 was tagged at the C-terminus, however a decrease of ~ 60 % was observed with a GFP tag and ~ 48 % with mRFP (Figure 4.6B). Similar to TPC1, TPC2 appears to also have cytosolic N- (Figure 4.6A) and C-termini (Figure 4.6B) and therefore an even number of transmembrane regions.

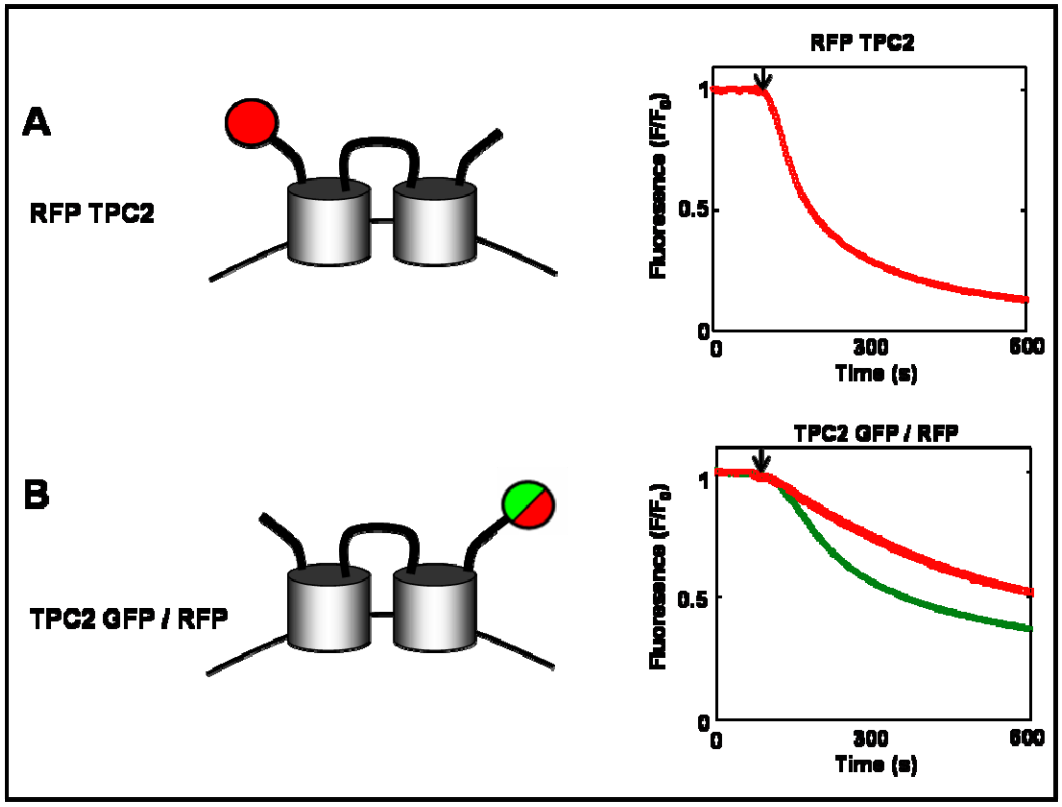

Figure 4.6. FPP analysis of differentially-tagged HsTPC2 indicates an even number of TM regions. HEK cells were transiently transfected with the indicated fluorescently-tagged TPC construct. After selective permeabilisation with digitonin, addition of trypsin (arrow) lead to a varying decrease in fluorescence intensity with all TPC2 constructs.

A TPC2 construct truncated after the first predicted hydrophobic domain was also investigated to determine the topology of an individual TPC domain. As $TPC2^{1-339}$ is without most of the domain linker, the second domain and the C-terminus, its localisation was first ascertained. Figure 4.7A shows that as with full-length TPC2, $TPC2^{1-339}$ colocalises with the lysosomal marker LAMP1, suggesting trafficking is not affected. When applied to the FPP assay, $TPC2^{1-339}$ GFP fluorescence decreased

by ~ 59 %, again indicative of a cytosolic location. This confirms that within TPC2 domain I there is an even number of transmembrane regions, likely six (Figure 4.7B).

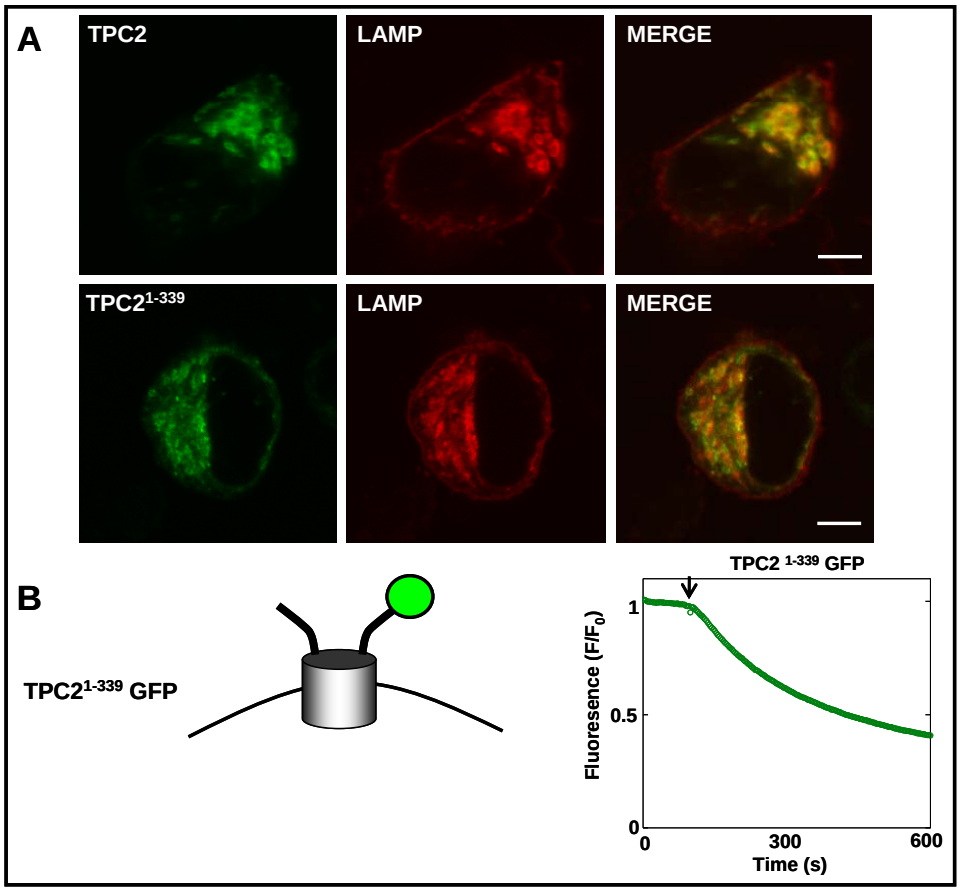

Figure 4.7. TPC2 domain I localises to the lysosome and has an even number of TM regions. (A) Full-length TPC2-GFP and TPC2$^{1-339}$ GFP expressed in SKBR3 cells colocalise with the lysosomal marker LAMP1-mRFP. (B) After selective permeabilisation by digitonin, the fluorescence intensity of TPC2$^{1-339}$ GFP expressed in HEK cells decreases upon trypsin addition as monitored by FPP analysis.

The extent of fluorescence intensity decrease at 600 s and initial rate of decrease upon trypsin addition for each of the constructs tested is summarised in Table 4.4. The extent decrease ranged from ~99 % to 48 % for degraded constructs and 33 % for the protected luminal tag of TPC1$^{1-628}$ GFP. Additionally the rate of decrease was least for TPC1$^{1-628}$ GFP (0.0009 U/s ± 0.000267) providing further evidence that tag of this construct is protected from degradation and therefore luminal.

Construct	n	% Extent at 600s	Initial Rate U/s
RFP TPC1	2	51	0.00102
TPC1$^{1-623}$ GFP	5	33 ± 6	0.0009 ± 0.000267
TPC1 RFP	2	99	0.0146
TPC1 GFP	2	92	0.0136
RFP TPC2	6	88 ± 6	0.00665 ± 0.00187
TPC2$^{1-393}$ GFP	5	59 ± 10	0.00224 ± 0.00060
TPC2 RFP	2	48	0.00132
TPC2 GFP	9	60 ± 6	0.00245 ± 0.00065

Table 4.4. Summary of FPP analysis. Extent of fluorescence intensity decrease at 600 s and initial rate calculated from the average of *n* experiments ± S.E.M (where applicable).

In summary FPP assays reveal that TPCs have cytosolic N- and C-termini and an even number of TM regions, most likely twelve with six TM regions in each domain.

4.3.3 Mapping of TPC antibody epitope sequences

The topology of TPCs was further investigated by exploiting different TPC antibody epitope sequences. A schematic of this principle is shown in Figure 4.8.

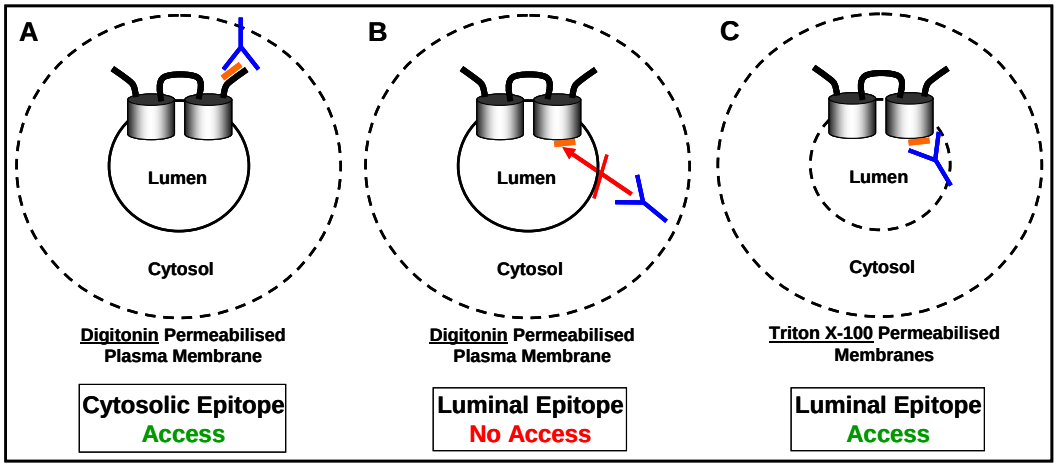

Figure 4.8. Antibody epitope mapping can discriminate between cytosolic and luminal epitopes. When the plasma membrane of the cell is selectively permeabilised by digitonin treatment, antibodies can bind epitope sequences (orange) that are cytosolic **(A)** but not luminal **(B)**. Luminal epitopes become accessible when the intracellular and plasma membranes are permeabilised by Triton X-100 treatment **(C)**.

As already shown by the FPP assay, digitonin selectively permeabilises the plasma membrane of the cell. This principle is also applied to the mapping of TPC antibody epitope sequences (Figure 4.8). When the plasma membrane is selectively permeabilised by digitonin treatment, epitope sequences that are cytosolic are accessible to antibody binding (Figure 4.8 A) however luminal epitopes are inaccessible (Figure 4.8 B) and no immunostaining is observed. Luminal epitopes can only be accessed upon permeabilisation of intracellular membranes by Triton X-100 (Figure 4.8C).

The results of epitope mapping by immunostaining are shown in Figure 4.9. TPC1 and TPC2 tagged with a fluorophore at the C-terminus were clearly visible in each population of cells (Figure 4.9 A-C, GFP or mRFP). The Santa Cruz antibody raised against a peptide sequence corresponding to the C-terminus of TPC1 is able to bind the protein when membranes are permeabilised with Triton X-100 or when the plasma membrane only is selectively permeabilised by digitonin (Figure 4.9A). This independently confirms the findings of the FPP assay that the C-terminus of TPC1 is cytosolic.

The same conclusion was reached when the location of the TPC2 C-terminus was mapped using an antibody raised to the C-terminus of TPC2 (Figure 4.9B). However using an antibody raised to a region adjacent to pore I of TPC2, antibody # 34 could only access the epitope when the intracellular membranes were permeabilised by Triton X-100 (Figure 4.9C). This places the epitope in a luminal location, as predicted in the 12 TM region model. The location of C-terminal epitopes as cytosolic and the region preceding pore I as luminal supports the conclusions of the FPP analysis.

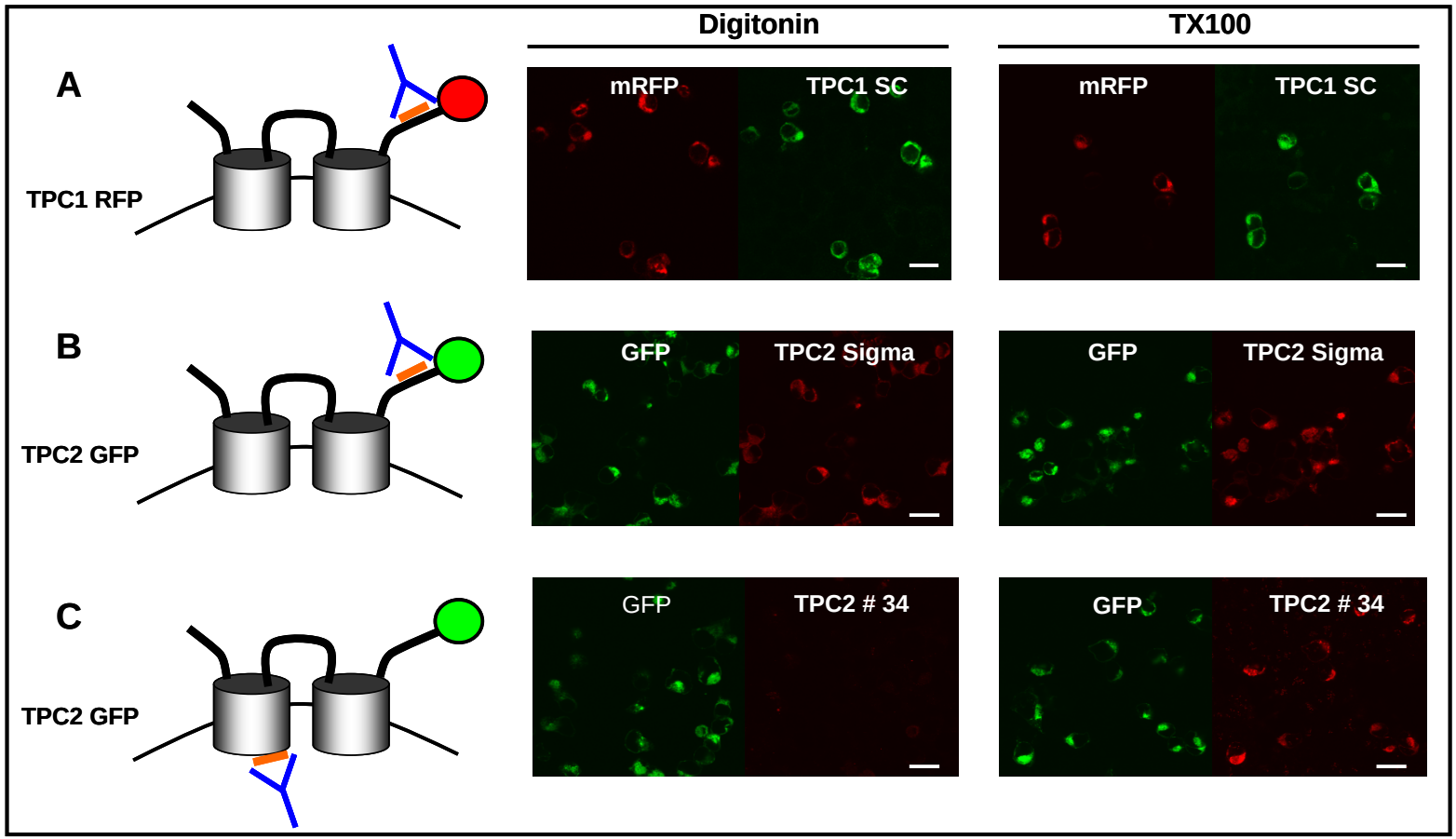

Figure 4.9. Mapping the epitopes of TPC antibodies after selective membrane permeabilisation reveals TPC topology. HEK cells expressing the indicated construct were permeabilised with either digitonin or Triton X-100 and the ability of antibodies to access epitope sequences was assessed by immunostaining. Cytosolic epitopes are accessible when the plasma membrane is selectively permeabilised by digitonin while luminal epitopes are not. Scale bar 20µm.

4.3.4 Mapping of HsTPC N-glycosylation sites

A third independent method with which TPC topology can be defined, is the mapping of N-glycosylation sites. N-glycosylation is the modification of luminal asparagine residues by the addition of carbohydrate side-chains (Kukuruzinska & Lennon, 1998). This has been demonstrated for SpTPCs (Figure 2.6) (Brailoiu *et al.*, 2010a;Ruas *et al.*, 2010) as well as mouse TPCs (Zong *et al.*, 2009) and HsTPC2 (Calcraft *et al.*, 2009). Mapping of glycosylated asparagine residues therefore defines luminal sites.

Following the demonstration that SpTPC1 and SpTPC2 are N-glycosylated (Figure 2.6), this analysis was extended to human TPC orthologues. Western blotting of HsTPC1-GFP reveals two bands at approximately 130 ± 5 kDa and 100 ± 5 kDa (n=8) which after treatment with PNGase F are decreased in size to a single band of 95 kDa ± 2 kDa (n=4) (Figure 4.10). Like the SpTPCs, the presence of two protein bands would seem to represent full and core glycosylated species of the protein which are consolidated into a single deglycosylated species upon PNGase F treatment. The same pattern is observed with HsTPC2 with two bands at ~ 100 ± 5 kDa and 82 ± 5 kDa (n=7), decreased in size to 77 ± 2 kDa after PNGase F pre-treatment. For TPC2, bands corresponding to a dimer molecular mass are also present (Figure 4.10, arrow).

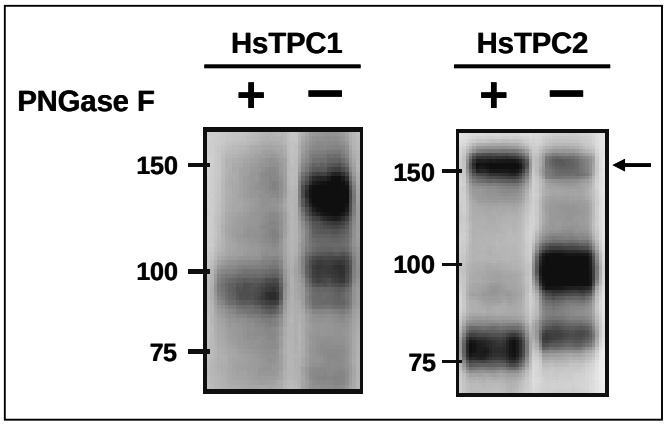

Figure 4.10. Treatment with PNGase F reveals HsTPCs to be glycoproteins. Western blot of solubilised HEK protein sample expressing either HsTPC1 or HsTPC2, mock treated (-) or treated with PNGaseF (+) to remove oligosaccharide side-chains before resolution by SDS-PAGE. The arrow indicates a possible dimer-sized protein band.

Therefore both TPC1 and TPC2 are N-glycosylated. This validates the localisation of luminal glycosylated asparagine residues as a means of defining TPC topology.

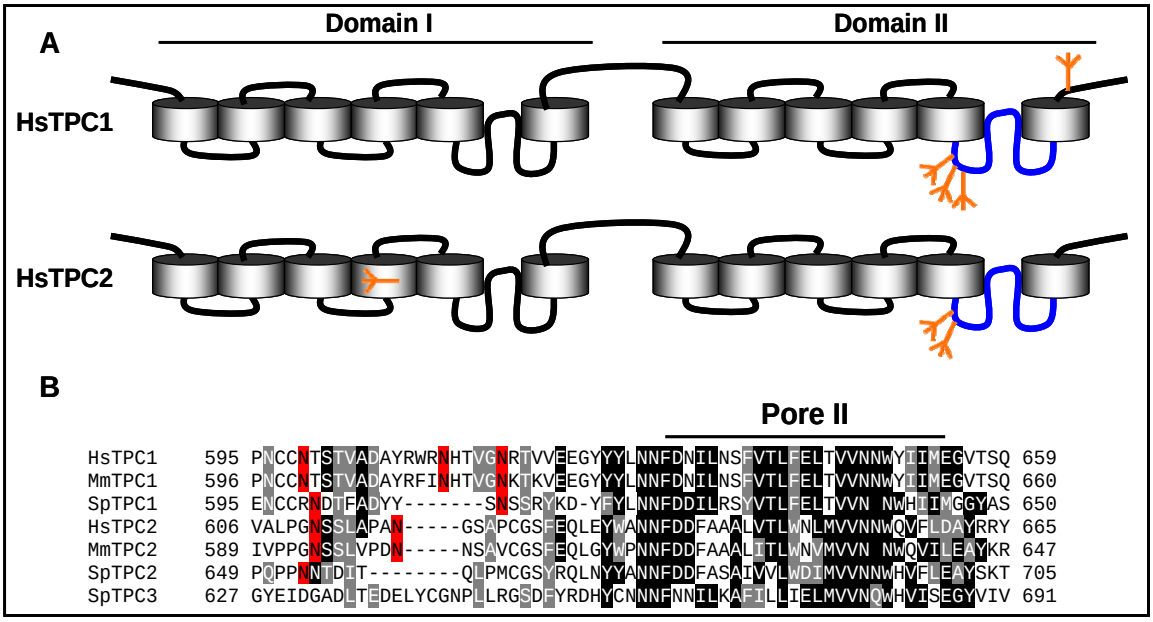

Figure 4.11. Conservation of TPC asparagine residues adjacent to pore II. (A) Schematic representation of TPC1 and TPC2 showing approximate locations of glycosylated asparagine side chains (orange). The region of the channel aligned in (B) is highlighted in blue. **(B)** Multiple sequence alignment of human (Hs), mouse (Mm) and sea urchin (Sp) TPCs sequence between transmembrane region five and six of domain II encompassing pore II.

The N-glycosylation of asparagine residues conforms to a well defined consensus sequence (NxT/S where x is any amino acid except P). Asparagine residues that are predicted to be N-glycosylated are marked on a schematic of TPC1 and TPC2 (Figure 4.11A). In both cases glycosylation is predicted in a luminal cluster preceding pore II. A multiple sequence alignment of human, mouse and sea urchin regions preceding and encompassing pore II shows that putative N-glycosylation sites are highly conserved in this region through the deuterostome lineage (Figure 4.11B). HsTPC1 has three predicted N-glycosylation sites in this region at Asn599, 611 and 616 and HsTPC2 has two at Asn611 and 618. HsTPC1 is also predicted to

have a glycosylated residue at Asn695 a site in the C-terminus which we have now confirmed to be cytosolic (Figures 4.5B & 4.9A) and can be discounted. HsTPC2 has a further asparagine residue predicted to be glycosylated at position 198. Although this is in a TM region that is poorly predicted by algorithms, FPP and epitope mapping has confirmed that TM 4 must be present. SpTPC3 has no asparagine residues in the pore II region that conform to the N-glycosylation consensus sequence and we have shown that SpTPC3 is not glycosylated (Figure 2.6). The cluster of putative N-glycosylated residues preceding pore II, specifically in HsTPC1 were therefore investigated.

To examine the glycosylation state of asparagine residues 599, 611 and 616 in TPC1, these residues were individually mutated to glutamine, an amino acid with similar polarity, hydrophobicity and neutral charge but unable to be N-glycosylated.

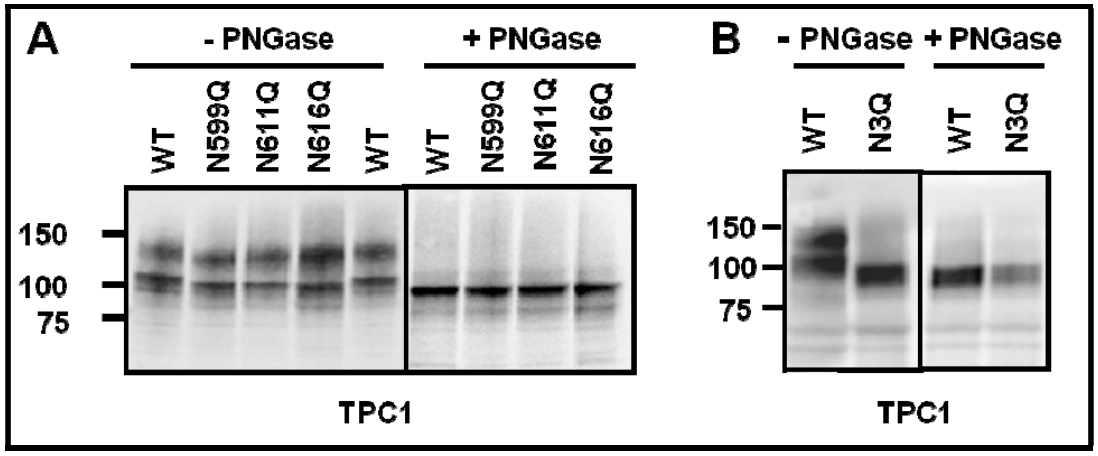

Figure 4.12. PNGase F treatment of glycosylation mutants reveals Asn599, 611 and 616 are responsible for N-glycosylation of TPC1. Western blot analysis of single point N-glycosylation mutants or the triple N3Q glycosylation mutant treated with (+) or without (-) PNGaseF and mobility compared to wild-type (WT) TPC1. No change in mobility is seen with the N3Q mutant in the presence or absence of PNGase F.

When any one of N599, N611 or N616 were mutated to glutamine, each caused a slight decrease in apparent size on SDS-PAGE compared to wild-type (WT) in the absence of PNGaseF treatment (Figure 4.12A). Upon treatment with PNGase F, all three mutants decrease in apparent size by SDS-PAGE, to a single deglycosylated species of ~95 kDa. However, when all three asparagine residues are mutated there

is no apparent change in mobility by SDS-PAGE between PNGase and mock treated samples. A protein band of ~95 kDa, a size that corresponds to WT TPC1 post PNGase treatment (Figure 4.13B) is present. This suggests that the three residues account for the total N-glycosylation of TPC1 and furthermore, confirms their location on the luminal face of the protein.

4.3.5 The localisation of TPC1^{N3Q}

N-glycosylation has been shown to regulate endo-lysosomal protein trafficking (Chikh *et al.*, 2004). The intracellular distribution of wild-type TPC1 and TPC1^{N3Q} expressed in HEK293 and SKBR3 cells was examined.

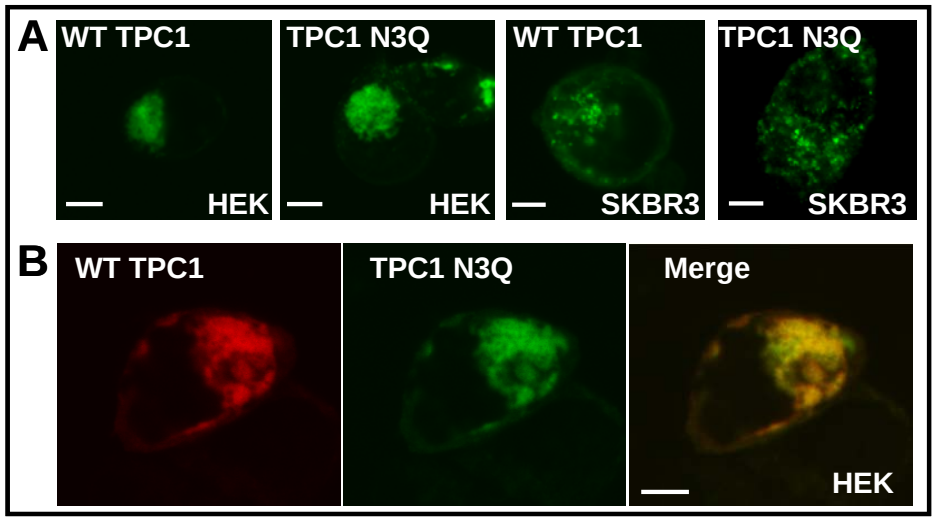

Figure 4.13. Localisation of TPC1 N3Q is not altered from wild-type. (A) WT TPC1 or TPC1 N3Q were expressed alone in HEK and SKBR3 cells to examine distribution. **(B)** HEK cells were also co-transfected with WT and N3Q TPC1. Scale bars 5µm.

When the distribution of protein was compared between WT TPC1 and TPC1 N3Q, both appeared to be intracellular and perinuclear with a punctate appearance indicative endo-lysosomal localisation. This was most apparent in SKBR3 cells (Figure 4.13A). Furthermore when co-expressed in the same cell (Figure 4.13B), WT and N3Q TPC1 colocalised, suggesting that the N3Q trafficking and localisation is not perturbed by the absence of glycosylation. Glycosylation therefore appears not to regulate trafficking of HsTPC1 to the endo-lysosomal system.

4.4 Discussion

Utilising unbiased prediction algorithms, FPP assays, antibody epitope mapping and the examination of glycosylated residues, the topology of TPCs was investigated. The exact architecture of the channel using an *in silico* approach was ambiguous with no consensus on the total number of TM regions predicted. FPP analysis demonstrated that both TPC isoforms have cytosolic N- and C-termini and therefore an even number of TM regions. Within individual domains, an even number of TM regions was also confirmed. The cytosolic location of the C-terminus was further supported by mapping of C-terminal antibody epitopes. Sites predicted to be luminal on the TPCs were also validated by FPP assay and epitope mapping. Luminal glycosylation sites adjacent to pore II of TPC1 were confirmed and shown not to be involved in expression or localisation of the channel. Overall the data supports the prediction that TPCs have an even number of TM regions, most likely 12, with cytosolic N and C termini. The findings and the residues examined to reach this conclusion are summarised in Figure 4.14.

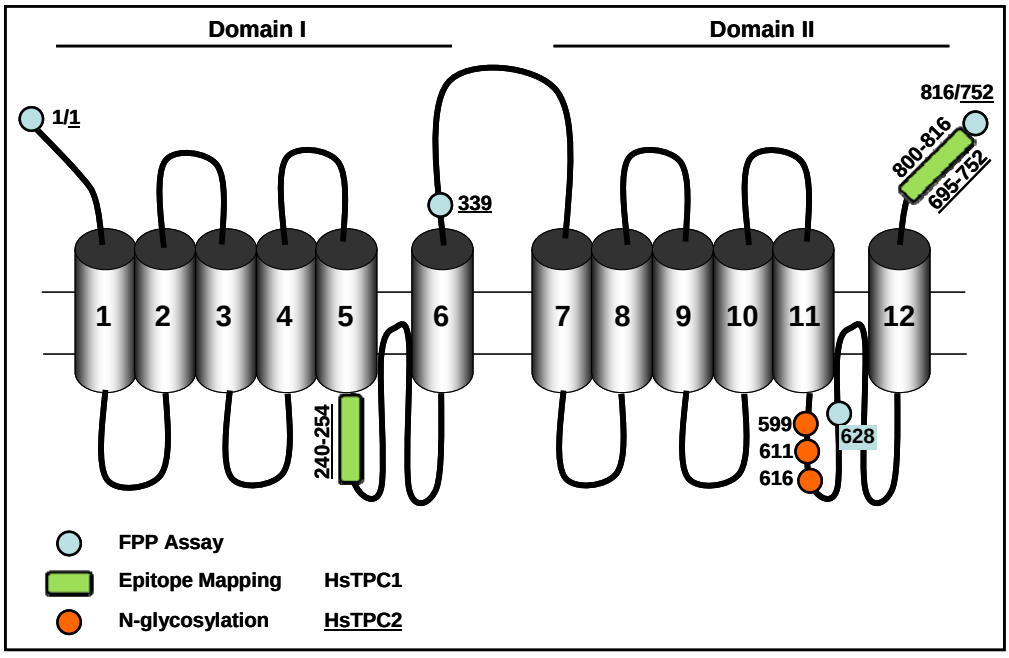

Figure 4.14. Schematic of a TPC based on experimental assessment of TPC topology. The position of residues defined in the preceding experiments from FPP, epitope mapping and glycosylation mutation are marked.

It was important to define the topology of the TPCs in order to understand their function and regulation. For example, an odd number of TM regions would place the termini on either side of the organelle membrane. As termini are important sites for protein interaction and oligomerisation in numerous channels (Lepage *et al.*, 2009;Feng *et al.*, 2011), this would influence channel regulation. If TPCs did not have two domains of six TM regions, this would make them distinct from the repeat pattern seen in voltage-gated Ca^{2+} and Na^{+} channels and perhaps preclude the necessity for a four-pore arrangement needed to form a functional channel.

TM region prediction algorithms failed to predict the fourth TM region in each domain. This is likely due to the presence of positively charged amino acid residues in this region (Figures 4.2 and 4.3). In voltage-sensitive channels, the fourth TM in each domain acts as the voltage sensor due to the presence of these positively charged amino acids (Liman *et al.*, 1991). It seems likely that TPCs have evolved from voltage-sensitive channels, although TPC2 does not appear to be voltage-sensitive (Brailoiu *et al.*, 2010b). Conversely, some algorithms predict the pore as a TM region. This is likely due to the presence of hydrophobic amino acids which may be necessary for the pore of the channel to form through the membrane. The putative pore region had previously been defined for TPC1 and TPC2 by mutation of conserved leucine residues (L273 and L265, respectively) to a helix-breaking proline residue, rendering the pore unable to conduct ions (Brailoiu *et al.*, 2009a;Brailoiu *et al.*, 2010b). The discrepancies seen between prediction algorithms therefore make experimental analysis of topology a necessity.

FPP analysis showed that TPCs have an even number of TM regions with cytosolic N- and C-termini, supporting the 12 TM region model. The luminal fluorophore of $TPC1^{1-628}$ supported the presence of TM regions 4 and 10 and indicated the putative pore region is not membrane spanning as predicted by some algorithms. The converse of this scenario would lead to a cytosolic fluorophore which would be degraded (Figure 4.5). Decreased fluorescence with $TPC2^{1-339}$ also confirmed an even number of TM regions within domain I (Figure 4.7). The N-terminus has been

determined to be cytosolic, therefore if the poorly predicted TM region 4 was absent there would be an odd number of TM regions in domain I and the fluorophore at position 339 would be luminal and thus protected. Therefore the most likely number of transmembrane regions is indeed six. By extension we can infer an even number of TM regions in domain II, again probably six, otherwise the C-terminus would be luminal if an odd number were present.

Further TPC truncated constructs have also been examined by FPP analysis (Hooper *et al.*, 2011). $TPC1^{1-225}$ was tagged after the poorly defined TM region 4 of domain I. A decrease in fluorescence upon trypsin addition placed this tag in the cytosol and provided further evidence of TM region 4. If TM4 did not exist, an odd number of TM regions would precede the tag at position 225, placing it in a luminal location. $TPC1^{1-347}$, tagged after domain I, also supported an even number of TM regions in TPC1 domain I as the tag was cytosolic and cleaved. This is in accordance with domain II of TPC2 (Figure 4.6).

Of interest is the variation between extent and rate of degradation of cytosolic fluorophores by FPP assay (Table 4.4). The extent of decrease in fluorescence for the N-terminus was much more pronounced for TPC2 (~88%) than TPC1 (~50%). Conversely the extent of decrease was less for the C-terminus of TPC2 (~55%) compared to TPC1 (~95%). This may suggest that some cytosolic fluorophores are more accessible than others. The variation between degradation of tags at predicted cytosolic termini could be due to folding of the termini or interaction between the termini and either other proteins or within the protein itself. Both TPC1 and TPC2 tagged at the C-terminus are functional (Brailoiu *et al.*, 2009a) arguing against misfolding of protein. Furthermore when TPC2-GFP was probed with an antibody that recognised a predicted luminal epitope in cells where only the plasma membrane had been permeabilised, no immunostaining was observed, suggesting that no sub-population of the protein is inserted into the membrane in an inverted orientation. This supports the notion that the termini themselves are variable between isoforms and may play a role in channel regulation.

The FPP assay utilised tagged protein that was greatly over-expressed. This makes possible interaction of termini with accessory proteins unlikely unless such proteins were highly abundant. It may therefore be that the termini are associating with regions on other TPCs or within the same channel protein. The N-terminus of TPCs could be mediating oligomerisation between TPC channels such as has been demonstrated for the N-terminus of TRPC4 (Lepage *et al.*, 2009). Alternatively the termini may be interacting with another region on the same protein such as the N-terminus of the hERG potassium channel which interacts with the TM 4-5 linker to regulate channel gating (de la Pena *et al.*, 2011). Subsequent to publication of the results detailed in this chapter (Hooper *et al.*, 2011), similar methodology was employed to determine the topology of TRPP2, a close relative of the TPCs (Hoffmeister *et al.*, 2010). TRPP2 was demonstrated to contain six TM regions with cytosolic N- and C-termini, analogous to half a TPC protein.

The slight loss of fluorescence seen with the predicted luminal tagged $TPC1^{1-628}$ GFP could be due to the heterogeneous distribution of TPC1 within acidic and unidentified organelles. Such a range of organelles may have slightly different membrane compositions (such as higher cholesterol) leading to more rapid permeabilisation by digitonin. TPC1 has been shown to be present in recycling endosomes (Calcraft *et al.*, 2009) and these are known to be enriched in cholesterol (Gagescu *et al.*, 2000;Hao *et al.*, 2002). This suggests that recycling endosomes could be more readily permeabilised by digitonin leading to cleavage of luminal GFP upon trypsin addition.

HsTPCs, like their sea urchin orthologues (Chapter 2, Figure 2.6) were shown to be N-glycosylated. For HsTPC1 the sum of this glycosylation was pinpointed to residues N599, N611 and N616, clustered adjacent to pore II (Figure 4.11, 4.12). In relation to topology, this confirms the location of these asparagine residues to the luminal face of the channel as only luminal residues can be N-glycosylated. When any one of these residues was mutated there was only a very slight shift in mobility

by SDS-PAGE (Figure 4.12).This may suggest that all three contribute equally to the glycosylation of HsTPC1, although it may not preclude some redundancy whereby only two of the residues may be glycosylated. The observed mobility shift when only one of the three asparagines residues was mutated did not appear to account for a third of the size difference between full and deglycosylated forms. The clustering of the residues may lead to steric hindrance whereby only two of the three possible asparagine residues can be glycosylated.

Calcraft et al first demonstrated that HsTPC2 is N-glycosylated as shown by sensitivity to PNGase F (Calcraft *et al.*, 2009) and Zong et al extended this to mouse TPC1 and TPC2 (Zong *et al.*, 2009). Zong et al. showed the lower protein band of both isoforms to be EndoH sensitive suggesting this represents the core-glycosylated species while the upper band is the mature, fully glycosylated channel. They demonstrated by mutagenesis that N-glycosylation of mouse TPC2 was accounted by the two asparagines residues adjacent to pore II. As shown in Figure 4.11 B, predicted mouse glycosylated asparagine residues show good conservation with HsTPC sequences.

It is interesting to note that SpTPC2 has only one predicted glycosylated asparagine residue adjacent to pore II (Figure 4.11 B). SpTPC2 does however have a cluster of three asparagine residues in a similar position, adjacent to pore I. It would be informative to examine the effect removal of glycosylation residues from either pore I or pore II in this isoform and how this compares to deglycosylated human TPCs. It would also be of interest to examine the distribution of glycosylated residues in species intermediate to the sea urchin (as a basal deuterostome) and humans to see if the switch in glycosylation from pore I to pore II evolved over time and for what reason.

Preventing N-glycosylation in $TPC1^{N3Q}$ did not appear to alter protein expression levels or degradation (Figure 4.12). When equal amounts of total protein were resolved by SDS-PAGE and visualised by Western blot, there was no apparent

difference in protein band intensity between wild-type and the N3Q mutant (Figure 4.12B). Glycosylation-defective mutants have previously been shown to have compromised expression, as demonstrated for the glucose transporter GLUT4 (Haga *et al.*, 2011). There was also no evidence of protein degradation products with the N3Q mutant. It therefore seems that the addition of oligosaccharides do not protect the protein from the harsh acidic environment of the endo-lysosome lumen as is observed with other lysosomal proteins such as LAMP1 (Kundra & Kornfeld, 1999) and P2X4 (Qureshi *et al.*, 2007). N-glycosylation has also been shown to regulate trafficking of proteins to the endo-lysosomal system, as with Niemann–Pick disease type C protein 2 (NPC2) (Chikh *et al.*, 2004). However, the localisation of the $TPC1^{N3Q}$ mutant does not seem to be perturbed as it is still present in intracellular vesicles and colocalises with wild-type TPC1 (Figure 4.14).

The position of the glycosylated residues adjacent to pore II lead us to suspect glycosylation could be regulating channel flux itself. When NAADP was microinjected into cells over-expressing the TPC1 N3Q mutant, a potentiation of intracellular Ca^{2+} release greater than wild-type was observed (Hooper *et al.*, 2011). It is clear that N-glycosylation adjacent to pore II is therefore serving to negatively modulate Ca^{2+} flux through the channel. The addition of oligosaccharide side-chains may result in structural changes to the channel pore that decrease channel conductance. Alternatively the negative charge of oligosaccharide side-chains may influence binding of luminal Ca^{2+} or H^{+}, both of which have been proposed to regulate TPC2 activity (Pitt *et al.*, 2010). As a post-translational modification, glycosylation could be a dynamic means of regulating channel activity, increasing or decreasing flux during translation as applicable.

Precedence exists for regulation of ion channels by glycosylation. In the voltage gated potassium channel $K_v12.2$, a cluster of glycosylated residues preceding the pore loop have been shown to cause a shift to more negative potentials in the activation threshold of the channel (Noma *et al.*, 2009). Thus removal of glycosylated residues leads to a channel which activates more readily. In the case of

K_v12.2 and TPC1, glycosylation is negatively regulating the channel. Conversely with TRPV1, mutagenesis to create a de-glycosylated channel results in a decreased EC_{50} and maximal response to the channel agonist capsaicin (Wirkner *et al.*, 2005). Endogenous glycosylation of TRPV1 is therefore potentiating channel flux. N-glycosylation represents a key modulator of ion channel function and can act to both inhibit and potentiate channel activity.

In summary, we determined the topology of TPCs by utilising FPP assays, mapping of TPC antibody epitopes and examination of putative N-glycosylation sites. These techniques revealed that TPCs have 12 TM regions, with cytosolic N- and C-termini.

Chapter 5 - TPC assembly

5.1 Introduction

In Chapter 4, the topology of the TPCs was defined. The next aim was to investigate how TPCs combine to form a channel. As discussed previously, TPCs are members of the voltage-gated ion channel superfamily (Yu *et al.*, 2005). A characteristic of this family is the formation of a functional channel pore by the arrangement of four-pore domains. This channel pore can be formed by a single polypeptide, such as with Ca_vs and Na_vs, which contains all four pore domains or the tetramerisation of four polypeptides, each containing a single pore domain, as with K_vs, K_{ir}s and TRP channels. A TPC protein encompasses two pore domains and is therefore believed to be an evolutionary intermediate between single-pore domain proteins and four-pore domain proteins. Since their initial cloning, it was postulated that TPCs form dimers to create a functional channel, preserving the four-pore arrangement (Ishibashi *et al.*, 2000). In this chapter I investigate the quaternary structure of TPCs.

5.2 Methods

Plasmids

The molecular cloning of HsTPC1-GFP and HsTPC2-GFP is described in Brailoiu et al. 2009 (Brailoiu *et al.*, 2009a). The cloning of HsTPC2$^{1-339}$ GFP is described in Hooper et al 2011 (Hooper *et al.*, 2011). The cloning of GFP-HsTPC2, HsTPC1$^{1-347}$-*myc*, HsTPC1$^{1-347}$-GFP, HsTPC1$^{348-426}$-*myc*, HsTPC1$^{427-816}$-*myc* and HsTPC1$^{427-816}$-GFP is described in Churamani et al (Churamani *et al.*, 2011). The cloning of HsTPC1-*myc* and HsTPC2-*myc* is described in Yamaguchi et al 2011 (Yamaguchi *et al.*, 2011). The ptdTomato-C1 vector and LAMP1-tdTom were kindly provided by Colin Taylor's lab (Cambridge). HsTPC2-tdTom was created by restriction digest of TPC2-GFP at XhoI/EcoRI sites and subsequent ligation of the product into the tdTomato vector. HsTPC2$^{1-339}$-*myc* was created by restriction digest of HsTPC2$^{1-339}$-GFP at XhoI/XbaI sites and subsequent ligation of the product into pCS2+-*myc*. TPC2$^{422-752}$ was generated by PCR amplification from full-length TPC2 using the gene specific primers (restriction sites underlined) 5'-CGCGAATTCATGGCGTTTCTGCAGAGCGCCCAG-3' (forward) and 5'-AGGCTCGAGCCTGCACAGCCACAGGT-3' (reverse) encompassing EcoRI and XhoI restriction sites respectively. PCR amplification was by Platinum® *Taq* DNA polymerase High Fidelity (Invitrogen) for 30 cycles with an annealing temperature gradient of 55°C ± 5°C. The elongation temperature was 68°C for 60 sec (30 sec / kb product). The 1,002 base pair PCR product was subsequently digested at EcoRI/XhoI restriction sites and ligated into pCS2+ with either a GFP or *myc* tag at the C-terminus.

The constructs utilised in this chapter are summarised in Figure 5.1.

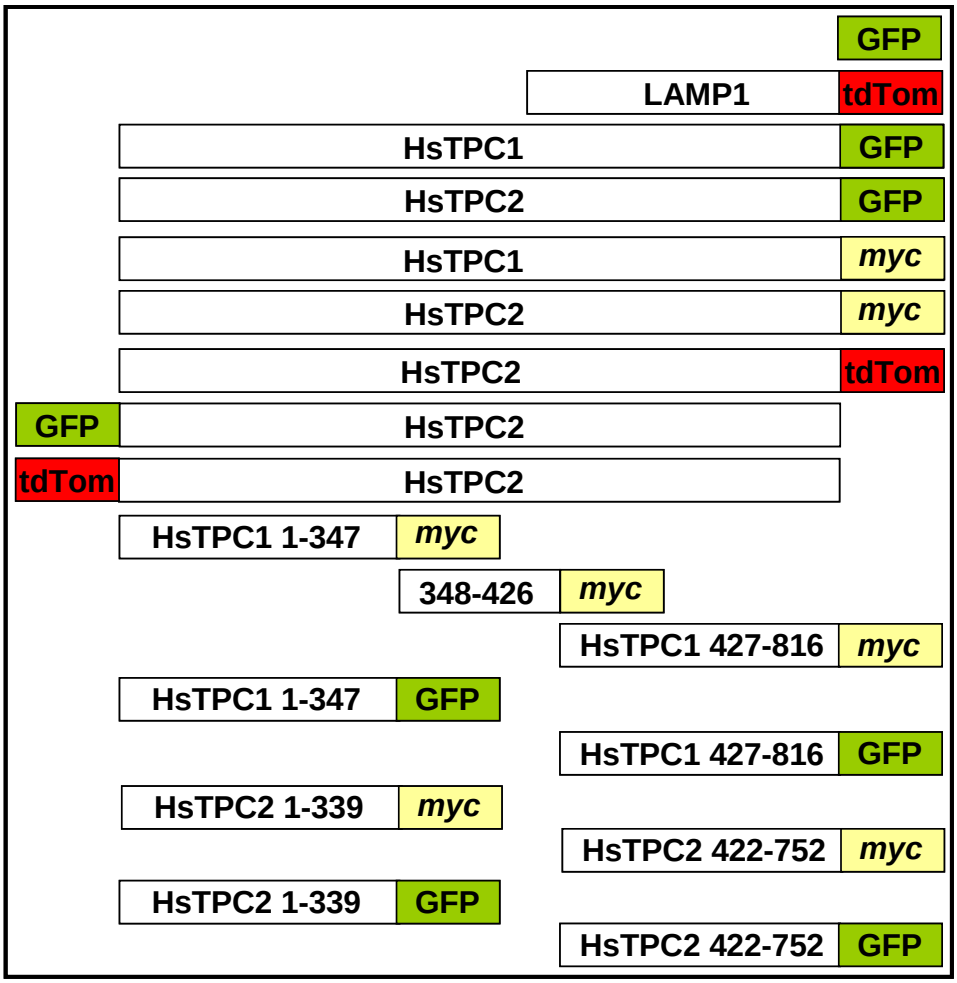

Figure 5.1. HsTPC clones utilised in the characterisation of channel assembly. A schematic illustrating differentially tagged full-length and truncated TPC constructs and other plasmids used to assess TPC assembly.

Fluorescence Resonance Energy Transfer (FRET) analysis

HEK293 cells were transiently transfected with the indicated combination of plasmids. After 24 hrs, cells were washed three times in HEPES buffered saline (HBS) before FRET analysis. Cells were imaged by excitation at 488 nm (GFP, donor) for 2 ms then bleached by a 60 sec exposure of 561 nm light (tdTomato, acceptor, bleaching > 90 %) then a final image is taken at 488 nm for 2 ms. The change in fluorescence at 488 nm before and after bleaching was then measured.

FRET efficiencies were corrected for background fluorescence and crosstalk of the 488 laser to the tdTomato tag as calculated by the following formula:

$$\mathbf{E} = 1 - \left(\frac{\left[\text{Donor}_{\text{Pre}} - \text{Donor}_{\text{BG}}\right] - \left[\left[\text{Acceptor}_{\text{Pre}} - \text{Acceptor}_{\text{BG}}\right] \text{x } 0.00299 \text{ x} \left(\frac{\text{Donor}_{\text{Exp}}}{\text{Acceptor}_{\text{Exp}}}\right)\right]}{\left[\text{Donor}_{\text{Post}} - \text{Donor}_{\text{BG}}\right] - \left[\left[\text{Acceptor}_{\text{Post}} - \text{Acceptor}_{\text{BG}}\right] \text{x } 0.00299 \text{ x} \left(\frac{\text{Donor}_{\text{Exp}}}{\text{Acceptor}_{\text{Exp}}}\right)\right]} \right)$$

BG (background), Exp (exposure ms), 0.00299 (correction factor for laser crosstalk between 488 nm laser and tdTomato tag as provided by Taylor lab).

Chemical cross-linking

Transiently transfected HEK cells were scraped in their media and washed once in PBS by centrifugation. Cell pellets were resuspended in PBS pH 8 (10 µl/cm^2 of adherent cells) supplemented with EDTA-free protease inhibitor mix (Roche) and sonicated for 3 x 5 seconds. The protein concentration of the cells homogenates was estimated by BCA assay. Cell homogenates (15 µg protein) were treated with twice concentrated Bis(sulfosuccinimidyl) suberate (BS3, Thermo Scientific) at 0.1 or 0.4 mM in PBS pH 8 or mock treated with PBS pH 8 alone, both for 10 min at 37°C. After 10 min the reaction was terminated by the addition of 20 mM Tris pH 7.2. Protein (2 µg) was subsequently resolved by SDS-PAGE then visualised by Western blot as per the methods in Chapter 2.

Protein insertion assay

Transiently transfected HEK cells were scraped in their media and washed once in PBS by centrifugation. Cell pellets were resuspended in intracellular-like buffer (10 µl/cm^2 of adherent cells) composed of 110 mM potassium acetate, 2 mM $MgCl_2$, 20 mM NaHepes (pH 7.2) supplemented with EDTA-free protease inhibitor mix

(Roche) then sonicated for 1 x 5 seconds. Homogenates were centrifuged at 1000 x g for 10 min at 4°C, to remove unbroken cells and nuclei. The pellet was discarded, the supernatant recovered and diluted in an equal volume of intracellular-like buffer. Homogenates were incubated for 60 minutes at 4°C then centrifuged (90,000 x g, 60 min, 4°C). The supernatant was recovered (S) and the pellet (P) was resuspended in the original volume of intracellular-like buffer. Protein was subsequently resolved by SDS-PAGE then visualised by Western blot as per the methods in Chapter 2.

Co-immunoprecipitation

Transiently transfected HEK cells were solubilised in 1 % Triton X-100-based buffer as described in Chapter 2. Solubilised material (250 µl) was incubated with 2.5 µg of *myc* antibody (9e10, Santa Cruz Biotechnology) overnight at 4°C on a rotator. Protein was immunoprecipitated by the addition of 3.75 µl Protein-L-Agarose-conjugated beads (0.5 ml agarose / 2 ml PBS, Santa Cruz Biotechnology) for 3 hours at 4°C on rotator then samples washed three times by centrifugation in solubilisation buffer. Beads were resuspended in solubilisation buffer with NuPAGE LDS-sample buffer (Invitrogen) containing 100 mM DTT and heated at 50 °C for 60 min. Samples were then centrifuged for 60 sec at 13,000 x g to pellet beads and the supernatant recovered then resolved by SDS-PAGE as described in Chapter 2.

Recurrent molecular biology methods

Cell culture, transfection, protein preparation, SDS-PAGE, Western blotting, gel filtration analysis and sucrose density gradient centrifugation were all performed as per the methods in Chapter 2.

5.3 Results

5.3.1 FRET analysis

The ability of TPCs to form oligomeric complexes was first assessed using Fluorescence Resonance Energy Transfer (FRET). FRET relies on two fluorophores being in close proximity, so that one can act as a donor, passing emission energy to the acceptor fluorophore when the donor is excited. If the acceptor fluorophore is bleached, it can no longer absorb emission energy from the donor and thus an increase in fluorescence intensity is seen at the emission wavelength of the donor. TPC2 has readily shown dimer sized protein bands by Western blot analysis, therefore FRET efficiency was investigated with TPC2 constructs. TPC2 was tagged at either the N- or C-terminus with GFP (donor) or tdTomato (acceptor) fluorophores and combinations of these coexpressed in HEK cells.

As seen in Figure 5.2, upon bleaching of TPC2-tdTomato (acceptor), an increase in fluorescence intensity can be observed with TPC2-GFP (donor).

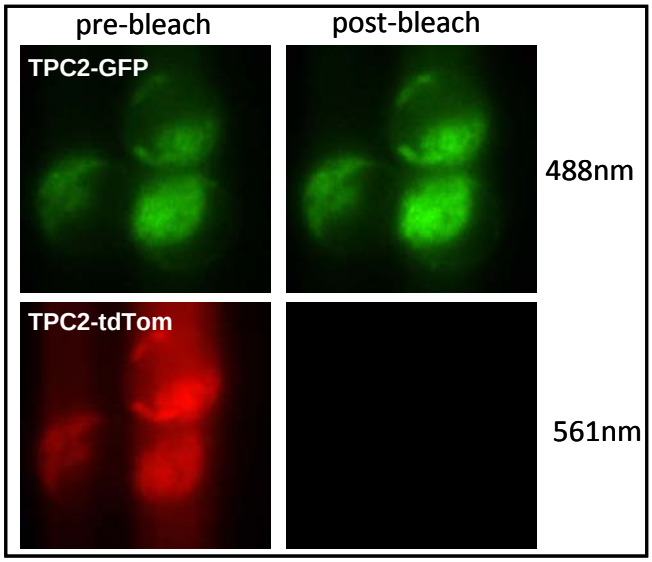

Figure 5.2. Bleaching of TPC2-tdTom causes an increase in TPC2-GFP fluorescence. HEK cells coexpressing TPC2-GFP and TPC2-tdTomato were imaged at the indicated emission wavelength before and after bleaching of the tdTomato fluorophore.

The FRET efficiencies of TPC2 constructs tagged at either the N- or C-terminus were quantified in Figure 5.3. FRET efficiency in cells coexpressing C-terminally tagged TPC2-GFP and TPC2-tdTom (C/C) was found to be ~ 0.33. When N-terminally tagged GFP-TPC2 and C-terminally tagged TPC2-tdTom (N/C) were coexpressed, FRET efficiency was lower at ~ 0.21. Similar results (FRET efficiency ~0.14) were obtained with C-terminally tagged TPC2-GFP and N-terminally tagged tdTom-TPC2 (C/N). Moreover, when N-terminally tagged GFP-TPC2 and tdTom-TPC2 (N/N) were coexpressed, FRET efficiency was ~ 0.17. FRET efficiency was therefore greatest when TPC2 plasmids were both tagged at the C-terminus. These data show that TPC2 forms oligomers and these oligomers orientate with C-termini in close proximity. The N-termini do not seem to be closely associated. When GFP-TPC2 or TPC2-GFP are coexpressed with the lysosomal marker protein LAMP1-tdTom FRET efficiency was 0.219 and 0.185 respectively. This suggests that FRET seen with C-terminal TPC2 constructs is not an artefact of protein overexpression in the confines of the lysosome.

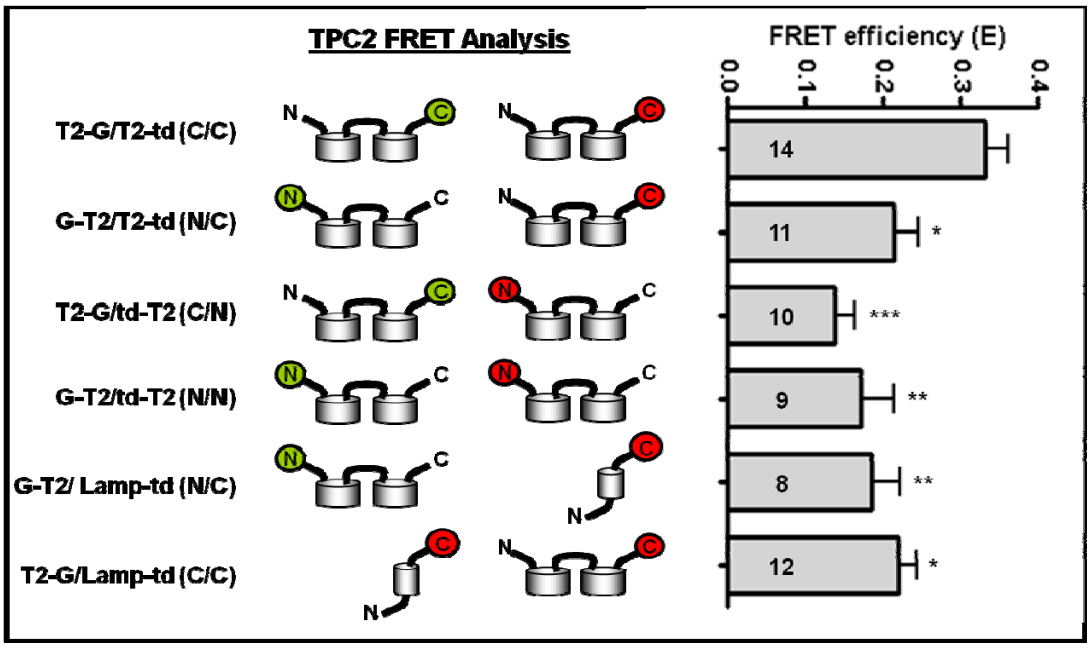

Figure 5.3. Quantification of FRET analysis reveals TPC2 forms oligomers that orientate with C-termini in close proximity. FRET efficiency was measured in HEK cells expressing the indicated combination of TPC2 (T2) or LAMP proteins tagged with either GFP (G) or tdTomato (td). Tags were introduced at either the N- or C-terminus as schematically depicted. Efficiency was corrected for background and laser crosstalk. Results are shown as mean ± s.e.m. *p = < 0.05, one-way ANOVA between T2-G/T2-td (C/C) and other combinations with Dunnett's post-test on indicated (*n*) repeats.

5.3.2 Size determination of HsTPC complexes

Having ascertained that TPC2 forms oligomers, I next sought to determine the size of these oligomers and therefore infer the stoichiometry of TPCs. The size of the native HsTPC channel was assessed by sucrose density gradient fractionation and gel filtration analysis. Sucrose density gradient centrifugation revealed the native channel molecular weight of HsTPC1 and HsTPC2 to be ~ 150 – 200 kDa (Figure 5.4A). This correlates to a dimer of TPC proteins. However gel filtration analysis determined the native channel to be > 400 kDa (Figure 5.4B) equivalent to at least a tetramer of TPC proteins. Aberrant migration of HsTPCs reflects that previously seen with the SpTPCs (Chapter 2).

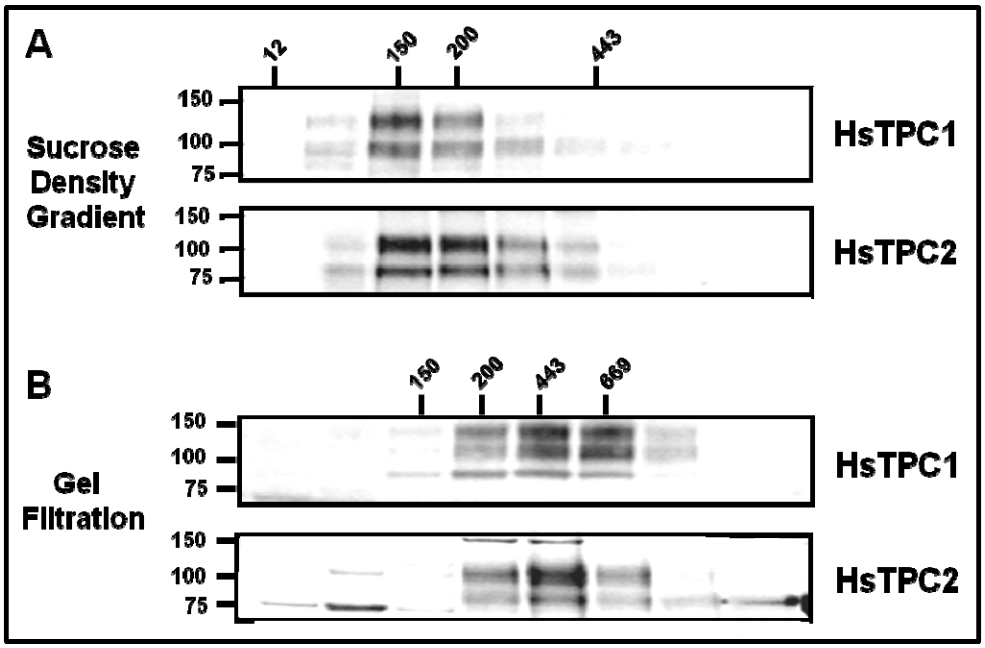

Figure 5.4. Fractionation of TPC homogenates, following sucrose density gradient centrifugation and gel filtration, reveals aberrant migration of TPCs. Western blot of fractions from HEK cell homogenates expressing TPCs, separated on a 5-20% sucrose gradient (**A**) or gel filtration column (**B**). HsTPCs appear in fractions corresponding to ~ 200 kDa by sucrose gradient centrifugation and > 400 kDa by gel filtration.

Gel filtration analysis and sucrose density gradient centrifugation do not therefore reach a consensus as to the size and therefore quaternary structure of a native HsTPC channel complex.

5.3.3 Cross-linking of TPCs

The failure of sucrose density gradient centrifugation and gel filtration column analysis to reach a consensus as to the native size of HsTPCs and SpTPCs lead to the use of chemical cross-linking agents to determine the oligomer size by Western blot. Chemical cross-linking using the lysine-reactive reagent BS3 forms stable amide-bonds between proteins within 11.4 Å, the linker arm length of BS3. These stable bonds preserve protein complexes during the reducing conditions of SDS-PAGE. BS3 cross-linking of HsTPC1 homogenates promoted the formation of a high molecular weight protein band (H) that was larger than 300 kDa in size (Figure

5.5A). HsTPC2 appeared as monomeric (1, ~100 kDa) and dimeric (2, ~ 200 kDa) forms in the absence of cross-linker. However, TPC2 was also promoted into a large complex (H) upon treatment with BS3 (Figure 5.5A). High molecular weight complexes were not seen when GFP was cross-linked, suggesting complex formation is not an artefact of the cross-linking reagent (Figure 5.5C).

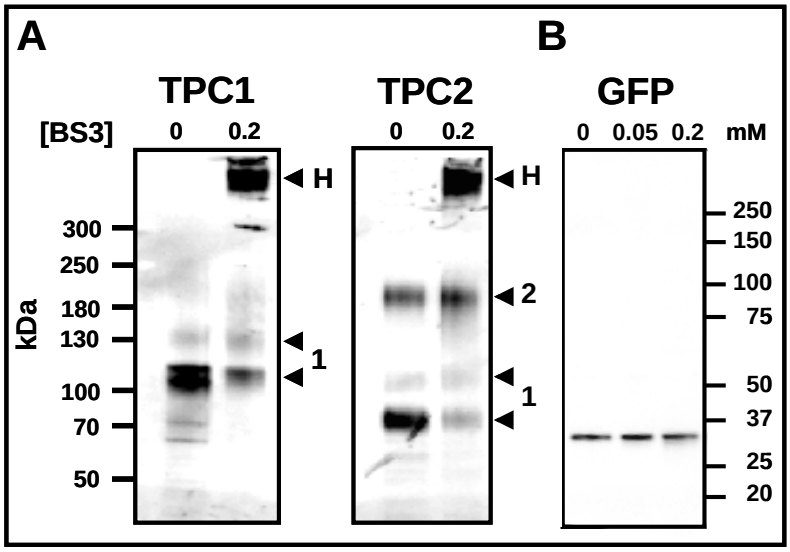

Figure 5.5. Cross-linking of TPCs promotes the formation of high molecular weight complexes. Western blot of TPC-*myc* **(A)** and GFP **(B)** expressing HEK homogenates treated with BS3 (0-0.2 mM) then resolved by SDS-PAGE and Western blot. Protein bands were visualised at sizes corresponding to monomers (1), dimers (2) and high molecular weight complexes (H).

TPCs therefore appear as high molecular weight complexes of > 300 kDa that are beyond our capacity to accurately size by SDS-PAGE.

5.3.4 Membrane insertion of TPC domains

To further investigate the quaternary structure of TPCs, the constituent domains were analysed. To validate the use of TPC domains, it was first ascertained if channel domains were capable of independently inserting into intracellular membranes. This is particularly crucial to establish for domain II, as the necessary information required for the protein to insert is more likely encoded towards the N-

terminus and insertion of domain II may occur cooperatively with domain I and not independently. TPC expressing homogenates were fractionated to yield a pellet fraction containing membrane bound protein and supernatant containing soluble, cytosolic proteins. Figure 5.6 reveals that when TPC1 is fractionated in intracellular-like buffer, domain I (DI) and domain II (DII) are resolved predominately in membrane fractions (83 % and 79 % recovery respectively). In contrast 90 % of the domain linker, which has previously shown to be cytosolic (Chapter 4), appears in the supernatant containing soluble proteins. This indicates that TPC1 domain I and domain II can independently insert into membranes. Multiple bands were observed for domain II but not domain I of TPC1, most likely representing N-glycosylation of sites adjacent to pore II.

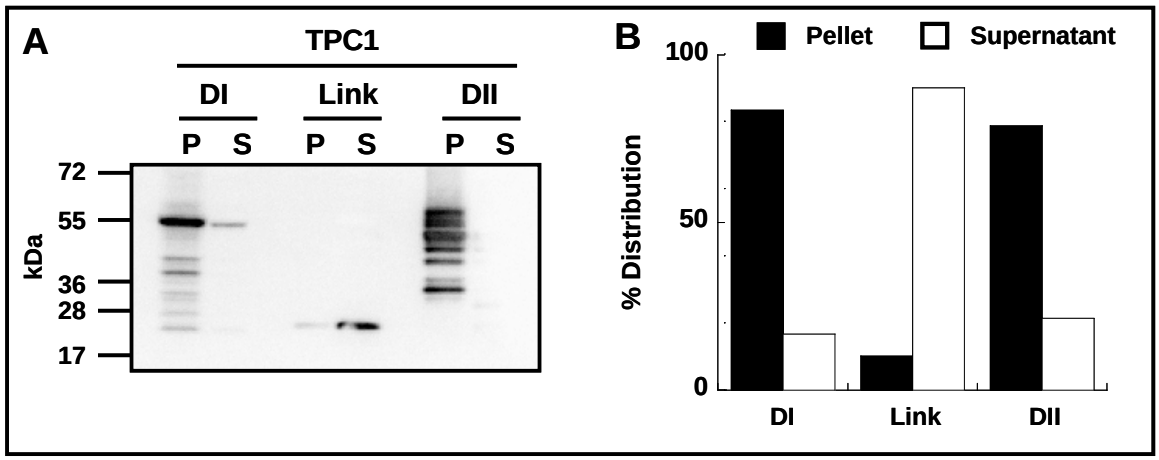

Figure 5.6. TPC1 hydrophobic domains independently insert into membranes while the domain linker is cytosolic and does not integrate. (A) Western blot of *myc*-tagged TPC1 domain I (DI), domain linker (Link) and domain II (DII) separated in intracellular-like buffer into membrane pellet (P) and cytosolic supernatant (S) fractions. (**B**) The percentage distribution between fractions was then analysed by densitometry of protein bands.

Similar results were observed for TPC2. Both TPC2 domain I (98 % pellet recovery) and domain II (DII 96 % pellet) could independently insert into membrane fractions in intracellular-like buffer (Figure 5.7) with domain II again showing evidence of multiple bands that may be indicative of N-glycosylation.

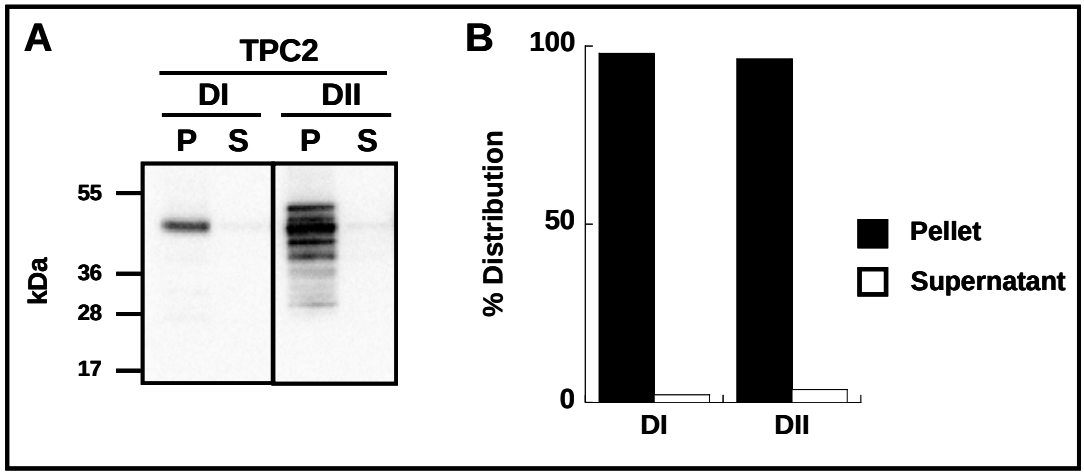

Figure 5.7. TPC2 hydrophobic domains independently insert into membranes. (A) Western blot of *myc*-tagged TPC2 domain I (DI) and domain II (DII) fractionated into the membrane protein pellet (P) or cytosolic protein supernatant (S) in intracellular-like buffer. (**B**) The percentage distribution between fractions was then analysed by densitometry of protein bands.

Both hydrophobic domains of TPC1 and TPC2 are therefore capable of independent insertion into the membrane without the necessity to be expressed in the context of the full-length protein.

5.3.5 Co-immunoprecipitation of TPC domains

Having established that individual TPC domains can insert into membranes in isolation, the contribution of these domains to the oligomerisation of TPCs was assessed by co-immunoprecipitation. Co-immunoprecipitation could establish whether potentially both domains contribute to the interaction between monomers in the formation of a stable channel and from this, inferences as to the orientation of domains in the channel oligomer could be made.

TPC domains tagged at their C-terminus with either *myc* or GFP were coexpressed in HEK cells. TPC1 domain I-*myc* was shown to immunoprecipitate with TPC1 domain I-GFP suggesting domain I in TPC1 forms interactions that can mediate oligomer formation. The same result was also observed with TPC1 domain II

(Figure 5.8A). Each individual domain of TPC1 is therefore able to form homointeractions. The individual domains of TPC2 were also able shown to form homologous interactions suggesting this capability is common to both isoforms.

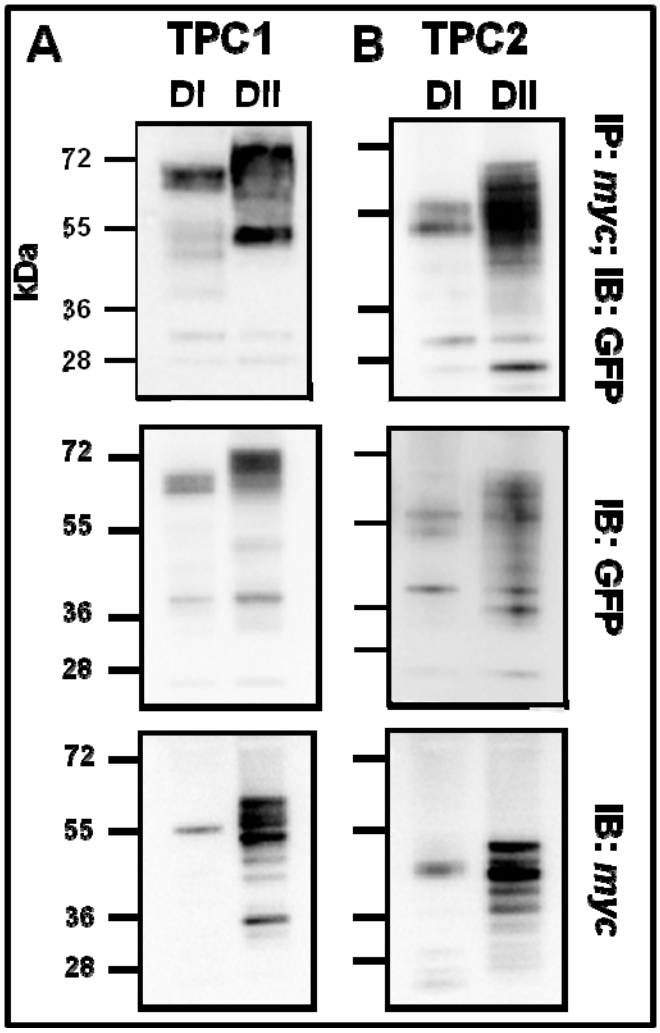

Figure 5.8. Co-immunoprecipitation of TPC hydrophobic domains reveals they are capable of homologous interaction. Western blots show HEK homogenates expressing TPC domain I (DI) or II (DII) tagged with GFP co-immunoprecipitate with homologous *myc*-tagged TPC domains (top) when over-expressed together. Homogenates were probed for GFP (middle) or *myc* (bottom) to visualise protein expression.

5.3.6 Cross-linking of TPC domains

Individual TPC domains can insert into the membrane and interact as shown by co-immunoprecipitation. Next the ability of these domains to oligomerise was assessed by chemical cross-linking. Full-length TPC constructs were promoted into high molecular weight complexes by cross-linking (Figure 5.5), therefore smaller, individual TPC domains were examined by SDS-PAGE and Western blot to more accurately resolve the size of TPC cross-linked complexes.

As shown in Figure 5.9A, TPC1 domain I is visualised as a protein band of ~ 66 kDa in the absence of cross-linking reagent (1). Upon the addition of 0.05 mM BS3, the formation of a protein band of ~ 138 kDa (2) was seen with a further concentration-dependent potentiation of a high molecular weight band at 0.2 mM BS3 (H). The 138 kDa band has a size ratio of ~ 2:1 with the 66 kDa band and is therefore likely a dimer. TPC1 domain II exists as monomeric and dimeric sized species in the absence of cross-linker while high-molecular weight complexes were readily induced with 0.05 mM BS3 (Figure 5.9B). With both TPC domains, protein bands corresponding to a dimer were visualised although high-molecular weight species that were beyond our capacity to accurately size persisted in the presence of cross-linker.

Examination of TPC2 domains revealed that TPC2 domain I also readily existed as a dimer sized species (~ 125 kDa) in the absence of cross-linking reagent (Figure 5.9C) as with TPC1 domain II. When the homogenates were treated with 0.05 mM BS3, the dimer sized band was potentiated (2), as seen by an increase in band intensity with a reciprocal decrease in the intensity of the monomeric species (1). BS3 at 0.2 mM then promoted the formation of high-molecular weight complexes (H) with a seeming further decrease in band intensity of the monomeric (1) and dimeric (2) species. This suggests increasing levels of higher-order complex are promoted, proportionate to the concentration of BS3. TPC2 domain II did not appear to exist as a dimer-sized species in the absence of cross-linking but formation of dimers was

promoted upon treatment with 0.05 mM BS3 (Figure 5.9D). This domain appeared more resistant to the formation of high molecular-weight complexes however, and only a small increase in the amount of dimer sized protein was visualised at 0.2 mM.

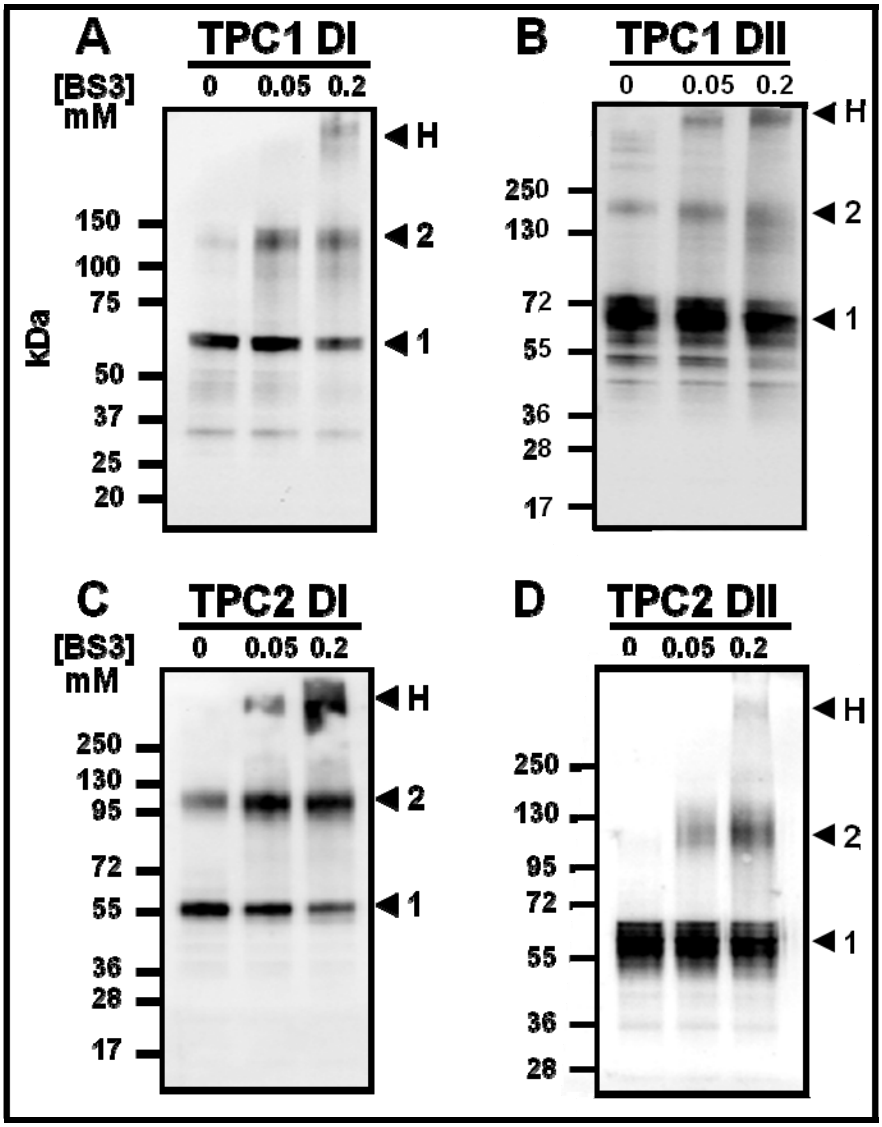

Figure 5.9. Cross-linking of TPC domains induces the formation of dimers, then high molecular weight complexes in a concentration dependent manner. Western blot analysis of HEK cell extracts expressing the indicated GFP-tagged TPC domain (A-D) either in the absence (0 mM) or presence of (0.05, 0.2 mM) BS3 prior to SDS-PAGE. Visualised bands correlate to either monomeric (1), dimeric (2) species of the domain or high-molecular weight complexes (H).

The size of the protein bands visualised by Western blot for each domain was calculated over multiple experiments and is presented in Figure 5.10. Larger protein bands are consistently visualised at a size ratio of ~ 2:1 compared to the monomeric species and are therefore likely to be dimers.

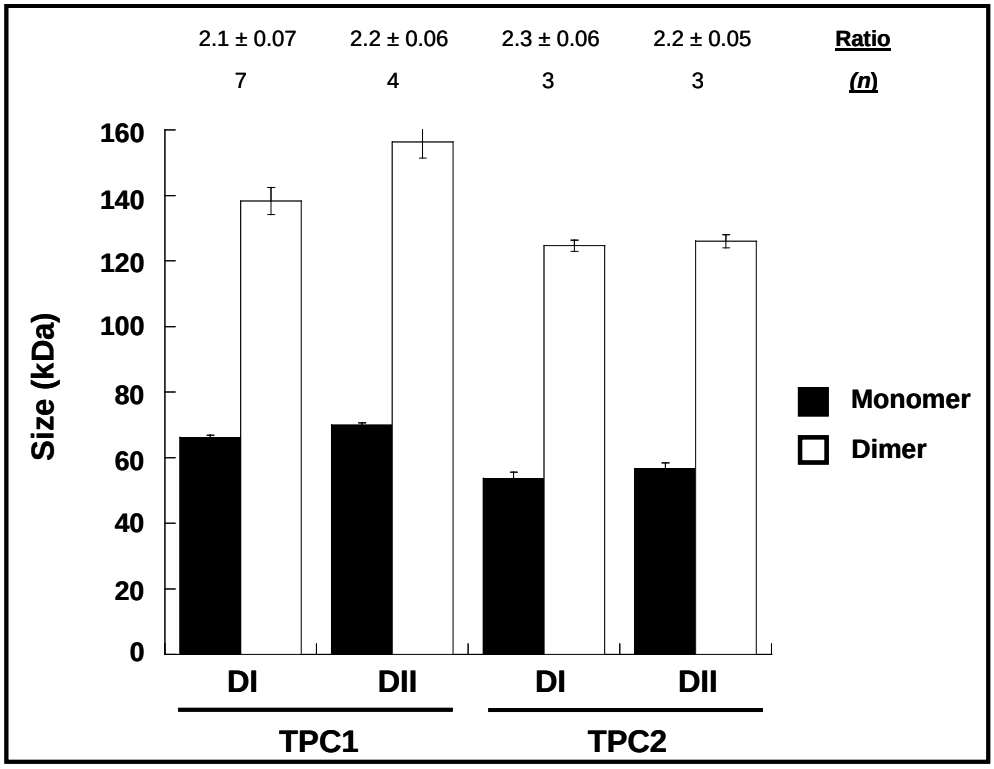

Figure 5.10. Quantification of cross-linking analysis reveals the formation of TPC domain dimers. The size of protein bands visualised by Western blot of TPC domains subject to cross-linking was plotted to show the relative size of protein species.

TPC domains are therefore capable of dimerisation, even in the absence of cross-linking reagent. These dimers are then promoted by BS3 in a concentration-dependent manner to form high-molecular weight complexes as was witnessed with the full-length protein.

5.3.7 Cross-linking of TPC1 domain I TM regions

It is believed that TPCs, with their two pores, dimerise to form a functional channel. Therefore if one of the pore regions of a TPC domain was dissected out of the protein, would it be capable of forming a tetrameric complex to reconstitute a pore? TPC1 domain I was dissected into its ancestral constituents of TM region 1-4 and TM region 5-6 and subject to BS3 cross-linking. Figure 5.11A shows that TM regions 1-4 are visualised as protein bands of ~ 50 and 100 kDa in the absence of cross-linker, likely corresponding to monomeric (1) and dimeric (2) forms. A decrease in the protein band intensity of the monomeric form was observed when cell homogenate was treated with 0.05 mM BS3 and the total amount of protein appeared to redistribute to the dimeric form. The formation of a high-molecular weight complex was subsequently apparent at 0.2 mM BS3 pre-treatment (H). In contrast, TM regions 5-6, appeared only as protein band corresponding to the monomer (1, ~ 40 kDa) in the absence of cross-linker treatment (Figure 5.11B). Upon treatment of cell extract with 0.05 mM BS3 the formation of higher order oligomers was seen. Prominent bands were visible at ~96 kDa and ~ 158 kDa, representing approximate dimeric (2) and tetrameric (4) forms. A less prominent band was also visible at ~ 122 kDa which may represent an intermediate trimer-sized protein (3). With 0.2 mM BS3 treatment the promotion of high-molecular weight complexes (H) is again apparent.

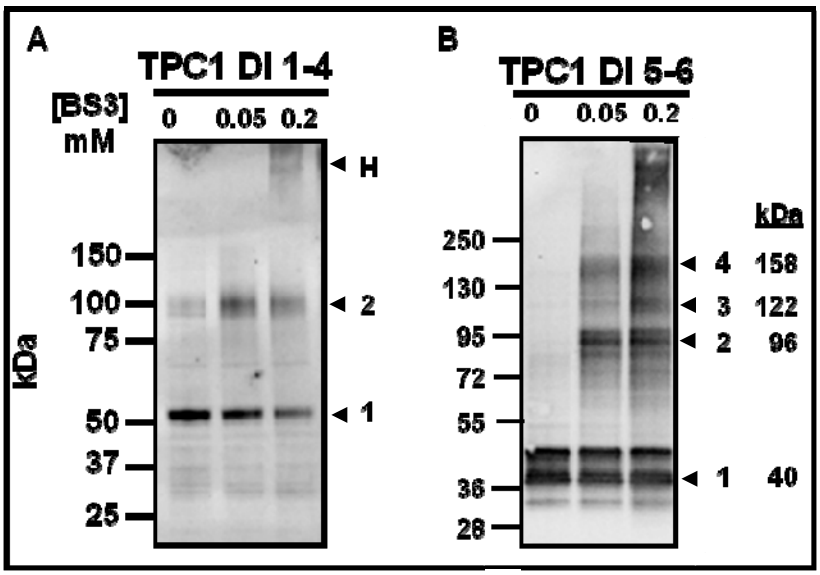

Figure 5.11. Cross-linking of TPC1 TM regions reveals that TM region 1-4 form dimers whereas TM regions 5-6 can form tetramers. Western blot analysis of GFP-tagged TPC1 domain I TM regions 1-4 (**A**) or 5-6 (**B**) treated with BS3. Cross-linking promotes the formation of higher order structure. Monomers (1), dimers (2), trimers (3), tetramers (4) and high molecular weight complexes (H) are visible.

The molecular dissection of TPC1 domain I into ancestral protein components reveals that TM regions 5-6 can form tetramers, preserving the four-pore arrangement seen in functional voltage-gated ion channels.

5.4 Discussion

With the topology of the TPCs determined, attention turned to higher order quaternary structure of the channel. FRET analysis revealed that TPC2 proteins interact to form oligomers, with the C-termini in close proximity. Accurately elucidating the size of this oligomeric complex proved problematic however, with the size determined by sucrose density gradient centrifugation ~ 200 kDa and gel filtration analysis > 400 kDa. Attempts to resolve this discrepancy by cross-linking TPCs with BS3 promoted high molecular weight complexes that were too large to size accurately. It was therefore reasoned that expressing individual TPC domains may decrease the size of the high molecular weight complexes and enable accurate size determination of these complexes. The constituent hydrophobic domains of TPCs were shown to insert into the membrane in isolation validating the expression of these individual domains in the investigation of TPC oligomerisation. Co-immunoprecipitation of TPC domains revealed each domain is capable of homologous interaction. Cross-linking of cell extracts expressing each hydrophobic domain demonstrated that domains were all capable of forming dimers, in some cases in the absence of cross-linker. When domain I of TPC1 was further dissected into its ancestral components, TM regions 1-4 were shown to form dimers, however TM regions 5-6 could form higher order tetramer-sized complexes. In summary TPCs can form oligomers, most likely dimers, to create a functional channel and preserve the four-domain arrangement, typical of voltage-gated ion channels.

FRET analysis of TPC2 showed the channel was capable of forming oligomers in live cells (Figure 5.3). FRET efficiency was greatest when TPC2 was coexpressed with C-terminal GFP or TdTomato tags opposed to when fluorophores were tagged at opposite termini of TPC2. This may suggest a “head-to-head” (Figure 5.12A) instead of a “head-to-tail” (Figure 5.12B) orientation between TPC proteins. In this model homologous domains would be orientated opposite each other, whereby domain I of one TPC monomer is parallel to domain I of a second TPC. FRET was low however when TPC2 was coexpressed with N-terminal fluorophore tags. This

suggests that although the C-termini are closely apposed, the N-termini are not. FRET analysis only shows the proximity of the protein at the point of the fluorophore tag addition therefore no conclusions can be inferred as to the relative proximity of domain I or domain II between monomers.

.

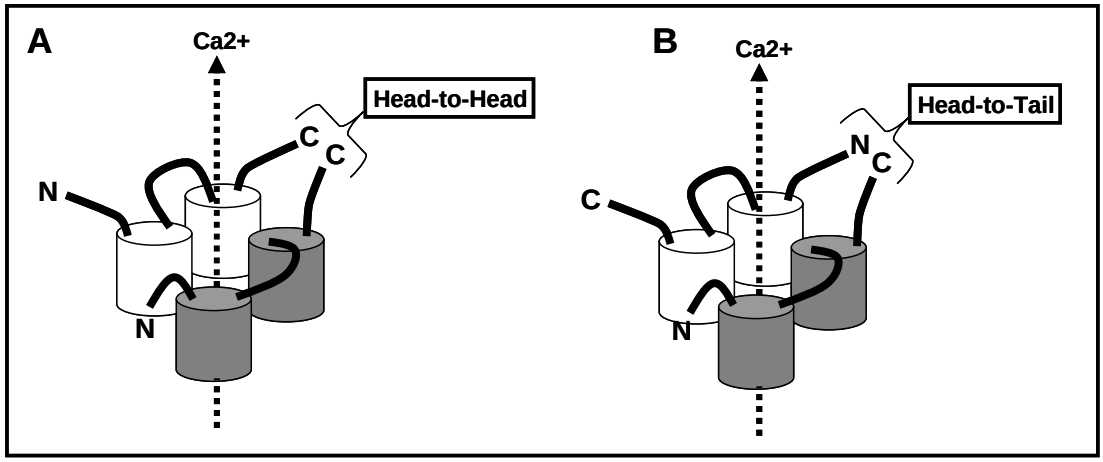

Figure 5.12. Schematic of the possible orientations of TPCs, to form a functional channel. TPCs are predicted to form dimers and this may occur in a "head-to-head" (**A**) or "head-to-tail" (**B**) orientation.

The likely formation of TPC oligomers was first shown when it was demonstrated that differentially tagged TPC2 constructs could co-immunoprecipitate (Zong *et al.*, 2009). TPC2 could not immunoprecipitate TPC1 however, suggesting heterointeractions were improbable. Further functional evidence that TPCs oligomerise also exists. Brailoiu et al introduced a mutation into the putative pore region of HsTPC1 resulting in NAADP-mediated Ca^{2+} release being diminished to below that of mock-transfected cells (Brailoiu *et al.*, 2009a). This suggested the mutant protein was interacting with endogenous wild-type protein to decrease the endogenous response. Ruas et al. also demonstrated that Ca^{2+} release triggered by NAADP was abolished when overexpression of their SpTPC3 clone in HEK293 cells, suppressed endogenous responses observed with mock transfected cells (Ruas *et al.*, 2010). Expression of SpTPC3 also diminished responses to overexpressed SpTPC2 suggesting the two isoforms can form hetero-oligomers. These data suggest

that when non-functional TPC mutants or isoforms are overexpressed, they interact with functional channels in a dominant-negative manner.

By determining the size of the TPC oligomer, the stoichiometry of TPCs within the complex could be inferred. In Chapter 4, HsTPC1-GFP was shown to be visualised by Western blot as a mature, glycosylated protein band at 130 kDa while HsTPC2-GFP appeared as a 100 kDa band. Oligomers would therefore appear as multiples of these monomeric sizes. Western blots of TPC2 also reveal the presence of dimer-sized protein bands, supporting the model of TPCs forming a dimer to preserve the four-pore arrangement of a functional ion channel.

Fractionation of sucrose density gradients gave an apparent molecular weight of ~ 200 kDa for the native TPC channel complex (Figure 5.4A). However gel filtration analysis determined the weight of the protein to be > 400 kDa (Figure 5.4B). This aberrant migration places the TPC complex at either a dimer size (200 kDa) or larger than a tetramer (> 400 kDa) and does not aid attempts to determine the stoichiometry of the channel. The observed migration mirrors that seen with SpTPCs (Chapter 2) and the endogenous sea urchin NAADP-binding protein (Berridge et al). It therefore appears that the characteristics of TPCs are consistent across the deuterostome lineage. As discussed previously (Chapter 2) this aberrant migration could be explained by dissociation of oligomeric complexes by high-speed centrifugation on sucrose gradients, alternatively, the association of TPCs with lipids (Churamani *et al.*, 2005) may underestimate the buoyant mass of the protein by this method.

In an attempt to size TPC oligomers, cell extracts expressing TPCs were treated with the cross-linking reagent BS3 (Figure 5.5). This irreversibly binds proteins that are within 11.4 Å corresponding to the linker "arm" length of BS3. Cross-linking of homogenates promoted the formation of high molecular weight TPC complexes that were too large to size accurately by protein standards on SDS-PAGE. These complexes may be aggregates however no aggregation was seen when GFP alone

was treated with cross-linking reagent. TPC2 was consistently visualised forming a dimer-sized protein band, although it is unclear why TPC1 failed to be promoted into a dimer intermediate. Titrating to lower concentrations of BS3 also failed to resolve TPC1 dimer intermediaries (data not shown).

The arrangement of TPCs into high molecular weight complexes may however be expected. TPCs could form complexes by channel clustering as seen with the IP_3 receptor. Functional IP_3 receptor channels exist as tetramers, preserving a four-pore arrangement also seen with members of the voltage-gated ion channel superfamily. Channel tetramers have been shown to form higher order "clusters" to dynamically regulate IP_3 receptor-mediated Ca^{2+} release between local and global Ca^{2+} release events (Rahman & Taylor, 2009). Clustering can be triggered by both Ca^{2+} and IP_3, which promote the prerequisite conformational change in the receptor for clustering to occur. Clustering of IP_3 receptors is reversible, however the molecular nature of the interaction that promotes and maintains clusters is unknown at present. Clustering also occurs in ryanodine receptors, with channel tetramers interacting with four other adjacent tetramers via a specific domain interaction (Fill & Copello, 2002) to bring together clusters of hundreds of receptors. It could therefore be reasoned that TPCs form clusters in order to generate Ca^{2+} release events above the threshold to trigger subsequent Ca^{2+} release from the ER. The high molecular weight complexes visualised upon cross-linking could therefore represent clusters of numerous TPC dimers.

Alternatively, TPCs could be interacting with other proteins to form a high molecular weight complex. TPCs have been shown to interact with TRPML1, yet maintain functional independence (Yamaguchi *et al.*, 2011). This may suggest that although TRPML1 does not form hetero-oligomers with TPCs (such as one TPC and two TRPML1 proteins forming a functional pore) functional channel complexes of both proteins may interact or cluster together. An increasing number of channel proteins are being shown to interact and form signalling microdomains. IP_3 receptors have been demonstrated to interact with Polycystin-1 and -2 (TRPP2, PKD2)

(Santoso *et al.*, 2011;Sammels *et al.*, 2010), Orai1 (Lur *et al.*, 2011), TRPC3 and STIM1 (Adebiyi *et al.*, 2011) to name a few examples.

A functional TPC protein may not be the sole component of the channel. The four-pore arrangement of functional Ca_vs and K_vs constitutes only the α1 pore-subunit. Although this pore unit governs many of the biophysical properties of the channel, the functional channel is formed in conjunction with accessory subunits which may also modulate channel properties (Dolphin, 2009). The Ca_v channels, for example, consist of the α1 pore-subunit but also the membrane-anchored, extracellular $\alpha_2\delta$ and cytosolic β subunits. These accessory subunits have been shown to regulate channel trafficking (Richards *et al.*, 2004), phosphorylation, protein interaction and channel expression. Given the structural homology of TPCs to half a Ca_v, it therefore seems most likely that TPCs may form only the α1 pore-subunit of the NAADP-mediated Ca^{2+} release channel. Indeed it is speculated from the original binding data that the NAADP binding site may be itself be located on an accessory protein (Calcraft *et al.*, 2009).

Of interest is the apparent homology between the alpha-interacting domain (AID) located on the domain I-II linker of Ca_v channels and a corresponding region on TPCs (Figure 5.13). The AID domain is the site of interaction on the α1 subunit (the Ca_v channel) with accessory β subunits (Richards *et al.*, 2004). K^+ channels have also been shown to have their own distinct complement of β subunits (Pongs & Schwarz, 2010). The homology of the TPC linker to the Ca_v AID may suggest that TPCs also have dedicated β subunits or perhaps more intriguingly, Ca_v β subunits could be more promiscuous than first thought.

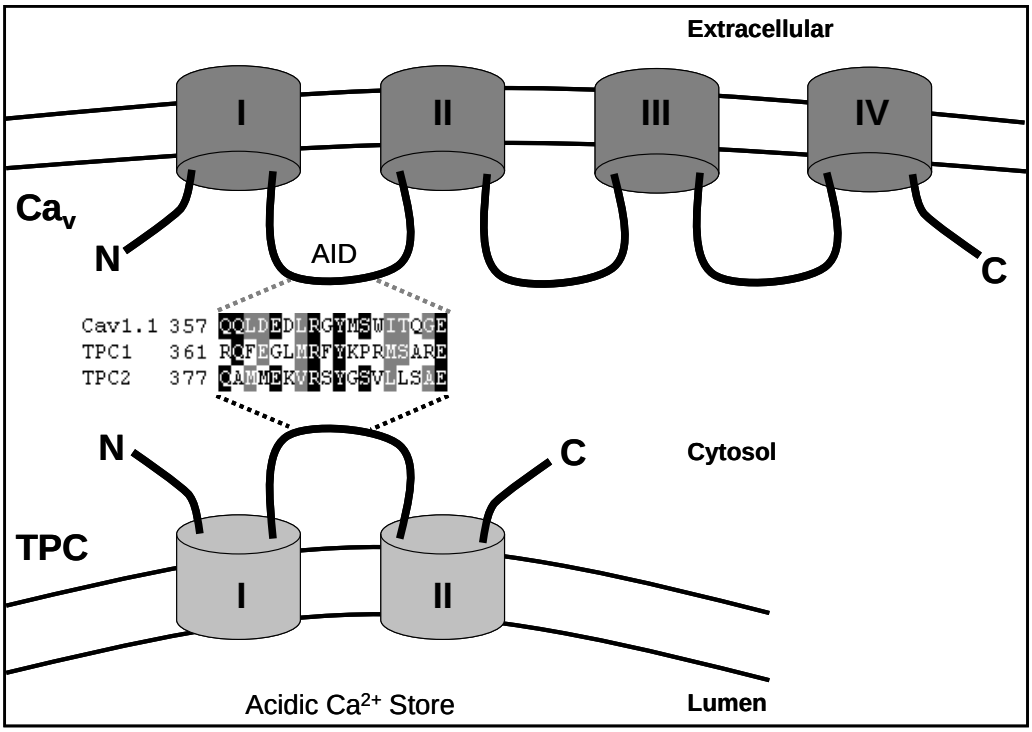

Figure 5.13. The Ca$_v$1.1 AID domain shares homology to an analogous region on TPCs. Multiple sequence alignment of Cav1.1 AID domain with TPC1 and TPC2 reveals identical (black shading) and similar amino acids (grey shading).

Having failed to determine the size of the TPC oligomer by cross-linking of the full length protein, it was reasoned that dissecting TPCs into their constituent domains may reduce the size of the channel complex and render the high molecular weight complex more amenable to accurate size estimation. First however, the ability of individual TPC domains to insert into the membrane in isolation was ascertained. Both hydrophobic domains of TPC1 were shown to be independently inserted into the membrane when cell extracts were fractionated, while the domain linker was shown to be cytosolic (Figure 5.6). The same results were obtained for TPC2 hydrophobic domains (Figure 5.7). When fractionated in intracellular buffer all hydrophobic domains were integrated into membranes and could therefore be used to assess TPC oligomerisation.

The ability of TPC hydrophobic domains to interact was examined by co-immunoprecipitation. All TPC hydrophobic domains were capable of self-immunoprecipitation, suggesting a level of redundancy within the protein (Figure

5.8). However domain II of both TPCs appeared to more readily immunoprecipitate than domain I as evidenced by the relative intensity of the protein bands. This may support the FRET analysis which revealed that while the C-termini are closely apposed in an oligomer, the N-termini are not (Figure 5.14A). Co-immunoprecipitation analysis extending this conclusion to show that domain I, is not as well associated as domain II leading to the speculative model proposed in Figure 5.14B. In this model TPC dimers orientate as a "chevron", with the C-termini in close proximity but the N-termini more distant.

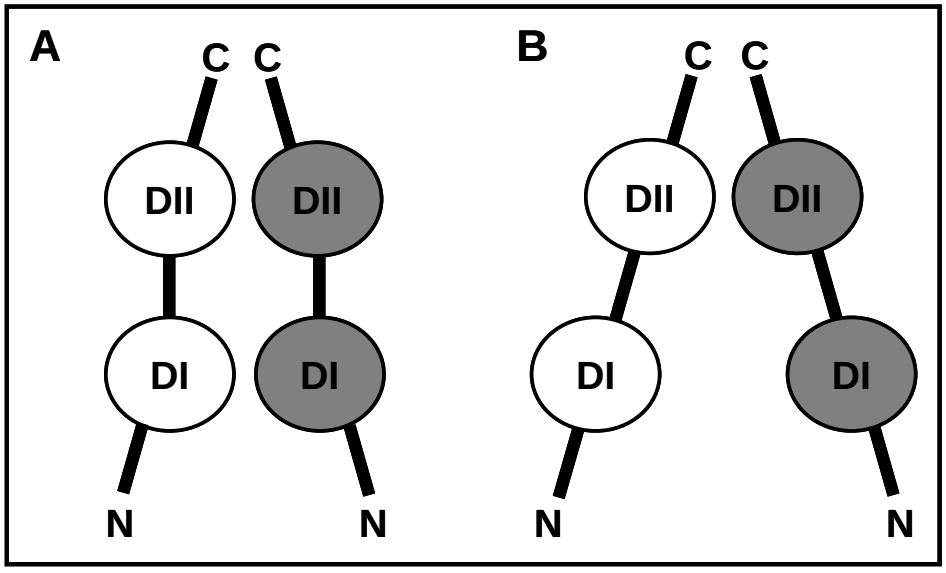

Figure 5.14. A model of TPC association shows the N-terminal portion of the protein is not as well associated as the C-terminal end. FRET analysis reveals the C-termini of TPC2 are in close proximity while the N-termini are not (**A**). Co-immunoprecipitation supports this theory and extends it to the conclusion that domain I (DI) is not as closely associated as domain II (DII) (**B**).

Finally the effect of cross-linking TPC domains was investigated. BS3 promoted the formation of a dimer-sized protein band upon treatment of TPC1 domain I, which was further potentiated into a high molecular weight complex (Figure 5.9A). In contrast TPC1 domain II appeared to exist as a dimer in the absence of cross-linker (Figure 5.9B). Dimer-sized bands have not been previously visualised with full-length TPC1 by Western blot and it may be, that in the context of the full-length protein, dimerisation is somehow inhibited and this constraint is lifted when

domains are expressed in isolation. It could be that binding of NAADP to the TPC or an accessory protein promotes a conformational change in TPC and mediates dimerisation to form a functional channel. Formation of TPC1 oligomers could therefore be promoted in the presence of NAADP and this could certainly be explored. TPC1 DII may be primarily involved in mediating any dimer formation of the full-length protein, as dimers of this domain were observed in the absence of cross-linker.

In contrast, dimers of full-length TPC2 are readily observable by Western blot after SDS-PAGE. It is therefore likely that the nature of the dimer interaction between the isoforms is different and indeed more robust for TPC2. Furthermore in contrast to TPC1, domain I of TPC2 appears as a dimer-sized protein in the absence of cross-linker, suggesting differences in the domains mediating dimerisation between isoforms (Figure 5.9C). Isoform specific regulation of dimerisation and channel function therefore seems likely. That domains only appear as dimers and not trimers or tetramers suggests each domain may only have one point of interaction with an adjacent domain which would preclude a complex larger than a dimer forming.

As previously discussed in Chapter 1, six-TM region channels are the evolutionary product of fusion between a four-TM region voltage-sensing protein and a two-TM region pore protein. It has been shown that when K_v or Na_v channels are dissected into TM region 1-4, the ancestral voltage sensor and TM region 5-6, the ancestral pore, that TM regions 5-6 are capable of forming tetramers to reconstitute a functional pore (Shaya *et al.*, 2011). TPC1 domain I was further dissected into TM regions 1-4 and TM regions 5-6 and cell extracts expressing these domains were treated with BS3 (Figure 5.11). BS3 treatment of extracts expressing TM regions 1-4 potentiated the formation of dimer-sized protein bands which were further promoted to high molecular weight complexes in a concentration-dependent manner, similar to TM regions 1-6 (DI). In contrast TM regions 5-6 exist solely as a monomeric species in the absence of cross-linker. BS3 treatment then induces the formation of prominent bands corresponding to dimer and tetramer sizes. This suggests the pore

region may dimerise then form a "dimer of dimers" to assume a tetrameric arrangement. The formation of tetramers also suggests that each pore region has two points of interaction, however these are usually constrained the presence of TM regions 1-4 as we have not previously witnessed tetramer sized protein bands with the hydrophobic domains. The ancestral pore region still seems capable therefore, of forming the tetramer required to reconstitute a pore. It would be interesting to carry out functional analysis of this construct to ascertain if pore activity can be observed.

In summary, TPCs form oligomers and these are most likely dimers which form a functional channel and preserve the classic four-pore arrangement seen with other members of the voltage-gated ion channel super-family.

Chapter 6 - Probing the regulation and physiology of the TPCs

6.1 Introduction

6.1.1 The molecular determinants of TPC regulation

The TPCs are now established as NAADP-sensitive Ca^{2+}-release channels (Galione, 2011;Patel *et al.*, 2011), however there is limited molecular understanding of how the channels are regulated. It has previously been shown that N-glycosylation of TPC1, at sites adjacent to pore II, appear to negatively regulate Ca^{2+} flow through the channel (Hooper *et al.*, 2011). The mechanism by which glycosylation-mediated regulation of TPC1 occurs is not known at present but we speculate glycosylation could either structurally alter the pore region or the negative charge of the oligosaccharides may interact with the binding of luminal Ca^{2+} or H^{+} ions, potential regulators of channel function (Pitt *et al.*, 2010).

Conservation of amino acid residues between species and isoforms is generally indicative of a key role in channel function. By examining the pore regions of TPC1 and TPC2, conserved leucine residues, L273 and L265, were identified in pore I of each isoform respectively. When these leucine residues were mutated to a helix-breaking proline residue, channel conductance was blocked (Brailoiu *et al.*, 2009a;Brailoiu *et al.*, 2010b). It is not clear whether this is a result of mutating the leucine per se or whether breaking the pore helix with a proline blocks the channel, but pore structure is essential for ion conductance. Another molecular determinant of channel regulation was proposed by Schieder et al. They speculated that acidic residues in the pore loop may confer Ca^{2+} selectivity on TPC2 (Schieder *et al.*, 2010b) as acidic residues fulfil this role in TRPV channels (Voets *et al.*, 2002;Voets *et al.*, 2004) and homology between the pore region in these channels and TPC2 was noted.

Other amino acid residues have been identified that target the TPCs to organelles of the endo-lysosomal system. Both TPC1 and TPC2 have lysosomal-targeting dileucine motifs in the N-terminus. Mutation of this motif in TPC2 prevents the channel trafficking to the lysosome and instead redirects it to the plasma membrane (Brailoiu *et al.*, 2010b). Mutation of the N-terminal dileucine in TPC1 does not result in defective localisation, suggesting there is redundancy in the targeting of this isoform. The localisation of TPCs to the endo-lysosomal system is required for functional coupling of these acidic Ca^{2+} stores to the ER and subsequent amplification of NAADP-mediated Ca^{2+} release by CICR.

We have previously shown that TPC1 over-expression can potentiate NAADP-mediated Ca^{2+} release (Brailoiu *et al.*, 2009a). The TPC1 construct utilised was tagged with fluorophores at the C-terminus. Zong et al fail to see a potentiated response to over-expression of N-terminally tagged TPC1 and concluded the channel is non-functional (Zong *et al.*, 2009). Moreover we have shown SpTPC3 to be functional while Ruas et al claim SpTPC3 is non-functional (Ruas *et al.*, 2010). Aside from polymorphic variation (as discussed in Chapter 2) another difference between the two plasmids used was the site of the fluorophore tag. Thus, like the Zong mouse TPC1 clone, the Ruas SpTPC3 clone was tagged at the N-terminus. The discrepancies in the data between lab groups therefore lead me to speculate that the N-terminus is involved in regulating TPC activity.

6.1.2 Molecular Physiology of the TPCs

With the identification of the TPCs as NAADP-sensitive Ca^{2+} channels, investigations have focussed on the role of TPCs in physiological processes in which NAADP had previously been implicated. Examination of the TPC2 knock-out mouse revealed that the channel mediates NAADP-evoked contraction in smooth muscle (Tugba Durlu-Kandilci *et al.*, 2010). Both TPC isoforms were implicated in the regulation of skeletal muscle differentiation after it was demonstrated that siRNA mediated knock-down of either TPC isoform caused a decreased differentiation index score (Aley *et al.*, 2010a). siRNA mediated knock-down of TPCs was also employed in endothelial cells to show that histamine-induced von Willebrand factor secretion was TPC-dependent (Esposito *et al.*, 2011).

Converse to the use of knock-down approaches, over-expression of SpTPCs in HEK293 cells lead to a perturbation of retrograde trafficking between endo-lysosomes and the Golgi which manifested as enlarged lysosomes (Ruas *et al.*, 2010). This phenotype could be prevented by the use of the TPC antagonist Ned-19. These findings support a role for TPCs in control of the highly dynamic endo-lysosomal system and the biogenesis of vesicles in this system. A role for TPCs in acidic organelle biogenesis is substantiated by findings in astrocytes, where NAADP was shown to potentiate the formation of autophagosomes. Levels of LC3II and beclin 1 also increased, indicative of autophagic induction (Pereira *et al.*, 2011). This increase could be abolished using Ned-19 or expressing the non-conducting TPC2 L265P pore mutant, which acted in a dominant-negative manner.

Preceding the identification of TPCs as NAADP-mediated Ca^{2+} release channels, TPC2 had been implicated in the determination of human hair colour by a genome-wide association study (Sulem *et al.*, 2008). Two non-synonymous, single nucleotide polymorphisms (SNPs) of TPC2 were found to correlate with blonde or brown hair colour in a European population. A link between calcium homeostasis and pigmentation had previously been proposed when a polymorphism in the

potassium-dependent sodium-calcium exchanger SL24A5 was associated with light skin pigmentation (Lamason *et al.*, 2005;Ginger *et al.*, 2008). Furthermore a mutation rendering the Ca^{2+} channel, TRPML3, constitutively active (Xu *et al.*, 2007) lead to a loss of pigmentation when expressed in mice (Di *et al.*, 2002). These data highlight a role for calcium in melanogenesis. To date the function of TPCs in the regulation of pigmentation remains unknown.

The aim of this chapter is therefore to investigate the role of the N-terminus in regulating TPC activity and to examine a possible role for TPC2 in pigmentation.

6.2 Materials and methods

Plasmids

The molecular cloning of HsTPC1-GFP and HsTPC2-GFP is described in Brailoiu et al. 2009 (Brailoiu *et al.*, 2009a). The cloning of HsTPC2^{L265P}-GFP is described in (Brailoiu *et al.*, 2010b). GFP-TPC1 and GFP-SC-TPC1 were cloned by Dr Dev Churamani with the vector containing a self-cleaving peptide sequence (Szymczak *et al.*, 2004), a kind gift from Dr Masa Tada (UCL).

The TPC constructs utilised in this chapter are summarised in Figure 6.1.

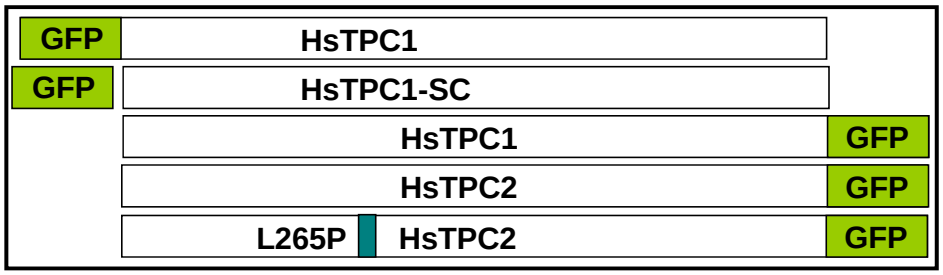

Figure 6.1. HsTPC clones utilised in the characterisation of channel activity and physiology. A schematic illustrating differentially tagged full-length and mutated TPC constructs used in the molecular characterisation of TPC regulation and physiology.

Microinjection of SKBR3 Cells

Microinjection was performed using Femptotips II microinjection pipettes backfilled with an intracellular-like buffer composed of 110 mM KCl, 10 mM NaCl and 20 mM HEPES, pH 7.2, supplemented with 10 nM NAADP. The InjectMan N12 and FemtoJet systems (Eppendorf) were used and the injection time was 0.5 sec. The injection pressure was 75 hPa with a compensatory pressure of 25 hPa.

Ca^{2+} imaging

SKBR3 cells were plated on poly-L-lysine coated glass coverslips and transiently transfected with the indicated construct as described in Chapter 2. Cells were incubated with 5 μM fura-2 AM for 45 min at room temperature then washed three times in Hank's Balanced Salt Solution (HBSS) and incubated for a further 45 min to allow deesterification of the fura-2. Only transfected cells, as viewed by expression of GFP-tagged protein at 488 nm, with a resting basal fura-2 ratio of < 0.5 were injected. Cells were imaged using a 40x NA 1.3 oil immersion objective and CCD camera (Roper Scientific, Optical Apparatus Co.) attached to an inverted microscope (Eclipse TE2000-U, Nikon). Fura-2 fluorescence (510 nm emission) was captured after alternative excitation at 340 and 380 nm with a frequency of 0.33 Hz.

Xenopus Oocyte expression and pigmentation assay

Xenopus laevis oocytes were mechanically defoliculated then washed in modified Barth's saline (88 mM NaCl, 1 mM KCl, 2.4 mM $NaHCO_3$, 0.82 mM $MgSO_4$, 0.33 mM $Ca(NO_3)_2$, 0.41 mM $CaCl_2$, and 20 mM HEPES-Tris, pH 7.5) for 3 hours with agitation. Oocytes were microinjected with the indicated TPC DNA plasmid (~ 8 ng DNA), 24 h post defoliculation, directly into the nucleus of the cell. Oocytes were imaged 48 h post injection at 24 h intervals. Imaging was either by confocal or light microscopy. Confocal microscopy images of oocytes bathed in Barth's solution were captured with a confocal scanner (MRC1024, BioRad Laboratories) attached to an Olympus AX70 microscope with a 40x NA 1.3 oil immersion objective. Transfected oocytes were visually examined for defects to pigmentation of the animal pole such as "banding" of the pigment or areas devoid of pigmentation. The percentage of TPC expressing oocytes with a pigmentation defect was then calculated.

Recurrent molecular biology methods

Cell culture, transfection, protein preparation, SDS-PAGE, Western blotting and confocal microscopy were performed as per the methods in Chapter 2.

6.3. Results

6.3.1. Does the N-terminus of TPC1 regulate channel activity?

6.3.1.1 Expression of GFP-SC-TPC1

One controversy in the NAADP-signalling field is the discrepant data between lab groups regarding the activity of TPC isoforms. It was noted that the Zong mouse TPC1 clone (Zong *et al.*, 2009) and the Ruas SpTPC3 clone (Ruas *et al.*, 2010) were tagged at the N-terminus and were inactive, while our HsTPC1 (Brailoiu *et al.*, 2009a) and SpTPC3 (Brailoiu *et al.*, 2010a) clones were tagged at the C-terminus and active. I therefore investigated a possible role for the N-terminus in regulating TPC1 function. To address this problem, HsTPC1 was tagged at the N-terminus with a GFP tag (Figure 6.2A) or with a GFP attached to the N-terminus by a peptide sequence that is endogenously cleaved to produce a soluble GFP protein and an effectively untagged TPC1 (Szymczak *et al.*, 2004) (Figure 6.2B). This technique utilises viral 2A peptide sequences which self-cleaves during translation between glycine and proline residues within a consensus sequence, to release active viral sequence (Palmenberg *et al.*, 1992).

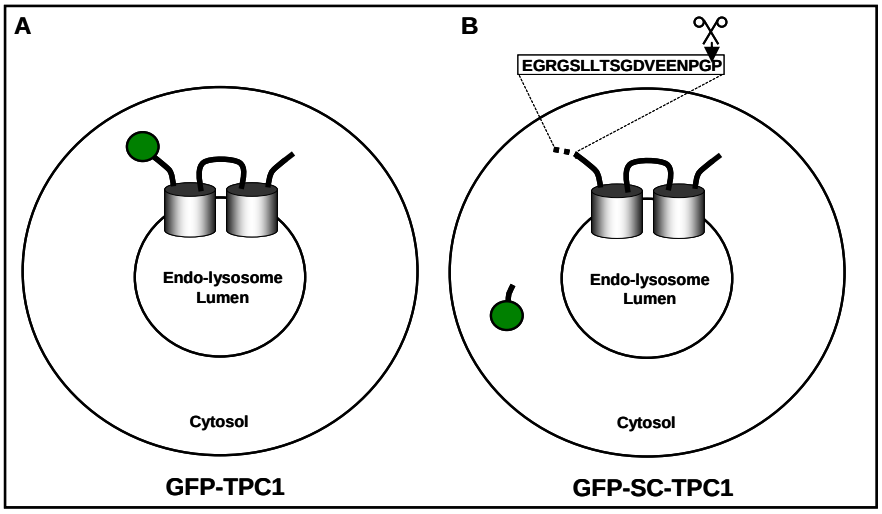

Figure 6.2. GFP is endogenously cleaved from the N-terminus of TPC1 at a "self-cleaving" peptide sequence. TPC1 is expressed either with an N-terminal GFP tag (A) or with an N-terminal tag joined to the protein via the indicated peptide sequence that is endogenously cleaved (B).

When GFP-TPC1 is expressed in SKBR3 cells, GFP fluorescence appears as intracellular puncta, likely reflecting the targeting of TPC1 to vesicles of the endo-lysosomal system (Figure 6.3A). GFP however appears to be diffusely expressed throughout the cell in GFP-SC-TPC1 expressing cells, indicative of GFP being cleaved from the TPC and redistributing as a soluble untargeted protein (Figure 6.3B).

When cell homogenates expressing GFP-TPC1 and GFP-SC-TPC1 were visualised by Western blot using a TPC1 specific antibody (Abcam) there is an appreciable decrease in the protein band sizes with the GFP-SC-TPC1 plasmid (Figure 6.3C). Both appear as a doublet, likely representing full and core-glycosylated protein as seen previously (Chapter 4). The fully glycosylated form of GFP-TPC1 is ~ 150 kDa while the upper protein band of GFP-SC-TPC1 is ~ 117 kDa, consistent with the cleavage of the GFP (~ 27 kDa) from the TPC1 construct.

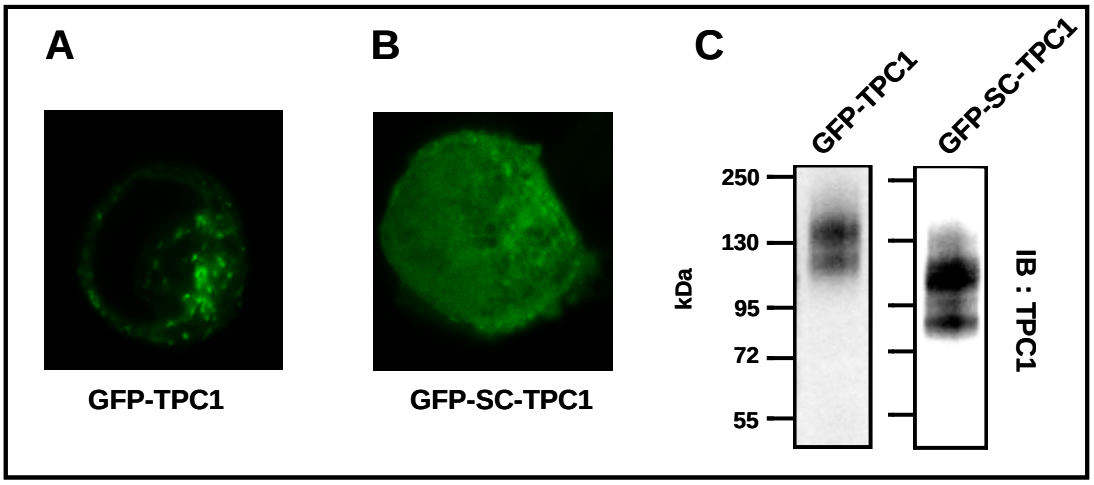

Figure 6.3. A "self-cleaving" peptide sequence removes the GFP tag from TPC1. GFP-TPC1 (**A**) and GFP-SC-TPC1 (**B**) were expressed in SKBR3 cells and the distribution of GFP viewed by confocal microscopy. When visualised by Western blot using an anti-TPC1 antibody (**C**) an appreciable size decrease of GFP-SC-TPC1 was seen, reflecting the cleavage of GFP from TPC1.

Both confocal microscopy and Western blotting indicate that the GFP-SC-TPC1 construct is effectively cleaved to yield a separate, soluble GFP protein from the TPC1 protein *in vivo*.

6.3.1.2 Microinjection of NAADP in cells expressing N-terminally tagged TPC1

Having ascertained that the GFP is cleaved from the N-terminus of TPC1 upon expression of GFP-SC-TPC1, functional Ca^{2+} release was investigated with this construct and GFP-TPC1. As shown in Figure 6.4A, microinjection of 10 nM NAADP into SKBR3 cells expressing GFP-TPC1 results in a modest release of intracellular Ca^{2+} to a cytosolic concentration of ~ 300 nM. When cells expressing GFP-SC-TPC1 are microinjected a ~ 3-fold increase in Ca^{2+} release relative to GFP-TPC1 is seen with intracellular Ca^{2+} concentration rising to ~ 900 nM (Figure 6.4B). With both constructs release is rapid upon microinjection and transient with a return to baseline.

N-terminal tagging of TPC1 therefore appears to be modulating intracellular Ca^{2+} release by NAADP.

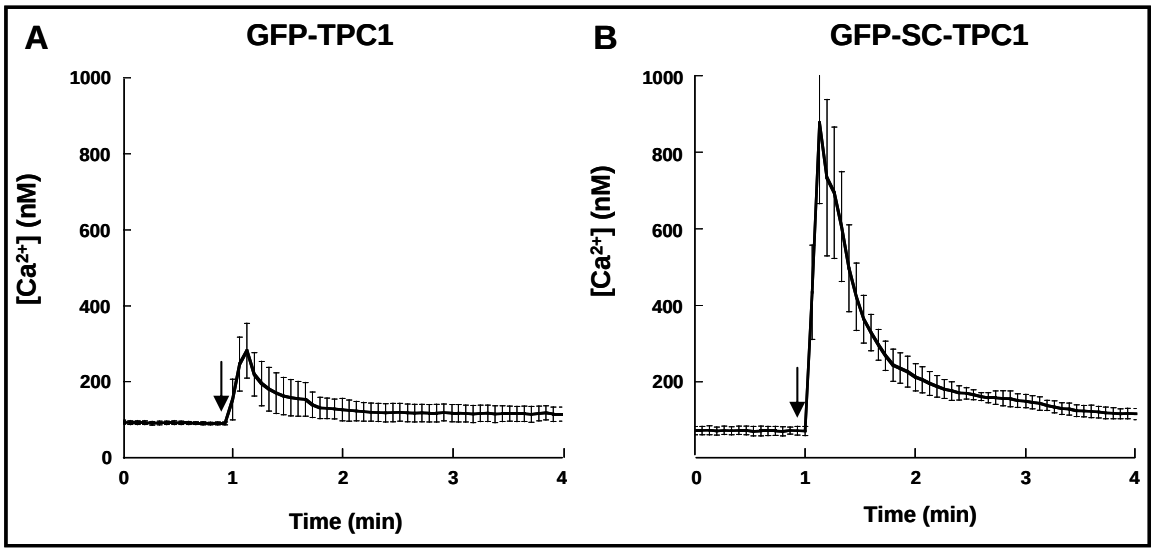

Figure 6.4. N-terminal tagging of TPC1 modulates activity. Average Ca^{2+} release by 10 nM NAADP in SKBR3 cells expressing GFP-TPC1 (*n*=4) or GFP-SC-TPC1 (*n*=5). Injection of NAADP is indicated by the arrow.

6.3.2. Investigating the role of TPC2 in pigmentation

6.3.2.1 TPC expression in *Xenopus laevis* Oocytes

Single nucleotide polymorphisms of TPC2 were linked to differences in hair pigmentation by a genome-wide association study (Sulem *et al.*, 2008). The role of TPC2 in regulating pigmentation was therefore investigated in *Xenopus* oocytes, a highly pigmented cell type. HsTPC1, HsTPC2 and the non-conducting pore mutant HsTPC2 L265P were tagged at the C-terminus with GFP and plasmid DNA microinjected into *Xenopus* oocytes. Post injection (48 h), heterologous expression was visualised by confocal microscopy at the pigmented animal pole of the oocyte. Figure 6.4 shows that all constructs are expressed as punctate, intracellular vesicles when viewed at a focal plain just below the ER (Figure 6.5).

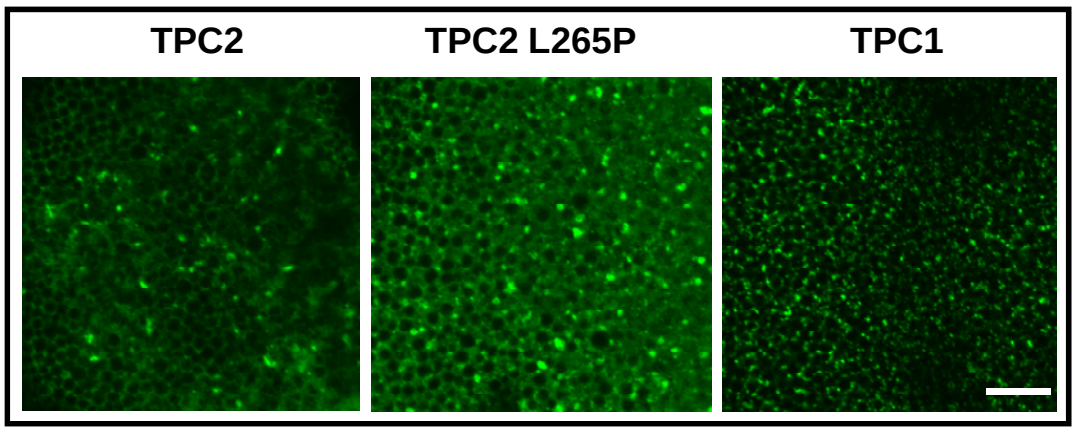

Figure 6.5. HsTPC constructs can be heterologously expressed in the *Xenopus* oocyte system. Confocal microscopy images of HsTPC-GFP constructs heterologously expressed at the animal pole of *Xenopus* oocytes, 48 h post microinjection of DNA into the nucleus.

Oocytes positive for TPC-GFP expression were visually examined for pigmentation defects such as whirling or banding of the pigment at the animal pole (Figure 6.6A). The percentage of oocytes expressing the indicated TPC construct with a pigmentation defect was then calculated (Figure 6.6B). Pigmentation defects with TPC2 increased over time and peaked at 71 %, 96 h post injection (Figure 6.6B).

Pigmentation defects were observed when TPC1 was expressed, however these were limited, peaking with only 17 % of oocytes displaying abnormalities. Despite robust expression, no pigmentation defect was seen when the non-conducting pore mutant TPC2 L265P was expressed.

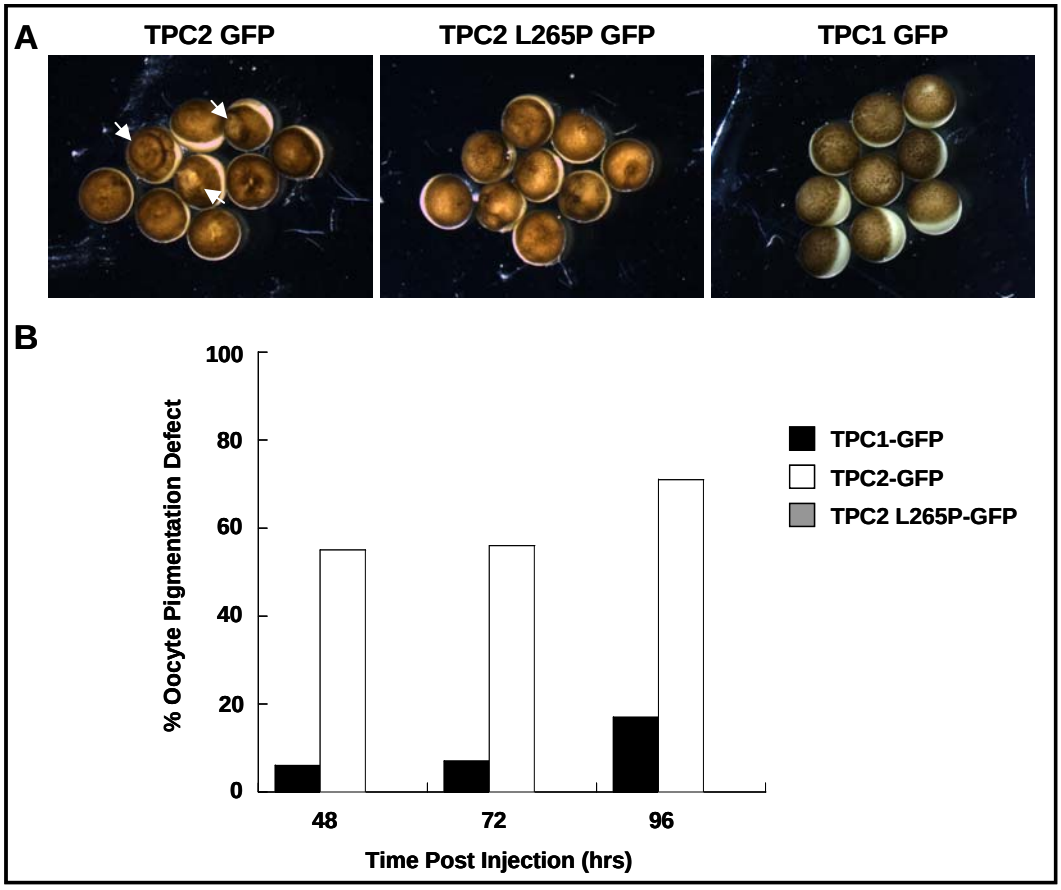

Figure 6.6. TPC2 expression causes an animal pole pigmentation defect in *Xenopus* oocytes. Cells were imaged by light microscopy (A) 48 h post microinjection with TPC DNA and subsequently at 24 h intervals. Oocytes with pigmentation defects (as indicated by arrows) were counted and the percentage of defective oocytes calculated (B). Note, no defects were observed for the TPC2 L265-GFP mutant and no single construct promoted a marked increase oocyte death above any other.

Expression of TPC2, but not TPC1, appears to specifically manifest a pigmentation defect in the animal pole of *Xenopus* oocytes which coincides with the localisation of expression. This suggests an isoform specific role for TPC2 in regulating pigmentation.

6.4 Discussion

6.4.1 The N-terminus of TPC1 regulates channel activity

When TPC1 is tagged at the N-terminus with a GFP fluorophore, Ca^{2+} release activity is greatly diminished upon injection of NAADP. If however, the tag is endogenously cleaved from the N-terminus during expression, Ca^{2+} release activity is restored. These data indicate that the N-terminus of TPC1 may regulate channel activity.

Zong et al utilised a mouse TPC1 clone tagged at the N-terminus which when over-expressed in HEK293 cells failed to elicit a Ca^{2+} transient upon application of NAADP. This is in contrast to our observation with human TPC1 tagged at the C-terminus which elicits a robust Ca^{2+} transient in response to NAADP. Human and mouse TPC1 share 94 % sequence similarity, it therefore seems unlikely that any major differences observed are due to sequence variation. The possibility that the location of the fluorophore tag may affect channel activity was supported when SpTPC3 acted in a dominant-negative manner when expressed with an N-terminal mCherry tag (Ruas *et al.*, 2010) in contrast to our C-terminally tagged SpTPC3 clone (Brailoiu *et al.*, 2010a). Furthermore SpTPC1 Ca^{2+}-release kinetics seemed markedly slower than SpTPC2 when both were tagged at the N-terminus again indicative of the N-terminus modulating channel function. This effect appears to be isoform specific as in all instances TPC2 isoforms show rapid Ca^{2+} release upon NAADP stimulation regardless of fluorophore location (Zong *et al.*, 2009;Ruas *et al.*, 2010). N-terminal regulation of TPCs may therefore be limited to TPC1 and TPC3 isoforms. As previously noted these isoforms are more closely related to each other than to TPC2 (Brailoiu *et al.*, 2009a;Zhu *et al.*, 2010;Galione *et al.*, 2009).

How could the N-terminus be regulating channel function? One possibility is that the fluorophore tag could be hindering N-terminal movement, interaction or perhaps be physically occluding the pore, preventing channel conductance. Zong et al

utilised an eGFP tag (~ 27 kDa) and Ruas tagged SpTPCs with an mCherry fluorophore (~ 29 kDa) both of which are of substantial size in the context of the terminus and likely to be to the detriment of terminal movement or interactions (Zong *et al.*, 2009;Ruas *et al.*, 2010). It would be interesting to see if smaller tags (such as *myc* or HA) also render the channel inactive.

N-termini of VGICs have been implicated in regulation of a variety of processes linked to channel function. One such example is the control of oligomerisation. The TRPC4 channel has two N-terminal interaction domains that contribute to the tetramerisation of the channel (Lepage *et al.*, 2009) while a single oligomerisation promoting domain was identified in the N-terminus of TRPP2 (Feng *et al.*, 2011). The N-terminus of TRPM2 has been shown to mediate total protein expression levels of the channel (Mei & Jiang, 2009). In TRPV5 deletion of the N-terminus retains the channel predominately in the ER and channel protein that did reach the plasma membrane was shown to be inactive (de Groot *et al.*, 2011). Therefore in TRP channels, close relatives of the TPCs, the N-terminus has been implicated in channel expression, trafficking, oligomerisation and activity. GFP-TPC1 appears to be expressed when visualised by confocal microscopy and Western blot (Figure 6.2). This is supported by data from the lab indicating that GFP-TPC1 remains localised to the endo-lysosomal system (Churamani unpublished). It therefore seems that N-terminal tagging may be more directly affecting channel function. The effect on oligomerisation of N-terminal tagging could be investigated using the methodology employed in Chapter 5. FRET analysis however indicates the N-termini may not be close proximity therefore tagging the N-terminus may not inhibit oligomerisation (Chapter 5, Figure 5.3).

One likely hypothesis could be a direct role for the N-terminus in channel gating. The N-terminus of the voltage-gated potassium hERG channel has been shown to be involved in gating, both activation and deactivation (Ng *et al.*, 2011) of the channel. It could be that tagging the N-terminus of TPC1 either maintains the channel in an inactive conformation or conversely the channel is constitutively "open" and the

endo-lysosomal stores are drained of Ca^{2+}. The N-terminus of TPC1 is negatively charged with a striking number of acidic amino acids and a theoretical pI of 4.3 (Figure 6.7). This would be ideal for electrostatic interaction with other proteins or intramolecular interactions within regions of the TPC1 protein. In the context of electrostatic interactions, I note that converse to the negative charge of the N-terminus, the domain linker of TPC1 is highly basic with a theoretical pI of 10.4 (Figure 6.7). It is not inconceivable therefore, that the long N-termini of TPC1 may form electrostatic interactions with domain linker. The C-terminus of TPC1 has a more neutral theoretical pI of 5.8 which may support the hypothesis that the N-terminus forms intramolecular electrostatic interactions but the C-terminus does not. Furthermore, the N-terminus of TPC2 is more neutral (pI 5.1) than TPC1 perhaps supporting an isoform selective mechanism.

Figure 6.7. The highly acidic N-terminus of TPC1 may interact with the basic domain linker to modulate channel activity. Primary sequence of predicted TPC1 N-terminal and domain linker regions with acidic (D/E) and basic (K/R) residues marked in red and green respectively.

Precedence exists for N-terminal intramolecular interactions within VGICs regulating channel activity. The mechanism of N-terminal regulation of the hERG channel (discussed above) has been shown to be partially due to interaction with the S4-S5 linker of the channel, a region which couples voltage sensing to channel gating (de la *et al.*, 2011). The N-terminus of Cav2.2 has also been demonstrated to form intramolecular interactions, in this instance with the domain I-II linker as I hypothesise for TPC1 (Agler *et al.*, 2005). Both regions contain domains that interact with G-protein coupled receptor βγ (G βγ) subunits to inhibit channel function. The use of peptides correlating to regions in the N-terminus and domain linker has demonstrated a direct interaction between these domains, which appear to

come together to form a interaction site for Gβγ to modulate the channel (Bucci *et al.*, 2011). Expression of N-terminal peptides of Cav2.2 can act in a dominant-negative manner to suppress channel currents (Page *et al.*, 2010). Intriguingly the region of the domain I-II linker which interacts with the N-terminus also corresponds to the Ca_v AID which we have previously shown to have homology to the domain I-II linker of TPCs (Chapter 5). It would therefore seem possible that the N-terminus of TPC1 interacts with the domain I-II linker to regulate channel activity.

6.4.2 TPC2 regulates pigmentation

The expression of TPC2 in *Xenopus* oocytes caused a defect in the pigmentation of the oocyte animal pole. The effect was specific to active TPC2 as pigmentation was unperturbed when either TPC1 or the inactive pore mutant of TPC2 was expressed. TPC2 is therefore involved in the regulation of pigmentation in the *Xenopus* oocyte.

TPC2 was first linked to a role in pigmentation by a genome-wide association study (Sulem *et al.*, 2008). The authors examined the association of sequence variation with pigmentation traits of the eye, skin and hair in a European population. Three non-synonymous variants were identified in the gene encoding TPC2, of which two could be linked to an association with blonde or brown hair colour. Mutations at M484L and G734E were correlated with brown versus blonde hair. Therefore if the TPC2 sequence encodes L484 or E734 it may be expected that this manifests as a lighter pigment tone as these are associated with the blonde hair phenotype.

Pigmentation is determined by the level and type of melanin pigment produced by melanocytes in the skin or hair cell follicles (Sturm, 2009). Within the melanocyte, melanin biogenesis occurs in the lysosome-related organelle, the melanosome. Lighter tones are the result of either the type of melanin or decreased melanin synthesis. Indeed the melanosomes in white skin have a lower pH, which is less optimal for melanin synthesis (Slominski *et al.*, 2004). Melanosomes, like

lysosomes, are believed to load Ca^{2+} via a H^+/Ca^{2+} exchanger (Luzio *et al.*, 2007). It therefore follows that any effect on Ca^{2+} homeostasis could impact on melanosomal pH and thus melanin production. This could implicate the TPCs, as Ca^{2+} channels of the endo-lysosomal system, in melanin production. Alternatively fusion events of the endo-lysosomal system have been shown to be sensitive to local Ca^{2+} levels when TPC2 over-expression was demonstrated to perturb endo-lysosomal trafficking (Ruas *et al.*, 2010). As a lysosome-related organelle, the biogenesis of melanosomes may also be sensitive to Ca^{2+} which could involve TPCs.

The effect of TPC2 in regulating pigmentation appears to be isoform selective as TPC1 does not replicate this phenotype. It has been shown that TPC2 is almost exclusively localised to the lysosome while TPC1 has a more heterogeneous distribution amongst acidic organelles (Brailoiu *et al.*, 2009a;Calcraft *et al.*, 2009). The localisation of TPCs to melanosomes in a pigmented cell line has not been investigated however. The effect on pigmentation of the *Xenopus* oocyte could therefore be due to the different localisation of the TPC isoforms or a direct result of differing channel functions between isoforms. Preliminary data indicates that when TPC2 is re-directed to the plasma membrane by mutation of an N-terminal lysosomal targeting motif, the pigmentation phenotype is not apparent (J. Marchant unpublished). This suggests that TPC2 has to be localised to the endo-lysosomal system for pigmentation to be perturbed. Over-expression of another lysosomal Ca^{2+} channel, TRPML1 could demonstrate whether the effect is deregulation of lysosomal Ca^{2+} or specific to TPC2. Furthermore expression of the pore mutant TPC2, which has been shown to be inactive, did not alter oocyte pigmentation. This suggests the pigmentation phenotype is a direct result of Ca^{2+} release through TPC2 when expressed on the lysosome.

A link between pigmentation defects and deregulation of Ca^{2+} has been demonstrated previously. A mutation of A419P in the Ca^{2+} channel TRPML3 renders the channel constitutively active (Xu *et al.*, 2007) and leads to the varitint-waddler mouse phenotype (Di *et al.*, 2002). This mouse displays pigmentation and

vestibular defects. TRPML3 is localised to the endo-lysosomal system and is highly expressed in melanocytes. The loss of pigmentation in varitint-waddler mice is consistent with loss of melanocytes in these mice, most likely due to Ca^{2+} toxicity from constitutively active TRPML3 leading to the death of melanocytes.

The potassium-dependent sodium-calcium exchanger NCKX5 is the most abundant sodium-calcium exchanger in human epidermal melanocytes (Ginger *et al.*, 2008)]. A non-synonymous SNP in the SLC4A5 gene encoding NCKX5 is associated with human skin colour variation (Lamason *et al.*, 2005). Knockdown of NCKX5 reduces melanin production in melanocytes, perhaps through a role in melanosome biogenesis as markers for this organelle were reduced after knockdown (Ginger *et al.*, 2008). Conversely levels of lysosome markers such as LAMP1 increased, suggesting a relationship between the synthesis of lysosomes and melanosomes. The A111T SNP, which confers a light skin colour, is linked to a decrease in exchanger activity. It has been proposed that NCKX5 localises to the melanosome (Lamason *et al.*, 2005) where a decrease in exchanger activity would lead to a decrease in Ca^{2+} uptake into the melanosome and a decrease in Na^{+} extrusion. Na^{+} uptake has been linked to H^{+} extrusion by another co-transporter, therefore if melanosome luminal Na^{+} levels remain high, H^{+} can not be extruded, leading to an acidification of the melanosome and a decrease in melanin production. This would link the SNP in NCKX5 to pale skin colour.

The standard TPC2-GFP plasmid expressed in the *Xenopus* oocytes and used throughout this thesis, corresponds to the M484/E734 SNP variant. While methionine at position 484 is the ancestral variant linked to brown hair, E734 is linked to the blonde hair phenotype by Sulem et al (Sulem *et al.*, 2008). This suggests that the E734 SNP in our clone is acting to perturb pigmentation in the *Xenopus* oocyte. Amino acid 734 is located at the C-terminus of the protein while position 484 is located in TM region 8 of domain II. Amino acid 484 is integral to a channel TM region and this may influence the structure or mechanics of the channel to alter Ca^{2+} flow through the channel. The cytosolic location of the C-terminal SNP

could influence binding of the TPC to other proteins which may regulate the channel. It would be interesting to examine the pigmentation of *Xenopus* oocytes injected with the TPC2 SNP variants then perform electrophysiological analysis or the microinjection Ca^{2+} release assay to investigate possible differences in gating or Ca^{2+} flux.

Both TRPML3 and NCKX5 demonstrate that melanin synthesis is intrinsically linked to Ca^{2+} homeostasis. This may be indirectly through the relationship between Ca^{2+} and regulation of the luminal pH of lysosomes and related organelles. It therefore seems possible that TPC2 and its associated SNP variants may also have different Ca^{2+} release properties that could govern Ca^{2+} homeostasis and luminal pH and thus modulate melanin synthesis and pigmentation.

In summary, TPC1 appears to be regulated by its N-terminus, providing an explanation for discrepant data between different lab groups regarding the functionality of this isoform. Furthermore, I present the first functional evidence linking TPC2 activity to pigmentation.

Chapter 7- General discussion & future aims

The two-pore channel (TPC) family of ion channels have recently been elucidated as the molecular targets of the intracellular, Ca^{2+}-mobilising, second messenger NAADP (Brailoiu *et al.*, 2009a;Calcraft *et al.*, 2009;Zong *et al.*, 2009). They represent a novel family of channels that were almost completely uncharacterised in animals before their recent association with NAADP. Therefore very little data exists about the channels and in particular the molecular properties that govern channel function. Properties such as how the TPCs integrate into the membrane upon expression, the topology they assume, the quaternary structure they subsequently form and ultimately how they are regulated have all been investigated here. While the work documented in this thesis and further data generated by our lab have helped to advance the understanding of the TPCs, many questions remain.

I reported in this thesis the cloning of a novel sea urchin TPC isoform, SpTPC3. The role of TPC3 isoforms is still open to debate however. SpTPC3 was shown to localise to acidic organelles (Brailoiu *et al.*, 2010a;Ruas *et al.*, 2010) and more specifically to endosomes,(Ruas *et al.*, 2010) as was chicken TPC3 (Calcraft *et al.*, 2009). Ruas et al report that membranes expressing SpTPC3 display enhanced NAADP binding (Ruas *et al.*, 2010). However expression of SpTPC3 acts in a dominant-negative manner to abolish the potentiation of NAADP-mediated Ca^{2+} release by expression of SpTPC2 as well as endogenous responses. They therefore conclude that the channel is non-functional. This is in contrast to our own data which suggests SpTPC3 is a functional NAADP-mediated Ca^{2+} release channel (Brailoiu *et al.*, 2010a). The functional differences observed may be due to SNP variation between SpTPC3 clones, alternatively the N-terminal tagging of the clone utilised by Ruas et al may inhibit channel function as has been demonstrated for HsTPC1 (Chapter 6). Using the N-terminal "self-cleaving" peptide to tag SpTPC3 may address functional differences seen between groups.

While TPC3 is present in most deuterostomes, including sea urchins, it is present as a pseudogene in humans (Brailoiu *et al.*, 2010a). Indeed the gene appears to have degenerated independently in both rodents and primates. Notably TPC3 is still present in New World monkeys and prosimians (Cai & Patel, 2010). This suggests selective pressures on the protein have ceased to exist leading to the degeneration of the channel in primates and rodents. Does this therefore infer that the channel mediates some long redundant function and may degenerate in further organisms? The TPC3 pseudogene is abundantly expressed in a sequence tag cluster found in the human reproductive organs, so it may have fulfilled a function in these tissues that is still required by certain animals. The localisation of TPC3 also overlaps with that of TPC1, therefore a degree of redundancy between TPC isoforms may exist. The characterisation of animal TPC3 from reproductive tissue, or other tissue in which TPC3 is shown to be the abundant isoform, may also be informative. Thus far analysis of TPC3 has been limited.

The topology and assembly of TPCs was also investigated. Both domains of TPC1 and TPC2 were capable of integrating independently into membranes suggesting a degree of redundancy in this mechanism. This is perhaps the result of protein evolution from single domain channels, such as the trp channels or voltage-gated K^+ channels, to TPCs. To investigate integration further, the domains could be dissected into individual or pairs of TM regions to observe which integrate with membranes. This would show whether TM regions integrate sequentially during translation or whether there is a degree of cooperation with certain domains facilitating the integration of others. A cooperative mechanism of TM region integration occurs in voltage-gated K^+ channels where negatively charged residues in the second TM region have been shown to interact with positively charged residues in the fourth TM region to promote integration (Tiwari-Woodruff *et al.*, 1997).

TPCs are members of the voltage-gated ion channel superfamily and as such their unique two-domain architecture makes it likely that they dimerise to preserve a four-pore functional channel arrangement. Redundancy was seen between domain

interactions with both domains of TPC1 and TPC2 capable of interacting with themselves, perhaps again a consequence of TPC evolution from single domain channels. Furthermore the nature of these domain interactions may differ between isoforms. Domain II of TPC1 and domain I of TPC2 appeared to form dimer sized oligomers in the absence of cross-linker, resistant to the reducing conditions required for SDS-PAGE and Western blot. Although immunoprecipitation suggests redundancy in domain interaction, TPC1 DII and TPC2 DI may be much more rigorously associated and thus the primary promoters of TPC assembly. A close relative of the TPCs, TRPP2, has three known dimerisation domains that contribute to the formation of the active tetrameric channel (Feng *et al.*, 2011). These dimer-mediating domains are found in the N- and C-termini as well as the linker between the putative 5^{th} and 6^{th} TM regions. TPC2 also contains a consensus sequence (GxxxA/G) within TM region 7, which has been implicated in the dimerisation of polytopic proteins, such as the ABC transporter protein G2 (Polgar *et al.*, 2010). It is possible this may function to mediate dimerisation of TPC2 also. Indeed unlike TPC1, dimer-sized protein bands have been consistently visualised for full-length TPC2 by Western blot.

Gel filtration chromatography, sucrose dentistry gradient fractionation and cross-linking of full length TPCs was unable to reach a consensus as to the size of the native TPC channel complex. Utilising other cross-linking reagents, such as 3,3'-dithiobis(sufosuccinimidylpropionate) (DTSSP) which reacts via amine groups (Staros, 1982) or other techniques to resolve native channel size, such as blue-native PAGE (Schagger & von Jagow, 1991) or perfluoro-octanoic acid (PFO)-PAGE (Ramjeesingh *et al.*, 1999) may reveal the stoichiometry of TPCs the functional channel.

From successful integration into ER membranes and formation of channels, the TPCs are next required to traffic to their site of action. The SpTPCs were shown to localise to acidic organelles with SpTPC1 appearing to be broadly distributed throughout the endo-lysosomal system, SpTPC2 localised to the lysosome and

SpTPC3 to the endosome (Chapter 2). This distribution reflects that observed for human TPCs (Brailoiu *et al.*, 2009a;Calcraft *et al.*, 2009;Zong *et al.*, 2009). Targeting of TPC2 to the lysosome is mediated by an N-terminal dileucine consensus sequence (Brailoiu *et al.*, 2010b). TPC1 has such motifs in the N and C-terminus but mutation of both was unable to redirect the protein to the plasma membrane as occurred with TPC2. The wide ranging distribution of TPC1 makes assessment of perturbed trafficking problematic, however with both these dileucine motifs mutated, TPC1 retained a punctuate intracellular distribution. Examination of the targeting of individual domains of TPC1 may reveal whether redundancy in targeting exists however. TPC1 contains tyrosine (YxxL/I/M/F) based consensus sequences in the domain linker, that are also implicated in endo-lysosomal targeting and perhaps these mediate trafficking of this isoform. The exact mechanism of TPC1 targeting remains elusive for now though.

Elucidating the topology of TPCs proposed a probable twelve transmembrane regions, arranged in two domains of six TM regions, and cytosolic termini. These cytosolic termini could contribute to oligomerisation, as with TRPP2 (discussed above), but could also mediate interactions with other proteins to form a channel complex or to modulate channel function. Indeed, both termini of TPC1 and TPC2 contain significant clusters of acidic and basic residues and are therefore primed for forming electrostatic interactions with other proteins. The domain linker is also cytosolic and may mediate protein interactions as well. In Chapter 5 it was postulated that the linker may interact with a "β-type" accessory protein due to the presence of sequence with homology to the Ca_v AID. Establishing the "interactome" of TPCs seems to me a key goal in TPC research, especially as it is proposed NAADP may bind an undefined accessory protein (Calcraft *et al.*, 2009;Galione, 2011). Defining the "interactome" could be achieved by methods such as a yeast-2-hybrid screen (Fields & Song, 1989) with cytosolic channel domains as the bait to screen for interacting partners. The distal C-terminus of TPC1 also contains a type-III consensus sequence for 14-3-3 protein binding (S/TX_{1-2}-COOH) (Coblitz *et al.*, 2006), as first identified in the plant TPC1 protein (MacRobbie & Smyth, 2010). 14-

3-3 proteins bind phosphorylated residues to modulate a wide range of effects, such as stabilising protein conformations to promote activation or inactivation, trafficking and interactions with other proteins (van Heusden, 2005). The inactivation properties of the $Ca_v2.2$ channel have been shown to be regulated by 14-3-3 proteins (Li *et al.*, 2006) and it would be interesting to investigate if TPC1 is also modulated by 14-3-3 binding. As discussed in Chapter 5, TPCs may form signalling microdomains as has been demonstrated for IP_3 receptors.

TPCs, located on the endo-lysosomal system may also interact with other channels to form signalling microdomains, as discussed in Chapter 5. In support of this theory, TPCs have recently been shown to interact with TRPML1, although the exact function of this interaction remains unknown (Yamaguchi *et al.*, 2011). Perhaps a close, even physical, interaction with ryanodine receptors in such a signalling microdomain, may explain why some data suggests ryanodine receptors are NAADP-sensitive (Dammermann & Guse, 2005). The high-molecular weight complexes seen by cross-linking may therefore represent TPC channel complexes with associated proteins.

In Chapter Six, the N-terminus of TPC1 was shown to regulate channel activity, perhaps by the formation of intra-molecular electrostatic interactions, as occurs in the hERG K^+ channel (de la *et al.*, 2011) and Cav2.2 (Agler *et al.*, 2005). It was notable from the FPP assays used to determine topology in Chapter 4, that the N-terminal fluorophore of TPC1 was the most resistant to trypsin degradation (~ 51%). This could be indicative of a terminus that is not fully accessible to trypsin digestion and is tightly associated with the channel. The channel activity of TRPV5 has been shown to be regulated by the N-terminus (de *et al.*, 2011) with N-terminal deletion constructs utilised to explore this. An incremental deletion approach could be applied to map N-terminal regions of TPC1 required for function and if TPCs dimerise these could act in a dominant negative manner, as shown for $Ca_v2.2$ (Raghib *et al.*, 2001). In contrast, TPC2 appears to retain activity with an N-terminal tag and therefore may be differentially regulated. A chimera of TPC1 expressing a

TPC2 N-terminus may also be informative to investigate channel regulation. The $Ca_v2.2$ channel has also been shown to be regulated by the N-terminal interaction with the DI-DII linker, as demonstrated by the use of inhibitory peptides corresponding to the N-terminus or DI-DII linker region (Bucci *et al.*, 2011). Such N-terminal peptides could also be developed for TPCs, where they may mediate channel inactivation in an isoform selective manner. This would be of use if TPC1 was implicated in a disease model and an antagonist was required for therapeutic intervention. The mechanism by which TPC1 (and potentially TPC3) is regulated by the N-terminus remains to be fully elucidated.

Other potential mechanisms of regulation that remain to be investigated include luminal pH and Ca^{2+}. Schieder et al were able to record TPC2 currents only at acidic luminal pH (Schieder *et al.*, 2010b) in contrast to work by ourselves (Brailoiu *et al.*, 2010b) and Pitt et al (Pitt *et al.*, 2010) where currents were recorded at more neutral pH. Furthermore Pitt et al proposed that TPC2 currents were sensitive to the luminal Ca^{2+} concentration. It therefore remains to be determined which, presumably luminal, residues confer potential sensitivity to pH and Ca^{2+}. This would represent an important mechanism of channel regulation, given the location of TPCs on acidic Ca^{2+} stores. In TRPM2, negatively charged (acidic) amino acids located in and adjacent to the putative pore loop have been implicated in pH sensitivity (Du *et al.*, 2009) and such residues are certainly present in the pore regions of TPCs. Numerous residues in TRP channels have been implicated in channel function either by scanning mutagenesis or characterisation of mutations associated with a disease phenotype. Some of these residues appear to show conservation with TPCs and may indicate a conserved function between the channel families. Notably, a multiple sequence alignment of TRPP2 with TPCs reveals conservation of TRPP2 amino acid D511 located in TM region 3 of the channel, with an aspartic acid residue of TPC1 and TPC2 located in TM region 3 of DII (data not shown). Mutation of this amino acid to a valine is associated with the PKD phenotype and manifests as a loss of TRPP2 currents. This residue may therefore also be important in regulating TPC activity.

Finally the physiology of TPC2 in the definition of pigmentation needs to be examined. Data in Chapter six indicated that TPC2 but not TPC1 mediated a pigmentation defect in the animal pole of the *Xenopus* oocyte, The role of the SNP variants of TPC2 remains to be explored. The decreased and perturbed pigmentation of the *Xenopus* oocyte animal pole may correlate to the blonde hair phenotype as this is caused by decreased amounts of the dark pigment eumelanin. It remains to test the full complement of TPC2 variants in the *Xenopus* pigmentation assay, where we would predict the ancestral SNP combination does not lead to a pigmentation defect. Towards this, I have already examined the effect of SNP variation on TPC2 localisation, expression and N-glycosylation (see Appendix). If the ancestral SNP variant does not lead to a pigmentation defect then the next logical step would be to utilise the SNP variants in the NAADP microinjection assay (Brailoiu *et al.*, 2009a) to examine if possible differences in Ca^{2+} release, and perhaps associated pH, determine pigment production.

As summarised in Figure 7.1, the questions raised from the data presented in this thesis are important for the progression of our knowledge regarding the molecular properties of the TPCs and will hopefully be investigated in the coming years.

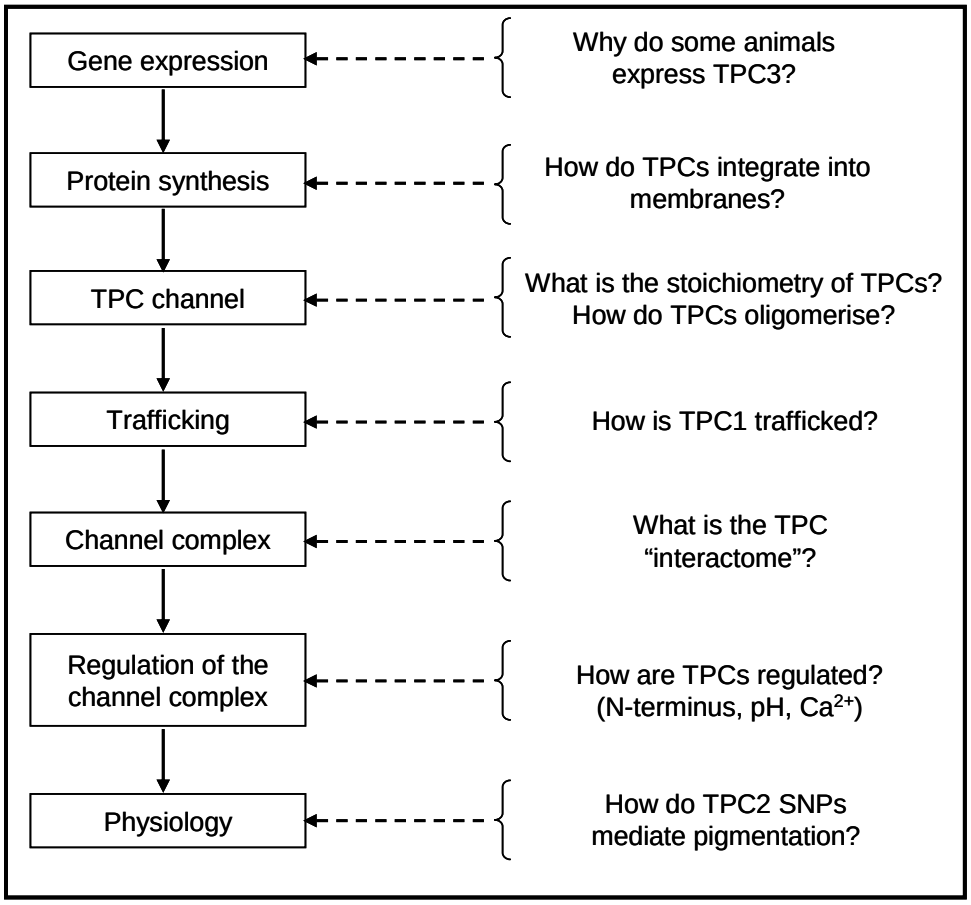

Figure 7.1. Schematic diagram of future aims for the characterisation of TPCs.

Appendix - Analysis of TPC2 SNP variants linked to pigmentation

In the study by Sulem et al, the determinants of pigmentation in Europeans were investigated and two exonic single nucleotide polymorphisms (SNPs) in the TPC2 gene, associated with blonde vs. brown hair colour, were identified (Sulem *et al.*, 2008). The identified SNPs encoded amino acids M484L and G734E, with methionine (M)484 and glycine (G)734 representing the ancestral allele correlating to brown hair colour. The standard TPC2-GFP plasmid expressed in the *Xenopus* oocyte in Chapter Six and used throughout this work, corresponds to the M484/E734 SNP variant. The four possible SNP combinations (ME, MG, LE, and LG) were cloned and the effect of each SNP investigated on localisation, expression and N-glycosylation.

TPC2 pigmentation SNP variants were created using the Stratagene QuikChange® Site-directed mutagenesis kit (as described in Chapter 4) and mutagenic primers listed in Table A.1.TPC2-GFP (M484/E734) was used as a template to create SNP variant TPC2 LE by mutagenesis using primer pair 1F and 1R. TPC2 MG was created by mutagenesis of TPC2 ME using primer pair 2F and 2R. TPC2 LG was created by using the TPC2 LE plasmid as a template and primer pair 2F and 2R. Mutagenesis was performed using Pfu Ultra II polymerase (Stratagene) with 16 cycles of PCR at an annealing temperature of 55°C and an extension temperature of 72°C.

Mutation	Primer	Sequence
M484L	1F	GTACTACCTGTTGGAG**TTG**CTGCTCAAGGTCTTTGCCC
	1R	GGGCAAAGACCTTGAGCAG**CAA**CTCCAACAGGTAGTAC
E734G	2F	GGGATATTCTGGAGGAGCCC**GGG**GAGGATGAGCTCACAGAGAGG
	2R	CCTCTCTGTGAGCTCATCCTC**CCC**GGGCTCCTCCAGAATATCCC

Table A.1 Primers for the creation of TPC2 pigmentation-linked SNP variants. The primer pair for the creation of each mutant is listed with sequences for the forward (F) and reverse (R) primer (5' to 3' direction).

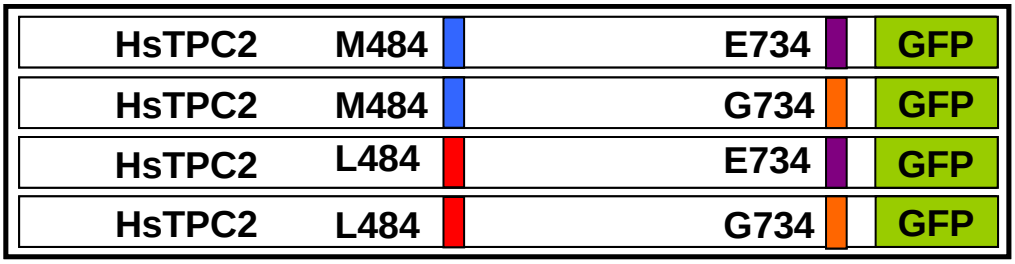

Figure A.1. TPC2 SNP clones utilised in the characterisation of TPC2 in the homeostasis of pigmentation. All TPC SNP variants were expressed with a GFP tag at the C-terminus.

First the effect of the expressing the SNP variants on TPC2 localisation was examined. Each SNP variant was over-expressed in SKBR3 cells with the lysosomal marker LAMP1. We have previously shown our TPC2 clone (TPC2 ME) to be localised almost exclusively within the lysosome. When the SNP variants were expressed their localisation coincided with the marker LAMP1, suggesting lysosomal targeting is not altered by SNP variation (Figure A.2). With all TPC2 SNPs, expression was intracellular and appeared to be on vesicular membranes as witnessed by large round vesicular structures that were clearly visible.

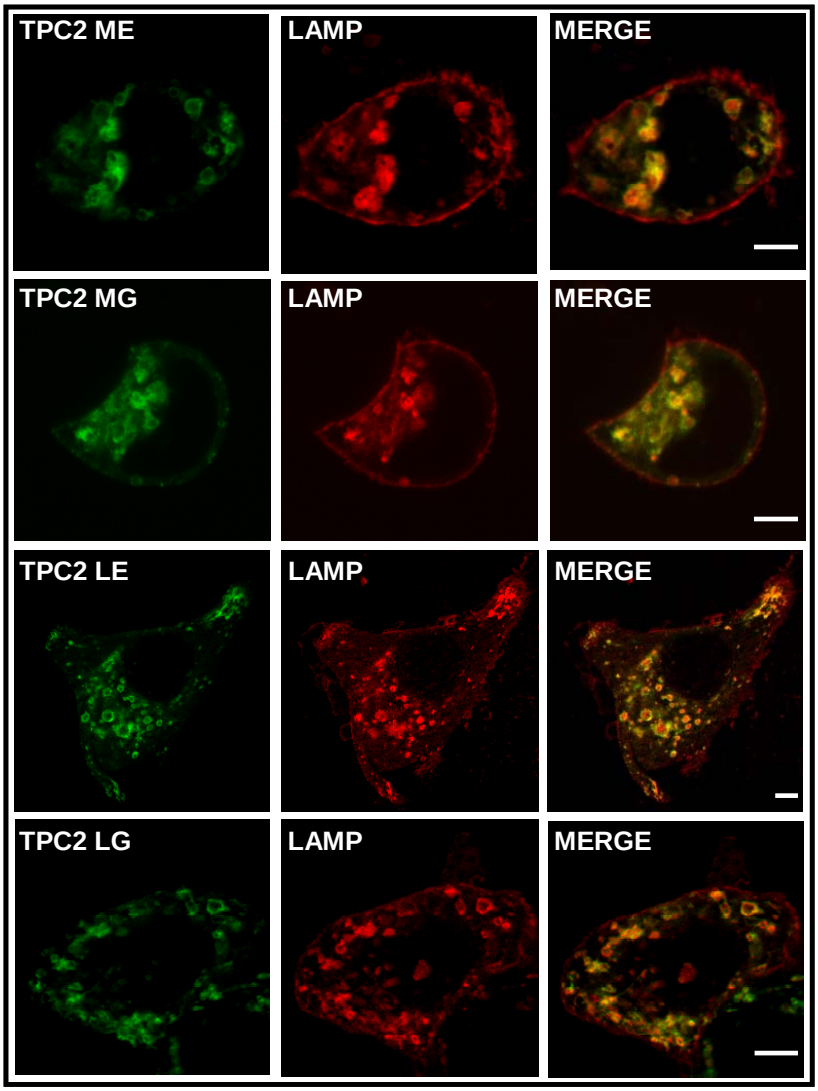

Figure A.2. Expression of TPC2 SNP variants does not alter TPC2 localisation. Confocal imaging of the four SNP variants of TPC2 tagged with a C-terminal GFP fluorophore and overexpressed in SKBR3 cells with the lysosomal marker LAMP1-RFP. All SNP variants showed good colocalisation between TPC2 and lysosomes. Scale bar 5 μm.

Having ascertained that localisation was unchanged, the expression, size and glycosylation were next examined by Western blotting and treatment of cell homogenates with the endoglycosidase PNGase F. Expression of the four SNP variants showed no change in apparent molecular weight in the absence or presence of PNGase F (Figure A.3). All appeared as a double protein band likely representing the full and core glycosylated forms of the protein and a single deglycosylated

species upon PNGase F treatment. The Western blot below appears to indicate that TPC2 LE is more abundant when equal amounts of protein is resolved by SDS-PAGE, however this is not consistent over multiple experiments (*n*=3) where protein levels seemed consistent. Therefore it is likely that the relative expression levels of TPC2 variants are unaffected by the SNPs implicated in pigmentation.

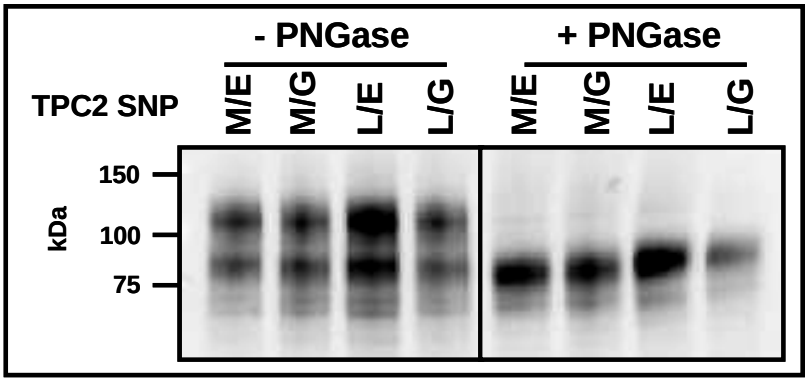

Figure A.3. SNP variants of TPC2 do not affect protein size or expression levels. Western blot of TPC2 SNP variants in the absence (- PNGase) or presence (+ PNGase) of PNGase F. No change in size or relative expression levels is seen across multiple experiments (*n*=3).

It remains to inject the full complement of TPC2 SNP variants in *Xenopus* oocytes and observe the pigmentation of the animal pole. It would also be informative to examine the Ca^{2+} release properties of TPC2 in SKBR3 cells with the NAADP-microinjection assay or redirect the proteins to the plasma membrane and subject them to record the electrophysiology of the channels.

Publications associated with this thesis

Brailoiu,E, Churamani,D, Cai,X, Schrlau,MG, Brailoiu,GC, Gao,X, **Hooper,R**, Boulware,MJ, Dun,NJ, Marchant,JS, Patel,S: Essential requirement for two-pore channel 1 in NAADP-mediated calcium signaling. J Cell Biol 186:201-209, 2009

Brailoiu,E, **Hooper,R**, Cai,X, Brailoiu,GC, Keebler,MV, Dun,NJ, Marchant,JS, Patel,S: An ancestral deuterostome family of two-pore channels mediates nicotinic acid adenine dinucleotide phosphate-dependent calcium release from acidic organelles. J Biol Chem 285:2897-2901, 2010

Brailoiu,E, Rahman,T, Churamani,D, Prole,DL, Brailoiu,GC, **Hooper,R**, Taylor,CW, Patel,S: An NAADP-gated two-pore channel targeted to the plasma membrane uncouples triggering from amplifying Ca^{2+} signals. J Biol Chem 285:38511-38516, 2010

Hooper,R, Churamani,D, Brailoiu,E, Taylor,CW, Patel,S: Membrane Topology of NAADP-sensitive Two-pore Channels and Their Regulation by N-linked Glycosylation. J Biol Chem 286:9141-9149, 2011

Churamani,D, **Hooper,R**, Brailoiu,E, Patel,S: Domain assembly of NAADP-gated two-pore channels. Biochem J ,441: 1, 317-323, 2012.

Hooper, R, Patel,S: Chapter 14: NAADP on target. Calcium Signaling, Advances in Experimental Medicine and Biology, Vol. 740. 2012. ISBN 978-94-007-2887-5.

Reference List

Adebiyi A, Narayanan D, & Jaggar JH (2011). Caveolin-1 assembles type 1 inositol 1,4,5-trisphosphate receptors and canonical transient receptor potential 3 channels into a functional signaling complex in arterial smooth muscle cells. *J Biol Chem* 286, 4341-4348.

Agler HL, Evans J, Tay LH, Anderson MJ, Colecraft HM, & Yue DT (2005). G protein-gated inhibitory module of N-type $Ca_v2.2$ Ca^{2+} channels. *Neuron* 46, 891-904.

Aley PK, Mikolajczyk AM, Munz B, Churchill GC, Galione A, & Berger F (2010a). Nicotinic acid adenine dinucleotide phosphate regulates skeletal muscle differentiation via action at two-pore channels. *Proc Natl Acad Sci U SA* 107, 19927-19932.

Aley PK, Noh HJ, Gao X, Tica AA, Brailoiu E, & Churchill GC (2010b). A functional role for nicotinic acid adenine dinucleotide phosphate in oxytocin-mediated contraction of uterine smooth muscle from rat. *J Pharmacol Exp Ther* 333, 726-735.

Anyatonwu GI, Estrada M, Tian X, Somlo S, & Ehrlich BE (2007). Regulation of ryanodine receptor-dependent calcium signaling by polycystin-2. *Proc Natl Acad Sci U S A* 104, 6454-6459.

Arif SH (2009). A Ca^{2+}-binding protein with numerous roles and uses: parvalbumin in molecular biology and physiology. *Bioessays* 31, 410-421.

Berg I, Potter BV, Mayr GW, & Guse AH (2000). Nicotinic acid adenine dinucleotide phosphate $NAADP^+$ is an essential regulator of T-lymphocyte Ca^{2+}-signaling. *J Cell Biol* 150, 581-588.

Berridge G, Dickinson G, Parrington J, Galione A, & Patel S (2002). Solubilization of receptors for the novel Ca^{2+}-mobilizing messenger, nicotinic acid adenine dinucleotide phosphate. *J Biol Chem* 277, 43717-43723.

Berridge MJ (1983). Rapid accumulation of inositol trisphosphate reveals that agonists hydrolyse polyphosphoinositides instead of phosphatidylinositol. *Biochem J* 212, 849-858.

Berridge MJ, Lipp P, & Bootman MD (2000). The versatility and universality of calcium signalling. *Nat Rev Mol Cell Biol* 1, 11-21.

Beyhl D, Hortensteiner S, Martinoia E, Farmer EE, Fromm J, Marten I, & Hedrich R (2009). The fou2 mutation in the major vacuolar cation channel TPC1 confers tolerance to inhibitory luminal calcium. *Plant J* 58, 715-723.

Blaustein MP & Lederer WJ (1999). Sodium/calcium exchange: its physiological implications. *Physiol Rev* 79, 763-854.

Boitier E, Rea R, & Duchen MR (1999). Mitochondria exert a negative feedback on the propagation of intracellular Ca^{2+} waves in rat cortical astrocytes. *J Cell Biol* 145, 795-808.

Bonaventure G, Gfeller A, Rodriguez VM, Armand F, & Farmer EE (2007). The fou2 gain-of-function allele and the wild-type allele of Two Pore Channel 1 contribute to different extents or by different mechanisms to defense gene expression in Arabidopsis. *Plant Cell Physiol* 48, 1775-1789.

Bowman EJ, Siebers A, & Altendorf K (1988). Bafilomycins: a class of inhibitors of membrane ATPases from microorganisms, animal cells, and plant cells. *Proc Natl Acad Sci U S A* 85, 7972-7976.

Brailoiu E, Churamani D, Cai X, Schrlau MG, Brailoiu GC, Gao X, Hooper R, Boulware MJ, Dun NJ, Marchant JS, & Patel S (2009a). Essential requirement for two-pore channel 1 in NAADP-mediated calcium signaling. *J Cell Biol* 186, 201-209.

Brailoiu E, Churamani D, Pandey V, Brailoiu GC, Tuluc F, Patel S, & Dun NJ (2006). Messenger-specific role for nicotinic acid adenine dinucleotide phosphate in neuronal differentiation. *J Biol Chem* 281, 15923-15928.

Brailoiu E, Hoard JL, Filipeanu CM, Brailoiu GC, Dun SL, Patel S, & Dun NJ (2005). Nicotinic acid adenine dinucleotide phosphate potentiates neurite outgrowth. *J Biol Chem* 280, 5646-5650.

Brailoiu E, Hooper R, Cai X, Brailoiu GC, Keebler MV, Dun NJ, Marchant JS, & Patel S (2010a). An ancestral deuterostome family of two-pore channels mediates nicotinic acid adenine dinucleotide phosphate-dependent calcium release from acidic organelles. *J Biol Chem* 285, 2897-2901.

Brailoiu E, Miyamoto MD, & Dun NJ (2001). Nicotinic acid adenine dinucleotide phosphate enhances quantal neurosecretion at the frog neuromuscular junction: possible action on synaptic vesicles in the releasable pool. *Mol Pharmacol* 60, 718-724.

Brailoiu E, Patel S, & Dun NJ (2003). Modulation of spontaneous transmitter release from the frog neuromuscular junction by interacting intracellular Ca^{2+} stores: critical role for nicotinic acid-adenine dinucleotide phosphate (NAADP). *Biochem J* 373, 313-318.

Brailoiu E, Rahman T, Churamani D, Prole DL, Brailoiu GC, Hooper R, Taylor CW, & Patel S (2010b). An NAADP-gated two-pore channel targeted to the plasma membrane uncouples triggering from amplifying Ca^{2+} signals. *J Biol Chem* 285, 38511-38516.

Brailoiu GC, Brailoiu E, Parkesh R, Galione A, Churchill GC, Patel S, & Dun NJ (2009b). NAADP-mediated channel 'chatter' in neurons of the rat medulla oblongata. *Biochem J* 419, 91-7, 2.

Brini M & Carafoli E (2011). The plasma membrane Ca^{2+} ATPase and the plasma membrane sodium calcium exchanger cooperate in the regulation of cell calcium. *Cold Spring Harb Perspect* Biol 3.

Bucci G, Mochida S, & Stephens GJ (2011). Inhibition of synaptic transmission and G protein modulation by synthetic $Ca_V2.2$ Ca^{2+} channel peptides. *J Physiol* 589, 3085-3101.

Cai X & Patel S (2010). Degeneration of an intracellular ion channel in the primate lineage by relaxation of selective constraints. *Mol Biol Evol* 27, 2352-2359.

Calcraft PJ, Ruas M, Pan Z, Cheng X, Arredouani A, Hao X, Tang J, Rietdorf K, Teboul L, Chuang KT, Lin P, Xiao R, Wang C, Zhu Y, Lin Y, Wyatt CN, Parrington J, Ma J, Evans AM, Galione A, & Zhu MX (2009). NAADP mobilizes calcium from acidic organelles through two-pore channels. *Nature* 459, 596-600.

Cancela JM, Churchill GC, & Galione A (1999). Coordination of agonist-induced Ca^{2+}-signalling patterns by NAADP in pancreatic acinar cells. *Nature* 398, 74-76.

Carlsson SR, Roth J, Piller F, & Fukuda M (1988). Isolation and characterization of human lysosomal membrane glycoproteins, h-lamp-1 and h-lamp-2. Major sialoglycoproteins carrying polylactosaminoglycan. *J Biol Chem* 263, 18911-18919.

Catterall WA (2011). Voltage-gated calcium channels. *Cold Spring Harb Perspect* Biol 3.

Chameau P, Van d, V, Fossier P, & Baux G (2001). Ryanodine-, IP3- and NAADP-dependent calcium stores control acetylcholine release. *Pflugers Arch* 443, 289-296.

Chikh K, Vey S, Simonot C, Vanier MT, & Millat G (2004). Niemann-Pick type C disease: importance of N-glycosylation sites for function and cellular location of the NPC2 protein. *Mol Genet Metab* 83, 220-230.

Chin D & Means AR (2000). Calmodulin: a prototypical calcium sensor. *Trends Cell Biol* 10, 322-328.

Chini EN & Dousa TP (1996). Nicotinate-adenine dinucleotide phosphate-induced Ca^{2+}-release does not behave as a Ca^{2+}-induced Ca^{2+}-release system. *Biochem J* 316 (Pt 3), 709-711.

Christensen KA, Myers JT, & Swanson JA (2002). pH-dependent regulation of lysosomal calcium in macrophages. *J Cell Sci* 115, 599-607.

Churamani D, Dickinson GD, & Patel S (2005). NAADP binding to its target protein in sea urchin eggs requires phospholipids. *Biochem J* 386, 497-504.

Churamani D, Dickinson GD, Ziegler M, & Patel S (2006). Time sensing by NAADP receptors. *Biochem J* 397, 313-320.

Churamani D, Hooper R, Brailoiu E, & Patel S (2012). Domain assembly of NAADP-gated two-pore channels. *Biochem J* 441, 317 – 323.

Churchill GC & Galione A (2000). Spatial control of Ca^{2+} signaling by nicotinic acid adenine dinucleotide phosphate diffusion and gradients. *J Biol Chem* 275, 38687-38692.

Churchill GC & Galione A (2001). NAADP induces Ca^{2+} oscillations via a two-pool mechanism by priming IP_3- and cADPR-sensitive Ca^{2+} stores. *EMBO J* 20, 2666-2671.

Churchill GC, O'Neill JS, Masgrau R, Patel S, Thomas JM, Genazzani AA, & Galione A (2003). Sperm deliver a new second messenger: NAADP. *Curr Biol* 13, 125-128.

Churchill GC, Okada Y, Thomas JM, Genazzani AA, Patel S, & Galione A (2002). NAADP mobilizes Ca^{2+} from reserve granules, lysosome-related organelles, in sea urchin eggs. *Cell* 111, 703-708.

Clapham DE, Runnels LW, & Strubing C (2001). The TRP ion channel family. *Nat Rev Neurosci* 2, 387-396.

Clapper DL & Lee HC (1985). Inositol trisphosphate induces calcium release from nonmitochondrial stores in sea urchin egg homogenates. *J Biol Chem* 260, 13947-13954.

Clapper DL, Walseth TF, Dargie PJ, & Lee HC (1987). Pyridine nucleotide metabolites stimulate calcium release from sea urchin egg microsomes desensitized to inositol trisphosphate. *J Biol Chem* 262, 9561-9568.

Coblitz B, Wu M, Shikano S, & Li M (2006). C-terminal binding: an expanded repertoire and function of 14-3-3 proteins. *FEBS Lett* 580, 1531-1535.

Cserzo M, Wallin E, Simon I, von HG, & Elofsson A (1997). Prediction of transmembrane alpha-helices in prokaryotic membrane proteins: the dense alignment surface method. *Protein Eng* 10, 673-676.

Dammermann W & Guse AH (2005). Functional ryanodine receptor expression is required for NAADP-mediated local Ca^{2+} signaling in T-lymphocytes. *J Biol Chem* 280, 21394-21399.

Davies A, Hendrich J, Van Minh AT, Wratten J, Douglas L, & Dolphin AC (2007). Functional biology of the alpha(2)delta subunits of voltage-gated calcium channels. *Trends Pharmacol Sci* 28, 220-228.

de la Pena P, Alonso-Ron C, Machin A, Fernandez-Trillo J, Carretero L, Dominguez P, & Barros F (2011). Demonstration of physical proximity between the N terminus and the S4-S5 linker of the human ether-a-go-go-related gene (hERG) potassium channel. *J Biol Chem* 286, 19065-19075.

de Groot T, van der Hagen EA, Verkaart S, Te B, V, Bindels RJ, & Hoenderop JG (2011). Role of the Transient Receptor Potential Vanilloid 5 (TRPV5) Protein N Terminus in Channel Activity, Tetramerization, and Trafficking. *J Biol Chem* 286, 32132-32139.

Di PF, Belyantseva IA, Kim HJ, Vogt TF, Kachar B, & Noben-Trauth K (2002). Mutations in Mcoln3 associated with deafness and pigmentation defects in varitint-waddler (Va) mice. *Proc Natl Acad Sci U S A* 99, 14994-14999.

Dickinson GD & Patel S (2003). Modulation of NAADP (nicotinic acid-adenine dinucleotide phosphate) receptors by K^+ ions: evidence for multiple NAADP receptor conformations. *Biochem J* 375, 805-812.

Dolphin AC (2009). Calcium channel diversity: multiple roles of calcium channel subunits. *Curr Opin Neurobiol* 19, 237-244.

Du J, Xie J, & Yue L (2009). Modulation of TRPM2 by acidic pH and the underlying mechanisms for pH sensitivity. *J Gen Physiol* 134, 471-488.

Esposito B, Gambara G, Lewis AM, Palombi F, D'Alessio A, Taylor LX, Genazzani AA, Ziparo E, Galione A, Churchill GC, & Filippini A (2011). NAADP links histamine H1 receptors to secretion of von Willebrand factor in human endothelial cells. *Blood* 117, 4968-4977.

Feng S, Rodat-Despoix L, Delmas P, & Ong AC (2011). A single amino acid residue constitutes the third dimerization domain essential for the assembly and function of the tetrameric polycystin-2 (TRPP2) channel. *J Biol Chem* 286, 18994-19000.

Fields S & Song O (1989). A novel genetic system to detect protein-protein interactions. *Nature* 340, 245-246.

Fill M & Copello JA (2002). Ryanodine receptor calcium release channels. *Physiol Rev* 82, 893-922.

Foskett JK, White C, Cheung KH, & Mak DO (2007). Inositol trisphosphate receptor Ca^{2+} release channels. *Physiol Rev* 87, 593-658.

Freise D, Held B, Wissenbach U, Pfeifer A, Trost C, Himmerkus N, Schweig U, Freichel M, Biel M, Hofmann F, Hoth M, & Flockerzi V (2000). Absence of the gamma subunit of the skeletal muscle dihydropyridine receptor increases L-type Ca^{2+} currents and alters channel inactivation properties. *J Biol Chem* 275, 14476-14481.

Furuichi T, Cunningham KW, & Muto S (2001). A putative two pore channel AtTPC1 mediates Ca^{2+} flux in Arabidopsis leaf cells. *Plant Cell Physiol* 42, 900-905.

Gabow PA, Kimberling WJ, Strain JD, Manco-Johnson ML, & Johnson AM (1997). Utility of ultrasonography in the diagnosis of autosomal dominant polycystic kidney disease in children. *J Am Soc Nephrol* 8, 105-110.

Gagescu R, Demaurex N, Parton RG, Hunziker W, Huber LA, & Gruenberg J (2000). The recycling endosome of Madin-Darby canine kidney cells is a mildly acidic compartment rich in raft components. *Mol Biol Cell* 11, 2775-2791.

Galione A (2011). NAADP receptors. *Cold Spring Harb Perspect Biol* 3, a004036.

Galione A (2006). NAADP, a new intracellular messenger that mobilizes Ca^{2+} from acidic stores. *Biochem Soc Trans* 34, 922-926.

Galione A, Evans AM, Ma J, Parrington J, Arredouani A, Cheng X, & Zhu MX (2009). The acid test: the discovery of two-pore channels (TPCs) as NAADP-gated endolysosomal Ca^{2+} release channels. *Pflugers Arch* 458, 869-876.

Galione A, Morgan AJ, Arredouani A, Davis LC, Rietdorf K, Ruas M, & Parrington J (2010). NAADP as an intracellular messenger regulating lysosomal calcium-release channels. *Biochem Soc Trans* 38, 1424-1431.

Genazzani AA & Galione A (1996). Nicotinic acid-adenine dinucleotide phosphate mobilizes Ca^{2+} from a thapsigargin-insensitive pool. *Biochem J* 315 (Pt 3), 721-725.

Ginger RS, Askew SE, Ogborne RM, Wilson S, Ferdinando D, Dadd T, Smith AM, Kazi S, Szerencsei RT, Winkfein RJ, Schnetkamp PP, & Green MR (2008). SLC24A5 encodes a trans-Golgi network protein with potassium-dependent sodium-calcium exchange activity that regulates human epidermal melanogenesis. *J Biol Chem* 283, 5486-5495.

Glauser G, Grata E, Dubugnon L, Rudaz S, Farmer EE, & Wolfender JL (2008). Spatial and temporal dynamics of jasmonate synthesis and accumulation in Arabidopsis in response to wounding. *J Biol Chem* 283, 16400-16407.

Grottesi A, Sands ZA, & Sansom MS (2005). Potassium channels: complete and undistorted. *Curr Biol* 15, R771-R774.

Gu X & Spitzer NC (1995). Distinct aspects of neuronal differentiation encoded by frequency of spontaneous Ca^{2+} transients. *Nature* 375, 784-787.

Gyorke I & Gyorke S (1998). Regulation of the cardiac ryanodine receptor channel by luminal Ca^{2+} involves luminal Ca^{2+} sensing sites. *Biophys J* 75, 2801-2810.

Hackney CM, Mahendrasingam S, Penn A, & Fettiplace R (2005). The concentrations of calcium buffering proteins in mammalian cochlear hair cells. *J Neurosci* 25, 7867-7875.

Haga Y, Ishii K, & Suzuki T (2011). N-Glycosylation Is Critical for the Stability and Intracellular Trafficking of Glucose Transporter GLUT4. *J Biol Chem* 286, 31320-31327.

Hao M, Lin SX, Karylowski OJ, Wustner D, McGraw TE, & Maxfield FR (2002). Vesicular and non-vesicular sterol transport in living cells. The endocytic recycling compartment is a major sterol storage organelle. *J Biol Chem* 277, 609-617.

Hashimoto K, Saito M, Matsuoka H, Iida K, & Iida H (2004). Functional analysis of a rice putative voltage-dependent Ca^{2+} channel, OsTPC1, expressed in yeast cells lacking its homologous gene CCH1. *Plant Cell Physiol* 45, 496-500.

Heinemann SH, Terlau H, Stuhmer W, Imoto K, & Numa S (1992). Calcium channel characteristics conferred on the sodium channel by single mutations. *Nature* 356, 441-443.

Hibino H, Inanobe A, Furutani K, Murakami S, Findlay I, & Kurachi Y (2010). Inwardly rectifying potassium channels: their structure, function, and physiological roles. *Physiol Rev* 90, 291-366.

Hirokawa T, Boon-Chieng S, & Mitaku S (1998). SOSUI: classification and secondary structure prediction system for membrane proteins. *Bioinformatics* 14, 378-379.

Hoffmeister H, Gallagher AR, Rascle A, Witzgall R (2010). The human polycystin-2 protein represents an integral membrane protein with six membrane-spanning domains and intracellular N- and C-termini. *Biochem J* 433, 285 – 394.

Hohenegger M, Suko J, Gscheidlinger R, Drobny H, & Zidar A (2002). Nicotinic acid-adenine dinucleotide phosphate activates the skeletal muscle ryanodine receptor. *Biochem J* 367, 423-431.

Hooper R, Churamani D, Brailoiu E, Taylor CW, & Patel S (2011). Membrane Topology of NAADP-sensitive Two-pore Channels and Their Regulation by N-linked Glycosylation. *J Biol Chem* 286, 9141-9149.

Hoth M & Penner R (1992). Depletion of intracellular calcium stores activates a calcium current in mast cells. *Nature* 355, 353-356.

Huang KP (1989). The mechanism of protein kinase C activation. *Trends Neurosci* 12, 425-432.

Hwang GS, Jian CY, Chen TJ, Chen ST, & Wang SW (2009). Effects of Hypoxia on Testosterone Release in Rat Leydig cells. *Am J Physiol Endocrinol Metab.*

Ishibashi K, Suzuki M, & Imai M (2000). Molecular cloning of a novel form (two-repeat) protein related to voltage-gated sodium and calcium channels. *Biochem Biophys Res Commun* 270, 370-376.

Islam MM, Munemasa S, Hossain MA, Nakamura Y, Mori IC, & Murata Y (2010). Roles of AtTPC1, vacuolar two pore channel 1, in Arabidopsis stomatal closure. *Plant Cell Physiol* 51, 302-311.

Jadot M, Colmant C, Wattiaux-De CS, & Wattiaux R (1984). Intralysosomal hydrolysis of glycyl-L-phenylalanine 2-naphthylamide. *Biochem J* 219, 965-970.

Jaffe LF (1983). Sources of calcium in egg activation: a review and hypothesis. *Dev Biol* 99, 265-276.

Juretic D, Zoranic L, & Zucic D (2002). Basic charge clusters and predictions of membrane protein topology. *J Chem Inf Comput Sci* 42, 620-632.

Kahsay RY, Gao G, & Liao L (2005). An improved hidden Markov model for transmembrane protein detection and topology prediction and its applications to complete genomes. *Bioinformatics* 21, 1853-1858.

Kall L, Krogh A, & Sonnhammer EL (2004). A combined transmembrane topology and signal peptide prediction method. *J Mol Biol* 338, 1027-1036.

Kawasaki H, Nakayama S, & Kretsinger RH (1998). Classification and evolution of EF-hand proteins. *Biometals* 11, 277-295.

Krogh A, Larsson B, von HG, & Sonnhammer EL (2001). Predicting transmembrane protein topology with a hidden Markov model: application to complete genomes. *J Mol Biol* 305, 567-580.

Kukuruzinska MA & Lennon K (1998). Protein N-glycosylation: molecular genetics and functional significance. *Crit Rev Oral Biol Med* 9, 415-448.

Kundra R & Kornfeld S (1999). Asparagine-linked oligosaccharides protect Lamp-1 and Lamp-2 from intracellular proteolysis. *J Biol Chem* 274, 31039-31046.

Lai FA, Erickson HP, Rousseau E, Liu QY, & Meissner G (1988). Purification and reconstitution of the calcium release channel from skeletal muscle. *Nature* 331, 315-319.

Lamason RL, Mohideen MA, Mest JR, Wong AC, Norton HL, Aros MC, Jurynec MJ, Mao X, Humphreville VR, Humbert JE, Sinha S, Moore JL, Jagadeeswaran P, Zhao W, Ning G, Makalowska I, McKeigue PM, O'donnell D, Kittles R, Parra EJ, Mangini NJ, Grunwald DJ, Shriver MD, Canfield VA, & Cheng KC (2005). SLC24A5, a putative cation exchanger, affects pigmentation in zebrafish and humans. *Science* 310, 1782-1786.

Lange I, Penner R, Fleig A, & Beck A (2008). Synergistic regulation of endogenous TRPM2 channels by adenine dinucleotides in primary human neutrophils. *Cell Calcium* 44, 604-615.

Larsen FL & Vincenzi FF (1979). Calcium transport across the plasma membrane: stimulation by calmodulin. *Science* 204, 306-309.

Lee HC (1997). Mechanisms of calcium signaling by cyclic ADP-ribose and NAADP. *Physiol Rev* 77, 1133-1164.

Lee HC & Aarhus R (1991). ADP-ribosyl cyclase: an enzyme that cyclizes NAD^+ into a calcium-mobilizing metabolite. *Cell Regul* 2, 203-209.

Lee HC & Aarhus R (1995). A derivative of NADP mobilizes calcium stores insensitive to inositol trisphosphate and cyclic ADP-ribose. *J Biol Chem* 270, 2152-2157.

Lee HC & Aarhus R (1997). Structural determinants of nicotinic acid adenine dinucleotide phosphate important for its calcium-mobilizing activity. *J Biol Chem* 272, 20378-20383.

Lee HC & Aarhus R (2000). Functional visualization of the separate but interacting calcium stores sensitive to NAADP and cyclic ADP-ribose. *J Cell Sci* 113 Pt 24, 4413-4420.

Lee HC, Walseth TF, Bratt GT, Hayes RN, & Clapper DL (1989). Structural determination of a cyclic metabolite of NAD^+ with intracellular Ca2+-mobilizing activity. *J Biol Chem* 264, 1608-1615.

Lepage PK, Lussier MP, McDuff FO, Lavigne P, & Boulay G (2009). The self-association of two N-terminal interaction domains plays an important role in the tetramerization of TRPC4. *Cell Calcium* 45, 251-259.

Li Y, Wu Y, & Zhou Y (2006). Modulation of inactivation properties of $Ca_V2.2$ channels by 14-3-3 proteins. *Neuron* 51, 755-771.

Liman ER, Hess P, Weaver F, & Koren G (1991). Voltage-sensing residues in the S4 region of a mammalian K^+ channel. *Nature* 353, 752-756.

Lloyd-Evans E, Waller-Evans H, Peterneva K, & Platt FM (2010). Endolysosomal calcium regulation and disease. *Biochem Soc Trans* 38, 1458-1464.

Lorenz H, Hailey DW, Wunder C, & Lippincott-Schwartz J (2006). The fluorescence protease protection (FPP) assay to determine protein localization and membrane topology. *Nat Protoc* 1, 276-279.

Ludtke SJ, Serysheva II, Hamilton SL, & Chiu W (2005). The pore structure of the closed RyR1 channel. *Structure* 13, 1203-1211.

Lur G, Sherwood MW, Ebisui E, Haynes L, Feske S, Sutton R, Burgoyne RD, Mikoshiba K, Petersen OH, & Tepikin AV (2011). InsPreceptors and Orai channels in pancreatic acinar cells: co-localization and its consequences. *Biochem J* 436, 231-239.

Luzio JP, Pryor PR, & Bright NA (2007). Lysosomes: fusion and function. *Nat Rev Mol Cell Biol* 8, 622-632.

Macgregor A, Yamasaki M, Rakovic S, Sanders L, Parkesh R, Churchill GC, Galione A, & Terrar DA (2007). NAADP controls cross-talk between distinct Ca^{2+} stores in the heart. *J Biol Chem* 282, 15302-15311.

MacRobbie EA & Smyth WD (2010). Effects of fusicoccin on ion fluxes in guard cells. *New Phytol* 186, 636-647.

Mandi M & Bak J (2008). Nicotinic acid adenine dinucleotide phosphate (NAADP) and Ca^{2+} mobilization. *J Recept Signal Transduct Res* 28, 163-184.

Mei ZZ & Jiang LH (2009). Requirement for the N-terminal coiled-coil domain for expression and function, but not subunit interaction of, the ADPR-activated TRPM2 channel. *J Membr Biol* 230, 93-99.

Mignery GA & Sudhof TC (1990). The ligand binding site and transduction mechanism in the inositol-1,4,5-triphosphate receptor. EMBO J 9, 3893-3898.

Minor DL, Jr. & Findeisen F (2010). Progress in the structural understanding of voltage-gated calcium channel (CaV) function and modulation. *Channels (Austin)* 4, 459-474.

Moccia F, Lim D, Kyozuka K, & Santella L (2004). NAADP triggers the fertilization potential in starfish oocytes. *Cell Calcium* 36, 515-524.

Mojzisova A, Krizanova O, Zacikova L, Kominkova V, & Ondrias K (2001). Effect of nicotinic acid adenine dinucleotide phosphate on ryanodine calcium release channel in heart. *Pflugers Arch* 441, 674-677.

Morgan AJ & Galione A (2007). Fertilization and nicotinic acid adenine dinucleotide phosphate induce pH changes in acidic Ca^{2+} stores in sea urchin eggs. *J Biol Chem* 282, 37730-37737.

Mushtaq M, Nam TS, & Kim UH (2011). Critical role for CD38-mediated Ca2+ signaling in thrombin-induced procoagulant activity of mouse platelets and hemostasis. *J Biol Chem* 286, 12952-12958.

Naylor E, Arredouani A, Vasudevan SR, Lewis AM, Parkesh R, Mizote A, Rosen D, Thomas JM, Izumi M, Ganesan A, Galione A, & Churchill GC (2009). Identification of a chemical probe for NAADP by virtual screening. *Nat Chem Biol* 5, 220-226.

Newton CL, Mignery GA, & Sudhof TC (1994). Co-expression in vertebrate tissues and cell lines of multiple inositol 1,4,5-trisphosphate ($InsP_3$) receptors with distinct affinities for $InsP_3$. *J Biol Chem* 269, 28613-28619.

Ng CA, Hunter MJ, Perry MD, Mobli M, Ke Y, Kuchel PW, King GF, Stock D, & Vandenberg JI (2011). The N-terminal tail of hERG contains an amphipathic alpha-helix that regulates channel deactivation. *PLoS One* 6, e16191.

Noma K, Kimura K, Minatohara K, Nakashima H, Nagao Y, Mizoguchi A, & Fujiyoshi Y (2009). Triple N-glycosylation in the long S5-P loop regulates the activation and trafficking of the Kv12.2 potassium channel. *J Biol Chem* 284, 33139-33150.

Ogunbayo OA, Zhu Y, Rossi D, Sorrentino V, Ma J, Zhu MX, & Evans AM (2011). Cyclic Adenosine Diphosphate Ribose Activates Ryanodine Receptors, whereas NAADP Activates Two-pore Domain Channels. *J Biol Chem* 286, 9136-9140.

Page KM, Heblich F, Margas W, Pratt WS, Nieto-Rostro M, Chaggar K, Sandhu K, Davies A, & Dolphin AC (2010). N terminus is key to the dominant negative suppression of Ca_V2 calcium channels: implications for episodic ataxia type 2. *J Biol Chem* 285, 835-844.

Palmenberg AC, Parks GD, Hall DJ, Ingraham RH, Seng TW, & Pallai PV (1992). Proteolytic processing of the cardioviral P2 region: primary 2A/2B cleavage in clone-derived precursors. *Virology* 190, 754-762.

Patel S, Churchill GC, & Galione A (2000a). Unique kinetics of nicotinic acid-adenine dinucleotide phosphate (NAADP) binding enhance the sensitivity of NAADP receptors for their ligand. *Biochem J* 352 Pt 3, 725-729.

Patel S, Churchill GC, Sharp T, & Galione A (2000b). Widespread distribution of binding sites for the novel Ca^{2+}-mobilizing messenger, nicotinic acid adenine dinucleotide phosphate, in the brain. *J Biol Chem* 275, 36495-36497.

Patel S, Joseph SK, & Thomas AP (1999). Molecular properties of inositol 1,4,5-trisphosphate receptors. *Cell Calcium* 25, 247-264.

Patel S, Marchant JS, & Brailoiu E (2010). Two-pore channels: Regulation by NAADP and customized roles in triggering calcium signals. *Cell Calcium* 47, 480-490.

Patel S, Ramakrishnan L, Rahman T, Hamdoun A, Marchant JS, Taylor CW, & Brailoiu E (2011). The endo-lysosomal system as an NAADP-sensitive acidic Ca^{2+} store: Role for the two-pore channels. *Cell Calcium*.
Peiter E (2011). The plant vacuole: Emitter and receiver of calcium signals. *Cell Calcium.*

Peiter E, Maathuis FJ, Mills LN, Knight H, Pelloux J, Hetherington AM, & Sanders D (2005). The vacuolar Ca^{2+}-activated channel TPC1 regulates germination and stomatal movement. *Nature* 434, 404-408.

Pereira GJ, Hirata H, Fimia GM, do Carmo LG, Bincoletto C, Han SW, Stilhano RS, Ureshino RP, Bloor-Young D, Churchill G, Piacentini M, Patel S, & Smaili SS (2011). Nicotinic acid adenine dinucleotide phosphate (NAADP) regulates autophagy in cultured astrocytes. *J Biol Chem.*

Pitt SJ, Funnell TM, Sitsapesan M, Venturi E, Rietdorf K, Ruas M, Ganesan A, Gosain R, Churchill GC, Zhu MX, Parrington J, Galione A, & Sitsapesan R (2010). TPC2 is a novel NAADP-sensitive Ca^{2+} release channel, operating as a dual sensor of luminal pH and Ca^{2+}. *J Biol Chem* 285, 35039-35046.

Polgar O, Ierano C, Tamaki A, Stanley B, Ward Y, Xia D, Tarasova N, Robey RW, & Bates SE (2010). Mutational analysis of threonine 402 adjacent to the GXXXG dimerization motif in transmembrane segment 1 of ABCG2. *Biochemistry* 49, 2235-2245.

Pongs O & Schwarz JR (2010). Ancillary subunits associated with voltage-dependent K^+ channels. *Physiol Rev* 90, 755-796.

Qureshi OS, Paramasivam A, Yu JC, & Murrell-Lagnado RD (2007). Regulation of P2X4 receptors by lysosomal targeting, glycan protection and exocytosis. *J Cell Sci* 120, 3838-3849.

Raghib A, Bertaso F, Davies A, Page KM, Meir A, Bogdanov Y, & Dolphin AC (2001). Dominant-negative synthesis suppression of voltage-gated calcium channel $Ca_v2.2$ induced by truncated constructs. *J Neurosci* 21, 8495-8504.

Rah SY, Mushtaq M, Nam TS, Kim SH, & Kim UH (2010). Generation of cyclic ADP-ribose and nicotinic acid adenine dinucleotide phosphate by CD38 for Ca^{2+} signaling in interleukin-8-treated lymphokine-activated killer cells. *J Biol Chem* 285, 21877-21887.

Rahman T & Taylor CW (2009). Dynamic regulation of IP_3 receptor clustering and activity by IP_3. *Channels (Austin)* 3, 226-232.

Ramjeesingh M, Huan LJ, Garami E, & Bear CE (1999). Novel method for evaluation of the oligomeric structure of membrane proteins. *Biochem J* 342 (Pt 1), 119-123.

Richards MW, Butcher AJ, & Dolphin AC (2004). Ca^{2+} channel beta-subunits: structural insights AID our understanding. *Trends Pharmacol Sci* 25, 626-632.

Rizzuto R, Brini M, Murgia M, & Pozzan T (1993). Microdomains with high Ca^{2+} close to IP_3-sensitive channels that are sensed by neighboring mitochondria. *Science* 262, 744-747.

Roberts WM (1993). Spatial calcium buffering in saccular hair cells. *Nature* 363, 74-76.

Rogers JH (1987). Calretinin: a gene for a novel calcium-binding protein expressed principally in neurons. *J Cell Biol* 105, 1343-1353.

Rosen D, Lewis AM, Mizote A, Thomas JM, Aley PK, Vasudevan SR, Parkesh R, Galione A, Izumi M, Ganesan A, & Churchill GC (2009). Analogues of the NAADP antagonist NED-19 indicate two binding sites on the NAADP receptor. *J Biol Chem.*

Ruas M, Rietdorf K, Arredouani A, Davis LC, Lloyd-Evans E, Koegel H, Funnell TM, Morgan AJ, Ward JA, Watanabe K, Cheng X, Churchill GC, Zhu MX, Platt FM, Wessel GM, Parrington J, & Galione A (2010). Purified TPC Isoforms Form NAADP Receptors with Distinct Roles for Ca^{2+} Signaling and Endolysosomal Trafficking. *Curr Biol.*

Sagara Y, Wade JB, & Inesi G (1992). A conformational mechanism for formation of a dead-end complex by the sarcoplasmic reticulum ATPase with thapsigargin. *J Biol Chem* 267, 1286-1292.

Sammels E, Devogelaere B, Mekahli D, Bultynck G, Missiaen L, Parys JB, Cai Y, Somlo S, & De SH (2010). Polycystin-2 activation by inositol 1,4,5-trisphosphate-induced Ca^{2+} release requires its direct association with the inositol 1,4,5-trisphosphate receptor in a signaling microdomain. *J Biol Chem* 285, 18794-18805.

Samso M, Wagenknecht T, & Allen PD (2005). Internal structure and visualization of transmembrane domains of the RyR1 calcium release channel by cryo-EM. *Nat Struct Mol Biol* 12, 539-544.

Santella L, Kyozuka K, Genazzani AA, De RL, & Carafoli E (2000). Nicotinic acid adenine dinucleotide phosphate-induced Ca^{2+} release. Interactions among distinct Ca^{2+} mobilizing mechanisms in starfish oocytes. *J Biol Chem* 275, 8301-8306.

Santo-Domingo J & Demaurex N (2010). Calcium uptake mechanisms of mitochondria. *Biochim Biophys Acta* 1797, 907-912.

Santoso NG, Cebotaru L, & Guggino WB (2011). Polycystin-1, 2, and STIM1 interact with IP_3R to modulate ER Ca release through the PI3K/Akt pathway. *Cell Physiol Biochem* 27, 715-726.

Schagger H & von Jagow G (1991). Blue native electrophoresis for isolation of membrane protein complexes in enzymatically active form. *Anal Biochem* 199, 223-231.

Schatzmann HJ (1966). ATP-dependent Ca++-extrusion from human red cells. *Experientia* 22, 364-365.

Schieder M, Rotzer K, Bruggemann A, Biel M, & Wahl-Schott C (2010a). Planar patch clamp approach to characterize ionic currents from intact lysosomes. *Sci Signal* 3, l3.

Schieder M, Rotzer K, Bruggemann A, Biel M, & Wahl-Schott CA (2010b). Characterization of two-pore channel 2 (TPCN2)-mediated Ca2+ currents in isolated lysosomes. *J Biol Chem* 285, 21219-21222.

Shaya D, Kreir M, Robbins RA, Wong S, Hammon J, Bruggemann A, & Minor DL, Jr. (2011). Voltage-gated sodium channel Na_V protein dissection creates a set of functional pore-only proteins. *Proc Natl Acad Sci U S A* 108, 12313-12318.

Shaywitz AJ & Greenberg ME (1999). CREB: a stimulus-induced transcription factor activated by a diverse array of extracellular signals. *Annu Rev Biochem* 68, 821-861.

Slominski A, Tobin DJ, Shibahara S, & Wortsman J (2004). Melanin pigmentation in mammalian skin and its hormonal regulation. *Physiol Rev* 84, 1155-1228.

Smith PK, Krohn RI, Hermanson GT, Mallia AK, Gartner FH, Provenzano MD, Fujimoto EK, Goeke NM, Olson BJ, & Klenk DC (1985). Measurement of protein using bicinchoninic acid. *Anal Biochem* 150, 76-85.

Staros JV (1982). N-hydroxysulfosuccinimide active esters: bis(N-hydroxysulfosuccinimide) esters of two dicarboxylic acids are hydrophilic, membrane-impermeant, protein cross-linkers. *Biochemistry* 21, 3950-3955.

Steen M, Kirchberger T, & Guse AH (2007). NAADP mobilizes calcium from the endoplasmic reticular Ca_{2+} store in T-lymphocytes. *J Biol Chem* 282, 18864-18871.

Streb H, Irvine RF, Berridge MJ, & Schulz I (1983). Release of Ca^{2+} from a nonmitochondrial intracellular store in pancreatic acinar cells by inositol-1,4,5-trisphosphate. *Nature* 306, 67-69.

Sturm RA (2009). Molecular genetics of human pigmentation diversity. *Hum Mol Genet* 18, R9-17.

Sulem P, Gudbjartsson DF, Stacey SN, Helgason A, Rafnar T, Jakobsdottir M, Steinberg S, Gudjonsson SA, Palsson A, Thorleifsson G, Palsson S, Sigurgeirsson B, Thorisdottir K, Ragnarsson R, Benediktsdottir KR, Aben KK, Vermeulen SH, Goldstein AM, Tucker MA, Kiemeney LA, Olafsson JH, Gulcher J, Kong A, Thorsteinsdottir U, & Stefansson K (2008). Two newly identified genetic determinants of pigmentation in Europeans. *Nat Genet* 40, 835-837.

Swann K & Whitaker M (1986). The part played by inositol trisphosphate and calcium in the propagation of the fertilization wave in sea urchin eggs. *J Cell Biol* 103, 2333-2342.

Szymczak AL, Workman CJ, Wang Y, Vignali KM, Dilioglou S, Vanin EF, & Vignali DA (2004). Correction of multi-gene deficiency in vivo using a single 'self-cleaving' 2A peptide-based retroviral vector. *Nat Biotechnol* 22, 589-594.

Tinker A & Williams AJ (1992). Divalent cation conduction in the ryanodine receptor channel of sheep cardiac muscle sarcoplasmic reticulum. *J Gen Physiol* 100, 479-493.

Tinker A & Williams AJ (1993). Probing the structure of the conduction pathway of the sheep cardiac sarcoplasmic reticulum calcium-release channel with permeant and impermeant organic cations. *J Gen Physiol* 102, 1107-1129.

Tinker A & Williams AJ (1995). Measuring the length of the pore of the sheep cardiac sarcoplasmic reticulum calcium-release channel using related trimethylammonium ions as molecular calipers. *Biophys J* 68, 111-120.

Tiwari-Woodruff SK, Schulteis CT, Mock AF, & Papazian DM (1997). Electrostatic interactions between transmembrane segments mediate folding of Shaker K^+ channel subunits. *Biophys J* 72, 1489-1500.

Toth B & Csanady L (2010). Identification of direct and indirect effectors of the transient receptor potential melastatin 2 (TRPM2) cation channel. *J Biol Chem* 285, 30091-30102.

Tugba Durlu-Kandilci N, Ruas M, Chuang KT, Brading A, Parrington J, & Galione A (2010). TPC2 proteins mediate nicotinic acid adenine dinucleotide phosphate (NAADP)- and agonist-evoked contractions of smooth muscle. *J Biol Chem* 285, 24925-24932.

Tusnady GE & Simon I (1998). Principles governing amino acid composition of integral membrane proteins: application to topology prediction. *J Mol Biol* 283, 489-506.

van Heusden GP (2005). 14-3-3 proteins: regulators of numerous eukaryotic proteins. *IUBMB Life* 57, 623-629.

Varnai P, Hunyady L, & Balla T (2009). STIM and Orai: the long-awaited constituents of store-operated calcium entry. Trends Pharmacol Sci 30, 118-128.
Venkatachalam K & Montell C (2007). TRP channels. *Annu Rev Biochem* 76, 387-417.

Voets T, Janssens A, Droogmans G, & Nilius B (2004). Outer pore architecture of a Ca2+-selective TRP channel. *J Biol Chem* 279, 15223-15230.

Voets T, Prenen J, Vriens J, Watanabe H, Janssens A, Wissenbach U, Bodding M, Droogmans G, & Nilius B (2002). Molecular determinants of permeation through the cation channel TRPV4. *J Biol Chem* 277, 33704-33710.

Walseth TF, Aarhus R, Kerr JA, & Lee HC (1993). Identification of cyclic ADP-ribose-binding proteins by photoaffinity labeling. *J Biol Chem* 268, 26686-26691.

Wang YY, Chang RB, Waters HN, McKemy DD, & Liman ER (2008). The nociceptor ion channel TRPA1 is potentiated and inactivated by permeating calcium ions. *J Biol Chem* 283, 32691-32703.

Wasserman RH & Taylor AN (1966). Vitamin d3-induced calcium-binding protein in chick intestinal mucosa. *Science* 152, 791-793.

Wirkner K, Hognestad H, Jahnel R, Hucho F, & Illes P (2005). Characterization of rat transient receptor potential vanilloid 1 receptors lacking the N-glycosylation site N604. *Neuroreport* 16, 997-1001.

Wu MM, Buchanan J, Luik RM, & Lewis RS (2006). Ca^{2+} store depletion causes STIM1 to accumulate in ER regions closely associated with the plasma membrane. *J Cell Biol* 174, 803-813.

Xu H, Delling M, Li L, Dong X, & Clapham DE (2007). Activating mutation in a mucolipin transient receptor potential channel leads to melanocyte loss in varitint-waddler mice. *Proc Natl Acad Sci U S A* 104, 18321-18326.

Yamaguchi S, Jha A, Li Q, Soyombo AA, Dickinson GD, Churamani D, Brailoiu E, Patel S, & Muallem S (2011). Transient Receptor Potential Mucolipin 1 (TRPML1) and Two-pore Channels Are Functionally Independent Organellar Ion Channels. *J Biol Chem* 286, 22934-22942.

Yamasaki M, Thomas JM, Churchill GC, Garnham C, Lewis AM, Cancela JM, Patel S, & Galione A (2005). Role of NAADP and cADPR in the induction and maintenance of agonist-evoked Ca^{2+} spiking in mouse pancreatic acinar cells. *Curr Biol* 15, 874-878.

Yu FH, Yarov-Yarovoy V, Gutman GA, & Catterall WA (2005). Overview of molecular relationships in the voltage-gated ion channel superfamily. *Pharmacol Rev* 57, 387-395.

Yusufi AN, Cheng J, Thompson MA, Chini EN, Grande JP (2001). Nicotinic acid–adenine dinucleotide phosphate (NAADP) elicits specific microsomal Ca^{2+} release from mammalian cells. *Biochem J* 353, 531 – 536.

Yusufi AN, Cheng J, Thompson MA, Burnett JC, & Grande JP (2002). Differential mechanisms of Ca^{2+} release from vascular smooth muscle cell microsomes. *Exp Biol Med* (Maywood) 227, 36-44.

Zhang F, Xu M, Han WQ, & Li PL (2011). RECONSTITUTION OF LYSOSOMAL NAADP-TRP-ML1 SIGNALING PATHWAY AND ITS FUNCTION IN TRP-ML1$^{-/-}$ CELLS. *Am J Physiol Cell Physiol.*

Zhu MX, Ma J, Parrington J, Galione A, & Evans AM (2010). TPCs: Endolysosomal channels for Ca^{2+} mobilization from acidic organelles triggered by NAADP. *FEBS Lett* 584, 1966-1974.

Zong X, Schieder M, Cuny H, Fenske S, Gruner C, Rotzer K, Griesbeck O, Harz H, Biel M, & Wahl-Schott C (2009). The two-pore channel TPCN2 mediates NAADP-dependent Ca^{2+}-release from lysosomal stores. *Pflugers Arch* 458, 891-899.

Zurborg S, Yurgionas B, Jira JA, Caspani O, & Heppenstall PA (2007). Direct activation of the ion channel TRPA1 by Ca^{2+}. *Nat Neurosci* 10, 277-279.